Reactor Physics Methods and Preconceptual Core Design Analyses for Conversion of the Advanced Test Reactor to Low-Enriched Uranium Fuel

Annual Report for Fiscal Year 2012

David W. Nigg
Sean R. Morrell

September 2012

Idaho National Laboratory

Reactor Physics Methods and Preconceptual Core Design Analyses for Conversion of the Advanced Test Reactor to Low-Enriched Uranium Fuel

Annual Report for Fiscal Year 2012

David W. Nigg
Sean R. Morrell

September 2012

Idaho National Laboratory
Nuclear Science and Technology Directorate
Idaho Falls, Idaho 83415

http://www.inl.gov

Nuclear Science and Technology Directorate

Reactor Physics Methods and Preconceptual Core Design Analyses for Conversion of the Advanced Test Reactor to Low-Enriched Fuel

Annual Report for Fiscal Year 2012

INL/EXT-12-27069
September 2012

Approval:

_9/14/2012_

David W. Nigg, Principal Investigator, Reactor Physics

_9/14/2012_

Sean R. Morrell, ATR LEU Conversion Project Manager

EXECUTIVE SUMMARY

Under the current long-term DOE policy and planning scenario, both the ATR and the ATRC will be reconfigured at an appropriate time within the next several years to operate with low-enriched uranium (LEU) fuel. This will be accomplished under the auspices of the Reduced Enrichment Research and Test Reactor (RERTR) Program, administered by the DOE National Nuclear Security Administration (NNSA). At a minimum, the internal design and composition of the fuel element plates and support structure will change, to accommodate the need for low enrichment in a manner that maintains total core excess reactivity at a suitable level for anticipated operational needs throughout each cycle while respecting all control and shutdown margin requirements and power distribution limits

The complete engineering design and optimization of LEU cores for the ATR and the ATRC will require significant multi-year efforts in the areas of fuel design, development and testing, as well as a complete re-analysis of the relevant reactor physics parameters for a core composed of LEU fuel, with possible control system modifications. Ultimately, revalidation of the computational physics parameters per applicable national and international standards against data from experimental measurements for prototypes of the new ATR and ATRC core designs will also be required for Safety Analysis Report (SAR) changes to support routine operations with LEU. This report is focused on reactor physics analyses conducted during Fiscal Year (FY) 2012 to support the initial development of several potential preconceptual fuel element designs that are suitable candidates for further study and refinement during FY-2013 and beyond.

In a separate, but related, effort in the general area of computational support for ATR operations, the Idaho National Laboratory (INL) is conducting a focused multiyear effort to introduce modern high-fidelity computational reactor physics software and associated validation protocols to replace several obsolete components of the current analytical tool set used for ATR neutronics support. This aggressive computational and experimental campaign will have a broad strategic impact on the operation of the ATR, both in terms of improved computational efficiency and accuracy for support of ongoing DOE programs as well as in terms of national and international recognition of the ATR National Scientific User Facility (NSUF). It will also greatly facilitate the LEU conversion effort, since the upgraded computational capabilities are now at a stage where they can be, and in fact have been, used for the required physics analysis from the beginning.

In this context, extensive scoping neutronics analyses were completed for six preconceptual candidate LEU fuel element designs for the ATR (and for its companion critical facility, ATRC). Of these, four exhibited neutronics performance in what is believed to be an acceptable range. However, there are currently some concerns with regard to fabricability and mechanical performance that have emerged for one of the four latter concepts. Thus three concepts have been selected for more comprehensive conceptual design analysis during the upcoming fiscal year.

CONTENTS

ACRONYMS

AGR	Advanced Gas Reactor
ATR	Advanced Test Reactor
ATRC	Advanced Test Reactor Critical Facility
CIC	Core Internals Changeout
CSAP	Core Safety Assurance Package
DOE	(US) Department of Energy
ENDF	Evaluated Nuclear Data File
FY	Fiscal Year
HPRR	High Performance Research Reactor
HEU	High-Enriched Uranium (>20% ^{235}U)
ICSBE	OECD International Criticality Safety benchmark Experiment Evaluation (Program)
ICBA	Integral Cladding Burnable Absorber
HPZ	Hafnium-Poisoned Zirconium
RE	Reduced Enrichment
ELF	Enhanced Low-Enrichment Fuel
ISBA	Integral Side Plate Burnable Absorber
INL	Idaho National Laboratory
IRPhE	OECD International Reactor physics Experiment Evaluation (Program)
LEP	(ATR) Life Extension Program
LEU	Low-Enriched Uranium (<20% ^{235}U)
NR	Bureau of Naval Reactors (DOE)
NST	Nuclear Science and Technology
NSUF	National Scientific User Facility
OECD	Organization for Economic Cooperation and Development
QA	Quality Assurance
RERTR	Reduced Enrichment for Research and Test Reactors
SAR	Safety Analysis Report
V&V	Verification and Validation

1.0 INTRODUCTION

The Advanced Test Reactor (ATR), located at the Idaho National Laboratory (INL), is one of only a few high-power research reactors of its general type in the world. Its capabilities support a variety of missions involving accelerated testing of nuclear fuel and other materials in a very high neutron flux environment, medical and industrial isotope production, and other applications. Along with its companion critical mockup (ATRC), the ATR is one of the key nuclear engineering research and testing facilities within the US Department of Energy (DOE) National Laboratory Complex. The ATR and ATRC also serve as the centerpieces of the recently-formed ATR National Scientific User Facility (NSUF), whose purpose is to facilitate the current trend toward broadening the applications of the ATR beyond its traditional base.

1.1 General Facility Description

The ATR (Figures 1.1 and 1.2) is one of six High-Performance Research Reactors (HPRR) in the USA. It is a highly-heterogeneous light-water and beryllium moderated, beryllium reflected, light-water cooled system with highly-enriched (93% ^{235}U) plate-type fuel elements arranged in a serpentine pattern. Gross reactivity and power distribution control during operation is achieved through the use of eight pairs of rotating control drums with hafnium neutron absorber plates on one side as can be seen in Figure 1.1. There are several design features incorporated into the ATR and ATRC (Figures 1.3 and 1.4) to optimize experimental capabilities. These features include: a) the use of flux traps to provide high thermal neutron fluxes for irradiation or experiments in nine regions, b) incorporation of special control shim design to retain axial flux symmetry throughout an ATR fuel cycle; and c) regional power control to provide capability for power shifting between core lobes to optimize the neutron flux distribution for a wide range of simultaneous experiments. The ATR can be operated at powers as high as 250 MW although most routine applications do not require the maximum power. Typical thermal neutron fluxes in the flux traps can be as high as 5.0×10^{14} n/cm^2-s. Typical operating cycle lengths are in the range of 45–60 days. The core fuel configuration and the experiment loadings are usually rearranged between cycles and each fuel element is typically burned for two or three cycles during its useful lifetime.

The ATRC is an open-pool nuclear mock-up of the ATR that typically operates at approximately 600 W and produces a thermal neutron flux in the traps that is in the range of 1.0×10^9 n/cm^2-s. As is the case for the ATR, the core consists of a 4-ft-high (122 cm), uniform-width, vertical 40-element fuel annulus shaped in a serpentine fashion between and around nine flux-trap regions located in a three-by-three square array. The cruciform fixture inside the serpentine is called the neck shim housing. The reactivity of the core is controlled by: (a) five vertically withdrawn safety rods that use cadmium as the poison material; (b) 24 vertically withdrawn hafnium neck shim rods; and (c) eight pairs of rotating outer shim control cylinders (OSCCs) that use hafnium poison plates.

ATRC criticality can normally be stably attained at a power as low as 0.25 mW and the maximum rated power is 5 kW. The ATRC facility is typically used with prototype experiments to characterize in advance, with precision and accuracy, the expected changes in core reactivity to be expected for the same experiments in the ATR. Useful physics data can also be obtained for evaluating the worth and calibration of control elements as well as thermal and fast neutron distributions.
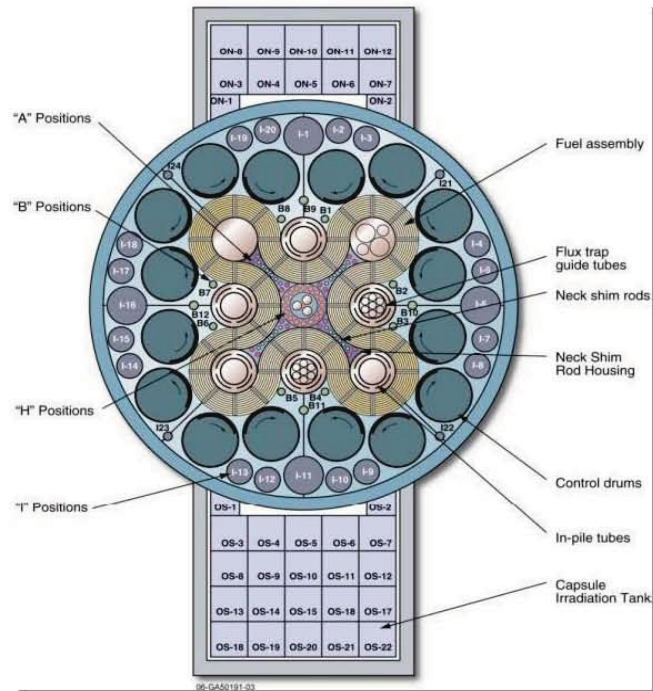
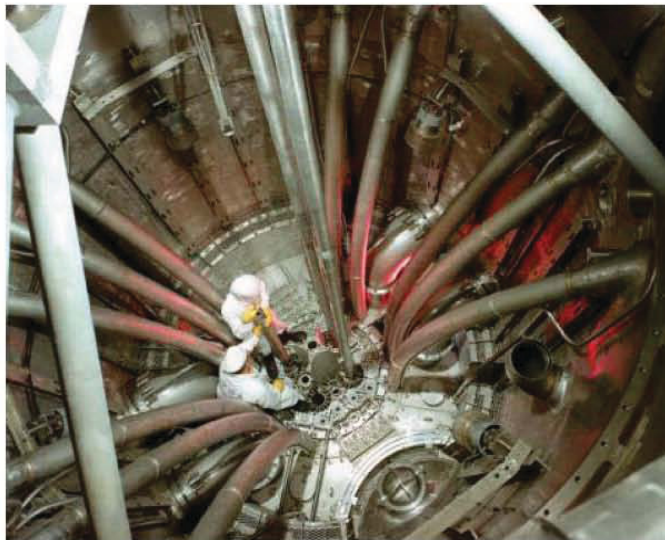Figure 1.1. Core and reflector geometry of the Advanced Test Reactor.

Figure 1.2. View into the ATR pressure vessel.

2

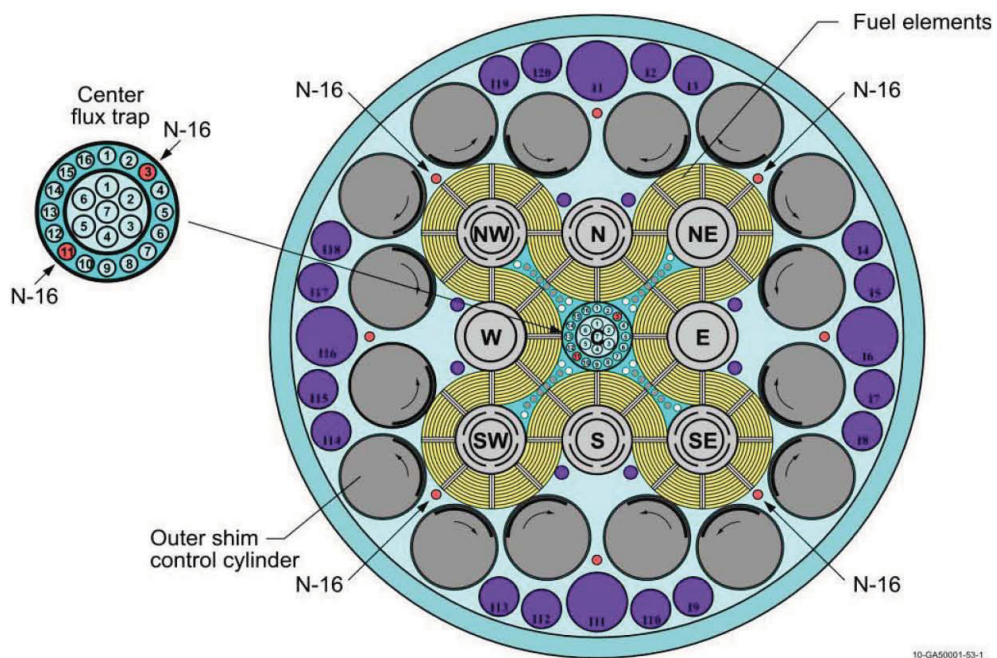Figure 1.3. The Advanced Test Reactor Critical Facility.

Figure 1.4. ATRC Configuration, showing the NW LIPT Flux Trap and six N-16 positions.

1.2 Reconfiguration of the ATR and ATRC to Low-Enriched Uranium Fuel

Under the current long-term DOE policy and planning scenario, both the ATR and the ATRC will be reconfigured at an appropriate time within the next several years to operate with low-enriched uranium (LEU) fuel. This will be accomplished under the auspices of the Reduced Enrichment Research and Test Reactor (RERTR) Program, administered by the DOE National Nuclear Security Administration (NNSA). LEU is defined to be uranium enriched to no more than 20% atom fraction ^{235}U. At a minimum, the internal design and composition of the fuel element plates and support structure will change, to accommodate the need for low enrichment in a manner that maintains total core excess reactivity at a suitable level for anticipated operational needs throughout each cycle. The internal element design may also include the use of burnable poisons at various locations within the element structure to help maintain reactivity margins throughout a given fuel cycle and to help control the spatial fission rate distribution within the element, just as is done in the case of the current HEU fuel. In addition it may be necessary to provide for variations in uranium loading per unit volume from one plate to another radially across the fuel element. Finally some active reactivity control system modifications may also be required. Such modifications could include placement of additional burnable poison components at various positions within the beryllium reflector and reconfiguration of neck shim loading patterns and compositions.

The complete engineering design and optimization of LEU cores for the ATR and the ATRC will thus require significant multi-year efforts in the area of fuel design, development and testing, as well as a complete re-analysis of the relevant reactor physics parameters for a core composed of LEU fuel, with possible control system modifications. Ultimately a complete revalidation of the computational physics parameters per applicable national and international standards against data from experimental measurements for prototypes of the new ATR and ATRC core designs will also be required for the necessary Safety Analysis Report (SAR) changes to support routine operations with LEU. Corresponding extensive thermal-fluids and structural integrity analyses with appropriate revalidation will also be required, but these latter subjects are outside of the scope of this report, which is focused on reactor physics analyses conducted during Fiscal Year (FY) 2012 to support the initial development of several potential preconceptual fuel element designs that are suitable candidates for further study and refinement during FY-2013 and beyond.

1.3 Overview of Computational Physics Methods for ATR Support

Computational reactor physics modeling is used extensively to support ATR experiment design, operations and fuel cycle management, core and experiment safety analysis, and many other applications. Experiment design and analysis for the ATR generally involves very detailed and sophisticated three-dimensional Monte Carlo analysis, typically using the internationally recognized continuous-energy MCNP5 code (Goorley et al., 2004) or an equivalent methodology, coupled to extensive fuel isotope buildup and depletion analysis where appropriate. On the other hand, the computational reactor physics software tools and protocols currently used for ATR core fuel cycle analysis and operational support are largely based on four-group diffusion theory in Cartesian geometry (Pfeifer et al., 1971) with heavy reliance on "tuned" nuclear parameter input data. These methods are not consistent with the state of current engineering practice and have been superseded in the general reactor physics community by high-fidelity multidimensional transport-theory-based methods. As a result, the historical approach to ATR reactor physics operational support is inconsistent with the state of modern nuclear engineering practice and nearly impossible to properly verify and validate (V&V) according to modern standards. Furthermore, some aspects of the analysis process are highly empirical in nature, with many "correction factors" and approximations that require very specialized experience to apply. But the legacy staff knowledge from the 1960s and 1970s that is essential for the successful application of these various approximations and outdated computational processes is rapidly being lost due to staff turnover and retirements.

4

In response to this situation, the INL is currently engaged in a major multiyear effort to modernize the computational reactor physics tools and validation protocols needed for support of ongoing ATR operations as well as for new applications, such as the design of suitable LEU fuel elements and corresponding LEU core configurations for the ATR and the ATRC. This effort, referred to as the "ATR Core Modeling Update Project" is currently completing its third full year under the auspices of the ATR Life Extension Program (LEP) funded by the DOE Office of Nuclear Energy. It is an aggressive computational and experimental campaign that will have a broad strategic impact on the operation of the ATR, both in terms of improved computational efficiency and accuracy for support of ongoing DOE programs as well as national and international recognition of the ATR NSUF.

Chapter 2 of this report provides a brief description of the Modeling Update Project, including its current status, recent accomplishments, and future plans. Chapter 3 summarizes the candidate preconceptual fuel designs that were selected for initial neutronics analysis using the new suite of computational tools, with translational support using the legacy tools, during Fiscal Year 2012. In Chapter 4 some observations, conclusions and a discussion of work planned for the upcoming fiscal year are provided. Finally, three Appendices provide detailed computational results produced during FY-2012 for all of the current candidate fuel element preconceptual designs.

2.0 ATR CORE MODELING UPDATE PROJECT – NEW COMPUTATIONAL CAPABILITIES AND RECENT ACCOMPLISHMENTS

Prior to the initiation of the Core Modeling Update Project in late 2009, the INL was already making a few efforts to modernize ATR reactor physics analysis capabilities using current standard software. Those efforts have produced some important progress, especially for experiment design and analysis as noted earlier. However, this was largely on an *ad-hoc* basis, and several key tasks remained. Those tasks included:

- Implementation of complementary, self-consistent multidimensional stochastic and deterministic neutron transport models of the ATR and ATRC cores using well-established and recognized science-based software packages consistent with current practice

- Standardized computational procedures and training, more easily transferred to new staff members

- Additional Verification &Validation, with development of standard apparatus and protocols for detailed neutron flux distribution and spectrum validation measurements in the core and selected flux traps that can be adapted as needed for changing experimental conditions and repeated on a regular basis. This also offers an opportunity to make much more effective use of ATRC both within the INL and as a key component of the National Scientific User Facility

2.1 Computational System Overview

Figure 2.1 shows the suite of new tools that are now becoming available and how they generally relate to one another. This illustration is not a computational flow chart or procedure *per se*. Specific computational protocols using the tools shown in Figure 1.6 for routine ATR support applications will be specified in approved procedures and other operational documentation. These documents will prescribe the geometric modeling input files, nuclear data files, and other aspects of each specific computational protocol. For example there will be a procedure for performance of core-follow calculations and computation of CSAP physics support data for a particular ATR operational cycle using the new tools.

The most recent release of the Evaluated Nuclear Data Files (ENDF/B Version 7.1 in 2012) is be used to provide the basic cross section data and other nuclear parameters required for all of the modeling codes. The ENDF nuclear data files are processed into computationally-useful formats using the standard

publically-available NJOY or AMPX (Radiation Safety Information Computational Center, 2010) codes as applicable to a particular module as shown at the top of the Figure.

As noted earlier, the MCNP5 three-dimensional stochastic simulation code is already used extensively for ATR experiment design and analysis and, to some limited extent, core analysis. Under the Core Modeling Update Project, we are also introducing the KENO stochastic simulation code (Hollenbach et al., 1996). The KENO code is useful both as a stand-alone analysis and verification tool as well as in conjunction with the TSUNAMI (Broadhead et al., 2004, Williams and Rearden, 2008) sensitivity-uncertainty analysis system available with the SCALE nuclear system analysis package (Bowman et al., 2009). Furthermore, during Fiscal year 2012, we investigated the possibility of incorporating the extremely sophisticated MC21 (Sutton et al., 2007) and SERPENT (Leppänen, 2012) stochastic simulation and depletion codes into the new suite, acquisition of both codes was initiated, and some initial demonstrations of applications of the SERPENT code to ATRC validation experiments were completed.

The right-hand side of Figure 2.1 shows the new high-fidelity deterministic transport computational tools that are being integrated into the system. HELIOS (Studsvik Scandpower, 2008) and ATTILA (McGhee et al., 2006) are commercial grade software products now in place at the INL under permanent sitewide licenses. NEWT (DeHart, 2006) together with its SCALE-based support infrastructure is a well-established and verified software tool developed within the DOE National Laboratory system. All three code packages have various strengths and weaknesses, but taken together they will provide the necessary high-fidelity deterministic neutron and gamma transport capability that is required for various aspects of ATR and ATRC core modeling according to modern standards of practice.
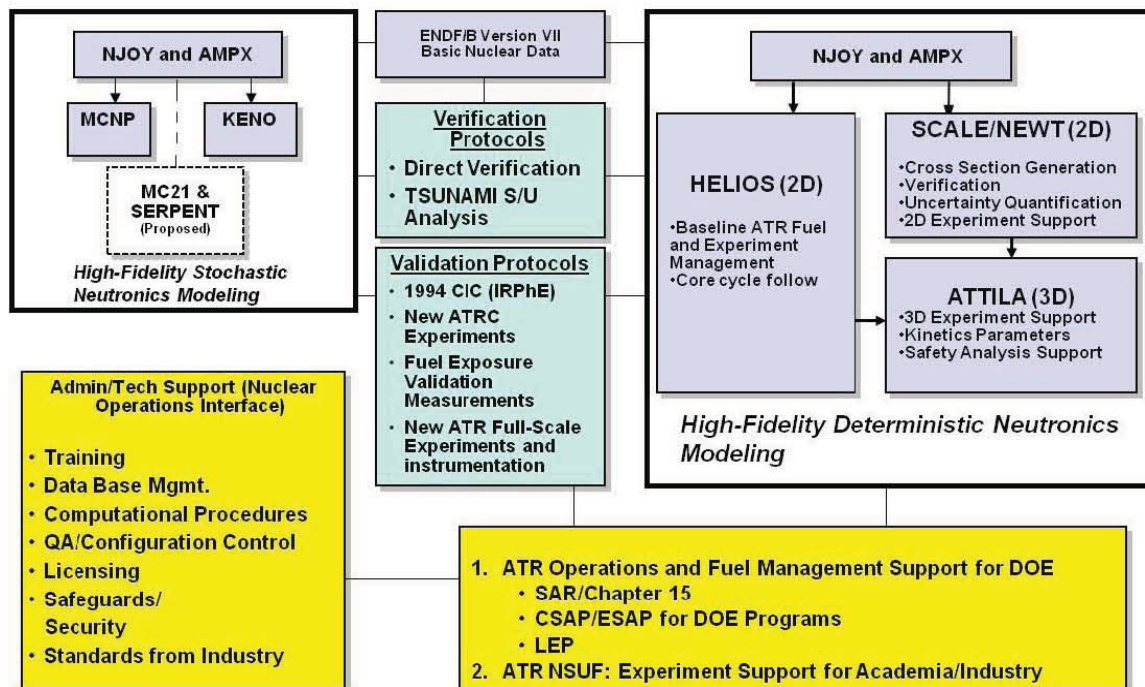

Figure 2.1. Advanced computational tool suite for the ATR and ATRC, with supporting verification, validation and administrative infrastructure.

2.2 Validation Protocols

As always, theory and experiment must be consistent in any scientific or engineering enterprise. The Core Modeling Update Project also includes several activities designed to incorporate historical validation data from earlier ATR and ATRC experiments as well as to develop new validation data specific to the new computational models and protocols. In particular, much of the initial model testing has been based on a very well documented critical experiment conducted as part of the 1994 ATR Core Internals Changeout (CIC) activity (Kim and Schnitzler, 2008). New core flux measurements in both ATRC and ATR are also underway, and the statistical analysis of the first four new ATRC validation experiments per ASTM Standard E944 (ASTM, 2008) was completed in FY-2012. Additional validation effort in FY-2012 was focused on obtaining initial data from a previously unanticipated "depressurized" low-power run (Cycle 152A) of the ATR late in 2012. This activity will continue in 2013 and additional new validation experiments in the ATRC are planned for FY-2013 and FY-2014 as well.

Validation protocols for the various computational ATR physics models are primarily based on neutron activation spectrometry in the near term. Additional validation capabilities using post-irradiation burnup measurements for selected fuel elements are anticipated in the longer term as well. The latter capabilities may be of particular importance with possible future LEU-fueled cores for the ATR, with their inevitable increased plutonium production relative to the current HEU fuel. Some basic equipment for activation experiments in the ATRC Northwest Large In-Pile Tube (NW LIPT), and in the surrounding NW Lobe core fuel elements as well as in the diametrically opposite SE Lobe fuel elements was fabricated during FY-2010, and initial scoping measurements to determine neutron flux spectra in these regions were completed during FY-2011. Corresponding fuel element fission power distribution measurements throughout the ATRC core were also completed using standard ATRC protocols. There have been four LEP-specific ATRC validation experiments in total, and complete statistical analyses for all four have been completed along with some initial analysis of additional measurements made during FY-2012 in the ATRC to support Cycle (152A) as noted earlier (Nigg and Steuhm, 2012).

Over the course of the upgrade project neutron spectrum measurements in the smaller flux traps and additional measurements in the core fuel elements are also planned, and some additional equipment was accordingly fabricated and assembled during FY-2012 to enable activation measurements within the southeast flux trap as well during 2013 and beyond. Ultimately a complete set of experimental apparatus and associated standard validation measurement protocols using neutron activation spectrometry will be available for future code and model validation measurements as needed in both the ATRC and, when feasible, in the ATR itself. The work described here builds on previous related INL experience at the ATR (e.g. Rogers and Anderl, 1995) as well as at other research reactor and accelerator facilities worldwide (e.g. Nigg et al., 2000). It is also intended that detailed Evaluated Benchmarks based on these measurements will ultimately be published for use by the international community under the auspices of the Organization for Economic Cooperation and Development (OECD, 2012). All of this validation protocol development will be directly transferrable to LEU core design model validation as needed.

2.3 Overview of Relevant Core Modeling Update Project Accomplishments

The current phase of the Core Modeling Update Project is expected to require approximately 60 months to complete, and is targeted for full implementation in phase with an anticipated ATR Core Internals Changeout (CIC) in the 2014-2015 time frame. Some key accomplishments in the first 38 months of the effort are briefly summarized below, along with a description of planned next steps in several areas during FY-2013 and beyond.

- HELIOS, NEWT, ATTILA, KENO, and MCNP models of ATR and ATRC are all operational. An initial SERPENT model has also been demonstrated.

- An initial demonstration-level HELIOS model of the ATR with fuel depletion and replacement is operational and "as run" analyses beginning with Cycle 145a (August 2009 startup

and proceeding through Cycle 151B) have been completed, with all experiments explicitly represented in the model database. This will provide the basis for more formal acceptance testing and qualification of the core fuel cycle computational models and protocols in 2013 and 2014, with the goal of enabling a decision to rely exclusively on the new computational methods and fuel cycle models for current ATR operation using HEU fuel by the end of Fiscal Year 2014. The acceptance testing calculations will be continued and refined in 2013 and beyond, with the HELIOS methodology running in parallel with the standard PDQ-based CSAP methodology.

- Initial critical shim rotation for Cycle 152A (Depressurized Physics Testing) was successfully modeled, and informal cycle follow calculations from 152A forward have been initiated.

- Capability for rigorous sensitivity-uncertainty analysis is available

- Validation protocol development and demonstration are underway, with a focus on consistency with ASTM-944, which establishes standard protocols for analysis of activation spectrometry data. Complete results of statistical validation analyses for the first four (of 6) ATRC irradiations were presented at the 2012 American Nuclear Society (ANS) Reactor Physics Topical Meeting and at the 2012 ANS Annual Meeting.

- In-canal feasibility measurements for construction of a permanent fuel burnup validation system were completed and proposal for new system construction has been submitted to DOE-NE.

- Initiated use of additional direct validation data referenced to ATR Cycle 152A ("Depressurized Run") and the corresponding ATRC supporting configurations.

- A new fuel element power fitting algorithm based on least-squares adjustment is also now operational and will be applied to support the depressurized operations of the ATR as well as future measurements in the ATRC.

- The INL team received significant national and international attention via refereed publications topical conferences (ANS, ASTM), culminating in an invited special session at the 2012 ANS Annual meeting and an invitation (accepted) for INL to have a representative on ASTM Standards Committee E10.5 (Nuclear Metrology)

- Acquisition of MC21 and SERPENT 3D stochastic simulation codes from DOE-NR and VTT-Finland was initiated and SERPENT is now operational at the INL as noted earlier, with MC21 soon to follow. These codes offer significant additional validation capability now, as well as a potential longer-term route to full 3D Monte Carlo CSAP analysis at an appropriate time in the future.

3.0 CURRENT STATUS OF CANDIDATE PRECONCEPTUAL LEU FUEL ELEMENT CONFIGURATIONS FOR THE ATR

Figure 3.1 shows a transverse cross section of a standard ATR fuel element. There are 19 fuel plates, with an aluminum-uranium dispersion fuel region (red areas) sandwiched within an aluminum fuel plate structure as shown. The fuel plates are structurally supported by aluminum side plates and a central aluminum rib. The black dots in various azimuthal positions between the fuel plates are standard locations for placement of uranium-aluminum flux wires for measurement of fission power distributions within the element and gold-copper flux wires for basic neutron spectral measurements. Use of the U/Al fission wires for power measurements has been a longstanding practice at the ATR. Use of the Au/Cu wires for spectral measurements was introduced in 2010 as part of the ATR Modeling Update Project, as an additional validation technique.

Plate 19
Plate 18
Plate 17
Plate 16
Plate 15
Plate 14
Plate 13
Plate 12
Plate 11
Plate 10
Plate 9
Plate 8
Plate 7
Plate 6
Plate 5
Plate 4
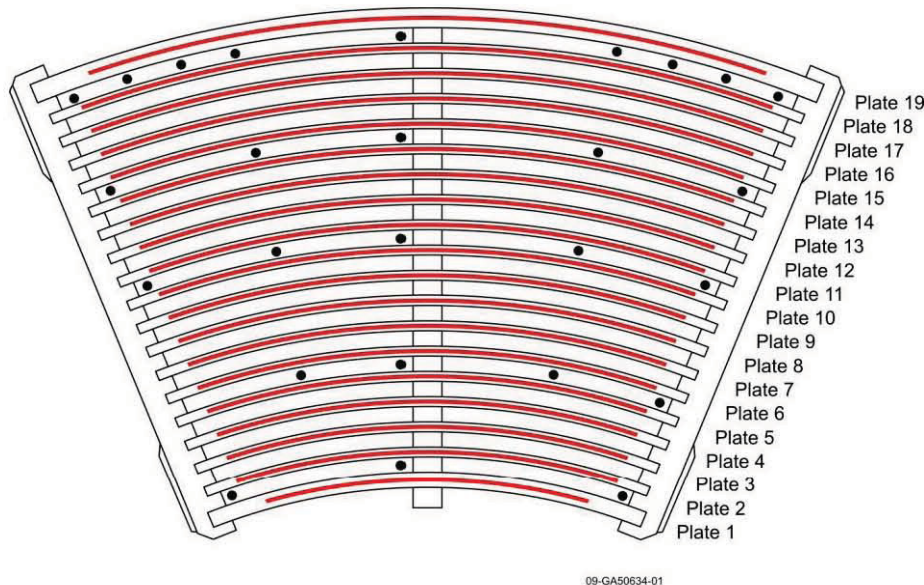Plate 3
Plate 2
Plate 1

09-GA50634-01

Figure 3.1. Transverse section through the axial midplane of a standard ATR fuel element.

A basic working assumption of the LEU conversion effort to this point has been that the external dimensions and overall fuel plate thicknesses and spacing of plates for LEU fuel elements will ideally be the same as those of the current HEU elements. This preserves the current beryllium reflector geometry as well as the basic thermal-hydraulic behavior of the core for a given heat flux distribution on the surface of each plate within an element. The various candidate fuel element preconceptual designs examined in FY-2012 maintain this assumption, and only the internal fuel region and support plate compositions and geometric details are modified in various ways summarized in the following paragraphs, and described in much more detail in Appendices A-C.

The primary considerations for ATR fuel element design include maintenance of sufficient excess reactivity throughout the fuel cycle, while simultaneously maintaining sufficient control and shutdown margins. In addition the transient behavior and thermal margins must remain within acceptable ranges for all normal and postulated off-normal operating conditions. External dimensions must also be unchanged if the element is to be geometrically compatible with the current reflector and fuel support structures. The current primary candidate for the active LEU fuel ("fuel meat") region of each fuel plate is an alloy composed of uranium metal enriched to no more than 20% ^{235}U and natural molybdenum ("U-Mo"). Six initial fuel element concepts based on these considerations were selected for scoping neutronics analyses during FY-2102:

- Integral Cladding, Burnable Absorber (ICBA): A distinct B4C foil is located outside the U-Mo fuel meat on each side to provide a burnable poison. This yields a 7-layer sandwich structure including a zirconium barrier layer under the cladding.

- Hafnium-Poisoned Zirconium (HPZ): The zirconium barrier layers in each fuel plate are composed of zirconium that contains 1%-2% hafnium, which is a common impurity in zirconium that normally is removed for reactor applications.

- Reduced Enrichment (RE): The enrichment of the fuel is reduced significantly below the 20% allowable maximum, to achieve the same initial excess core reactivity as the HPZ design.

9

- Enhanced LEU Fuel (ELF): Fuel element features variable fuel meat thicknesses from plate to plate for power peaking and reactivity control.

- Integral Side-plate Burnable Absorber - Boron (ISBA-B): Boron is homogeneously alloyed into the side plates and possibly the central rib of each fuel element to provide a burnable poison.

- Integral Side-plate Burnable Absorber – Cadmium (ISBA-Cd): Cadmium wires are placed in the side plates of each fuel element to provide a burnable poison.

Extensive details of the scoping analyses for these concepts are provided in Appendix A (ICBA), Appendix B (HPZ, RE, and ELF), and Appendix C (ISBA-B and ISBA-Cd). Based on the results of these analyses the HPZ and RE designs were eliminated from further consideration. The ICBA design was shown to be neutronically attractive, but fuel fabrication and mechanical performance concerns have made this option a low-priority candidate for the moment. Thus the ELF and the two ISBA designs are the current priority options for further consideration.

4.0 FUTURE DIRECTIONS

As summarized above, six initial preconceptual LEU fuel element designs were identified and analyses to determine their basic neutronics performance characteristics in the current ATR geometric core configuration were conducted during FY-2012. These analyses were based on a simple enveloping 3-cycle fuel management scheme without replacement. In FY-2013, much more detailed physics, thermal-fluids, and structural analysis will be conducted for these and possibly one or two additional concepts with the objective of downselecting one or perhaps two concepts that are the most attractive from all relevant aspects by the end of the fiscal year.

A second, related, activity will involve initiation of studies needed for updates to the ATR Safety Analysis Report to accommodate the use of LEU fuel. This will require various supporting reactor physics analyses to provide the necessary parameters for the development of a suitable RELAP-5 model. Such parameters will include the neutron generation time, the effective delayed neutron fraction (which will change significantly during the fuel cycle in the case of LEU), power distribution and reactivity feedback weighting functions, etc.

Finally, the LEU conversion effort will continue to be carefully coordinated with the ATR Modeling Update project in areas of shared benefit. One such area will be the ongoing code validation campaign, which is currently focused on development of qualified validation data in connection with the ATR Cycle 152A core physics characterization effort and the supporting ATRC measurements.

5.0 REFERENCES

ASTM (American Society for Testing and Materials), "Standard Guide for Application of Neutron Spectrum Adjustment methods in Reactor Surveillance", ASTM-E944-08 (2008)

Bowman, S. M. (Ed.), *SCALE: A Modular Code System for Performing Standardized Computer Analyses for Licensing Evaluation*, ORNL/TM-2005/39, Version 6, Vols. I–III, Oak Ridge National Laboratory, Oak Ridge, Tennessee, January 2009. Available from Radiation Safety Information Computational Center at Oak Ridge National Laboratory as CCC-750.

Broadhead, B. L., Rearden, B. T., Hopper, C. M., Wagschal, J. J. and Parks, C. V., "Sensitivity- and Uncertainty-Based Criticality Safety Validation Techniques," *Nucl. Sci. Eng.* **146**, 340–366 (2004).

DeHart, M. D., Advancements in Generalized-Geometry Discrete Ordinates Transport for Lattice Physics Calculations, A154.pdf in Proc. of PHYSOR–2006, American Nuclear Society Topical Meeting on Reactor Physics: Advances in Nuclear Analysis and Simulation, September 10–14, 2006, Vancouver, British Columbia, Canada.

Hollenbach, D.F., Petrie, L.M., Landers, N.F., KENO-VI: A General Quadratic Version of the KENO Program, ORNL/TM-13011, Lockheed Martin Energy Research Corp., Oak Ridge National Laboratory, 1996.

Kim, S. S. and Schnitzler, B. G., Advanced Test Reactor: Serpentine Arrangement of Highly Enriched Water-Moderated Uranium-Aluminide Fuel Plates Reflected by Beryllium" HEU-SOLTHERM-022, *International Handbook of Evaluated Criticality Safety Benchmark Experiments*, NEA/NSC/DOC(95)03, OECD-NEA (2008).

Leppänen, J., 2012b. "Serpent Progress Report 2011", VTT Technical Research Centre of Finland (2012), VTT-R-05444-12.

McGhee, J.M., Wareing, T.A., Barnett, D.J., ATTILA Version 5: User Manual, Transpire Inc., Gig Harbour WA, USA (2006).

D.W. Nigg, K. A. Steuhm (Editors), Advanced Test Reactor Core Modeling Update Project Annual Report for Fiscal Year 2012, INL/EXT-11-27059, September 2012.

Pfeifer, C.J., PDQ Reference Manual II, WaPD-TM-947(L), 1971.

Radiation Safety Information Computational Center, NJOY99- Code System for Producing Pointwise and Multigroup Neutron and Photon Cross Sections from ENDF/B Data and AMPX77- Modular Code System for Generating Coupled Multigroup Neutron-Gamma Libraries from ENDF/B, Oak Ridge National Laboratory (http://www-rsicc.ornl.gov), 2010.

Rempe, J.L., Nigg, D.W., Imel, G. R., Unruh, T., FY-10 Irradiation Experiment Plan for the ATR National Scientific User Facility – Idaho State University Project Evaluating Flux Sensors, PLN-3351, Revision 0, Idaho National Laboratory, 2010.

Studsvik Scandpower, HELIOS Methods (Version 1.10), 2008.

Sutton, T.M., et al., The MC21 Monte Carlo Transport Code, Knolls Atomic Power Laboratory and Bettis Laboratory, LM-06K144, 2007.

Williams, M.L., Rearden, B.T., SCALE 6 Sensitivity/Uncertainty Methods and Covariance Data, *Nucl. Data Sheets* **109** (2008), p. 2796.

Appendix A - Evaluation of RERTR LEU Conversion Core Physics Analysis Methods

Mark D. DeHart and William Skerjanc
Reactor Analysis and Design Department

Brian K. Castle
International Safeguards Department

TEM-10200-1
09/30/2011
Rev. 05

**ENGINEERING CALCULATIONS
AND ANALYSIS**

Page 1 of 39

Title: **Evaluation of RERTR LEU Conversion Core Physics Analysis Methods**
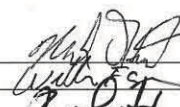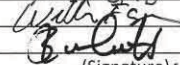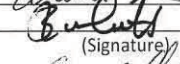
ECAR			Project File			
No.: ECAR-1819	ECAR Rev. No.: 0		No.: 31230		Date: 2/20/2012	

Engineering Calculations and Analysis

ECAR Title: Evaluation of RERTR LEU Conversion Core Physics Analysis Methods

ECAR No.: ECAR-1819
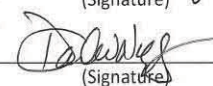
	(Name)	(Organization)	(Signature)	(Date)
Performers:	Mark DeHart	C100		2/20/2012
	William Skerjanc	C100		2/20/2012
	Brian Castle	D200		2/20/2012
	(Name)	(Organization)	(Signature)	(Date)
Checker[1]:	Gray Chang	C100	Gray S Chang	2/21/2012
	(Name)	(Organization)	(Signature)	(Date)
Independent Peer Reviewer[2]:	David W. Nigg	C100		2/21/12
	(Name)	(Organization)	(Signature)	(Date)
CUI Reviewer:	N/A			
	(Name)	(Organization)	(Signature)	(Date)
Principal Investigator[3]:	David W. Nigg	C100		2/21/12
	(Name)	(Organization)	(Signature)	(Date)
Owner[4]:	Sean R. Morrell	D210		2/21/12
	(Name)	(Organization)	(Signature)	(Date)
Nuclear Safety[4]:	N/A			
	(Name)	(Organization)	(Signature)	(Date)
Cognizant Engineer[4]:	N/A			
	(Name)	(Organization)	(Signature)	(Date)
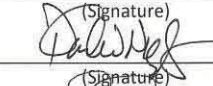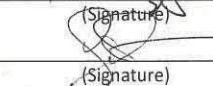
14

1. Introduction

A number of activities related to Low-Enriched Uranium (LEU) fuel design for the Advanced Test Reactor (ATR) are underway at the Idaho National Laboratory (INL) under the auspices of the Reduced Enrichment Research Test and Training Reactor (RERTR) Program. The primary focus to date has been on computational and experimental materials performance studies for uranium-molybdenum composites. A fuel element design based on a U-10Mo composite has been proposed with a 13 mil fuel plate thickness encased in 1 mil zirconium centered in 50 mil Al 6061 plates. This fuel is the basis for the Full Element (FE) fuel assembly test planned for initial neutronics evaluation in the Advanced Test Reactor Critical Facility (ATRC), followed by insertion and irradiation in the ATR.

Experimental work has been supplemented by a number of computational RERTR fuel studies to determine potential performance of different fuel designs covering a broad range of fuel characteristics. Computational neutronics studies to support the possible conversion of the ATR to LEU are also underway.

Simultaneously, INL is engaged in a physics methods upgrade project to put into place modern computational neutronics tools for future support of ATR fuel cycle and experiment analysis. The computational methods selected include Helios [1], Attila [2], and portions of the SCALE code system [3] for reactor physics calculations. MCNP [4], long used for detailed ATR analysis, will also be employed in ATR analysis for independent confirmation of computational models. A number of experimental measurements have been performed in the ATRC in support of the methods upgrade project, and are being used to validate the new core physics methods.

The current computational neutronics work is focused on performance of scoping calculations for the ATR core loaded with a candidate LEU fuel design, using the tools identified above. In the absence of a final fuel element design, the emphasis has been placed on development of candidate designs informed by ATR operational requirements, and on evaluation of the reactor physics performance of such cores. Ultimately, the goal of this work is to complete a preliminary assessment of the capabilities of new core analysis methods for LEU fuel. Note that a complete assessment will ultimately require measured in-core data with as-designed LEU fuel for code validation. Initially, it is planned to obtain some early neutronics measurements for LEU fuel in the ATR via coordination with the FE experiment mentioned previously.

The following sections describe the initial plan for the supporting neutronics analytical effort, the modeling approach used and the most significant results of work completed to date. This work is far from complete, and several departures have been made from the initial analysis plan described below.

Initial RERTR Core Physics Analysis

In January 2011 the following strategy was proposed for initial scoping RERTR core physics analysis:

- Perform initial calculations using multigroup KENO-VI
  - A validated (94-CIC) KENO-VI model has been developed
  - KENO-VI runs much faster than MCNP
  - KENO-VI can be used within TRITON for full core depletion calculations
  - Sensitivity/uncertainty studies can be performed using KENO-VI within TSUNAMI

- Starting with the 94-CIC model, replace the highly-enriched uranium (HEU) fuel in the model with an acceptable candidate design for RERTR fuel.

- Note that the full RERTR fuel assembly has not been finalized (specifically, power peaking control for the inner and outer plates) at this time.
- Final reactor physics analysis will hinge on the final engineering design on to model the RERTR fuel performance.
- In lieu of a final design, conceptual fuel designs can be analyzed, assuming the current 13 mil fuel meat. As a starting point, the following three concepts were initially considered:
  1) A model with boron in the 4 inner and 4 outer fuel plates, with a uniform initial loading that will reproduce the critical state of the ATR from the 94-CIC measurement.
  2) Reduced enrichment used in inner and outer fuel to reduce reactivity in place of or in conjunction with B_4C poison.
  3) A model with a thinner fuel meat in the inner and outer 4 plates that to reduce reactivity in place of or in conjunction with B_4C poison.
- The most feasible of these candidates (in a reactor physics sense) should be used in following depletion/decay calculations to quantify transuranic isotope production.

- Given a working fuel assembly design, it will be necessary to determine the likely shim positions for critical. With this design, it may be possible calculate kinetics parameters for this core. However, the approach for determination of kinetics parameters has not yet been determined.

- Analysis of the candidate designs should be performed to determine generate drum worth curves and safety rod worth curves, along with flux tilt calculations (to see if the same tilts can be achieved), thermal penalty estimates, and burnup calculations. Burnup calculations will be important for determination of fuel life, and for determination of Pu contents and source term inventories. It may be necessary to use NEWT for burnup calculations so that a critical buckling correction may be applied during depletion. This capability is not available in available Monte Carlo depletion packages.

- Ultimately control element worth calculations and thermal penalties should be evaluated as a function of burnup.

The preliminary studies considered a number of candidate fuel designs, which demonstrated essentially that a uniform fuel loading in all 19 fuel plates of an element is not feasible. The amount of poison required to reduce innermost and outermost plate powers to an acceptable level would result in an excessive net reactivity penalty and possible fabrication issues. Hence, a reduced fuel loading would be required in innermost and outmost fuel plates, either by thinner fuel regions or by reduced enrichment.

A draft report was prepared describing these analyses and comparison to an existing LEU design report [5]. The draft report was never finalized and because of a departure from the parameters assumed in these analyses relative to subsequent analysis.This report has been substantially revised here to represent the more recent work. For completeness, however, the results of the earlier studies are included herein (see Appendix A).

In the current study, the current HEU ATR core design is compared to a single proposed LEU design to assess relative performance of the two designs. The HEU core is based on the 94-CIC configuration as documented in Ref. 6. Chang refers to the LEU fuel type of interest to this study as Integral Cladding Burnable Absorber (ICBA); this nomenclature is used in this report to identify the LEU fuel design. Calculations with the ICBA fuel design used the same core model, but fuel elements were replaced by a fuel concept that has been designed and analyzed by G. Chang in (currently) unpublished work; the draft of Chang's report that was used as a basis for the LEU fuel studied in this report is included as Appendix

B. Note that the terms "ICBA" and "LEU" are used interchangeably in this report; in description of specific models both terms represent the Chang fuel design.

One change was made to the dimensions of the fuel plates listed in Table 2 of Appendix B. Subsequent to that report, a minor change was made to fuel thickness dimensions to allow a better match in power profiles shapes between LEU and HEU fuels. Specifically, the fuel meat thickness of in plates 4 and 16

Table 1. Integrated Thermal Fluxes and Spectral Shift for ICBA LEU Configuration

Fuel Plate No.	Fuel Thickness, cm (mils)	Boron Thickness, cm (mils)
1	0.02032 (8)	0.0127 (5)
2	0.02032 (8)	0.0127 (5)
3	0.0254 (10)	
4	0.0254 (10)	
5	0.03302 (13)	
6	0.03302 (13)	
7	0.03302 (13)	
8	0.03302 (13)	
9	0.03302 (13)	
10	0.03302 (13)	
11	0.03302 (13)	
12	0.03302 (13)	
13	0.03302 (13)	
14	0.03302 (13)	
15	0.03302 (13)	
16	0.0254 (10)	
17	0.0254 (10)	
18	0.02032 (8)	0.0127 (5)
19	0.02032 (8)	0.0127 (5)

were reduced from 12 mils (0.03048 cm) to 10 mils (0.0254 cm). For completeness, fuel plate thicknesses are provided in Table 1.

Modeling Approach

In the majority of this work, components of the SCALE 6.0 package [3] were used for cross section processing, criticality and depletion calculations. Specifically, the following functional and control modules were applied in these analyses:

Functional Modules:

BONAMI - used to perform Bondarenko calculations for resonance self-shielding in unresolved resonance energy regions. Cross sections and Bondarenko factor data are input from an AMPX master library.

CENTRM - computes continuous-energy neutron spectra in zero- or one-dimensional systems, by solving the Boltzmann transport equation using a combination of pointwise and multigroup nuclear data. It is used mainly to calculate problem-specific fluxes on a fine energy mesh (10,000–70,000 points), which may be used to generate self-shielded multigroup cross sections for subsequentcriticality or shielding analysis.

PMC - generates problem-dependent multigroup cross sections from an existing AMPX multigroup cross section library, a pointwise nuclear data library, and a pointwise neutron flux file produced by CENTRM. It is used primarily to produce self-shielded multigroup cross-sections over the resolved resonance range of individual nuclides in the system of interest. The self-shielded cross sections are obtained by integrating the pointwise nuclear data using the CENTRM problem-specific, continuous-energy flux as a weight function for each spatial zone in the system.

KENO-VI - KENO-VI is a 3-D generalized geometry Monte Carlo code initially developed for criticality safety analysis. The ability to use holes and arrays in the geometry allows very complex problems to be constructed without having to explicitly specify every region in every location. KENO-VI can be run in both multigroup and continuous-energy modes; however, within TRITON depletion calculation KENO-VI runs only in multigroup mode.

NEWT – a transport computer code with flexible meshing capabilities that allow two-dimensional (2-D) neutron transport calculations using complex geometric models. The differencing scheme employed by NEWT allows a computational mesh based on arbitrary polygons. Such a mesh can be used to closely approximate curved or irregular surfaces to provide the capability to model problems that were formerly difficult or impractical to model directly with discrete-ordinates methods. Automated grid generation capabilities provide a simplified user input specification in which elementary bodies can be defined and placed within a problem domain. NEWT can be used for eigenvalue, critical-buckling correction, and source calculations, and it can be used to prepare collapsed weighted cross sections in AMPX working library format.

ORIGEN – a depletion/decay code that applies a matrix exponential expansion model to calculate time-dependent concentrations, activities, and radiation source terms for a large number of isotopes simultaneously generated or depleted by neutron transmutation, fission, and radioactive decay. Provisions are made to include continuous nuclide feed rates and continuous chemical removal rates that can be described with rate constants for application to reprocessing or other systems that involve nuclide removal or feed.

Control Modules

CSAS6 - The Criticality Safety Analysis Sequence with KENO-VI (CSAS6) was developed within the SCALE code system to provide automated, problem-dependent, cross-section processing followed by calculation of the neutron multiplication factor for the system being modeled using KENO-VI. This control sequence activates the cross-section processing codes BONAMI, to provide resonance corrected cross sections in the unresolved resonance range, and CENTRM and PMC, to provide resonance-corrected cross sections in the resolved resonance range.

TRITON - a multipurpose SCALE control sequence for transport, depletion, and sensitivity and uncertainty analysis. TRITON can be used to provide automated, problem-dependent cross-section processing followed by multigroup transport calculations for one-, two-, and three-dimensional configurations, using XSDRNPM, NEWT and KENO, respectively. Additionally, this functionality can be used in tandem with the ORIGEN depletion module to predict isotopic concentrations, source terms, and decay heat, as well as to generate few-group homogenized cross sections for nodal core calculations.

Both KENO-VI and NEWT models of the 94-CIC configuration were developed at INL in separate work and were validated against the critical benchmark configuration described in Ref. 2. For this configuration, KENO-VI calculates k_{eff} = 1.00572 +/- 0.00084. NEWT is a 2-D model of the core at the axial mid-plane of the fuel region and hence over-predicts the reactivity of the core at 1.0317 with $\varepsilon = 10^{-4}$; however, with axial buckling applied for a 48" core NEWT calculates k_{eff} = 0.991114. Power distributions within a fuel element and for the 40 individual elements have been shown to be in good agreement for KENO-VI, NEWT, MCNP, and HELIOS, and for measured data for the 40 elements. Figure 1 provides a rendered image of the KENO-VI model for the ATR 94-CIC specification.
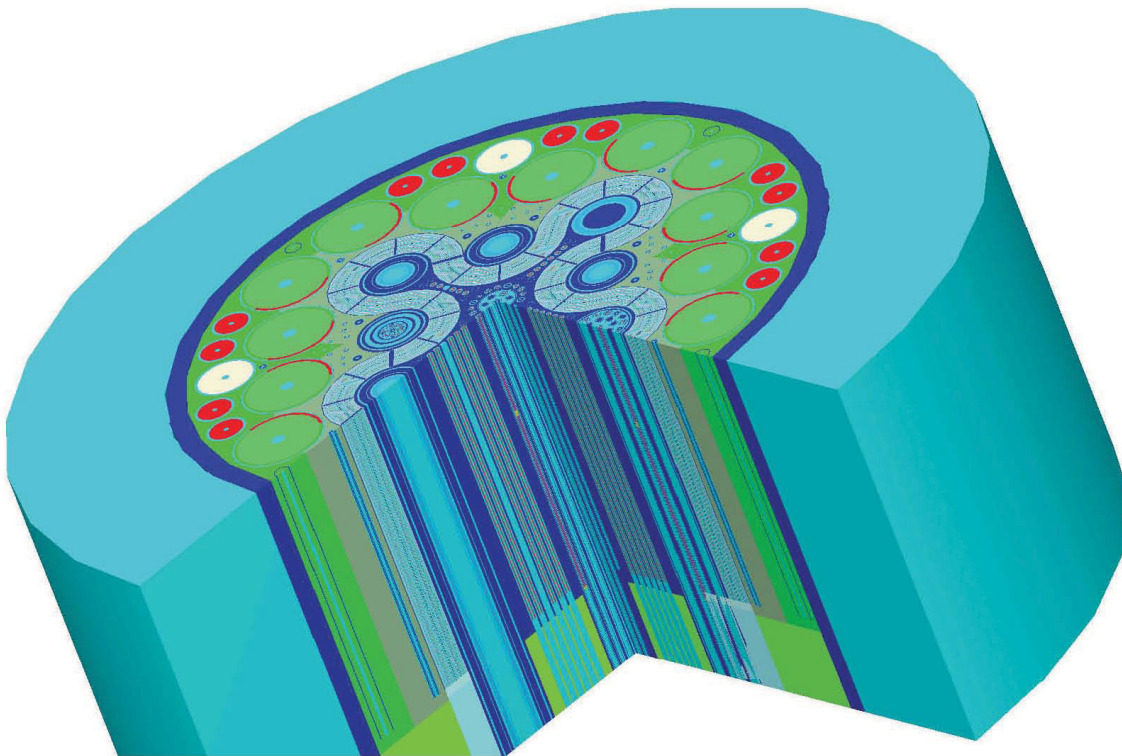
Fig. 1. Cut-away view of lower half of ATR core from KENO-VI model.

For the ICBA fuel design, the fuel element model used within the 94-CIC core design was replaced with a fuel element based on ICBA fuel dimensions. The outer dimensions of all plates within the element were unchanged; only the inner and outer radius of each fuel region was altered, and four burnable poison regions were added. Dimensions and number densities were extracted from the MCNP model used for the analyses documented in Appendix B.

All SCALE calculations were performed using ENDF/B-VII cross sections. Early calculations were performed using the SCALE *v7-238* 238-energy-group library; later work used the ATR spectrum to collapse this library to a 47-energy-group library named *xn49v7_atr*. The 47-group library was useful for deterministic NEWT calculations to accelerate the solution, and was used in depletion calculations.
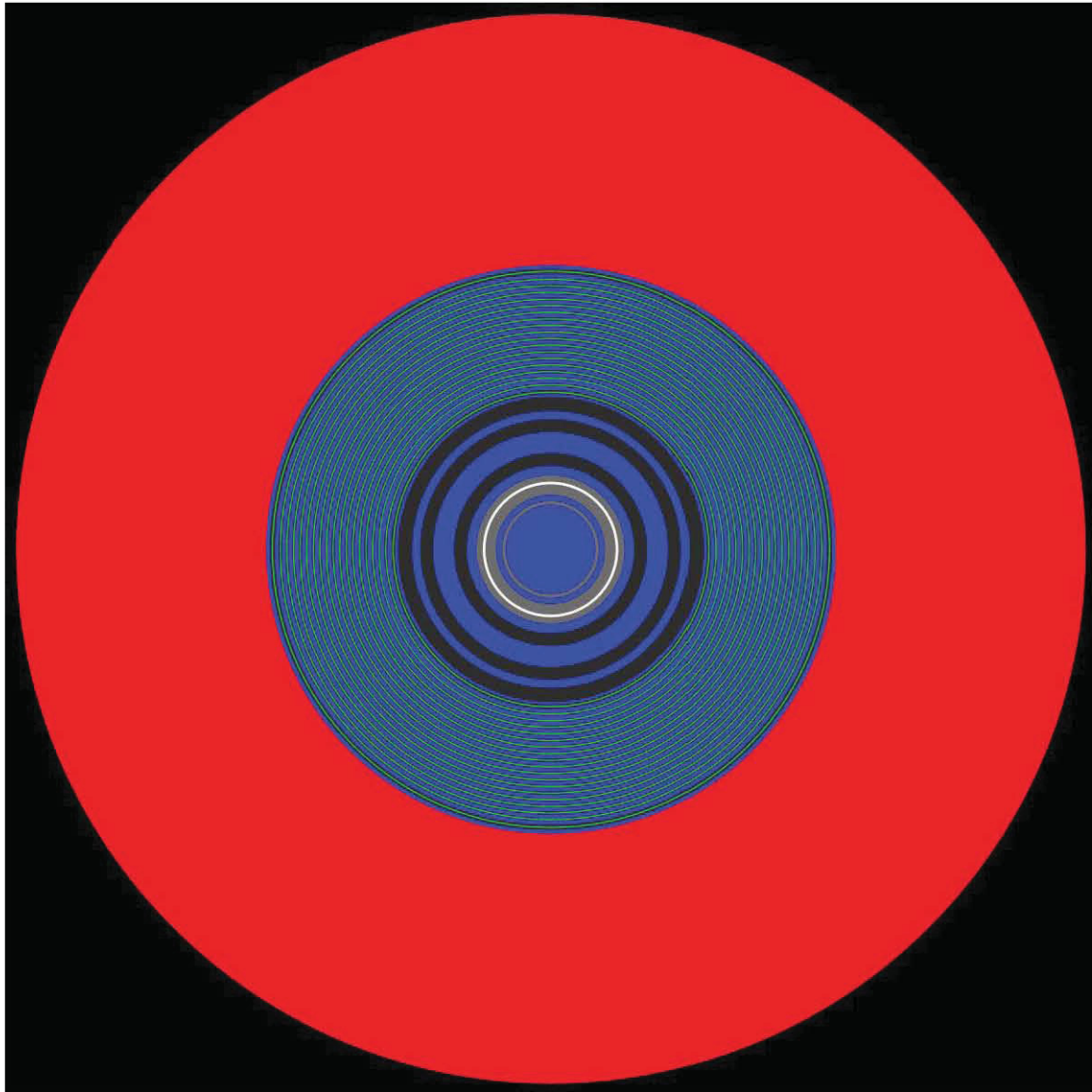
Fig. 2. Two-dimensional representation of CENTRM fuel cell model for HEU fuel.

The *csas6* sequence of the CSAS6 module was used for KENO-VI criticality calculations; the *t-newt* sequence of TRITON was used for corresponding NEWT calculations. For depletion analysis, TRITON's *t-depl* (NEWT) and *t6-depl* (KENO-VI) were used. All sequences used CENTRM and PMC

for cross section processing, based on a 1D representation of a fuel element. To capture the spectral effects of the ATR core within the 1D limitations of CENTRM, fuel element cross sections were computed based on an approximation of the core created by assuming a southeast flux trap configuration, surrounded by a 360° ring of fuel plates, enclosed in a beryllium moderator/reflector region. Compositions of SS-348, Al 6061-T6 alloy, water, fuel, and beryllium were based on 94-CIC isotopic specifications, all at a uniform temperature of 310.9K. Fuel plates 1-4 and 16-19 contained B_4C integral within the fuel meat. Figure 2 illustrates the cell model assumed in HEU CENTRM calculations. Figure 3 shows a close-up of the same cell to illustrate details of the fuel plates. Differences between the current HEU fuel and the proposed LEU ICBA design are clear; The most notable features of the ICBA design are the introduction of a distinct burnable poison region and significantly reduced fuel thickness in plates 1,2, 18 and 19. Plates 3, 4, 16, and 17 do not contain burnable poison, and although slightly thinner than remaining fuel regions are not noticeably so in the figure.
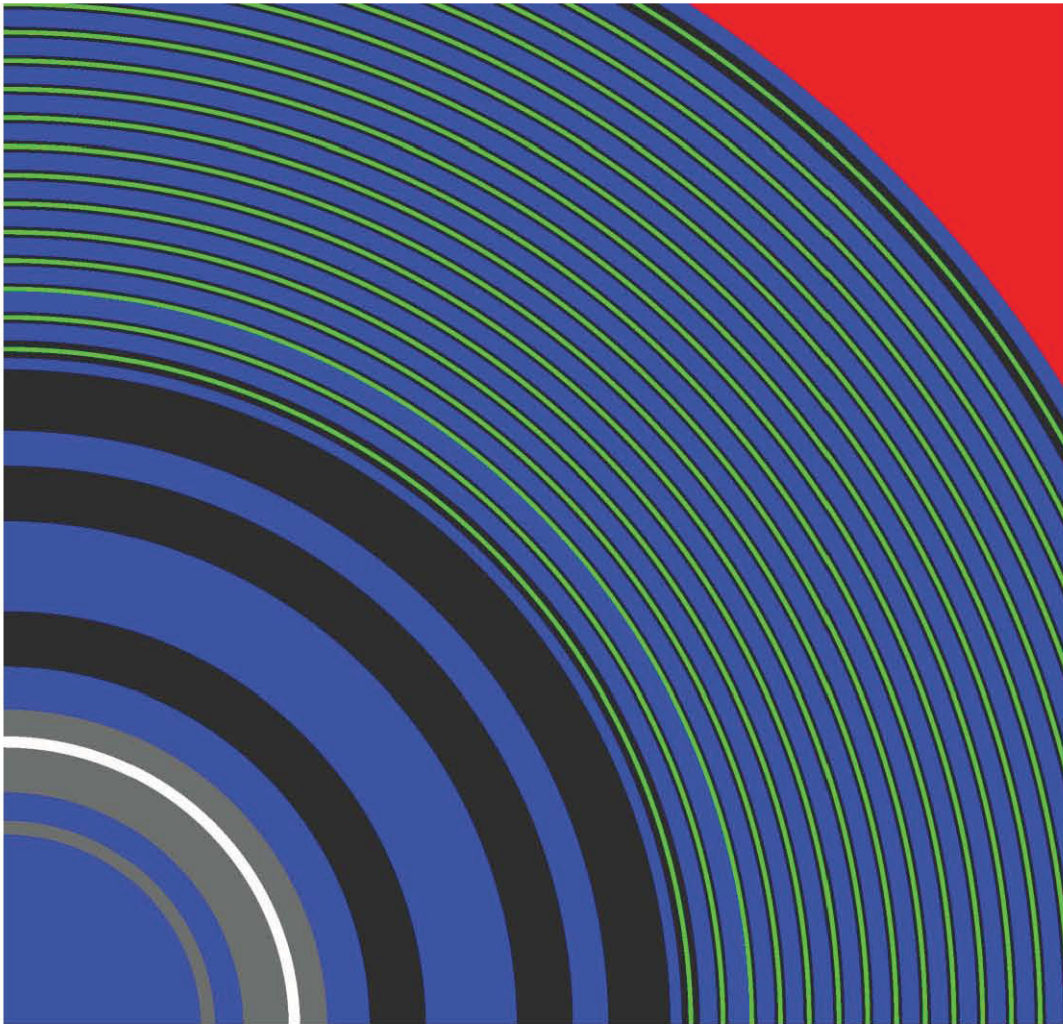
Fig. 3. Close-up of fuel cell model for HEU fuel.
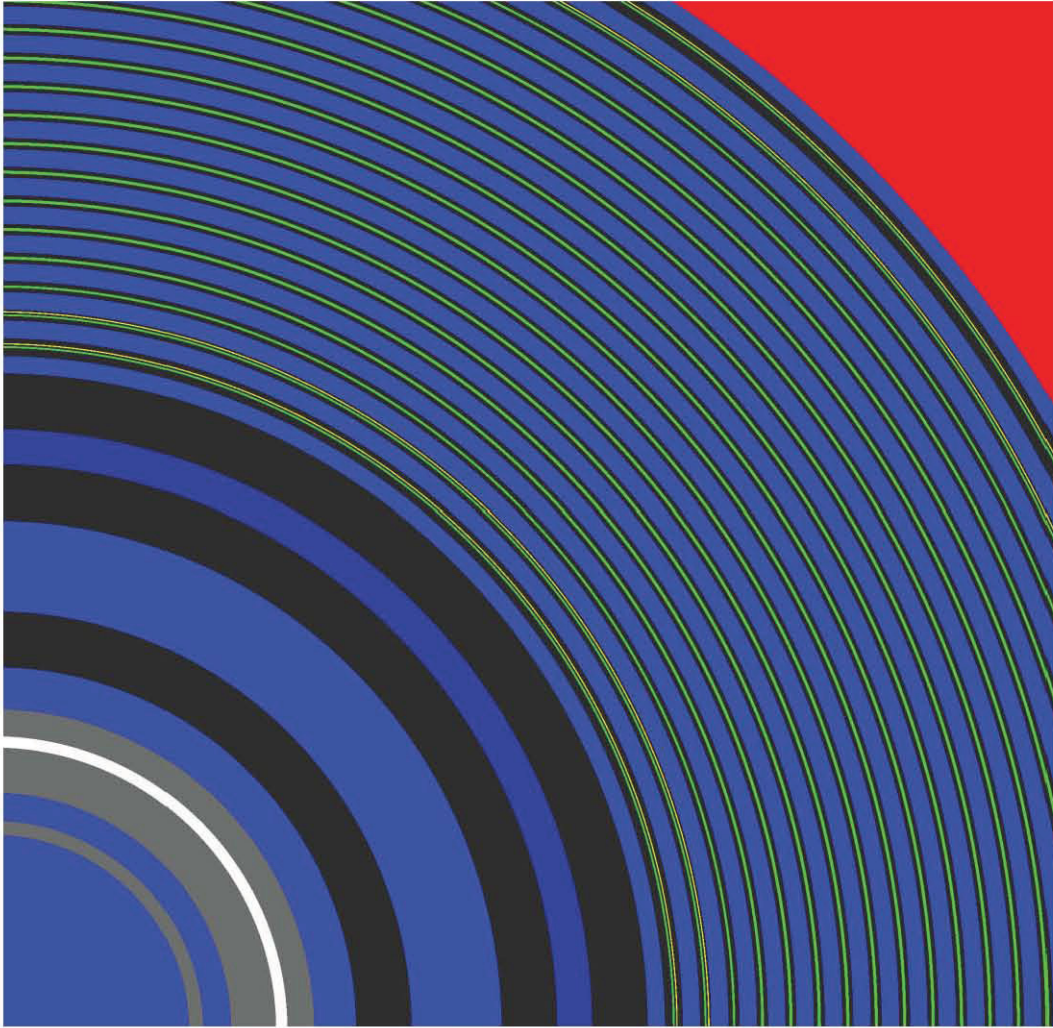
Fig. 4. Close-up of fuel cell model for ICBA fuel.

Comparison of Fuel Element Design Performance

Given working KENO-VI models for the existing HEU core and for a modified core based on the ICBA fuel design, calculations were performed to determine similarities and differences in core behavior. The following subsections discuss each of the various studies.

Initial Eigenvalue

Based on a critical configuration, the HEU model results in a k_{eff} value of 1.00393 +/- 0.00041 with the SCALE v7-238 library. There is an additional 0.5% uncertainty in the eigenvalue due to fundamental nuclear data uncertainties, so this eigenvalue is in excellent statistical agreement with the measurement. To obtain a critical configuration, this model had two neck shims represented as fully withdrawn with remaining shims fully inserted. In addition, OSCC drums were uniformly rotated to 51.8°. For the ICBA fuel loaded into this core model, KENO-VI calculated k_{eff} = 0.97250 +/- 0.00042. (not including the anticipated additional 0.5% uncertainty due to nuclear data) Thus, the ICBA design as currently specified is slightly less reactive than the HEU fuel element, $-\rho$=3.13%. This is in the same range as a reactivity of -3.63% calculated by Chang for beginning of life fuels with 105° OSCC rotation.
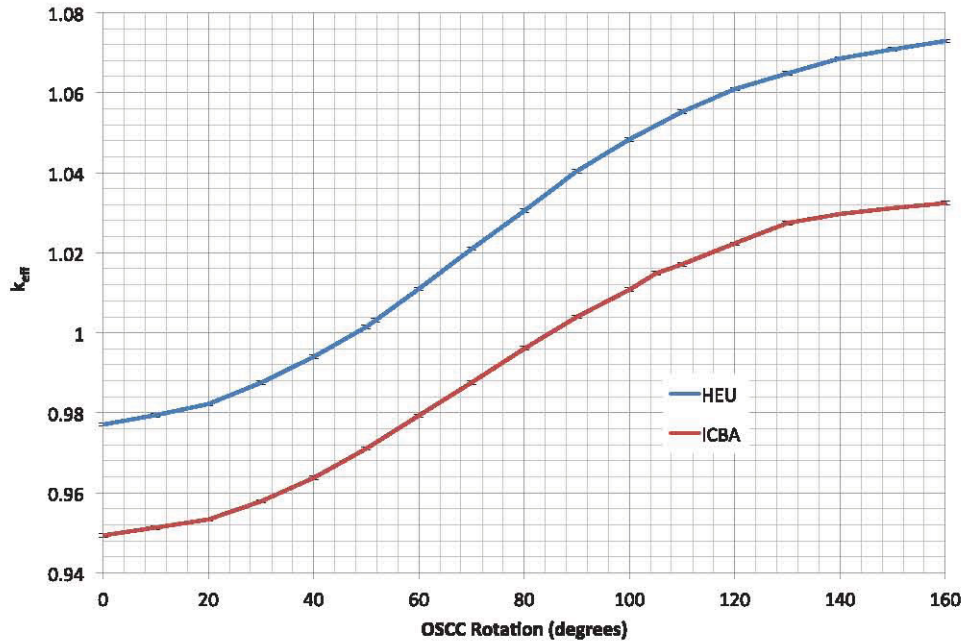
**Fig. 5. Neutron multiplication factor as a function
of OSCC rotation for two fuel types.**

OSCC Worth

The next set of calculations were performed to determine the worth of the OSCCs as a function of drum rotation. Eigenvalue calculations were performed beginning with a drum rotation of 0°, repeated in 10° increments to 160°. Figure 5 illustrates the calculated k_{eff} values as a function of drum rotation; the curve generated for the ICBA fuel appears to be slightly flattened relative to the HEU fuel curve. To better compare the results, the two curves were normalized as $\Delta k = k_{eff}(\Omega) - k_{eff}(\Omega=0)$, where Ω is the drum rotation angle, and plotted in Fig. 6. This plot shows that the total drum worth is reduced to about 85% of its HEU reactivity for the LEU ICBA design. This behavior is not unexpected; increased resonance absorption (resulting from the substantially increased [238]U inventory in the LEU fuel) hardens the spectrum generated within the fuel by reducing the thermal neutron flux at constant fission power. With fewer thermal neutrons, the amount of thermal capture in hafnium will also be reduced. In fact, this behavior is most likely only loosely coupled to the fuel design itself, as the spectrum for any candidate design will be largely influenced by the [238]U fraction, which will remain near 80% of total U inventory for any LEU design.
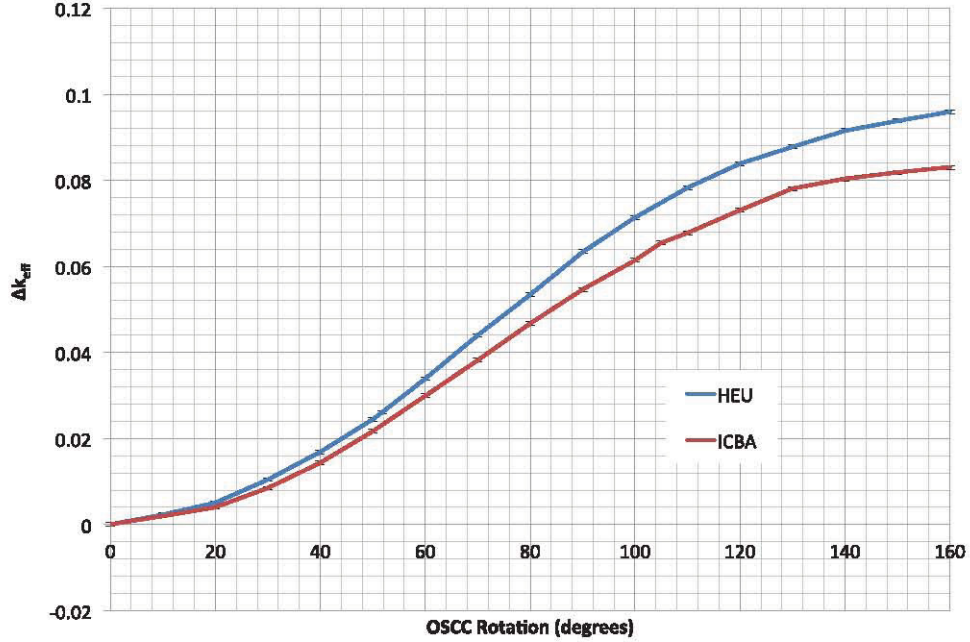
Fig. 6. Δk_{eff} as a function of OSCC rotation for two fuel types.

It was asserted above that there is spectral hardening in the fuel; this is best demonstrated by examination of fuel fluxes. Figure 7 is a plot of the neutron flux within plate 10 (the radially central plate) from element 1. Relative to the spectrum in the HEU fuel, there is a clear reduction of the neutron population in the ICBA design beginning around 1keV and moving down into the thermal energy range; there is also somewhat more resonance structure apparent in the resonance energy range between roughly 500eV to 1 eV.

Because the control drums are in close proximity to the fuel with little hydrogen moderation, the reduced thermal flux is still important at the drum locations. However, as will be shown later, flux trap positions are not as strongly influenced by the spectral hardening, as water in the vicinity of the targets serves to restore much of the thermal neutron flux.
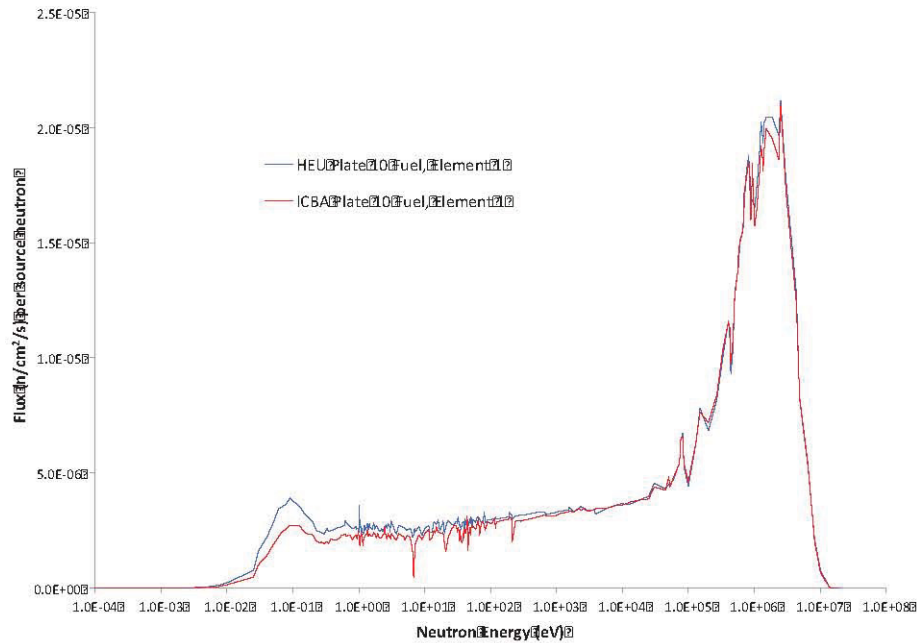
**Fig. 7. Neutron flux spectrum within plate 10 of element 1
from HEU and ICBA core models.**

Power Distributions

Using the initial model with a 51.8° OSCC rotation, calculations were performed to estimate element and plate powers for the 40 fuel elements. Calculations were initially performed with KENO-VI, but a bug was uncovered in KENO-VI resulting from the use of quadratic elements to define fuel plate boundaries in the ICBA fuel model. This bug would be uncovered when running a large number of histories to obtain converged spatial fluxes and would cause the code to halt. An alternate modeling approach was used to represent the ICBA fuel such that the model could be run. However, concern introduced in the use of KENO-VI and the modified model led to the preparation of a 2-D NEWT model of the 94-CIC core with both fuel types to provide an independent check on KENO results.

First, plate power distributions were averaged over all 40 fuel elements for each plate position. Total power was calculated for each plate position, and normalized to an average power of 1.0. Figure 8 shows the power distribution in the two fuel element designs as calculated by KENO-VI. Figure 9 illustrates the corresponding calculation in the NEWT calculation. With the exception of very small power differences in plates 1 and plate 18, the results are essentially identical. These results demonstrate that Chang's proposed fuel design very closely approximates the power distribution for the current HEU fuel – this feature is key to being able to use an approach similar to the current approach for core safety analysis.
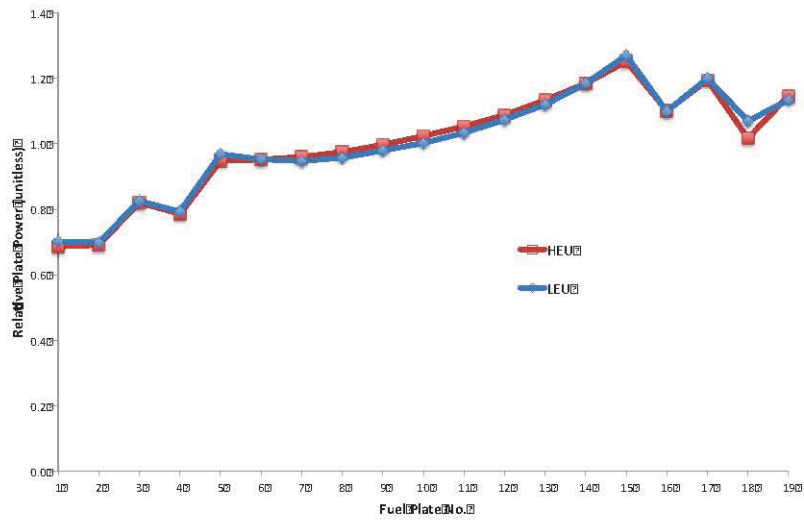
Fig. 8. KENO-VI prediction of average plate powers for two fuel types in 94-CIC core.
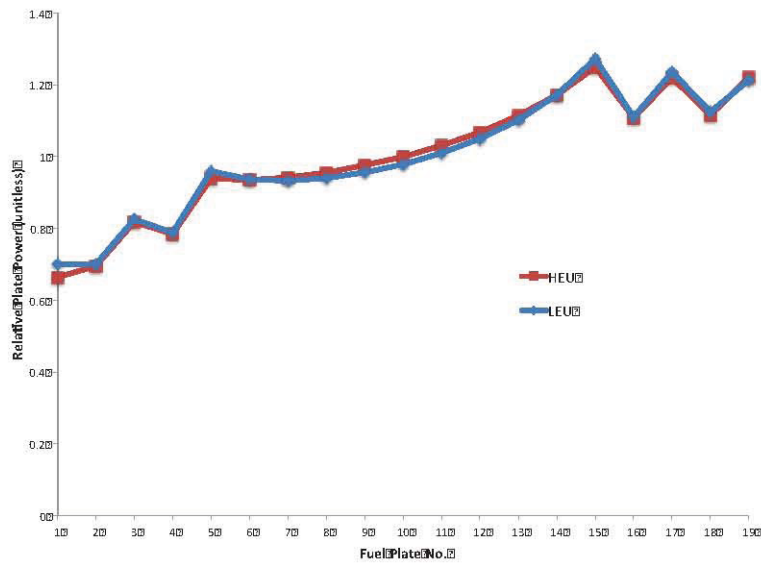
Fig. 9. NEWT prediction of average plate powers for two fuel types in 94-CIC core.

Next, the results of the same calculations were used to generate integral estimates of the average power in each fuel element position. Average element powers were calculated by summing the plate powers in each element. Element powers were then normalized such that the average over all elements was 1.0. Figure 10 plots the power in each of the 40 element positions as calculated using KENO-VI, with standard ATR element numbering. Figure 11 illustrates the same power distribution as calculated by NEWT. Figure 12 shows the ATR configuration, and illustrates the location of each element by number. From Figs. 10-12 it can be seen that the peaks in the power distribution occur in assemblies located toward the interior of the core near the center lobe; the minima occur at the outer lobe exteriors nearest the control drums.
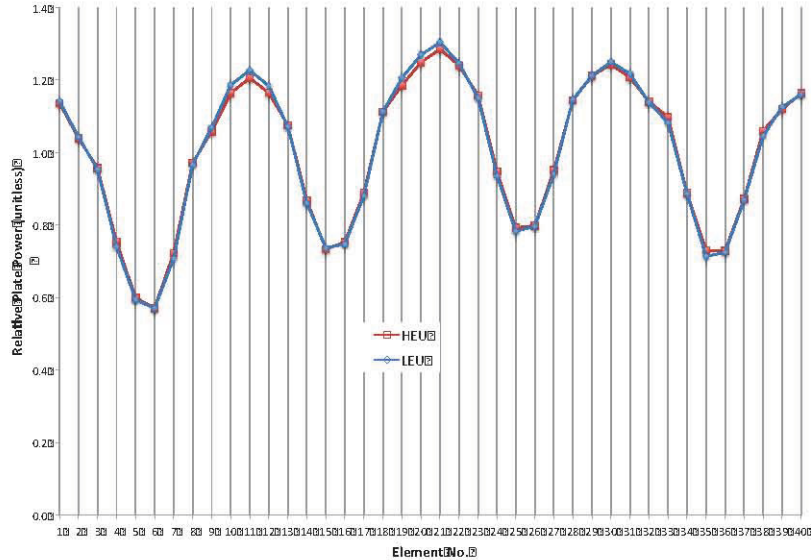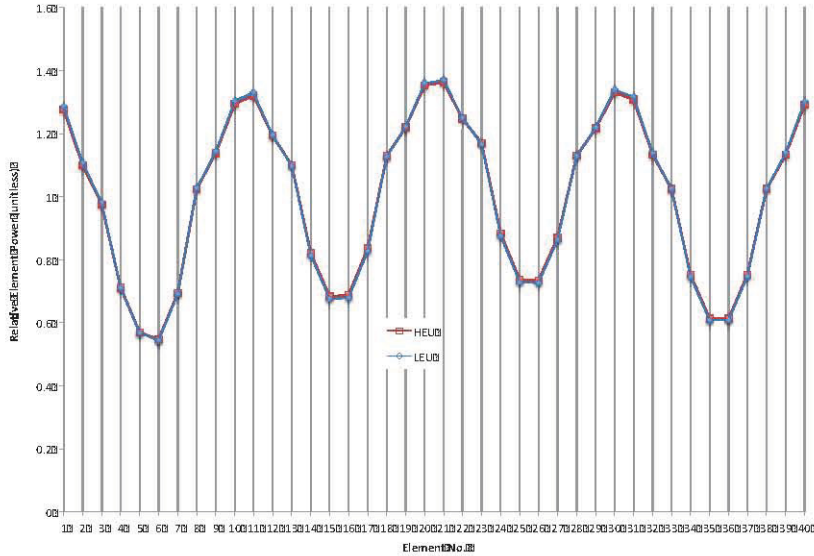
Fig. 10. KENO-VI prediction of average element powers for two fuel types in 94-CIC core.

Fig. 11. NEWT prediction of average element powers for two fuel types in 94-CIC core.

Both sets of results show that the HEU and ICBA designs result in very similar power profiles. NEWT results show an almost identical profile; KENO shows very similar profiles, but with slightly higher powers in the highest power element locations (center lobe elements) for the LEU fuel. Profiles in outer lobe positions (the four dips in the figures) are nearly identical for both codes; there is a slight difference

27

in the shape of the four peaks. The reason for this is not clear; it may result from 3-D versus 2-D modeling. Further investigation is not warranted at this time, but this could be easily studied using a 2-D-like KENO-VI model.

Flux Ratios

The key concern in transition to a low-enrichment fuel is the impact that this change will have on the neutron flux in target positions. Since the primary purpose of the ATR is to provide neutrons in irradiation positions to assess material behaviors, it is desirable to minimize changes in the neutron spectrum in target locations. Unfortunately, the large amout of ^{238}U in low-enrichment fuels (~80% by weight) will unavoidably alter the spectrum within the reactor for any critical configuration. In the resonance energy range, the fission cross section of ^{238}U is very small (about 5 orders of magnitude less than that of ^{235}U), but the absorption cross section of ^{238}U is about an order of magnitude larger than the fission cross section of ^{235}U. Thus, during the thermalization of neutrons, low-enrichment fuels will have a smaller resonance escape probability, and a reduced thermal population within the fuel regions at constant fission power. However, neutrons can continue to lose energy as they migrate away from the fuel into the target areas, so that the impact of the fuel change can be diluted. Nevertheless, as illustrated in Fig. 6, the reduced thermal neutron population does have an impact on hafnium absorption.

To study the potential effect of the ICBA fuel design on target fluxes, two positions were analyzed. In the 94-CIC configuration, the experiment position in the NW flux trap was a solid aluminum dummy (~9cm OD), and would represent perhaps the hardest spectrum of all targets due to the lack of moderating material. The SW flux trap had a ~4.4cm central water hole, representing a much more thermalized spectrum. Figure 13 shows fluxes calculated by KENO-VI for models with HEU and ICBA (LEU) fuel loadings, integrated over the full volume of the aluminum insert and normalized to the same total
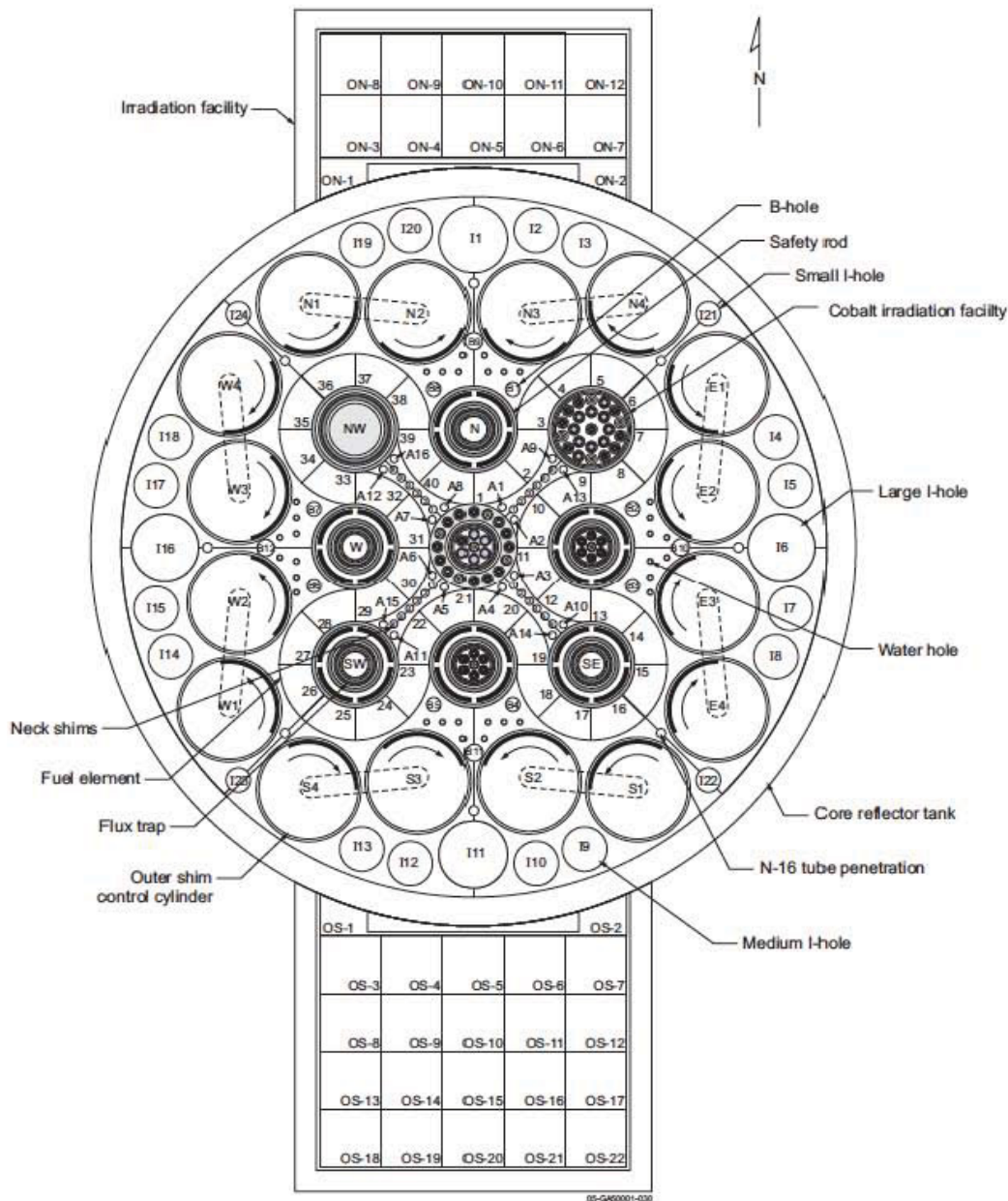
Fig. 12. ATR core configuration showing fuel element locations by number (Ref. 6)

flux
integrated over energy. This plot shows a slight reduction in the thermal flux peak for the LEU-fueled core. Figure 14 shows the same data within just the thermal energy
range, and includes error bars representing one standard deviation in estimated fluxes. Clearly, the difference between the two flux profiles is outside the range of statistical error. Similarly, Figs. 15 and 16 show the full spectrum and thermal fluxes, respectively, for the water region in the SE flux trap. In this case, the reduction is thermal flux is much smaller and within or close to the uncertainty range of the fluxes for this calculation.

29
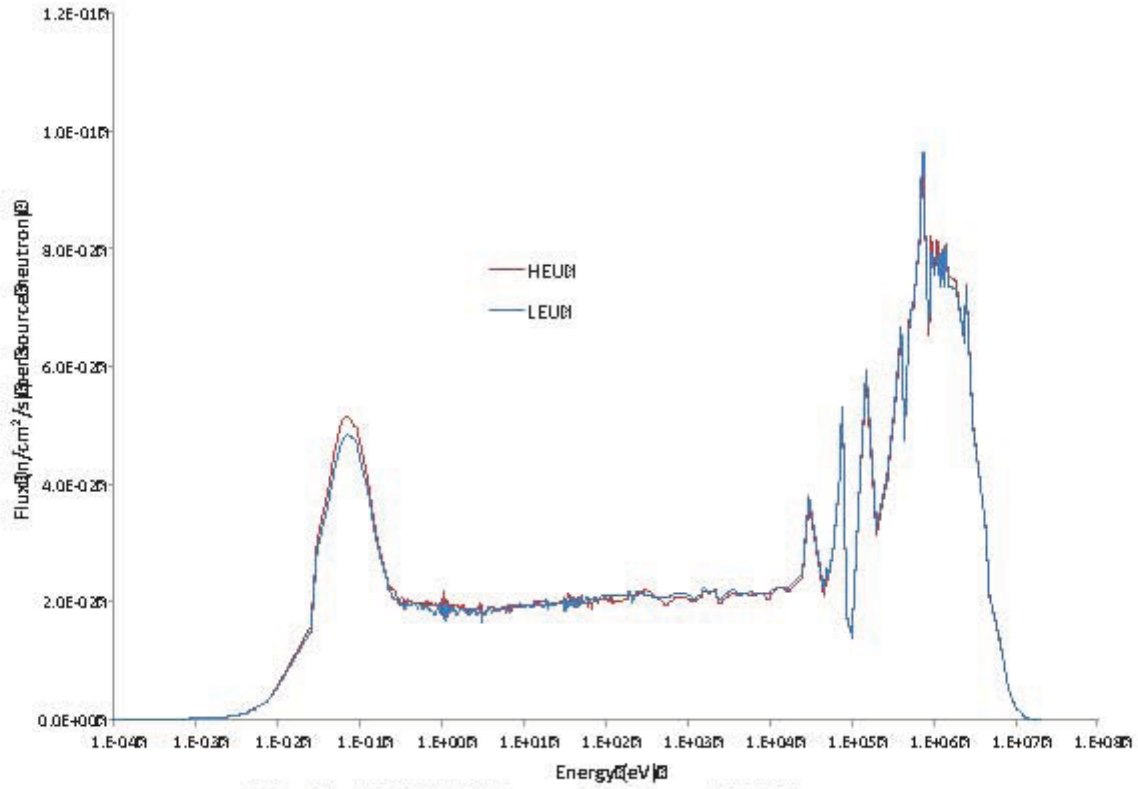
Fig. 13. KENO-VI fluxes in center of NW flux trap.

It is desirable to better quantify the thermal fluxes and any spectral shift associated with the LEU fuel relative to the HEU fuel. Hence, for the purposes of comparison, the thermal flux is defined here as the integrated neutron flux from 0 to 1.25 eV:

$$f_{\phi_{th}} = \int_0^{1.25 eV} \phi(e) dE = \sum_{g=171}^{238} \phi_g.$$

30
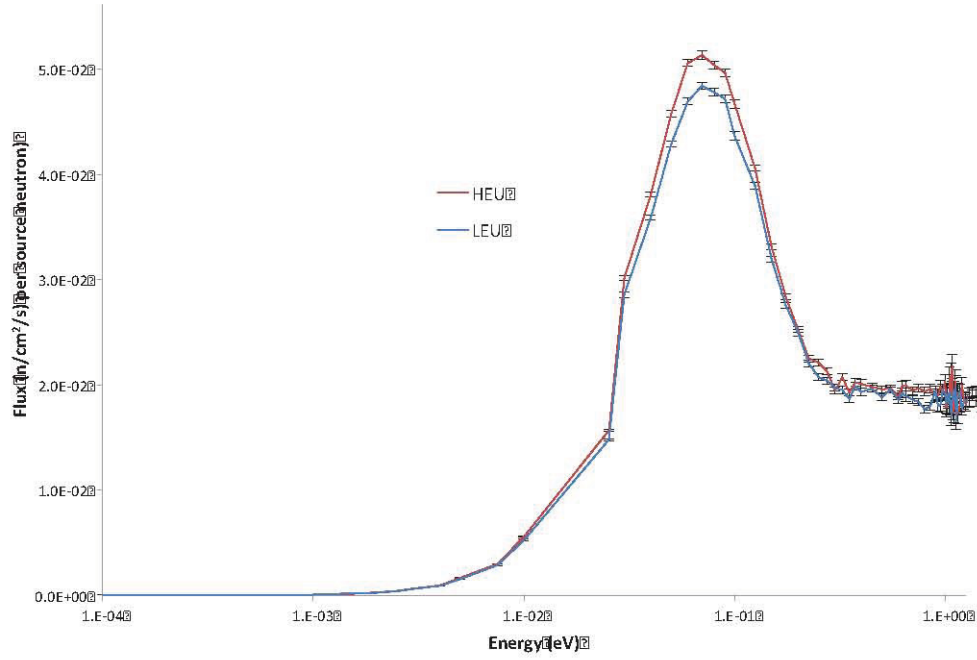
Fig. 14. KENO-VI thermal fluxes with error bars in center of NW flux trap.
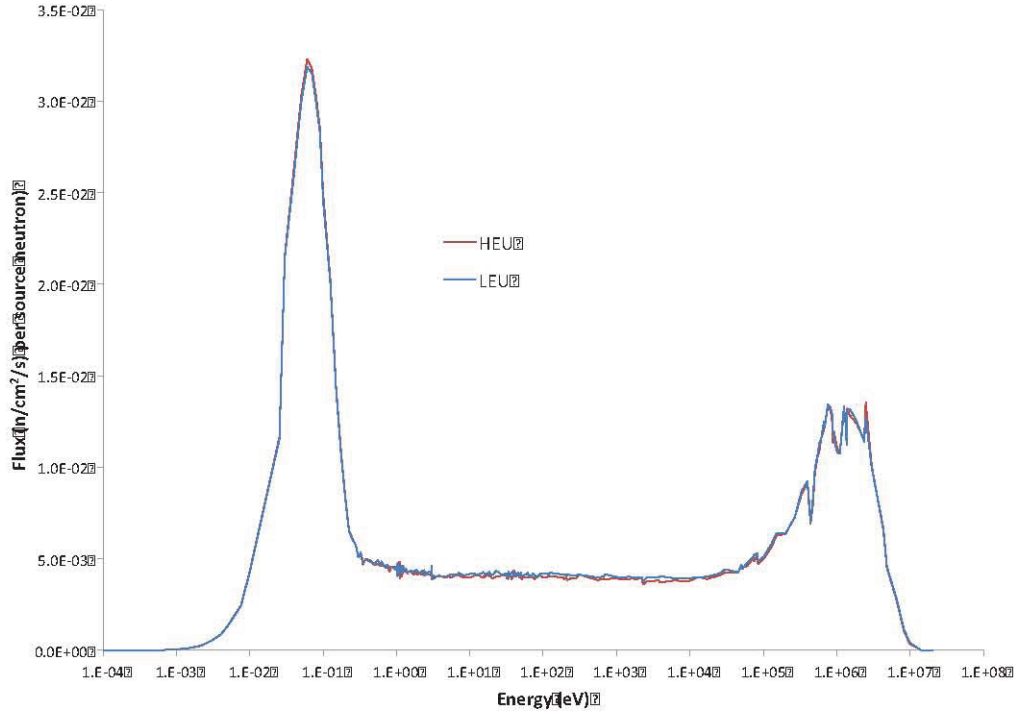
Fig. 15. KENO-VI fluxes in center of SE flux trap.
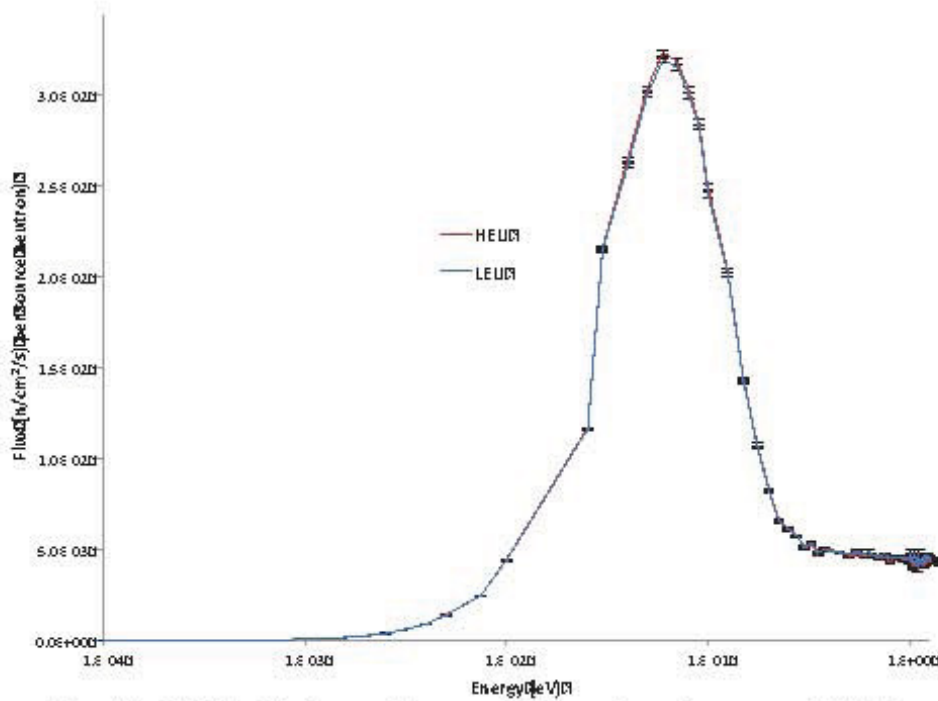
Fig. 16. KENO–VI thermal fluxes with error bars in center of SE flux trap.

where group fluxes were accumulated using the SCALE 238-group energy structure, and group 171 is the group with an upper energy boundary of 1.25 eV within this library. The thermal shift is then defined as:

$$S_{th} = \left| \frac{f_{\phi_{th}}(LEU)}{f_{\phi_{th}}(HEU)} - 1 \right| \times 100\%.$$

Table 2. Integrated Thermal Fluxes and Spectral Shift for ICBA LEU Configuration

	NW Al Tube	SE Water Hole
LEU Thermal Flux (per source neutron)	1.32E-01	7.11E-02
HEU Thermal Flux (per source neutron)	1.39E-01	7.17E-02
S_{th} (%)	-4.78	-0.87

Table 2 lists the integrated thermal fluxes, respectively, for both HEU- and LEU-fueled cores. These results indicate that the integral thermal flux may be reduced by as much as 5% in a solid target; however, with a moderating region very little change is seen, on the order of less than 1%. However, this does not account for power shift between lobes that could occur. As discussed earlier and illustrated in Fig. 10, there is a shift of power toward the central lobe with the ICBA fuel design. Averaging element powers for the elements associated with each lobe provides the lobe powers shown in Tables 3 and 4. Table 3

32

provides the lobe power for each of the 5 ATR lobes with the HEU fuel loading; Table 4 provides the lobe power computed with ICBA fuel, and also provides the percentage change relative to the HEU core.

Table 3. Relative Lobe Powers for HEU Core

NW 0.955		NE 0.834
	Center 1.207	
SW 1.031		SE 0.973

Table 4. Relative Lobe Powers for ICBA Core with Change Relative to HEU Core

NW 0.948 (-0.71%)		NE 0.830 (-0.46%)
	Center 1.220 (+1.07%)	
SW 1.026 (-0.43%)		SE 0.975 (+0.21%)

Table 5 contains adjustments made to fluxes to reflect relative lobe powers for NW and SE lobes, and corrected thermal flux reduction corresponding to operation as identical lobe powers. The thermal flux in the SE location is decreased by less than a percent; this is essentially in the uncertainty range of the

Table 5. Adjusted Thermal Fluxes and Corrected Spectral Shift for ICBA LEU Configuration

	NW Al Tube	SE Water Hole
LEU Thermal Flux (per source neutron)	1.25E-01	6.93E-02
HEU Thermal Flux (per source neutron)	1.33E-01	6.98E-02
Thermal Flux S_{th} (%)	-5.73	-0.63

calculation and may be negligible. A more significant thermal flux reduction of on the order of 6% is possible in the NW flux trap with complete moderator exclusion. This should perhaps be considered to be an upper limit on thermal flux reduction in flux trap locations.

Fast fluxes were not evaluated in this study. Fast flux is directly proportional to fission power to first order, and is not affected significantly by [238]U content; hence for a given power of operation, fast fluxes should be comparable for any fuel design.

Finally, it is important to note that thermal fluxes and the flux ratio will undoubtedly change with burnup, which will require further study. Spectral hardening is a natural consequence of burnup, but the relative amount of spectral hardening and its affect on fluxes is difficult to predict without extensive further analysis.

Fuel Depletion

The final phase this analysis is a study of fuel behavior as a function of burnup. To compare with analyses performed by Chang for these fuels, a depletion history was developed based on three 50-day cycles with a core power of 110 MW; each burn cycle was followed by a 7 day down time. Calculations were performed used KENO-VI within the TRITON depletion sequence. To get the best comparison of behavior, control drums were rotated to obtain a critical system for each fuel type at hot zero power for BOL fuel. The HEU-fueled core was burned with a drum rotation of 45°, while the ICBA-fueled core was set to critical with an 88° rotation. Drums were held in a fixed position for the entire depletion cycle and neck shims were not withdrawn. Figure 17 shows the core eigenvalue as a function of time during burn and down times. The shapes of the depletion curves are consistent with those generated by Chang for this fuel type (see Appendix B) and show that the LEU design would have an extended lifetime relative to the current fuel, presumably due to plutonium breeding in the LEU fuel. This is important, as the LEU fuel would start with a lower initial reactivity – the reactivity gain will offset the initial reduction to allow the fuel to complete a minimum of three fuel cycles.

One key difference is observed between these results and those reported by Chang, with respect to the shape of the two depletion curves following the initial xenon/samarium-driven reactivity drop. Chang's calculations show an initial increase in reactivity during the first 50 days; while the current calculation shows a slight decrease in reactivity during this same period. Increasing reactivity with burnup early in life is due to depletion of poison at a faster rate than introduction of negative reactivity due to fuel depletion and fission product buildup. TRITON calculations are capturing this effect, but the poison is being burned out more slowly. The cause of this behavior is not clear and should be investigated further.
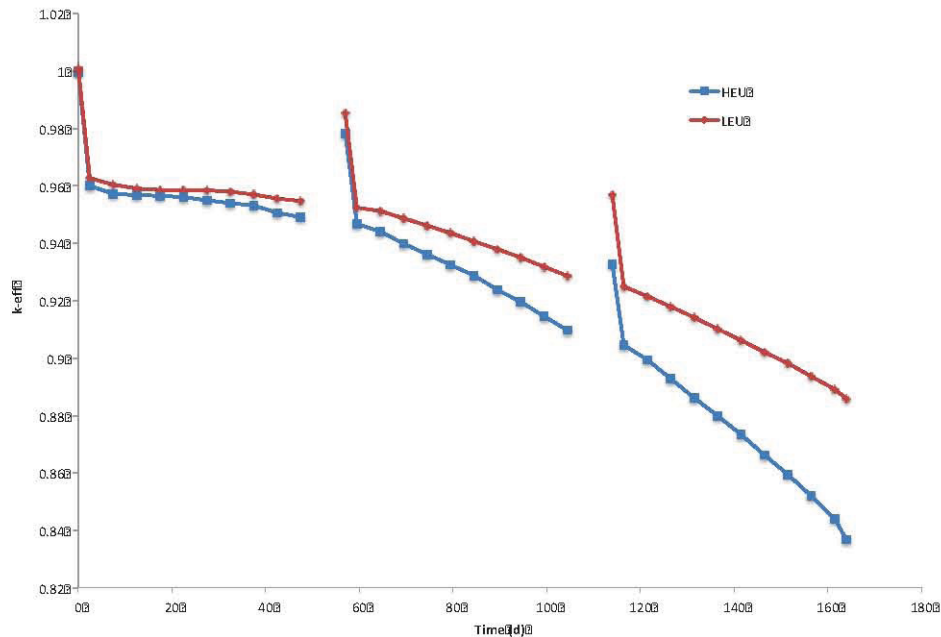
Fig. 17. TRITON KENO-VI depletion of HEU and ICBA fuel designs.

Differences in the value of k_{eff} are due to isotopic changes with burnup. The increased mass of ^{238}U in LEU fuel results in significantly increased plutonium production by neutron capture; the process for production of various plutonium nuclides is illustrated in Figure 18.
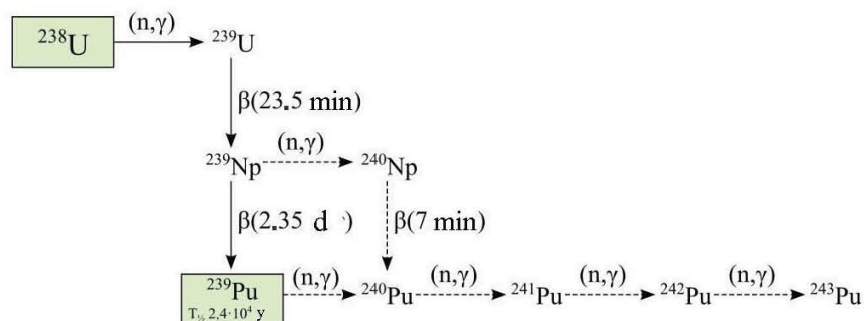
Fig. 18 Process for Pu production by successive neutron capture reactions beginning with ^{238}U. However, numerous other capture/decay reactions in uranium result in a variety of higher actinides as well. Hence, a comparison of actinide inventories at discharge may be instructive. From the results of the above depletion calculations, the majority of the mass of transuranics would be comprised of actinides americium, curium, neptunium and plutonium. Table 5 lists the masses (g) of primary actinides (nuclides with discharge masses greater than 0.01 g) predicted at discharge for full cores loaded with current HEU and proposed LEU fuels. The third column provides the ratio of masses of each nuclide for LEU/HEU.

Table 5. Comparison of Actinide Masses at Discharge

Isotope	HEU Discharge Mass (g)	LEU Discharge Mass (g)	Ratio (LEU/HEU)
Am-241	0.05	0.65	**13.51**
Am-243	0.11	0.76	**7.22**
Cm-242	0.01	0.10	**9.25**
Cm-244	0.01	0.06	**5.86**
Np-237	112.85	102.71	0.91
Np-238	0.00	0.63	—
Np-239	4.10	69.72	**16.98**
Pu-238	12.74	9.32	0.73
Pu-239	78.39	1629.20	**20.78**
Pu-240	14.84	239.79	**16.16**
Pu-241	9.80	125.48	**12.80**
Pu-242	1.44	12.09	**8.38**
Th-232	0.00	0.00	1.00
U-234	367.09	1.53	0.00
U-235	22899.20	35552.00	1.55
U-236	3634.81	3505.10	0.96
U-237	16.32	14.01	0.86
U-238	**2446.10**	**220240.00**	90.04
U-239	0.03	0.49	16.93
Total	29597.89	261503.64	
Initial mass	*46230.00*	*278450.00*	

Ratios of greater than 2.0 are highlighted in boldface. Note that ^{238}U inventories are 90 times larger in spent fuel; however, this is a result of the initial ^{238}U loading in the LEU fuel. These results confirm the

assertion that plutonium is produced in significant quantities in operation of LEU fuel; this design, under the assumed operating conditions, will produce 20 times more ^{239}Pu that an HEU core, with a mass of 1.6kg. However, relative to commercial power plant LWR fuel, much less plutonium is produced during a fuel lifetime. In these calculations, a total of approximately 2 kg of plutonium is present in the fuel, relative to 36 kg of ^{235}U. For LWR fuels the mass of plutonium at discharge is on the order of or slightly greater that the mass of ^{235}U. This is due largely to the fact that LWR fuels contain 95+% ^{238}U in fresh fuel, resulting in increased ^{238}U capture over the fuel lifetime.

Discharge fission product inventories were also reviewed. Findings here were unremarkable – with very few exceptions, the number densities of fission products are essentially the same between the two fuel types. Table 6 lists the most significant fission products (by mass) at discharge. Because plutonium fission is not a large component of total fission at end of life, the shifted fission yield from plutonium fission is not present to the extent to significantly alter the fission product distribution. The only interesting feature of this table is the significant increase in ^{135}Cs in LEU fuel relative to HEU fuel. ^{135}Cs is not produced in appreciable quantities as a fission product; it is produced largely from the decay of ^{135}Xe. ^{135}Xe is in turn produced by the decay of ^{135}I, which represents about 6% of the fission product inventory. As was discussed earlier and illustrated in Fig. 7, the increase ^{238}U inventory results in a significant reduction in the thermal flux within the fuel. It is possible that the increased ^{135}Cs inventory results from decreased ^{135}Xe absorption in LEU fuel (^{135}Xe is an extremely strong thermal absorber), which in turn results in increased ^{135}Xe decay, producing ^{135}Cs.

Standard ATR operation involves removal of negative reactivity over an operating fuel cycle – this is accomplished by a combination of depletion of the boron in the fuel elements, rotation of OSCCs, and removal of neck shims. Between cycles, fuel shuffling and addition of fresh fuel is also used to offset the reactivity loss during a cycle. The current study has not tried to evaluate such dynamic behavior – the computational effort required would be significant, and other analysis tools being incorporated into the upgraded ATR analysis suite are more appropriate for such calculations. However, there is still much to be learned about fuel behavior. From the results of these depletion calculations, it is possible to examine the radial distribution of power as a function of burnup. Figures 8 and 9 illustrated the distribution of powers within an average fuel element at beginning of life for both LEU and HEU fuels. It is desirable to understand the change in this distribution as a function of burnup, resulting from depletion of burnable poisons and of fissile material. Because safety limits are determined based on the hottest flow channel in the core, it is important to understand potential changes in the location of the hot channel over the lifetime of a fuel element.

Table 6. Comparison of Primary Fission Product Masses at Discharge

Isotope	HEU Discharge Mass (g)	LEU Discharge Mass (g)	Ratio (LEU/HEU)
Ba-138	659.15	664.26	1.01
Ce-140	534.53	537.59	1.01
Ce-142	594.18	594.94	1.00
Cs-133	551.18	568.49	1.03
Cs-135	71.19	605.52	**8.51**
Kr-86	112.46	110.60	0.98
La-139	625.16	630.85	1.01
Mo-100	444.55	448.26	1.01
Mo-97	420.74	423.19	1.01
Mo-98	400.02	409.22	1.02
Nd-143	439.80	464.37	1.06
Nd-144	176.90	152.52	0.86
Nd-145	380.06	385.86	1.02
Nd-146	330.64	328.23	0.99
Nd-148	184.46	184.86	1.00
Pr-141	408.51	413.98	1.01
Rb-87	159.39	156.49	0.98
Rh-103	124.82	139.48	1.12
Ru-101	363.06	376.40	1.04
Ru-102	316.04	327.40	1.04
Ru-104	140.06	158.77	1.13
Sm-150	122.72	122.66	1.00
Sr-88	219.55	215.29	0.98
Sr-90	364.60	357.19	0.98
Tc-99	393.03	416.21	1.06
Te-130	166.14	170.88	1.03
Xe-131	213.41	226.10	1.06
Xe-132	429.45	434.86	1.01
Xe-134	749.55	756.97	1.01
Xe-136	1186.98	1190.20	1.00
Y-89	177.70	175.41	0.99
Zr-91	209.51	207.66	0.99
Zr-92	390.27	385.58	0.99
Zr-93	412.88	410.08	0.99
Zr-94	430.54	428.46	1.00
Zr-96	429.47	430.68	1.00

Figures 19 and 20 show the average power calculated as a function of burn time for the three-cycle, 110 MW core power scenario discussed earlier. Figure 19 illustrates the behavior of the HEU fuelled core, while Fig. 20 shows the behavior of the core operated with the ICBA fuel design. It is significant to note that the most significant change in power distribution is seen in the innermost and outermost plates in the current HEU design. Figure 20 indicates that LEU fuel will deplete in a similar fashion; however, the change in the power distribution near the inner and outer edges is not as significant as for its HEU

counterpart. This seems counterintuitive   the thinner plates near the edges of the assembly result in reduced fuel masses in these regions. Intuition suggests that the reduced mass would be depleted faster at a given power level. However, the production of plutonium in LEU may cause this behavior. Spectral hardening due to boron poisons in outermost plates will further enhance production of plutonium in those fuel plates, resulting in significantly more breeding than is seen in interior fuel plates.
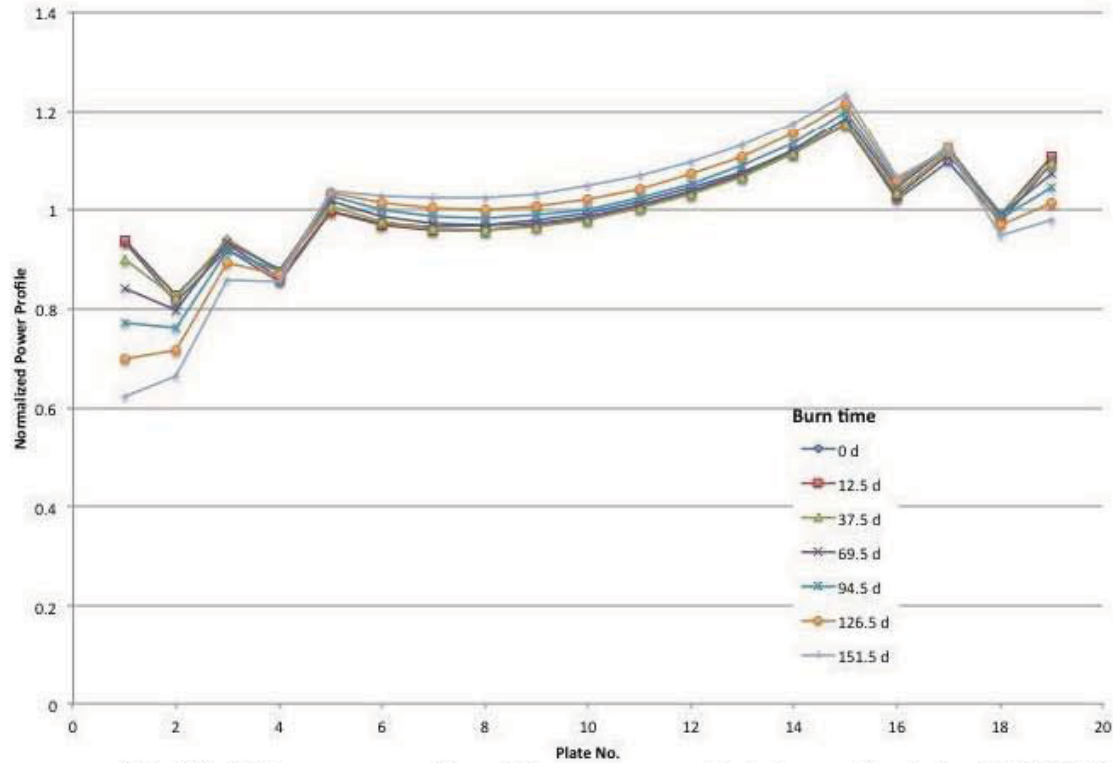
Fig. 19. Plate power profile within an average fuel element loaded with HEU fuel.
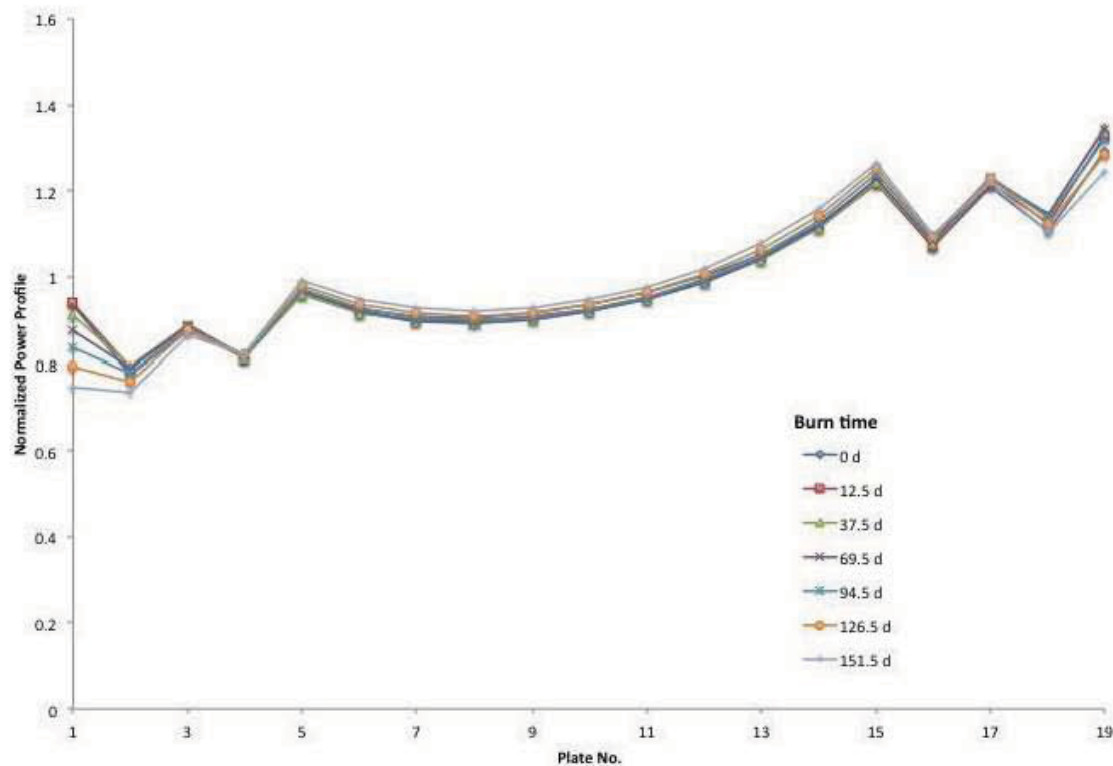
Fig. 20. Plate power profile within an average fuel element loaded with LEU fuel.

Other Core Models

Presently INL staff are engaged in a physics methods upgrade project to put into place modern computational neutronics tools for future support of ATR fuel cycle and experiment analysis. The computational methods selected include Helios, Attila, and portions of the SCALE code system for reactor physics calculations. MCNP, long used for detailed ATR analysis, will also be employed in ATR analysis for independent confirmation of computational models. Ultimately, these updated methods will be required to be applied to an ATR configuration loaded with LEU fuel. Work presented to date has illustrated the ability to perform analysis for ATR using NEWT and KENO-VI modules within SCALE 6. Appendix B provides a portion of work completed using MCNP and MCWO, which has been used to confirm the performance of SCALE modules.

As the calculations reported here have proceeded, models for the ATR for both HEU and LEU (ICBA) have been developed for Helios and Attila, and confirmatory analysis are underway. Calculations reported previously for NEWT and KENO-VI have been completed using Helios. Figure 6 illustrated KENO-VI results for OSCC worth as a function of rotation. The 3D KENO-VI calculation showed slightly less reactivity worth and that total drum worth is reduced to about 85% of its HEU reactivity for the LEU ICBA design. The results of 2D Helios calculations (Fig. 21) indicate that the reduction is on the order of 90%. This agreement is remarkably good in a comparison between 2D and 3D methods with totally different treatment of the basic input nuclear cross section data, and confirms the assessment of reduced drum worth at BOL for LEU fuel.
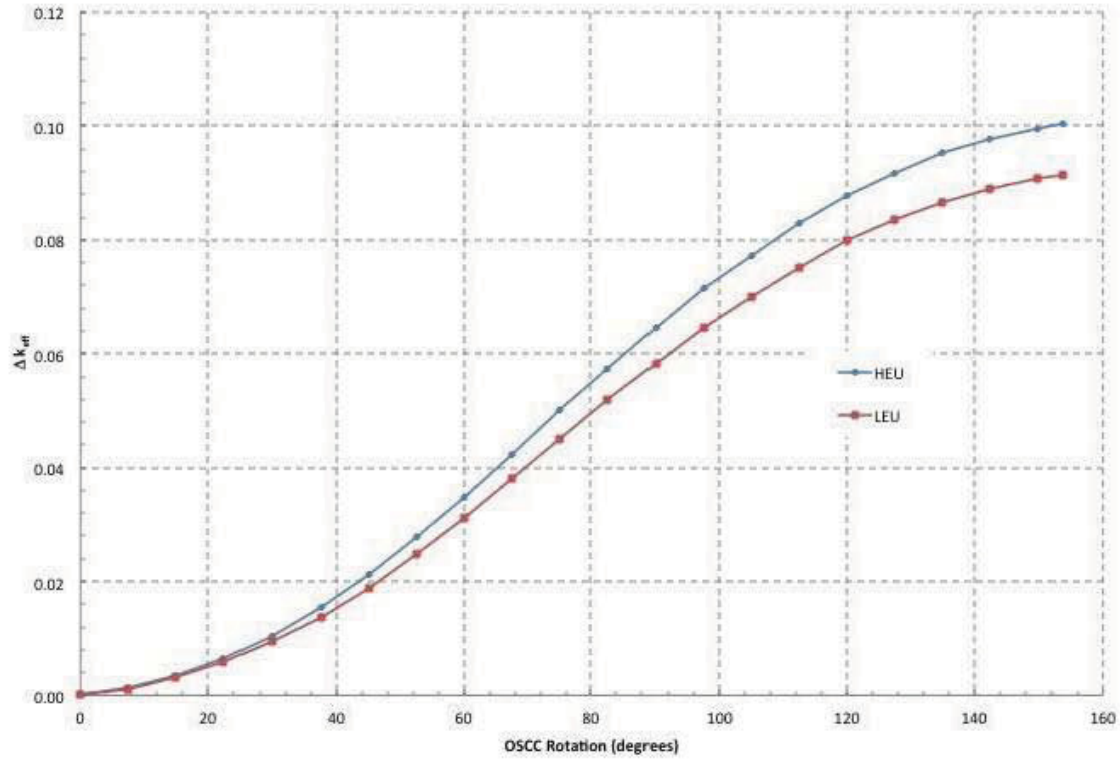
Fig. 21. Helios calculation for Δk_{eff} as a function of OSCC rotation for two fuel types.

Figures 8 and 9 showed results of KENO-VI and NEWT calculations, respectively, for the normalized plate power distribution in an average assembly at BOL. Figure 22 illustrates the results of a corresponding Helios calculation to obtain the average element power distribution under the same conditions. These results are essentially identical to the NEWT plate power distribution.
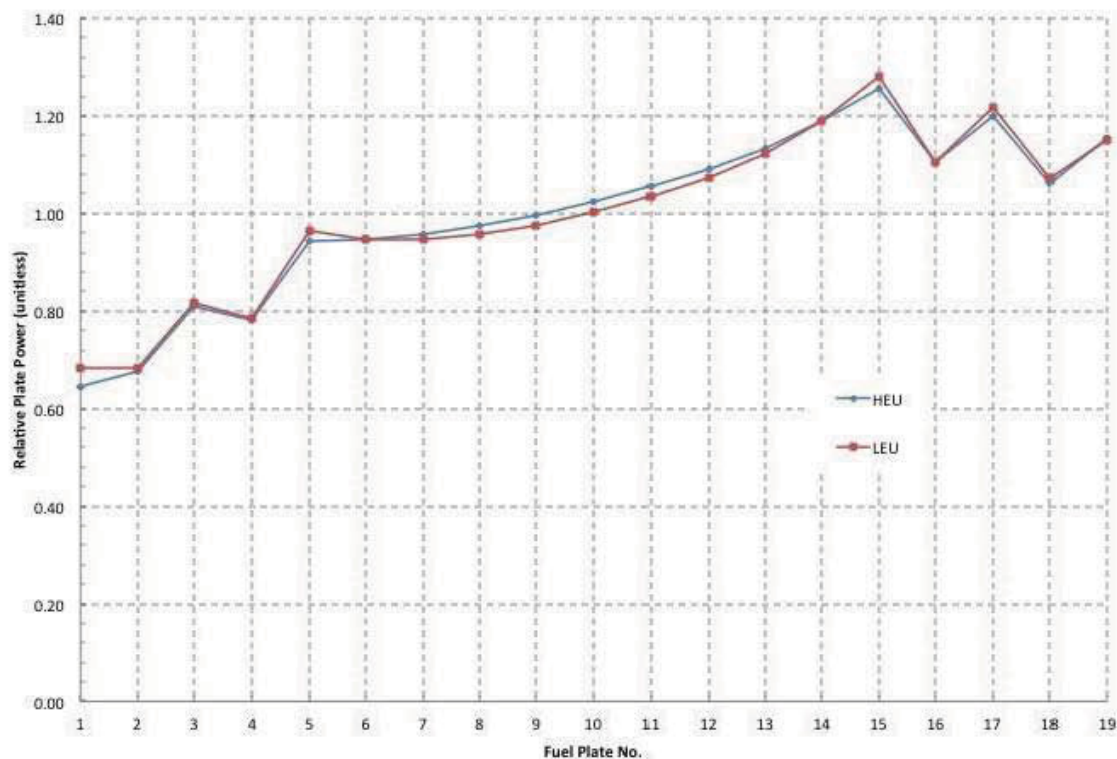
Fig. 22. Helios prediction of average plate powers for two fuel types in 94-CIC core.

Figures 10 and 11 showed the distribution of powers in the 40 fuel elements by core position, for calculations performed by KENO-VI and NEWT, respectively. Figure 23 shows the same distribution as calculated by Helios. This time, Helios results are more consistent with the KENO-VI results. NEWT results tend to show the same magnitude for peaks and valleys around the core; KENO-VI and Helios indicate a power shift toward elements 20 and 21, between the South and Center flux traps. Reasons for this are not clear – this may result from modeling differences, perhaps in the loading of the South flux trap.

Finally, Figure 24 is a plot of k_{eff} as a function of burnup as calculated by Helios. These results are in very good agreement with TRITON KENO-VI depletion results plotted in Fig. 17. Slight differences in reactivity at EOL may also be due to multidimensional effects.

41
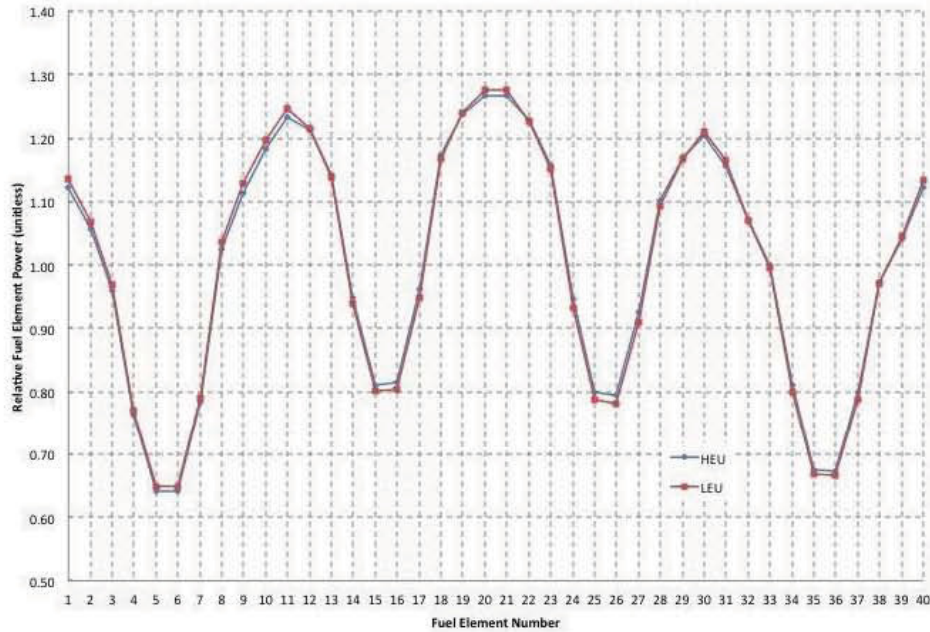
Fig. 23. Helios prediction of average element powers
for two fuel types in 94-CIC core.
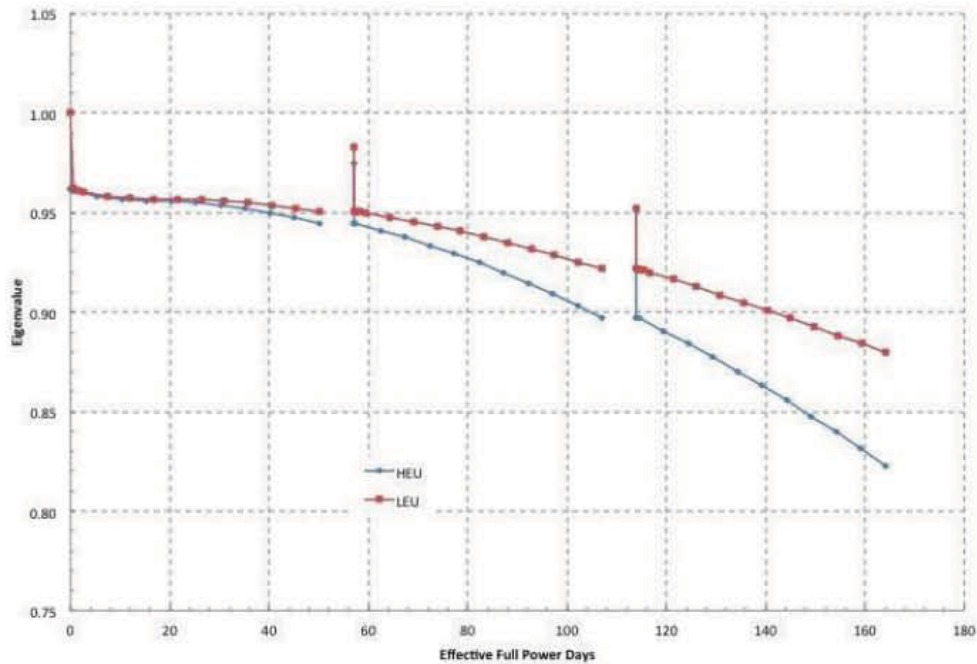
Fig. 24. Depletion of both LEU and HEU fuel using Helios.

A 3D Attila model has also been developed for HEU fuel in the 94-CIC configuration as part of the ATR Physics Methods Upgrade project. ATR models have been developed at INL using SolidWorks [7], a 3D CAD/CAM engineering design tool. SolidWorks models can be exported in Parasolid format, which can be read into Attila; this solid model can then be meshed as a 3D tetrahedral mesh for deterministic transport calculations. The ICBA design has been modeled within SolidWorks (see Fig. 25) and inserted as a part, replacing the HEU fuel element part in the existing 94-CIC model (see Fig. 26). This solid model has been imported into Attila and a full-core mesh developed, as illustrated in a partial-core

42

snapshot in Fig. 27. SCALE has been used to generate problem-specific cross sections using the 47-energy-group library *xn49v7_atr*, which has also been imported into Attila. At present, test calculations are being performed to optimize MPI-based distributed-memory parallel calculations on more than 100 CPUs on INL's Icestorm compute cluster. Preliminary fuel plate and assembly power calculations are anticipated to be completed in the very near future. Depletion calculations are expected to challenge the Attila system and may require further development before practical application for the ATR.
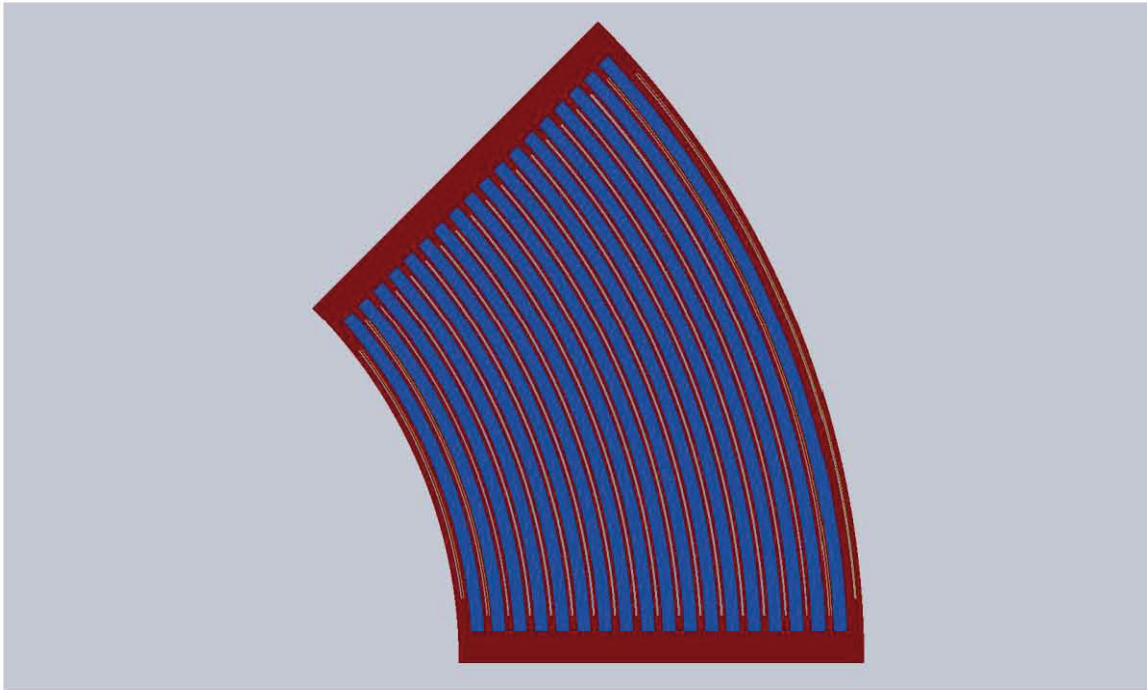
Fig. 25. SolidWorks representation of the LEU ICBA fuel design.

However, Attila is likely to serve as a very useful special purpose computational workhorse for ATR calculations, and is likely to have value for LEU applications. Specifically, Attila may be utilized to provide a means for future full core sensitivity/uncertainty calculations.
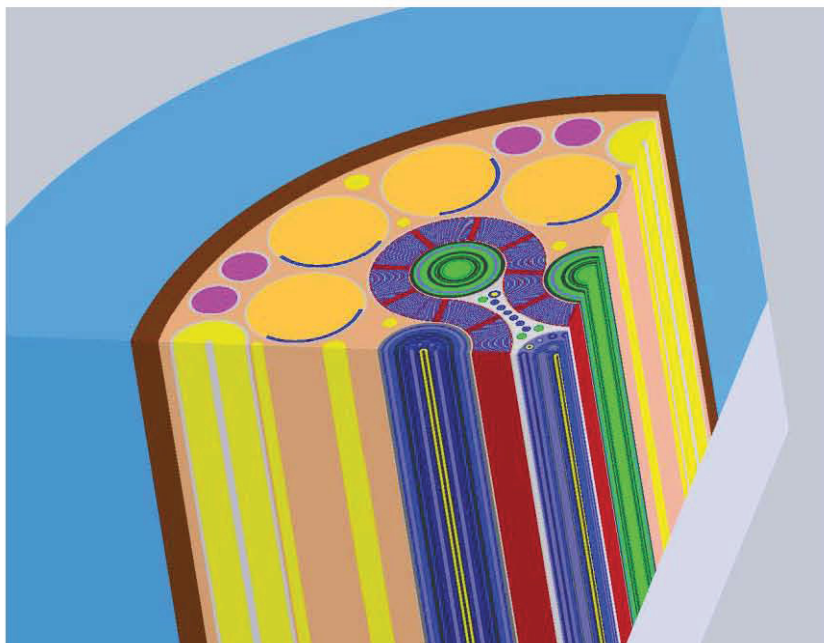
Fig. 26. Quarter-core cutaway from SolidWorks representation of ATR with ICBA fuel assemblies.
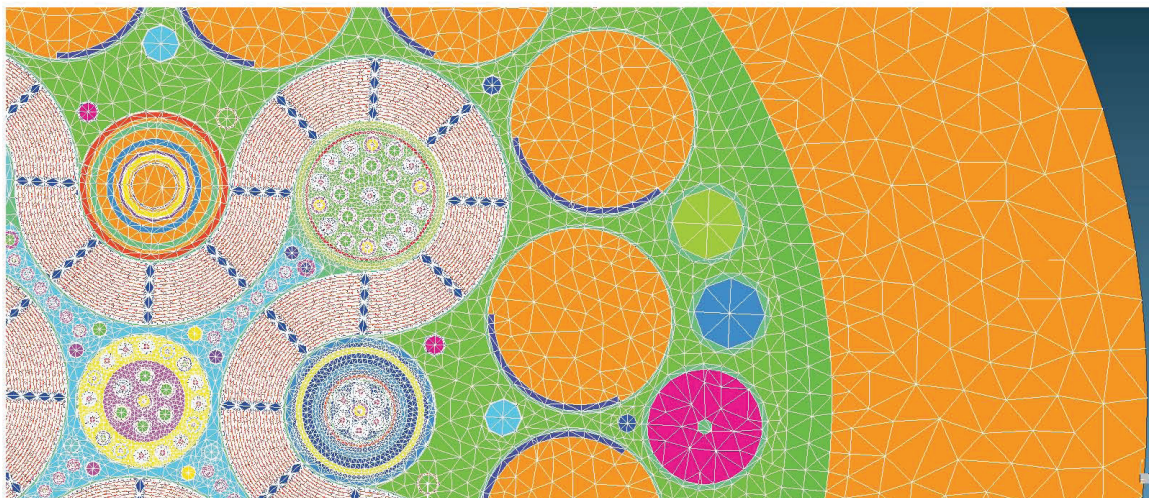
Fig. 27. Attila-generated mesh for ICBA fuel in ATR on axial midplane.

Conclusions

This report summarizes the results of an evolving set of calculations that sought to determine the performance characteristics of the ATR from a physics perspective using modern computational analysis methods. In the absence of a final LEU fuel design, a plausible conceptual design has been used as a basis for this evaluation. The primary goal of this work has been to evaluate the use of a new suite of computational packages for LEU core physics calculations. The KENO-VI and NEWT transport modules within the TRITON sequence of SCALE, along with Helios, Attila, and MCNP are currently being validated for application to the ATR under the INL Life Extension Program (LEP). The current work has been used as a starting point to assess the physics performance of the ATR fueled with LEU fuel with updated physics methods – the predicted performance of the such a core is been shown to be consistent between the various tools applied in these studies. To that end, this work has thus far shown expected levels of consistency.

From the calculations that have been completed to date, observations can be made regarding evaluation of the selected neutron transport packages:

- Calculations performed using elements of the SCALE code system for ATR analysis have shown consistency with independent MCNP calculations. This is important because components of SCALE will be part of the analysis suite that is currently being evaluated for physics methods upgrades for the current HEU core. Preliminary Helios calculations have been completed and also show agreement with SCALE and MCNP calculations. The use of Attila for LEU fuel studies, although not yet completed, is well underway.

- Helios is currently being deployed as the next-generation core management tool for the current ATR fuel design and operating envelop. In the absence of operational data for LEU fuel, further code to code testing and review and fine-tuning of models will be necessary to show that Helios will provide adequate analysis capabilities for LEU operation. Some combination of MCNP, SCALE, and/or Attila will provide a three-dimensional virtual reactor environment to be able to be used to continue to evaluate Helios.

Relative to the performance of the ATR driven by a prototypic LEU fuel design, the calculations performed herein indicate:

- In an LEU-fueled core based on the ICBA design, a thermal flux reduction on the order of up to 6% may be seen a single in-pile location if there is very little moderation associated with that experiment. However, this is considered to be a conservative and limiting value, and for typical experiment configurations no significant thermal flux reduction should be seen. Other ATR experiment positions more closely resemble the SE flux trap, and are not expected to see a significant reduction in thermal flux.

- Because of the power shifting that is available in the ATR, any thermal flux deficit seen in a given experiment position can be ameliorated by a small power shift toward that lobe. There is no evidence that there would be a core-wide reduction in thermal flux – future work should evaluate all 9 flux trap positions; however, G. Chang has already performed such analyses and has seen no net reduction in thermal flux over the entire core.

- From a physics point of view, the work completed here indicates that the ICBA fuel design proposed by Chang is an excellent candidate for LEU conversion. Although this fuel has a reduced reactivity on the order of 3-4% relative to HEU fuel, the natural breeding of plutonium in the ^{238}U inventory reduces the slope of reactivity decrease with burnup, offsetting the initial reduced reactivity at end of cycle.

- Earlier work included here for completeness (Appendix A) showed a potential for up to a 15% reduction in thermal flux in the NW position. However, that work was based on a different fuel design concept than the ICBA fuel, and clearly would not perform as well as the ICBA design. In addition, the earlier work did not evaluate redistribution of power between lobes, which would potentially change the effective flux reduction (flux per unit power) in the various lobes.

- Depletion calculations demonstrate that plutonium production in LEU fuel results decreased rate of reactivity loss over simple three-cycle burn scenario. Such behavior is fully expected to be manifest in real operations; use of fuel for an extra fuel cycle may be possible from a reactivity perspective.

- Significant differences in discharge isotopics are seen for uranium and transuranic metals; fission product distributions are largely unchanged in an LEU fuel. Plutonium and higher actinide inventories are not as large a component of discharged fuel as is typically seen in commercial nuclear fuel.

- Results reported here are generally consistent with those provided in Appendix B. The ICBA fuel element design was modified subsequent to the analysis reported in that work to provide closer agreement to HEU fuel assembly radial profiles. Differences observed between MCNP and other physics codes with respect to boron depletion may be a result of this fuel design difference, but this has not been demonstrated.

Note that calculations performed to-date including those described herein have been subject to independent intercode verification, but are largely unvalidated as yet, due to the unavailability of pertinent experimental data at this point. Further, more detailed, analysis will certainly be necessary; however, a final or near-final LEU fuel design will be needed to allow a focused study on core physics fuel performance. Nevertheless, the ICBA LEU fuel design recommended by Chang appears to be an appropriate replacement for the current HEU fuel element from both reactor physics and fuel cycle isotopic performance perspectives. This warrants more detailed study of this design for reactor physics, materials, and safety considerations.

References

1. R. Stamm'ler et al., "User's Manual for HELIOS," Studsvik/Scandpower (1994).
2. D. S. Lucas, "Core Modeling of the Advanced Test Reactor with the Attila Code," M&C 2005: International Topical Meeting on Mathematics and Computation, Supercomputing, Reactor Physics, and Nuclear and Biological Applications, Avignon, France, 2005.
3. M. D. DeHart and S. M. Bowman, "High-Fidelity Lattice Physics and Depletion Analysis Capabilities of the SCALE 6.0 Code System Using TRITON," *Nuclear Technology*, **174**, 2, 196-213, May 2011.
4. F. B. Brown, et al., "MCNP Version 5," Trans. Am. Nucl. Soc., **87**, 273 (November 2002).
5. G. S. Chang M. A. Lillo R. G. Ambrosek, "Neutronics and Thermal Hydraulics Study for Using a Low-Enriched Uranium Core in the Advanced Test Reactor 2008 Final Report," INL/EXT-08-13980, Idaho National Laboratory, June 2008.
6. S.S. Kim, B.G. Schnitzler, "Advanced Test Reactor: Serpentine Arrangement of Highly Enriched Water-Moderated Uranium-Aluminide Fuel Plates Reflected by Beryllium", NEA/NSC/DOC/(95)03/II, Volume II, HEU-MET-THERM-022.
7. D. Planchard and M. Planchard, "Engineering Design with SolidWorks 2012," SDC Publications, Mission, Kansas (2012)

Appendix A: Earlier Studies of Candidate Fuel Designs

In the absence of a final LEU design, a number of potential fuel designs have been evaluated: (1) a fuel element with uniform fuel thicknesses and boron poison in inner and outer fuel plate locations (similar in concept to the current HEU design), (2) a fuel element with graded (reduced) enrichment in inner and outer fuel plates to reduce plate powers, and (3) a fuel element based on earlier work performed by G. Chang using thinner fuel plates combined with B_4C poison. The following sub-sections detail the key aspects of studies completed at this point.

Borated 13 mil Fuel Plate Design

Initial studies began by assuming a boron-poisoned design similar to that used in the current HEU design. The goal was to obtain a power profile similar to that obtained with the HEU fuel, as the radial power profile would drive the maximum operating power. Because of the quantity of ^{238}U present in the LEU fuel, the relative thermal neutron density is reduced at a given power level (spectral hardening), and more boron is needed to obtain a given reactivity reduction. A candidate power profile was determined that would be similar to the current HEU design in terms of the average radial power profile. Table 1 lists the ^{10}B concentration (in natural B) used in each plate; the last column gives the volume fraction of B_4C that would be required to achieve the boron concentration in the LEU design, since large quantities of this poison might result in fabrication concerns. However, as will be discussed later, this becomes a non-issue as B_4C poisoning is not practical for other reasons.

Table 1. Boron Poison Plate Loading for Boron-Poisoned LEU Design

Fuel Plate No.	^{10}B, HEU	^{10}B, LEU	Ratio LEU/HEU loading	LEU B_4C Volume fraction
Plate 1	1.55E-04	3.10E-03	20.0	2.12%
Plate 2	1.60E-04	2.39E-03	14.9	1.64%
Plate 3	8.57E-05	8.54E-05	1.0	0.06%
Plate 4	8.34E-05	8.30E-05	1.0	0.06%
...				
Plate 16	8.30E-05	8.27E-05	1.0	0.06%
Plate 17	8.28E-05	8.25E-05	1.0	0.06%
Plate 18	1.59E-04	1.59E-03	10.0	1.09%
Plate 19	1.61E-04	3.21E-03	19.9	2.20%

Figure 1 shows the resulting radial power profile for this fuel design. Additional "tweeking" could be used to improve the alignment of power profiles, but for current purposes this was not necessary.
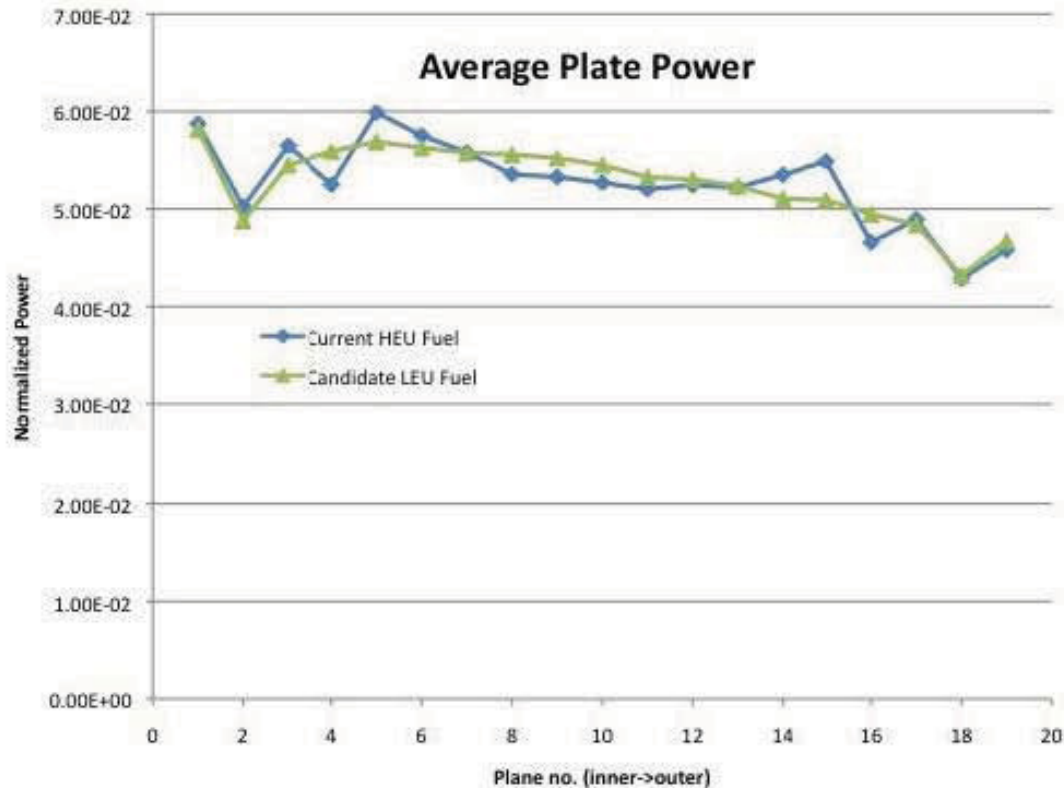
Fig. 1. Average plate power distribution for boron-poisoned LEU fuel element design.

Eigenvalue calculations were performed to determine the neck shim and OSCC positions that would be needed to achieve criticality. Unfortunately, it was determined that so much boron poisoning is need to flatten the power profile that a core loaded with all fresh assemblies could not be made critical. Figure 2 shows k_{eff} as a function of drum rotation for this design with all neck shims removed; the expected S-curve is obtained, but the core cannot be brought even close to critical. Hence, the use of 13mil fuel plates with B_4C poison was abandoned. Other design modifications may be possible that would make the use of boron poison feasible; however, the goal of this work is not to design a fuel element.

Graded Enrichment Fuel Plate Design

The next candidate design studied was based on reduced U enrichment in plates 1-4, 16-19, reducing plate reactivity by reducing the ^{235}U concentration. This option was selected for two reasons: (1) reduced or graded enrichments are common in LWR fuel designs for reactivity control and manufacture of variable enrichments is thus not a technical challenge, and (2) it is not known if manufacture if fuels of less that 13mils in thickness is feasible. This approach appeared much more promising, and it was much simpler to converge on the desired radial power profile. Table 2 lists the enrichment by plate that was used to obtain the radial profile illustrated in Fig. 3. A slightly decreased enrichment in plate 5 was necessary to reduce the peak in this plate. Further enrichment variations could be pursued to better match the initial HEU profile, but again the goal here was to obtain a representative profile, not to design a new fuel element.

Table 2. Fuel Plate ^{235}U Enrichment for Graded LEU Design

Fuel Plate No.	^{235}U Enrichment (wt %)
Plate 1	10.00
Plate 2	10.00
Plate 3	13.00
Plate 4	13.00
Plate 5	18.75
Plates 6-15	19.75
Plate 16	15.00
Plate 17	14.00
Plate 18	10.00
Plate 19	10.00

To assess the net reactivity of the fuel design, eigenvalue calculations were performed with OSCC drums rotated to 160° and with all neck withdrawn (to get maximum k_{eff} value), and with drums rotated to 0% and all neck shims inserted (to obtain the corresponding minimum k_{eff} value). Calculations were performed for the HEU-fuelled core (based on the 94 CIC configuration) and for the same core loaded with the graded fuel design. Results indicate that the two designs are similar in terms of reactivity worth at beginning of life. This will not remain true as the fuel is irradiated. The production of fissile ^{239}Pu in the LEU design will result in a slower decrease in reactivity in the LEU-fuelled core relative to the current HEU core.
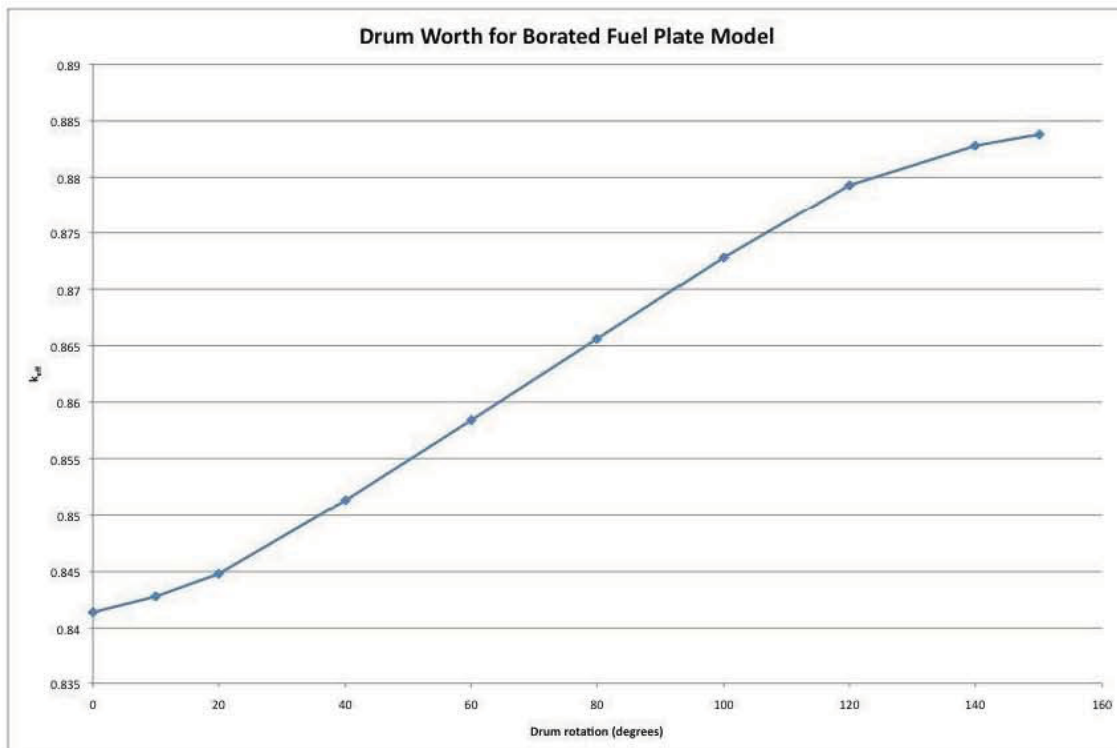
Fig. 2. OSCC worth for boron-poisoned LEU fuel element design.
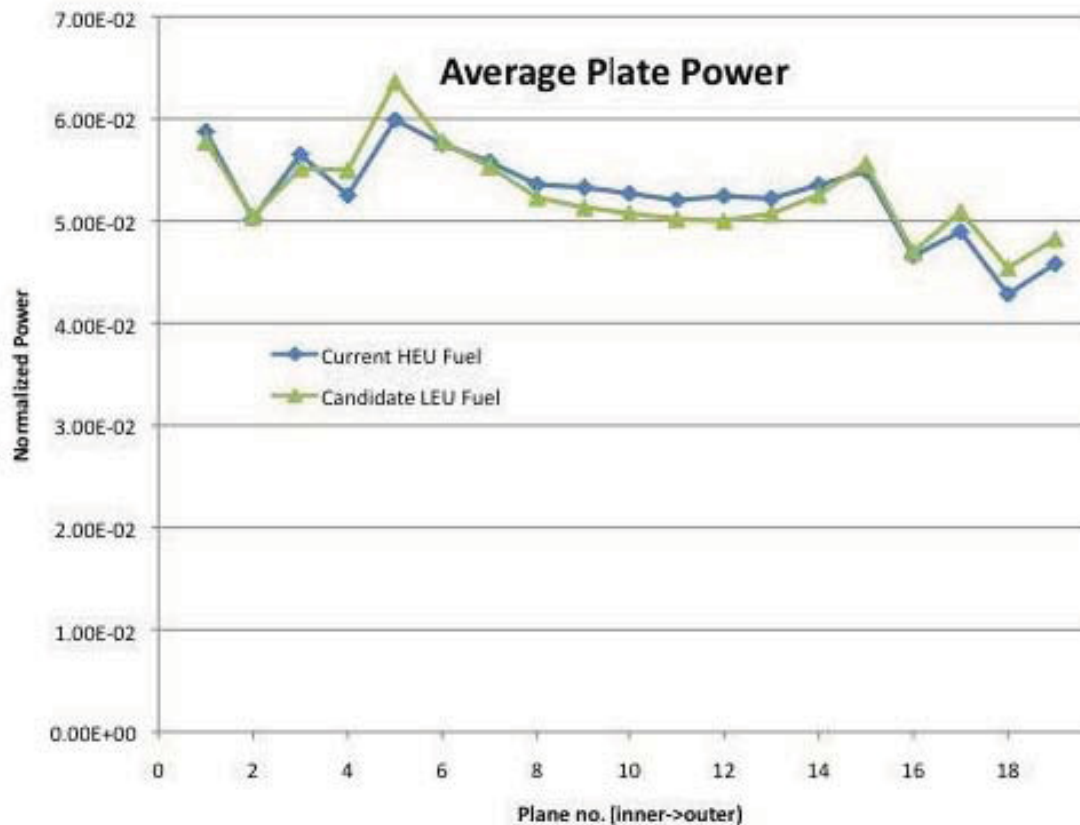
Fig. 3. Average plate power distribution for graded-enrichment LEU fuel element design.

Results indicate that the graded enrichment model would provide a good starting point for comparison of potential LEU performance to the current HEU core. Hence, additional study of the physics performance of this model was justified.

Perhaps the most significant issue to be resolved in the changeover to LEU fuel is the neutron spectral shift. Because of significant resonance absorption in ^{238}U during the neutron slowing down process, the increased concentration of ^{238}U in LEU fuels results in a decreased thermal flux relative to the HEU fuel. KENO-VI calculations were performed with 10^7 neutron histories to obtain statistically meaningful energy-dependent neutron fluxes, for both the HEU fuel and graded LEU fuel cores. Figure 4 illustrates the fluxes predicted in the aluminum insert present in the NW in-pile tube in both HEU and LEU models, averaged over the entire volume of the insert. Similarly, Fig. 5 shows the calculated neutron flux for both HEU and LEU fuel in the central water region on the SE tube; again, fluxes are averaged over the entire water volume within the SE position. These two experiment positions represent two extremes: the Al-filled NW position will have the hardest spectrum, while the water-filled SE position represents a highly thermalized spectrum.
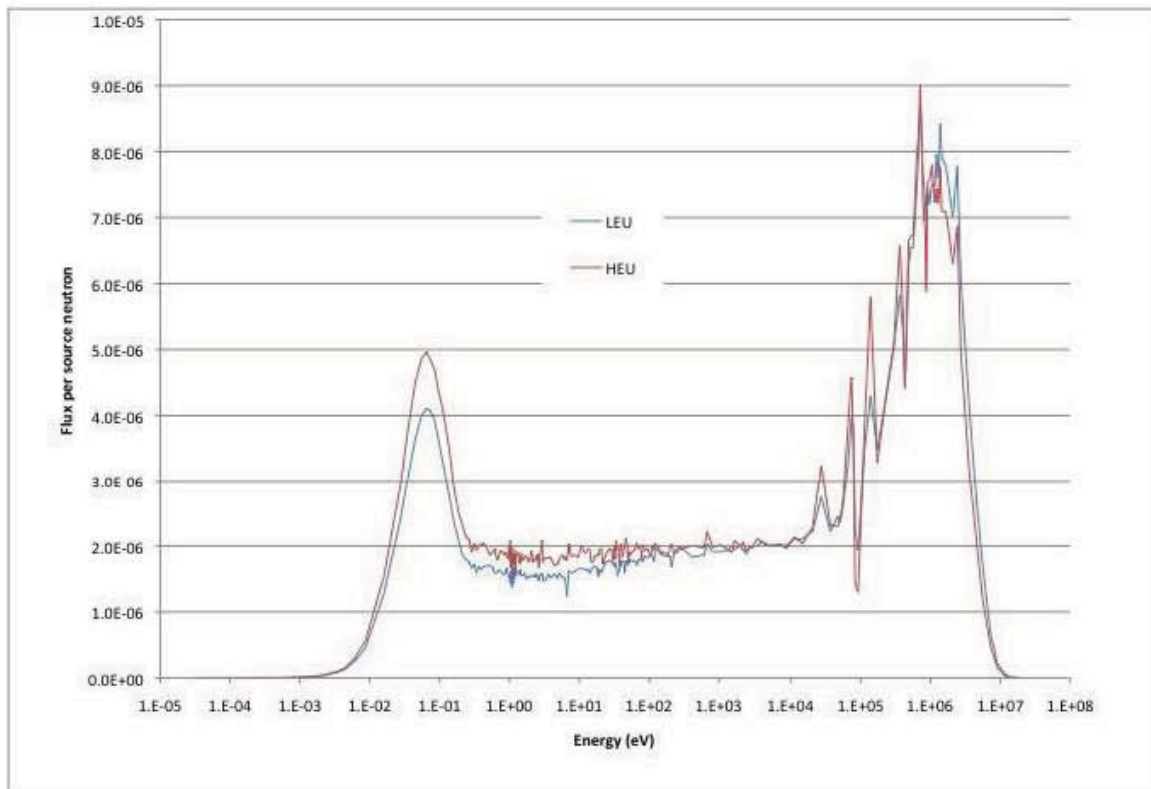
Fig. 4. KENO-VI calculated fluxes within the Al insert of the NW IPT (based on the 94-CIC configuration).
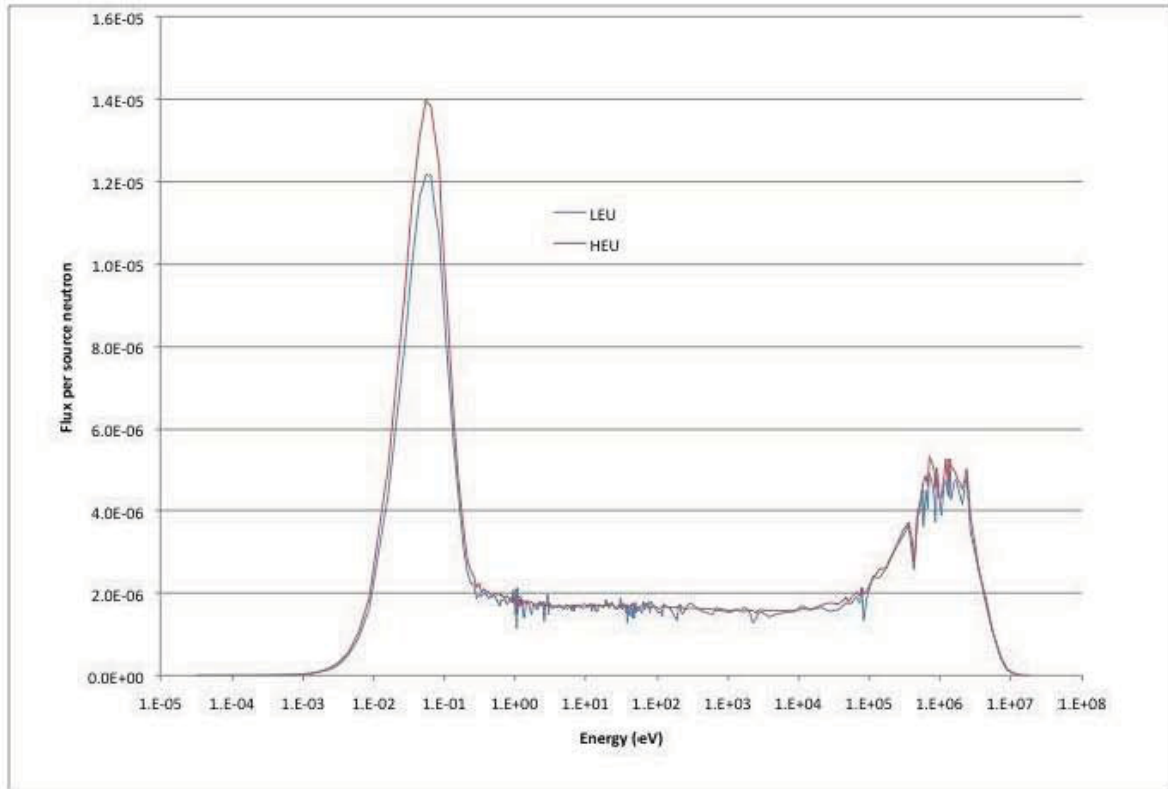
Fig. 5. KENO-VI calculated fluxes within the central water region of the SE IPT (based on the 94-CIC configuration).

Clearly, for this LEU fuel concept, the relative thermal flux is reduced for LEU vs HEU in both locations. However, to be able to make comparisons of different approaches, it is necessary to quantify the thermal flux and the penalty associated with the LEU thermal flux relative to the HEU simulation. For the purposes of comparison, the thermal flux is defined as the integrated neutron flux from 0 to 1.25eV. Hence, the thermal flux has been defined in this work as:

$$ f_{\phi_{th}} = \int_{0}^{1.25 eV} \phi(E)dE = \sum_{g\ 175}^{238} \phi_g $$

where group fluxes were accumulated using the SCALE 238-group energy structure, and group 175 is the group with an upper boundary of 1.25 eV within this library. The thermal penalty was then defined as:

$$ P_{th} = 1 - \frac{f_{\phi_{th}}(LEU)}{f_{\phi_{th}}(HEU)} \times 100\% $$

Table 4 lists relative thermal fluxes for both HEU and graded enrichment LEU cores. If these two configurations bound all irradiation locations, then a 9-16% relative thermal flux reduction would be expected in an ATR core fueled with this design. However, it is important to note that

52

these fluxes and the flux ratio will undoubtedly change with burnup, which will require additional study.

Table 4. Integrated Thermal Fluxes and Flux Changes for Graded LEU Configuration

	NW IPT	SE IPT
LEU Thermal Flux (per source neutron)	1.091E-04	1.917E-04
HEU Thermal Flux (per source neutron)	1.300E-04	2.109E-04
Thermal Flux Reduction (%)	16.1	9.1

Next a study of fuel behavior as a function of burnup is appropriate. As a starting point, a single cycle (50 d), high power (250 MW) depletion calculation was performed for HEU and LEU fuels. The TRITON t6-depl sequence of SCALE was used in these analyses, using KENO-VI 3D Monte Carlo transport coupled with ORIGEN depletion. Because of the scoping nature of these studies and the time required to complete detailed 3D depletion calculations, KENO was run with 2×10^6 neutron histories. In addition, shim positions were fixed for the entire calculation – an initial OSCC position was selected such that BOL core reactivities would be similar. Figure 6 is a plot of k_{eff} as function of time for the nominal HEU core and the graded enrichment LEU core. The relatively flat reactivity change region from roughly 5 to 25 days on the HEU curve is a result of the burnup of ^{10}B in the fuel.

Use of a burnable poison, which causes the relatively flat reactivity change region from roughly 5 to 25 days on the HEU curve, could be used in conjunction with graded enrichment to further extend the life of LEU fuel by adding additional ^{235}U to the fuel. Although not studied here, earlier work by Chang[1] indicates that it is perhaps feasible. Although the initial calculations described here showed that B_4C poisoning could not be effectively applied with 13 mils of 19.75 wt % fuel, Chang shows that B_4C could be added in conjunction with reduced ^{235}U inventory in the poisoned plate locations. KENO calculations performed with the Chang fuel design are described in the following subsection.
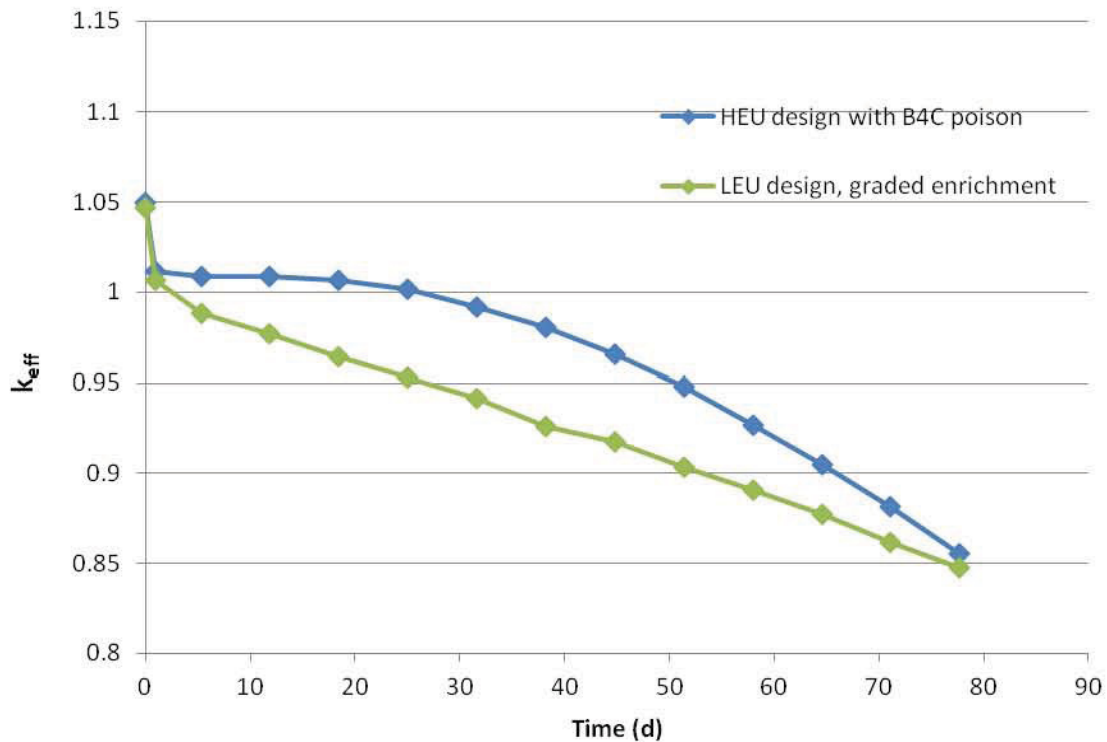
Modified Fuel Plate Thickness with B_4C Poison (Chang) Design

As mentioned above, previous work performed by Chang[1] has shown that another fuel design (using reduced fuel plate thicknesses combined with B_4C poisoning in four innermost and outermost plates) is also feasible. Because analysis of this model with KENO-VI would provide a mechanism for comparison to earlier MCNP calculation, and would reinforce validation of KENO analysis, the decision was made to perform additional scoping analysis for this fuel design.

Table 5 lists the fuel region thickness and ^{10}B mass provided by the Case-C LEU design of Ref. 1. The corresponding number density of natural boron used in KENO-VI calculations is listed in the last column of the table; the model used B_4C homogenized within the fuel material. Chang's model assumed 19.70 wt. % enrichment rather than the 19.75 wt. % used in plates 6-15 of the graded enrichment LEU model; hence for consistency a 19.70 wt. % enrichment was used in the KENO-VI models described here.

The analysis reported in Ref. 1 were based on a 1/8 core model. KENO-VI calculations performed thus far and described earlier are based on a full-core model, which in turn was based on a validated 94-CIC model. Thus calculations performed here are also based on a full-core model, and may show slight differences from the results reported in Ref. 1. Differences in the configurations for each of the experiment tubes will cause variations in the flux profile around the core, and will result in slightly different average fluxes relative to 1/8 modeling.

Analysis of this design began with calculation of the radial power profile. This calculation is currently being rerun with changes made in B_4C number densities (as listed in Table 5).

However, minimum and maximum reactivities for the Case-C LEU design from Ref 1 (referred to hereafter as the reduced fuel thickness LEU design) have been computed and are compared to the standard HEU fuel in Table 6. Note that because of the of the borated fuel, this fuel assembly design has significantly less excess reactivity. Hence, other core modifications may be necessary to support the use of borated LEU fuel; however, that is beyond the scope of the current study.

Table 5. Fuel Plate ^{235}U Enrichment for Graded LEU Design

Fuel Plate No.	Fuel meat thickness (mils)[a]	^{10}B Mass (g)[a]	Corresponding number densities in B$_4$C (atoms/b-cm)[b]	
		0.063	^{10}B	3.39496E-04
			^{11}B	1.36652E-03
Plate 1	7.8		C	4.26503E-04
		0.178	^{10}B	6.13898E-04
			^{11}B	2.47102E-03
Plate 2	10.4		C	7.71230E-04
		0.044	^{10}B	3.16145E-04
			^{11}B	1.27253E-03
Plate 3	11.7		C	3.97168E-04
		0.005	^{10}B	1.53966E-05
			^{11}B	6.19736E-05
Plate 4	11.7		C	1.93426E-05
Plates 5-15	13.0	0.000	0.0000E-00	
		0.001	^{10}B	2.33030E-06
			^{11}B	9.37979E-06
Plate 16	11.7		C	2.92752E-06
		0.033	^{10}B	8.89157E-05
			^{11}B	3.57897E-04
Plate 17	10.4		C	1.11703E-04
		0.133	^{10}B	3.18540E-04
			^{11}B	1.28216E-03
Plate 18	7.8		C	4.00176E-04
		0.343	^{10}B	9.53998E-04
			^{11}B	3.83997E-03
Plate 19	6.5		C	1.19849E-03

[a]From Ref. 1.
[b]Calculated number densities for elements in B$_4$C to obtain specified ^{10}B mass.

Table 6. Comparison of Fresh Core Reactivities for HEU and Reduced Fuel Thickness LEU.

Fuel type/Control state	k_{eff}
HEU (based on 94-CIC specs)	
160° OSCCs, neck shims out	1.12104 + or - 0.00065
0° OSCCs, neck shims in	0.97495 + or - 0.00057
LEU (reduced fuel thickness)	
160° OSCCs, neck shims out	1.06598 + or - 0.00086
0° OSCCs, neck shims in	0.93847 + or - 0.00086

References

1. G. S. Chang M. A. Lillo R. G. Ambrosek, "Neutronics and Thermal Hydraulics Study for Using a Low-Enriched Uranium Core in the Advanced Test Reactor 2008 Final Report," INL/EXT-08-13980, Idaho National Laboratory, June 2008.

ATR LEU MONOLITHIC FOIL-TYPE FUEL WITH INTEGRAL CLADDING BURNABLE ABSORBER DESIGN – NEUTRONICS PERFORMANCE EVALUATION

Gray S. Chang
Idaho National Laboratory
2525 N. Fremont Ave.
Idaho Falls, ID 83415-3870
Email: gray.chang@inl.gov

ABSTRACT

The Advanced Test Reactor (ATR), currently operating in the United States, is used for material testing at very high neutron fluxes. Powered with highly enriched uranium (HEU), the ATR has a maximum thermal power rating of 250 MWth. Because of the large test volumes located in high flux areas, the ATR is an ideal candidate for assessing the feasibility of converting HEU driven reactor cores to low-enriched uranium (LEU) cores. The burnable absorber – ^{10}B, was added in the inner and outer plates to reduce the initial excess reactivity, and to improve the peak ratio of the inner/outer heat flux. The present work investigates the LEU Monolithic foil-type fuel with ^{10}B Integral Cladding Burnable Absorber (ICBA) design and evaluates the subsequent neutronics operating effects of this proposed fuel designs.

1.   Introduction

The Advanced Test Reactor (ATR) at the Idaho National Laboratory (INL) is a high power density and high neutron flux research reactor operating in the United States. Powered with highly enriched uranium (HEU), the ATR has a maximum thermal power rating of 250 MWth with a maximum unperturbed thermal neutron flux rating of 1.0×10^{15} n/cm^2-s. The conversion of nuclear test reactors currently fueled with HEU to operate with low-enriched uranium (LEU) is being addressed by the reduced enrichment for research and test reactors (RERTR) program.

The scope of this task is to assess the feasibility of converting the ATR HEU fuel to LEU fuel while retaining all key functional and safety characteristics of the reactor. Using the current HEU ^{235}U enrichment of 93.0 % as a baseline, this study will evaluate the LEU uranium density required in the fuel meat to yield an equivalent K-eff between the ATR HEU core and an LEU core after 150 effective full power days (EFPD) of operation with a total core power of 115 MW. A lobe power of 23 MW is assumed for each of the five lobes. Then, the LEU ^{235}U loading that yields an equivalent K-eff as the HEU ^{235}U loading will be used to predict radial, axial, and azimuthal power distributions. ^{10}B loading for LEU case studies will have 0.635 g in the LEU fuel meat at the inner 2 fuel plates (1-2) and outer 2 fuel plates (18-19), which can achieve peak to average ratios similar to those for the ATR reference HEU case study. The investigation of this paper shows the optimized LEU Monolithic (U-10Mo) Foil-type with Integral Cladding

Burnable Absorber (ICBA) (MF-ICBA) case can meet the LEU conversion objectives. The heat rate distributions will also be evaluated for this core and used to predict the core performance as it relates to the current Upgraded Final Safety Analysis Report (UFSAR) and the associated Technical Safety Requirements (TSRs).

2.   MCNP ATR Fuel Plate-by-Plate Full Core Model

The ATR CIC-1994 (NT-3 of Cycle 103A-2) core configuration was chosen[1] to built the ATR MCNP full core model in this work. The ATR was loaded with 40 new (fresh) type 7F fuel elements. The Large Inpile Tube (LIPT) in the northwest flux trap was loaded with a flux monitor wire holder with IR-1, 2, 3, and 4. The Standard Inpile Tube (SIPT) in the north, west, southwest, and southeast flux traps had stainless steel flow tubes installed. The northeast flux trap was loaded with the 23-position Large Irradiation Housing Assembly (LIHA), with aluminum fillers in positions NE-2, NE-9 and NE-15 through NE-21, with Low Specific Activity (LSA) Cobalt capsule trains loaded in positions NE-3, NE-5 through NE-7, NE-10, NE-12 through NE-14, and NE-22, and the remaining positions (NE-1, NE-4, NE-8, NE-11, and NE-23) containing flux monitor wire holders. Six of the Small Irradiation Housing Assembly (SIHA) positions in the east flux trap were loaded with LSA Cobalt. Positions H-1, H-4, H-5, H-7 through H-9, H-12, H-13, H-15, and H-16 were loaded with LSA Cobalt. For the detailed Cycle 103A-2 core configuration data refers to Table 1 in ECAR-1357.

The built detailed 19 fuel plate-by-plate and Integral ICBA ATR full core MCNP model is shown in Figure 1. This model is used to optimize the ^{235}U and minimize ^{10}B loading in the LEU core by minimizing the K-eff differences with respect to the HEU core after 150 EFPD of operation with a total core power of 115 MW (23 MW per lobe).
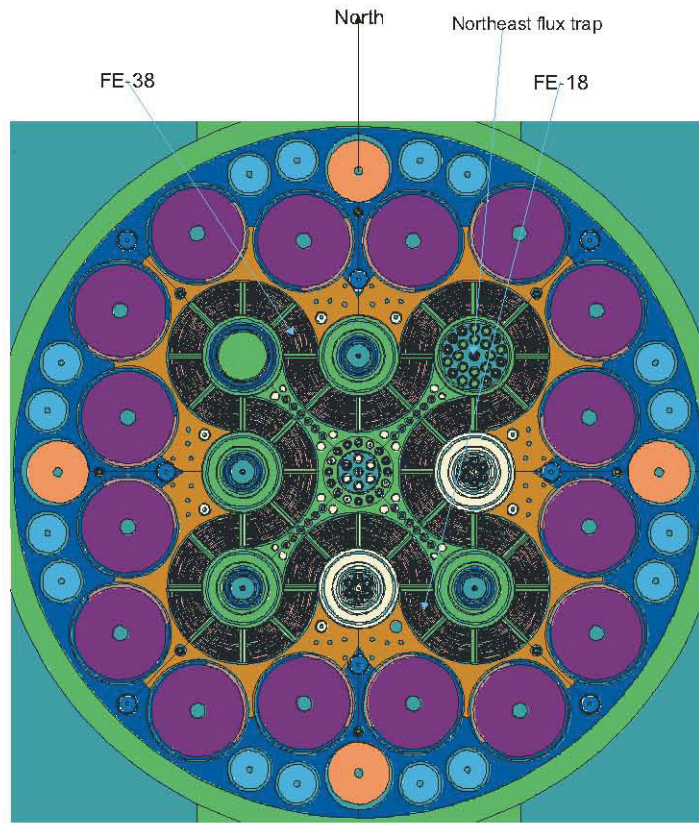
Figure 1. ATR MCNP full core model with 19 fuel plates per fuel element.

4.   MCWO – Fuel Burnup Analysis Tool

The fuel burnup analysis tool used in this study consists of a BASH (Bourne Again Shell) script file that links together the two FORTRAN data processing programs, m2o.f and o2m.f. [5] This burnup methodology couples the Monte Carlo transport code MCNP [6,7] with the radioactive decay and burnup code ORIGEN2. [8] The methodology is known as <u>M</u>onte <u>C</u>arlo <u>w</u>ith <u>O</u>RIGEN2, or MCWO. [4,9]

The MCWO methodology produces criticality and burnup data based on various material feed/removal specifications, core power(s), and irradiation time intervals. MCWO processes user-specified input for geometry, initial material compositions, feed/removal specifications, and other problem-specific parameters.

The MCWO methodology uses MCNP-calculated one-group microscopic cross sections and fluxes as input to a series of ORIGEN2 burnup calculations. ORIGEN2 depletes/activates materials and generates isotopic compositions for subsequent MCNP calculations.

MCWO performs one MCNP and one or more ORIGEN2 calculations for each user-specified time step. Due to the highly time-dependent nature of the physics parameters and material compositions of the modeled reactor system, the MCWO-calculated results are typically more accurate if long irradiation cycles are broken up into smaller intervals. It should be noted that an increase in the number of ORIGEN2 calculation steps does not significantly impact the overall MCWO execution time because MCNP dominates the MCWO execution time.

For each MCNP calculation step, MCNP updates the fission power distribution and burnup-dependent cross sections for each fuel plate, then transfers the data to ORIGEN2 for cell-wise depletion calculations. The MCNP-generated reaction rates are integrated over the continuous-energy nuclear data and the space within the region.

5.   ATR HEU Reference Case and LEU MF-ICBA Models Description

The typical ATR 7F fuel element (FE) was chosen in the HEU reference case model. The detailed 19 plate FE model with burnable absorbers is described in Section 5.1. Then, the proposed LEU Monolithic Foil-type and Integral Cladding Burnable Absorber (MF-ICBA) detailed FE model is described in Section 5.2.

5.1   Detailed ATR 7F Fuel Element Model

ATR has four fuel element types, which are designated 7F, 7NB, 7NBH, and YA. [10] They are all versions of the zone loaded fuel element design and are identically constructed, varying only in the content of the fuel matrix. The 7F FE was chosen as the reference HEU Case-A in this study. Table 1 shows the nominal ^{235}U and ^{10}B loadings for each fuel plate of the 7F FE. In the 7F fuel element, all 19 fuel plates are loaded with 93% enriched uranium in an aluminum matrix to a total of 1075 g U-235. The eight outer plates (plate-1 to plate-4 and plate-16 to plate-19) contain boron as a burnable poison for a total of 0.66 g ^{10}B. The detailed HEU FE-18 with 8 fuel plates with ^{10}B (Plates-1 to -4 and -16 to -19) are plotted in Figure 2.

Table 1. Specifications for a ATR reference HEU (^{235}U 93wt%) FE with B-10 in the 4 inner/outer fuel plates.

HEU Plate	Fuel Meat Thickness (mil)	Fuel Meat Volume (cc)	^{235}U Mass (g)	^{10}B Mass (g)	^{235}U Density (g/cc)
Plate-1	20	23.69	24.3	0.063	1.026
Plate-2	20	29.54	29.1	0.078	0.985
Plate-3	20	31.12	38.7	0.044	1.243
Plate-4	20	32.7	40.4	0.045	1.235
Plate-5	20	34.29	52.1	–	1.52
Plate-6	20	35.87	54.6	–	1.522

HEU Plate	Fuel Meat Thickness (mil)	Fuel Meat Volume (cc)	^{235}U Mass (g)	^{10}B Mass (g)	^{235}U Density (g/cc)
Plate-7	20	37.45	57	–	1.522
Plate-8	20	39.03	59.4	–	1.522
Plate-9	20	40.61	61.8	–	1.522
Plate-10	20	42.19	64.2	–	1.522
Plate-11	20	43.78	66.6	–	1.521
Plate-12	20	45.36	69	–	1.521
Plate-13	20	46.94	71.4	–	1.521
Plate-14	20	48.52	73.8	–	1.521
Plate-15	20	50.1	76.3	–	1.523
Plate-16	20	51.69	64	0.071	1.238
Plate-17	20	53.27	65.9	0.073	1.237
Plate-18	20	54.22	53.8	0.143	0.992
Plate-19	20	52.64	52.6	0.143	0.999
Total		792.99	1075	0.66	–
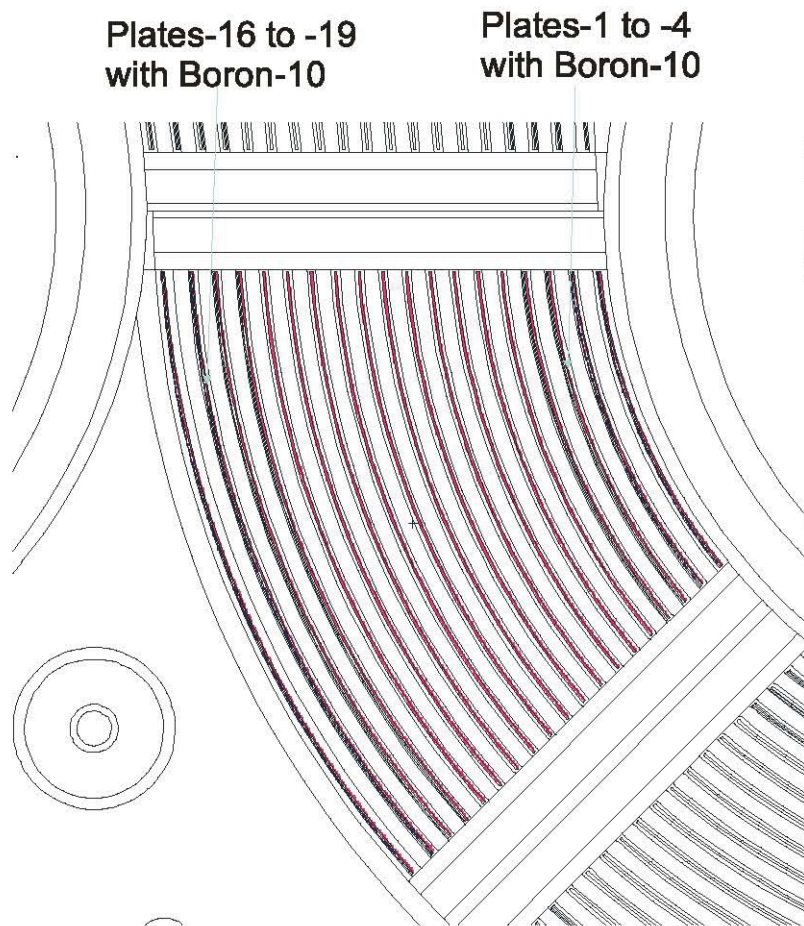
Figure 2. ATR MCNP model HEU-7F FE-18 detail.

The detailed, full core MCNP ATR model was used to perform the evaluation of the ATR reference HEU case with burnable absorber ^{10}B at the beginning of cycle (BOC) condition. Then, MCWO was used to evaluate the fuel cycle performance versus the EFPD using the following assumptions:

- Each nominal operating cycle was 50 EFPD, followed immediately by a seven day outage.
- Each 50 EFPD cycle was subdivided into 5 EFPD time step intervals.
- The OSCC positions were set to 105°.
- The resultant MCNP-calculated tallies were normalized to a core source power of 115 MW.

5.2   LEU Monolithic Foil-type and Integral Cladding Burnable Absorber Detailed FE model

A LEU monolithic fuel design with varied fuel meat thickness in the four inner plates (plate-1 to plate-4) and four outer plates (plate-16 to plate-19) was recommended in Ref. [1. However, those LEU fuel designs did not include the ^{10}B loading minimization. Because the ^{10}B (n,α) reaction will produce Helium-4 (He-4), which can degrade the LEU foil fuel (U10Mo) type fuel performance. An alternative burnable absorber loading option – Integral Cladding Burnable Absorber (ICBA) is proposed in this study. In monolithic plates the fuel-cladding interface is protected with Zr diffusion barrier. Therefore an addition of layer of burable absorber (5 mil) in ICBA was proposed, where the burnable absorber ^{10}B can be totally separated from not only the LEU foil-type fuel meat, but also from the fuel-cladding Zr diffusion barrier.

The optimization was achieved by reducing the fuel meat thickness as well as loading the two inner/outer plates with 0.635 g of ^{10}B in LEU ICBA Case. The isotopic concentration of ^{10}B in the boron of the burnable absorber is 20 wt%. The optimized LEU fuel plate specifications for the ICBA Case are given in Table 2. Table 2 shows that the nominal fuel meat thickness is 0.0330 cm (13 mil). The varied four inner plates (plate-1 to plate-4) fuel meat thicknesses are 0.0203 cm (8 mil), 0.0203 cm (8 mil), 0.0354 cm (10 mil), and 0.0305 cm (12 mil), respectively. While the varied 4 outer plates (plate-16 to plate-19) fuel meat thicknesses are 0.0305 cm (12 mil), 0.0354 cm (10 mil), 0.0203 cm (8 mil), and 0.0203 cm (8 mil), respectively. The detailed FE-18 model of LEU monolithic foil type ICBA Case is shown in Figure 3. The ^{10}B loading specification of ICBA in plates-1, -2, -18, and -19 are tabulated Table 3. The detailed MF-ICBA FE-18 with 4 fuel plates with ^{10}B (Plates-1 to -2 and -18 to -19) are plotted in Figure 4.

In summary, the ATR MCNP full core model is 3-dimentional (3D) because the axial fission power density and U-235 depletion burnup-dependent profiles are important parameter in controlling the lobe-power allocation and core K-eff during the cycle operation. The effective fuel meat and ICBA plate length is 48 inches. To investigate the axial fission power density and U-235 depletion burnup-dependent profiles impact on the fuel cycle performance, for each fuel element, we divide the fuel meats and Integral Cladding Burnable Absorber (ICBA) plates into 8 evenly divided axial cells. Due to the symmetry of the chopped-cosine shaped power profile, we can combine axial cells-4 and -5 in to one, which does not sacrifice much of the accuracy in the fuel burnup calculation. Therefore, a total of 7 axial cells per each fuel plate are used. With a full core of 40 fuel elements, there are 40 x 19 x 7 = 5320 fuel depletion cells. There are a total of 40 x 4 x 7 = 1120 ICBA ^{10}B depletion cells. The monolithic foil-type with ICBA 7-axial divided cells model has been through a series of de-bug processes. The verified model is in the attached file: icbaf1. In the first phase of the ATR LEU fuel cycle performance analysis, the MCNP-3D full core model (icx1f1) with one axial cell for the fuel meat and ICBA plate was used in this paper.

Table: 2. LEU Monolithic (U10Mo) Foil-type with ICBA (Boron-10) Specification

LEU Plate ID	Fuel Meat Total U g/cc	Thickness mil.	Fuel meat Vol. (cc)	U-235 Mass (g)	Boron_10 Mass (g)	U-235 Density (g/cc)
Plate-1	15.21	8	10.947	32.876	0.058	3.00
Plate-2	15.21	8	11.660	35.016	0.149	3.00
Plate-3	15.21	10	15.367	46.150	0	3.00
Plate-4	15.21	12	16.153	48.512	0	3.00
Plate-5	15.21	13	22.030	66.162	0	3.00
Plate-6	15.21	13	23.057	69.247	0	3.00
Plate-7	15.21	13	24.087	72.339	0	3.00
Plate-8	15.21	13	25.123	75.450	0	3.00
Plate-9	15.21	13	26.150	78.536	0	3.00
Plate-10	15.21	13	27.178	81.623	0	3.00
Plate-11	15.21	13	28.205	84.707	0	3.00
Plate-12	15.21	13	29.237	87.805	0	3.00
Plate-13	15.21	13	30.257	90.869	0	3.00
Plate-14	15.21	13	31.293	93.981	0	3.00
Plate-15	15.21	13	32.315	97.049	0	3.00
Plate-16	15.21	12	25.655	77.049	0	3.00
Plate-17	15.21	10	26.444	79.417	0	3.00
Plate-18	15.21	8	21.789	65.439	0.111	3.00
Plate-19	15.21	8	22.544	67.704	0.317	3.00
Total			449.490	1349.931	0.636	

Notes: Only 4 Plates-1, -2, -18, and -19 are the Integral Cladding Burnable Absorber (ICBA) with Boron-10.
The proposed Monolithic foil type fuels are well developed fuel types.

Table: 3. Integral Cladding Burnable Absorber (ICBA) with Boron-10 Specification

ICBA ID	Boron-10 g/cc	Thickness mil.	ICBA Vol. (cc)	Boron-10 Mass (g)
ICBA-01	0.008	5	6.888	0.058
ICBA-02	0.020	5	7.332	0.149
ICBA-18	0.008	5	13.663	0.111
ICBA-19	0.022	5	14.138	0.317
Total			42.021	0.635
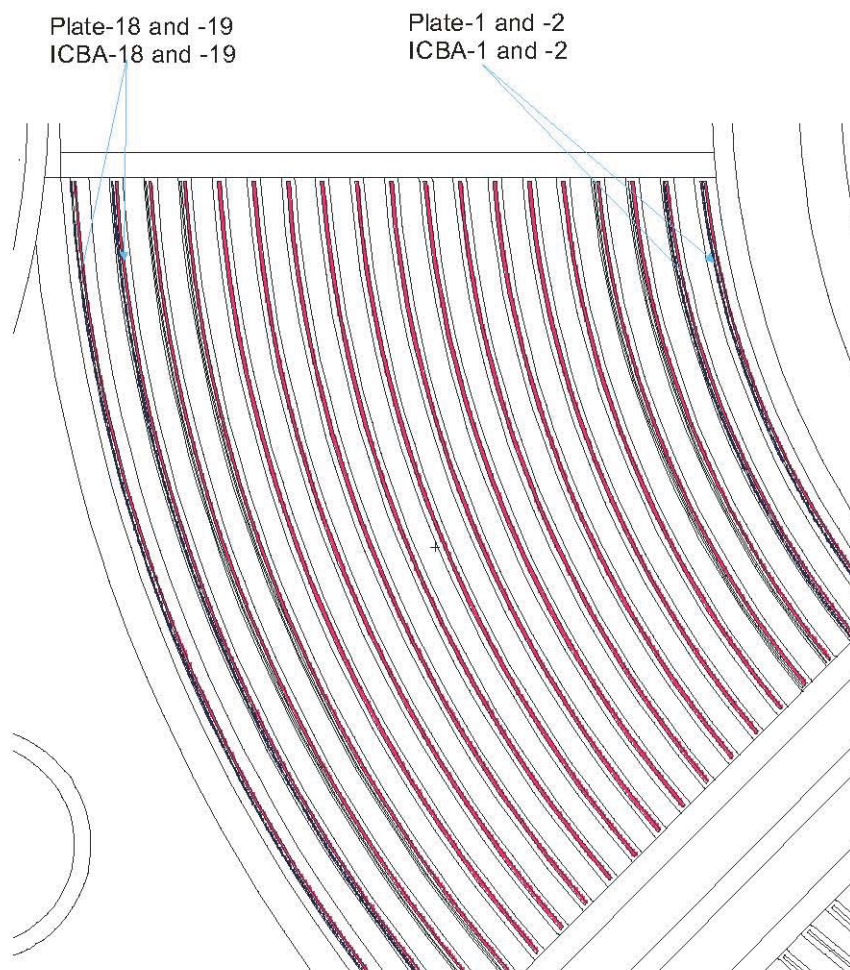
Figure 3. Monolithic foil-type with ICBA fuel element detailed configuration.
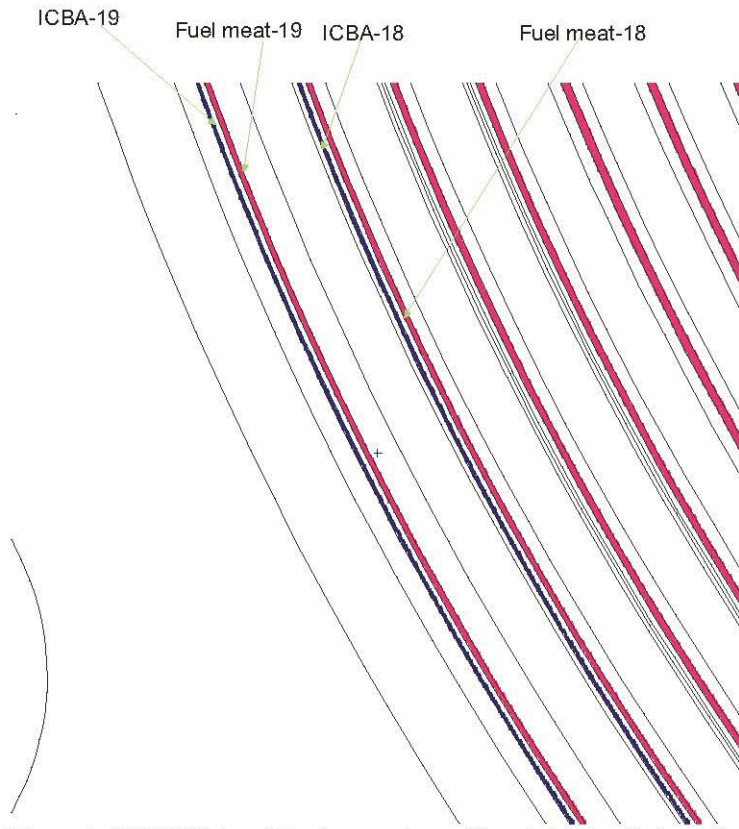
Figure 4. LEU ICBA and Fuel meat plates-18 and -19 detailed configuration.

6. HEU Reference Case and LEU Monolithic foil-type with ICBA Fuel Neutronics Performance Evaluation

For Case-C, the LEU dispersed (U7Mo) fuel type, the ^{235}U loading in the inner and outer four plates was varied. Based upon the comparison between Case-A , Case-B, and Case-C relative heat flux L2AR profiles, the ^{235}U contents and fuel meat thickness of the inner/outer plates were evaluated and optimized in order to reduce the difference of K-eff profiles versus EFPD and LEU fuel peak heat flux L2AR. The LEU fuel loading was optimized such that the L2AR at the four inner/outer plates closely matches the ATR reference HEU Case-A.

The optimization was based upon a comparison of the MCWO-calculated K-eff versus EFPD and the radial power L2AR profile for various LEU fuel and ^{10}B loading schemes. In order to reduce the ^{10}B depletion impact on the fuel plate performance, ^{10}B was modeled in the two inner plates (plate-1 and plate-2) and two outer plates (plate-18 and plate-19). The LEU fuel (^{235}U enrichment 19.7wt%) loading schemes included varying parameters such as fuel meat thickness within the monolithic U10-Mo LEU fuel type as Case-B.

6.1 HEU Reference Case and LEU MF-ICBA Radial Fission Power Profiles Versus Burnup

The above tables, Table 2 and Table 3, summarize the fuel and ^{10}B minimization loading parameter variations that resulted in the flattest radial fission heat profile while still maintaining sufficient reactivity within the LEU core. Not surprisingly, the optimal LEU fuel loading is similar to the HEU reference case. The optimal LEU fuel loading has thinner plates at the inner/outer plate positions. For the purposes of determining the feasibility of HEU to LEU conversion, the present study demonstrates a satisfactory loading scheme to achieve acceptable reactivity for three nominal 50 EFPD fuel cycles as well as maintain the radial heat flux L2AR profile.

The MCWO fuel burnup analysis code was used to calculate the relative radial plate fission power heat flux for the HEU Case-A and LEU Case-B at the beginning of the first cycle (BOC), 1st End of Cycle (EOC), 2nd, and 3rd EOC. For Fe-18 at BOC, the respective peak heat fluxes L2AR for Case-A and Case-B were determined to be 1.25 and 1.20, respectively, as shown in Figure 5. Figure 5 also indicates that HEU Case-A and LEU Case-B have a very similar fission power density profiles.

Results for Case-A and Case-B at the 1st, 2nd, and 3rd EOC are plotted in Figures 6, 7, and 8. These plot demonstrates that Case-A and Case-B yield very similar radial L2AR profiles versus burnup. Figures also indicate that the fission power density profiles are flattened toward the discharged burnup. These studies indicate that the LEU radial L2AR profiles can achieve flattened profiles bounded by HEU reference Case-A by varying fuel meat thickness of the inner/outer 2 plates. However, the fission power density (W/cm^3) L2AR profiles for the LEU cases with varied fuel meat thickness produced larger peaks within the inner/outer plates. This power density peaking will not result in a large, undesirable heat flux profile.

68
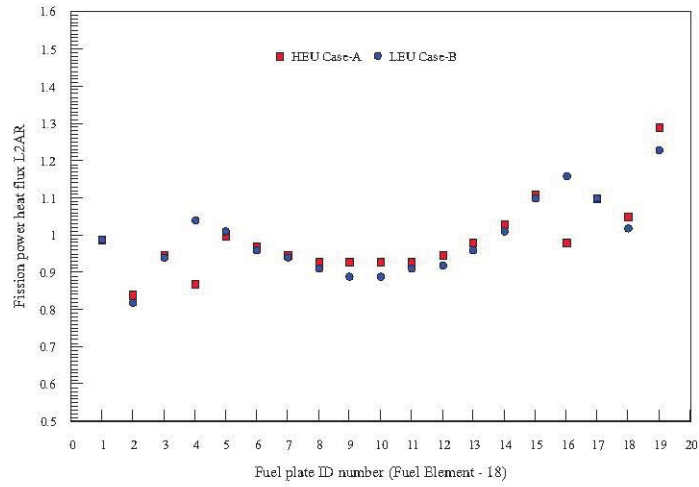
Figure 5. Fission power heat flux L2AR radial profiles for HEU Case-A and optimized LEU Case-B at BOC.
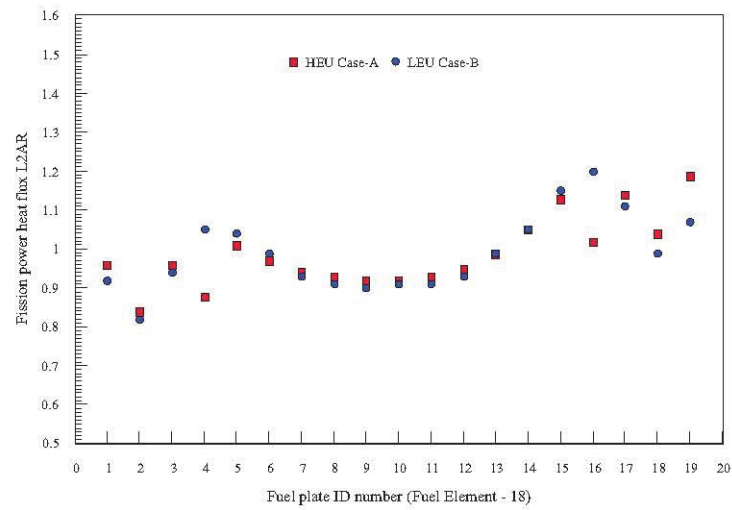
Figure 6. Fission power heat flux L2AR radial profiles for HEU Case-A and optimized LEU Case-B at 1st EOC.
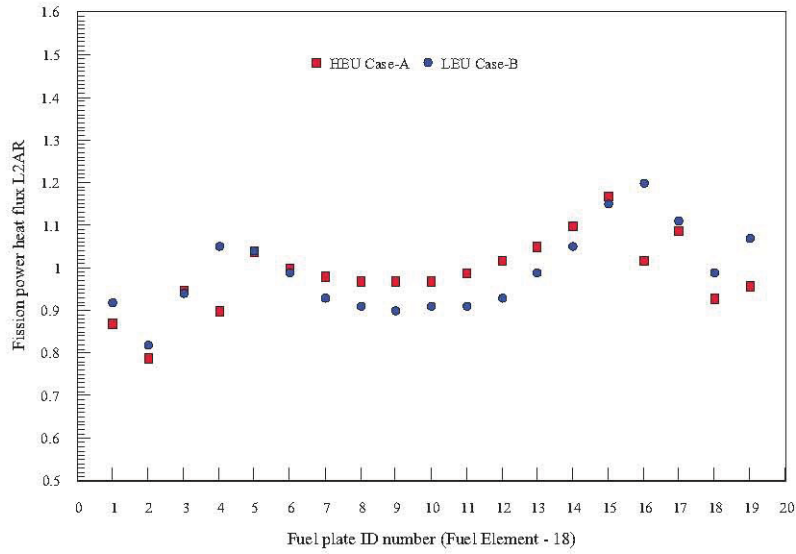
Figure 7. Fission power heat flux L2AR radial profiles for HEU Case-A and optimized LEU Case-B at 2nd EOC.
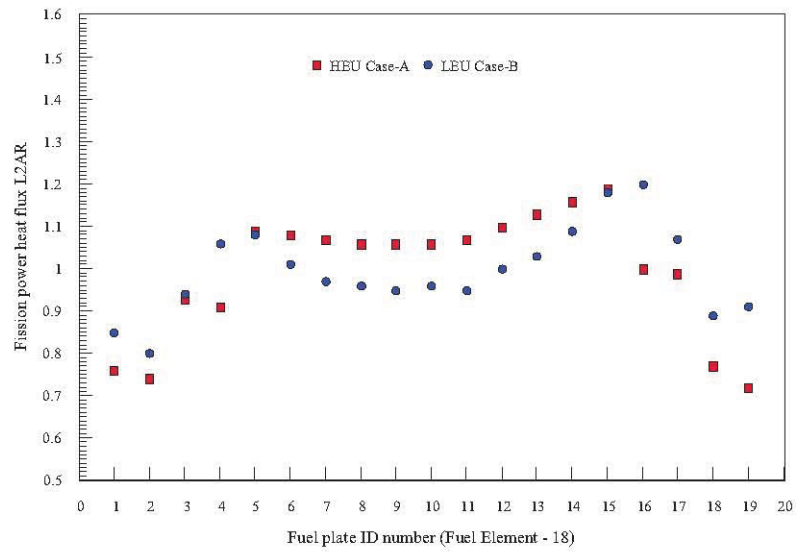
Figure 8. Fission power heat flux L2AR radial profiles for HEU Case-A and optimized LEU Case-B at 3rd EOC.

6.2   HEU Reference Case and Optimized LEU Case K-eff versus EFPD

Using the optimized LEU fuel loading, the MCWO-calculated K-eff for LEU Case-B as a function of EFPD as compared to the ATR reference HEU Case-A is shown in Figure 9. Note that the LEU fuels contain 80.25 wt% U-238, which can be transmuted to Pu-239. Although the LEU cases have a lower K-eff at the BOC when compared with HEU Case-A, the LEU cases sustain operation for the same EFPD as HEU Case-A (150 EFPD). The K-eff of HEU Case-A with and without ^{10}B at BOC are 1.1025 and 1.1969, respectively, which represents a hold-down reactivity of $9.94. While, the K-eff of LEU Case-B with and without ^{10}B at BOC are 1.0625 and 1.1389, respectively, which represents a hold-down reactivity of $8.77. The Figure 9 indicates that Case-A and Case-B has a small K-eff difference toward the end of three cycles EFPDs.
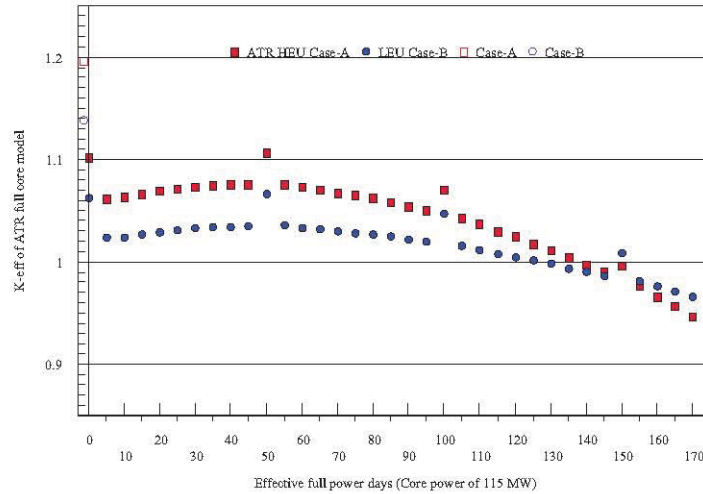
Figure 9. MCWO-calculated K-eff versus EFPD for ATR reference HEU Case-A and optimized LEU Case-B.

For a typical ATR new core fuel loading consists of about 1/3 fresh, 1/3 once-burnt at 1st EOC, and 1/3 twice-burnt at 2nd EOC fuel elements. Although the K-eff of all 40 fuel elements approaching the discharged burnup is about 0.988, which is less than 1. We believe (In phase-II, the LEU fuel cycle performance analysis can validate that it is the case.) that the typical new core fuel loading can provide an adequate K-eff for the complete cycle operation.

7.   Conclusion and Recommendations

The detailed plate-by-plate MCNP ATR full core model used in this study handles complex spectral transitions at the boundaries between the plates in a straight forward manner. The MCWO-calculated K-eff versus EFPD results indicate that LEU Case-B provide adequate excess

reactivity versus burnup while providing fission heat profiles similar to the ATR reference HEU Case-A. The LEU core conversion designer will be able to optimize the ^{235}U fuel loading so that the K-eff and relative radial fission heat flux profile are similar to Case-A. To achieve the flattened heat flux profile, the LEU monolithic core designer can fix the ^{235}U enrichment of 19.75wt% and vary the thickness of the four inner/outer plates, as well as adjust the amount of burnable absorber in the two inner/outer plates. The investigation of this paper shows the optimized LEU Monolithic (U-10Mo) case can all meet the LEU conversion objectives. As a result, it has been concluded that LEU core conversion for the ATR is feasible.

The LEU core designer can use the detailed plate-by-plate MCNP ATR full core model to optimize the ^{235}U loading by either minimizing K-eff differences with respect to the HEU core during the 150 EFPD of operation at a total core power of 115 MW (23 MW per lobe), or by reducing the higher L2AR of heat flux at the inner/outer plates. However, to demonstrate that the LEU core fuel cycle performance can meet the UFSAR safety requirement, a further study will be necessary in order to investigate the detailed radial, axial, and azimuthal heat flux profile variations versus EFPD. In addition, the safety parameters such as void reactivity and Doppler coefficients, control components worth (outer shim control cylinders, safety rods and regulating rod), and shutdown margins between the LEU cores need to be evaluated in depth.

8.   References

[1]   G. S. Chang, M. A. Lillo, R. G. Ambrosek (retired), 'Neutronics and Thermal Hydraulics Study for Using a Low-Enriched Uranium Core in the Advanced Test Reactor 2008 Final Report,' INL/EXT-08-13980, June 2008.

[2]   Roth, P. A., 2004a, letter to J. D. Abrashoff, PAR-17-04, revision 1, "Startup Outer Shim Prediction for ATR Cycle 134A-1, Revision 1," December 20, 2004.

[3]   ASUDAS report from DAC Hourly Control History for Cycle 134A-1/A-2 End of Cycle; provided by email from D. V. Thomas to M. A. Lillo, July 11, 2005.

[4]   Cook W. C., Smith A. C., "ATR CSAP Package on the Workstation Version 1," PG-T-96-002, May, 1996.

[5]   G. S. Chang, "MCWO - LINKING MCNP AND ORIGEN2 FOR FUEL BURNUP ANALYSIS," Proceedings of 'The Monte Carlo Method: Versatility Unbounded In A Dynamic Computing World,' Chattanooga, Tennessee, April 17–21, 2005, on CD-ROM, American Nuclear Society, LaGrange Park, IL (2005).

[6]   Tim Goorley, Jeff Bull, Forrest Brown, et. al., "Release of MCNP5_RSICC_1.30," MCNP Monte Carlo Team X-5, LA-UR-04-4519, Los Alamos National Laboratory, November 2004.

[7]   X-5 Monte Carlo Team, "MCNP—A General Monte Carlo N-Particle Transport Code, Version 5," Volume I (LA-UR-03-1987) and Volume II (LA-CP-0245), Los Alamos National Laboratory April 24, 2003 (Revised 6/30/2004).

[8]   G. Croff, "ORIGEN2: A Versatile Computer Code for Calculating the Nuclide Compositions and Characteristics of Nuclear Materials, Nuclear Technology," Vol. 62, pp. 335-352, 1983.

[9]   G. S. Chang and J. M. Ryskamp, "Depletion Analysis of Mixed Oxide Fuel Pins in Light Water Reactors and the Advanced Test Reactor," Nucl. Technol., Vol. 129, No. 3, p. 326-337 (2000).

[10]   Safety Analysis Report, "Safety Analysis Report for the Advanced Test Reactor," Idaho National Laboratory, SAR-153, Nov. 2003.

[11]   G. S. Chang, M. A. Lillo, "MCWO Neutronics Analysis of RERTR Full Element Demonstration in Position 38 of the ATR," Idaho National Laboratory ECAR-1357, Rev. 1, June 2011.

Appendix B – Analysis of Candidate LEU Fuel Designs for ATR

Mark D. DeHart
Reactor Analysis and Design Department

TEM-10200-1
02/20/2012
Rev. 00

**ENGINEERING CALCULATIONS
AND ANALYSIS REPORT**

Page 1 of 52

Title:	**Analysis of Candidate LEU Fuel Designs for ATR**					
ECAR No.:	ECAR-1997	ECAR Rev. No.: 0		Project File No.: XXXXX		Date: 8/29/2012

Engineering Calculations and Analysis

ECAR Title:	Analysis of Candidate LEU Fuel Designs for ATR	
ECAR No.:	ECAR-1997	

	(Name)	(Organization)	(Signature)	(Date)
Performers:	Mark D. DeHart	C100		9/5/12
Checker[1]:	Gray S. Chang	C100		09/05/20
Independent Peer Reviewer[2]:	David W. Nigg	C100		9/05/2012
CUI Reviewer:	N/A			
Principal Investigator[3]:	David W. Nigg	C100		9/05/2012
Owner[4]:	Sean R. Morrell	D200		9/12/12
Nuclear Safety[4]:	N/A			
Cognizant Engineer[4]:	N/A			

1. Introduction

A number of activities related to Low-Enriched Uranium (LEU) fuel design for the Advanced Test Reactor (ATR) are underway at the Idaho National Laboratory (INL) under the auspices of the Reduced Enrichment Research Test and Training Reactor (RERTR) Program. The primary focus to date has been on computational and experimental materials performance studies for uranium-molybdenum composites. A fuel element design based on a U-10Mo composite has been proposed with a 13 mil fuel plate thickness encased in 1 mil zirconium centered in 50 mil Al 6061 plates. This fuel has been proposed as the basis for the Full Element (FE) fuel assembly test planned for initial neutronics evaluation in the Advanced Test Reactor Critical Facility (ATRC), followed by insertion and irradiation in the ATR.

Experimental work has been supplemented by a number of computational RERTR fuel studies to determine potential performance of different fuel designs covering a broad range of fuel characteristics. A range of computational neutronics studies to support the possible conversion of the ATR to LEU have also been performed. [1-5] Simultaneously, INL is engaged in a physics methods upgrade project to put into place modern computational neutronics tools for future support of ATR fuel cycle and experiment analysis. The computational methods selected include Helios [6], Attila [7], Serpent [8] and portions of the SCALE code system [9] for reactor physics calculations. MCNP [10], long used for detailed ATR analysis, will also be employed in ATR analysis for independent confirmation of computational models. A number of experimental measurements have been performed in the ATRC in support of the methods upgrade project, and are being used to validate the new core physics methods.

The current computational neutronics work is focused on performance of scoping calculations for the ATR core loaded with a candidate LEU fuel design, using the tools identified above. In the absence of a final fuel element design, the emphasis has been placed on development of candidate designs informed by ATR operational requirements, and on evaluation of the reactor physics performance of such cores. Ultimately, the goal of this work is to complete a preliminary assessment of the capabilities of new core analysis methods for LEU fuel. Note that a complete assessment will ultimately require measured in-core data with as-designed LEU fuel for code validation. Initially, it is planned to obtain some early neutronics measurements for LEU fuel in the ATR via coordination with the FE experiment mentioned previously.

One of the most significant challenges in fuel design for the conversion of the ATR to LEU fuel is the nature of reactivity control for fresh fuel. To be able to run three full cycles, ATR fuel elements have historically used burnable poisons to control excess reactivity. Control of the excess reactivity in the current HEU design is accomplished by boron poisons integrated into the U-Al fuel matrix. However, for the U-10Mo fuel matrix, boron cannot be added due to materials performance issues. Studies of the use of a distinct B_4C foil located outside the fuel meat have been performed [4], but performance concerns remain due to helium production as a result of neutron capture in boron, resulting in fuel plate failure. More recent studies (as yet unpublished) have studied the potential for reactivity control by either using a borated aluminum for fuel element side plates, or by placement of thin cadmium wires within the side plates.

The use of boron foils manufactured within fuel plates has been shown to be acceptable from a reactor physics perspective, but in addition to blistering concerns this introduces a manufacturing challenge for fuel plate fabrication. Use of cadmium wires also presents a manufacturing challenge, albeit much less than that required for fuel element fabrication; however, cadmium is also of concern for occupational exposure. Use of borated aluminum would add the need to develop a new material and test its performance, although borated aluminum does have a long history in the nuclear industry. Nevertheless, both appear to be promising options from a reactor physics performance perspective.

A third option that has been recently considered, and which is the initial focus of this study, is the use of hafnium within the zirconium barrier of the current U-10Mo design for reactivity control. The current U-10Mo fuel plate design being considered uses a zirconium diffusion barrier layer outside the fuel. [12] Natural zirconium typically contains approximately 1-2% hafnium; zirconium and hafnium are chemically very similar and difficult to separate – at present an expensive separations process is used to reduce hafnium content in zirconium used for fuel barrier material to less than 40 ppm. In this work, the use of the natural hafnium fraction (perhaps with additional Hf enrichment) in the barrier material for reactivity control is studied.

The goal in this work is to be able to match the performance of a hafnium-based fixed poison design with the current HEU fuel in the ATR from a physics perspective. A number of aspects of performance are studied, including fuel reactivity as a function of time, fuel plate heat source terms as a result of fission, and changes in target region fluxes. Results will show, however, that hafnium poison results in too much negative reactivity near end of life for a core. However, follow-on calculations, described in the Phase II section of this report, show that an unpoisoned fuel element with variable fuel meat thicknesses could provide an acceptable alternative to fuel-element-embedded boron poisoning for power peaking and reactivity control.

This report is divided into three technical sessions. The *Modeling Approach* section provides an overview of the code and models used in the subsequent analyses and initial validation. The section entitled *Phase I: Comparison of Fuel Element Design Performance* describes the initial phase of this study to assess the possibility and impact of a hafnium-poisoned fuel element. Although this concept appeared promising at first, the fact that hafnium is essentially a fixed (as opposed to a burnable) poison over the lifetime of a fuel element, it results in too much negative reactivity toward end of life for a realistic core. The final technical section, *Phase II: Viability of an Alternative Unpoisoned Fuel Element Design*, examines at alternative to the hafnium-poisoned design in which all poisons are removed. These analyses demonstrate that such an approach may be feasible. The final section of the report provides a summary of the results of these calculations.

Modeling Approach

As has been done in previous work, calculations were performed using the benchmark ATR core configuration developed based on the 1994 core internals changeout. [13] Calculations were performed using the Monte Carlo reactor physics code Serpent [8], which is being integrated into the standard set of neutronics codes for ATR analysis. Serpent provides a number of capabilities that makes it a valuable tool for the calculations being performed here, including:

- Robust combinatorial geometry three-dimensional modeling capabilities (similar to MCNP),
- Ability to run multithreaded and MPI-based parallel calculations for speed to obtain a needed level of statistical convergence in a reasonable time period,
- Continuous energy calculations using NJOY-derived data,
- Significantly more efficient and faster than MCNP and SCALE,
- Powerful reaction-rate tally capabilities with little effect on performance,
- Calculation of reactor physics parameters including effective delay neutron fractions and half-lives,
- Built-in depletion capabilities.
- In-line Doppler broadening of resonance materials
- Powerful plotting capabilities for visualization and plotting of reaction rate tallies.

These capabilities made it possible to complete initial analyses within a 2 week period.

Models of the ATR (94-CIC configuration) and the ATRC (recent irradiation experiments) have been developed under separate work; the 94-CIC model was used as a starting point for this work. Figures 1 and 2 show the Serpent model of this configuration. The results of the Serpent calculations are shown in Table 1 for calculations performed using ENDF/B-VII and JEFF 3.1 data. Serpent calculates approximately 0.5% high for both libraries, but this is within the range of propagated nuclear data uncertainties and considered to be in statistical agreement with the measurement (k_{eff} = 1.000). Note that remaining calculations performed in this report are based on ENDF/B-VII, and that for other Serpent models, a calculated value of 1.005 is considered to be critical.

Initially, three fuel element designs were selected for comparison: (1) the current ATR Mark VII (HEU) design, (2) the Integral Clad Burnable Absorber (LEU ICBA) design that was studied in Ref. 4, and (3) new hafnium-poisoned zirconium (LEU HPZ) design. Subsequently, a fourth design was added in which the hafnium was removed from the zirconium barrier (replaced by pure zirconium), and the fuel enrichment reduced to near critical (LEU RE). The reason for this addition will be discussed later in this report. Thus, differences between models are basically a change of thicknesses and material compositions within the 19 fuel plates. Table 2 provides the fuel thicknesses assumed for each fuel design. Other dimensions of the fuel element design were unchanged.

Table 1. Results of Serpent Calculations for the 94-CIC Benchmark [13]

Cross Section Library	k_{eff}	Monte Carlo Statistical Uncertainty (1σ)
ENDF/B-VII	1.00530	± 0.00019
JEFF 3.1	1.00563	± 0.00019
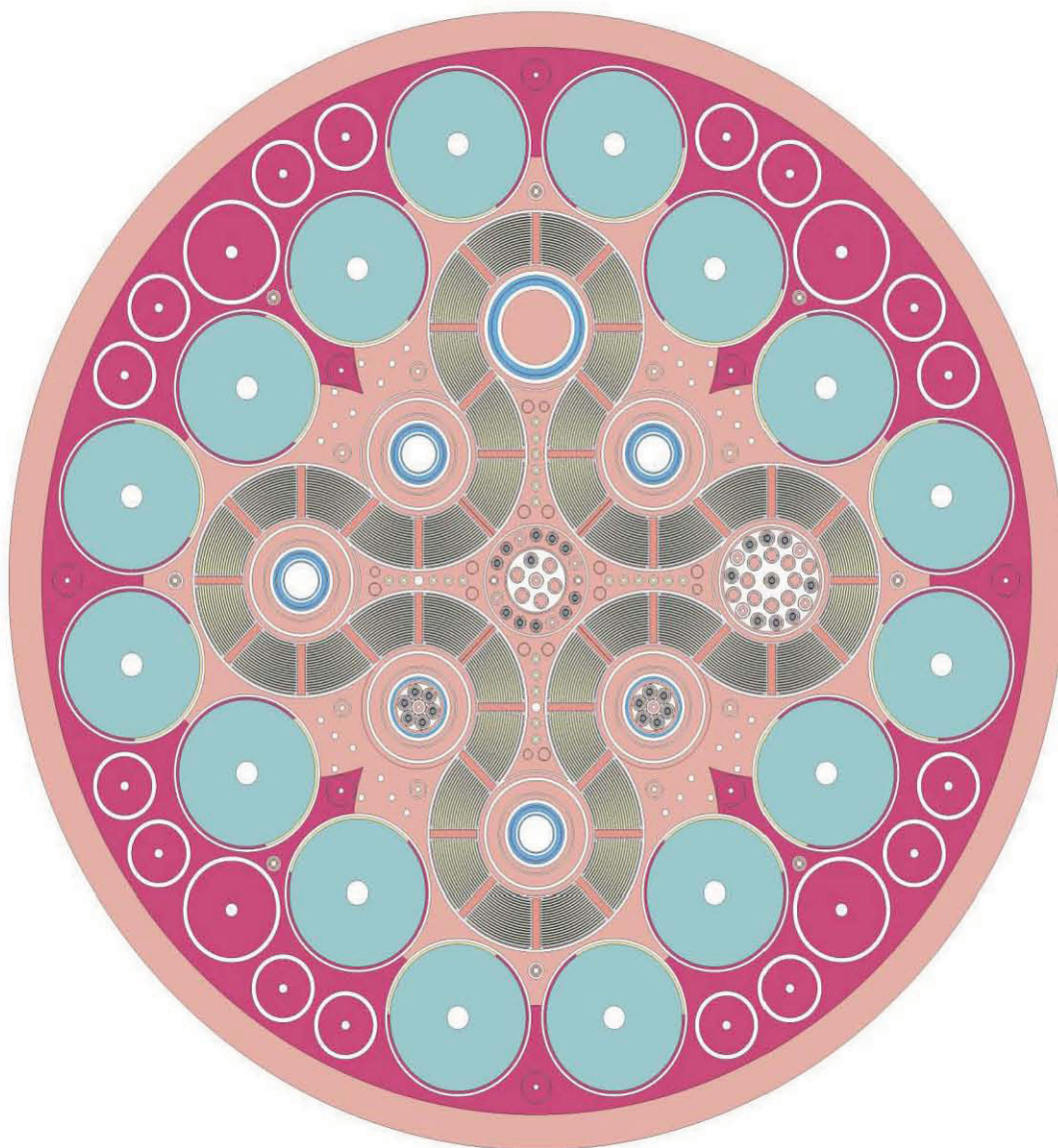
Fig. 1. Serpent model of ATR 94-CIC configuration
(x-y slice at the axial midplane).
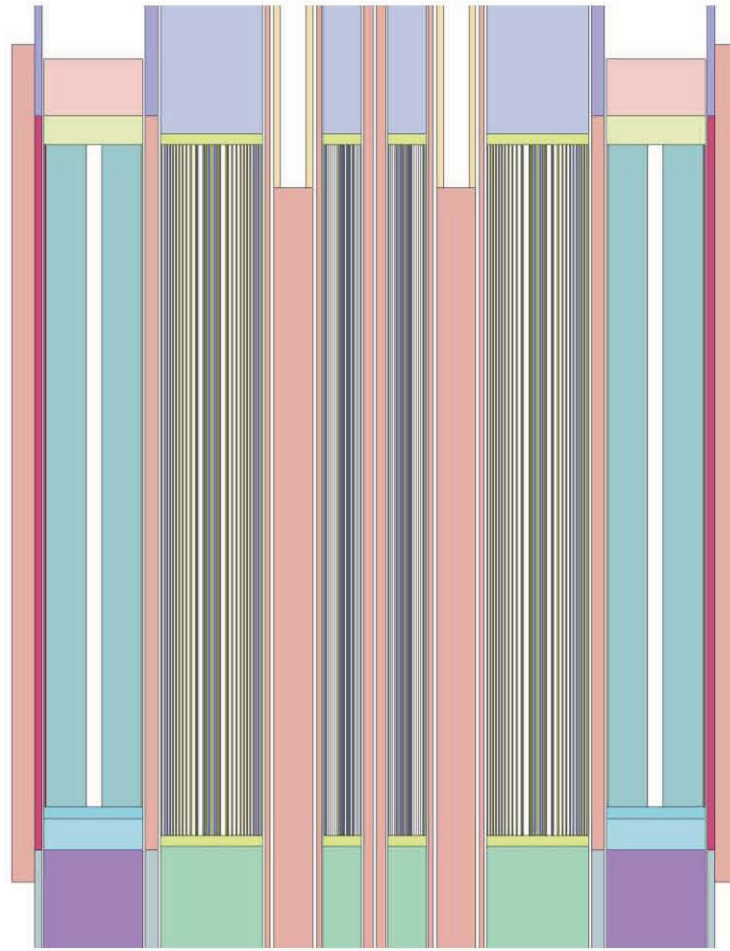
Fig. 2. Serpent model of ATR 94-CIC configuration (y-z slice at the x=10; portions of N and E flux traps are seen with safety rods partially inserted).

Note that fuel plate dimensions have been substantially revised for the LEU HPZ/RE designs. Removal of the boron plates results in slightly increased powers in the innermost and outermost plates. Chang [14] has proposed the dimensions provided in Table 2 for these two fuel designs to flatten power profiles. Chang has acknowledged that manufacturing tolerances will allow fuel thicknesses specified to the closest 1 mil, so that a final fuel design using fractional thicknesses in mils is highly unlikely. However, in absence of an alternative specification, the theoretical thicknesses proposed by Chang were assumed for these analyses.

Table 2. Fuel Meat and Poison Thicknesses for Four Analysed Designs

Fuel Plate No.	HEU Mark VII	LEU ICBA (Fuel)	LEU ICBA (B$_4$C poison)	LEU HPZ and LEU RE (plus 1 mil Zr barrier, not included here)
1	0.0508 (20)	0.02032 (8)	0.0127 (5)	0.02286 (9)
2	0.0508 (20)	0.02032 (8)	0.0127 (5)	0.02286 (9)
3	0.0508 (20)	0.0254 (10)		0.0254 (10)
4	0.0508 (20)	0.0254 (10)		0.02794 (11)
5	0.0508 (20)	0.03302 (13)		0.03302 (13)
6	0.0508 (20)	0.03302 (13)		0.03683 (14.5)
7	0.0508 (20)	0.03302 (13)		0.03683 (14.5)
8	0.0508 (20)	0.03302 (13)		0.03683 (14.5)
9	0.0508 (20)	0.03302 (13)		0.03683 (14.5)
10	0.0508 (20)	0.03302 (13)		0.03683 (14.5)
11	0.0508 (20)	0.03302 (13)		0.03683 (14.5)
12	0.0508 (20)	0.03302 (13)		0.03683 (14.5)
13	0.0508 (20)	0.03302 (13)		0.03683 (14.5)
14	0.0508 (20)	0.03302 (13)		0.03302 (13)
15	0.0508 (20)	0.03302 (13)		0.02794 (11)
16	0.0508 (20)	0.0254 (10)		0.0254 (10)
17	0.0508 (20)	0.0254 (10)		0.02032 (8)
18	0.0508 (20)	0.02032 (8)	0.0127 (5)	0.01778 (7)
19	0.0508 (20)	0.02032 (8)	0.0127 (5)	0.01524 (6)

Note: Dimensions are in cm, followed by mils in parentheses.

With a single exception, analyses were performed in the same core configuration for all four fuel element designs. The single exception was for the LEU ICBA design – this fuel design was proposed in independent work by Chang (see Refs 3 and 4) and has a lower initial reactivity than the other fuel designs. With this fuel element, OSCCs were rotated to 96.5° to bring the core to a critical state.

Serpent provides the ability to include external files that contain some portion of the full model. For this work, different files were created to represent each of the four fuel assembly designs, but all other files referenced were common to all models, to guarantee consistency between models. For the LEU ICBA

case, the base model references OSCC drums rotated to 96.5° while other models referenced (included) OSCC drums rotated to 51.8°.

Initial search calculations were performed to find the drum rotation necessary to obtain critical ($k_{eff} \sim$ 1.005) for the LEU ICBA model, to find the mass fraction of natural hafnium require to obtain criticality for the LEU HPZ model, and to find the uranium enrichment to take the LEU RE model to the critical state. Table 3 summarizes the results of the critical search calculations. The four eigenvalues are considered to be statistically identical.

Phase I: Comparison of Fuel Element Design Performance

The key concern in this study is the performance of the LEU HPZ fuel design concept relative to HEU fuel. The LEU ICBA design results are included as a reference for an alternative LEU design, and to help understand differences between boron, which typically burns out over the length of one fuel cycle, and hafnium, which would burn out much more slowly. In performance of preliminary analysis, a question was asked about the value of hafnium since it is not burned out over a fuel element lifetime; specifically, what would be the difference between using hafnium as a poison and reducing ^{235}U enrichment to the same initial reactivity. Hence, the LEU RE design was proposed calculations were performed for comparison to the LEU HPZ design.

After adjusting all fuel designs to the same initial eigenvalues, depletion calculations were performed to determine if the LEU HPZ design could match the burnup lifetime of HEU fuel; the other two designs were included for comparative purposes. However, performance must be measured in other terms as well. For the ATR, the impact of fuel design changes on experiment irradiation locations must be assessed to ensure that customer's needs will be met. From a safety limits perspective, any new design should show heat flux loads in each fuel plate do not significantly exceed those of the HEU design. Calculations of fluxes in target locations will be used to show the effect of fuel design changes on fluxes in key locations. Calculations of OSCC worth are performed here to assess the affect of design changes on reactor control systems, and calculations are performed to assess changes in the delayed neutron fraction as a function of burnup.

Table 3. Initial (Critical) State for Four Fuel Element Designs

Element Type	Modification Needed to Obtain Initial Criticality	Value of Modified Parameter	Calculated Core Multiplication Factor, k_{eff}
HEU Mark VII	—	—	1.00530 ± 0.00019
LEU Integral Control Burnable Absorber (ICBA)	OSCC rotation	96.5°	1.00531 ± 0.00020
LEU Hafnium-Poisoned Zirconium (HPZ)	Added natural hafnium to zirconium barrier	2.1 wt % natural Hf 97.9 wt % natural Zr	1.00519 ± 0.00020
LEU Reduced Enrichment (RE)	Reduced ^{235}U enrichment	17.7 wt % ^{235}U 83.3 wt % ^{238}U	1.00514 ± 0.00020

The following subsections describe the results of scoping calculations performed to assess this partial range of performance parameters.

Depletion Calculations

A key performance attribute is for a fuel element to provide sufficient excess reactivity to maintain criticality and provide power for suitable lifetime. For the purposes of this study, it was assumed that a typical fuel element lifetime would be three 60-day cycles operating at a power of 2.75 MW per fuel element, average (110 MW total core power), without fuel replacement between cycles. Furthermore, it was assumed that the reactivity of the core (initially composed of 40 fresh HEU elements) at the end of three cycles would determine the lower acceptable limit for end-of-life reactivity.

Rather than attempt to follow the rather complicated operational history of an ATR fuel element over its lifetime, depletion calculations were simplified to assume no fuel shuffling, no neck shim or OSCC adjustment, and an operating history as described in Table 4. Fuel was assumed to be removed from the core for one cycle between each burn cycle (although this does not appear to have an appreciable affect on fuel reactivity).

Table 4. Assumed Depletion History for Burnup Calculations

Core Power (MW)	Time (d)
110	60
0	60
110	60
0	60
110	60

Results of the calculations, in terms of the core multiplication factor k_{eff}, are shown in Fig. 3. These analyses show that for the two boron-bearing designs (HEU and LEU ICBA), the boron poison burns out at a rate such that the loss of reactivity from fuel depletion is more than offset by the gain in reactivity due to boron depletion for most of the first cycle. After the first cycle, the fuel reactivity decreases almost linearly with burnup. The large drops in reactivity at the beginning of each fuel cycle are due to the rapid buildup of equilibrium ^{135}Xe.

For both the HPZ and RE fuel designs, reactivity decreases in a nearly linear fashion for all three fuel cycles. The non-linear tail at beginning of life after the ^{135}Xe drop is due to the buildup of an equilibrium level of ^{149}Sm; this feature is present in the other fuel design depletion results as well, but is obscured by boron poisoning effects. The HPZ results show that hafnium is not rapidly depleted in the manner of boron poisoning; however, at the end of three cycles, the HPZ fuel design has more net reactivity than the current HEU fuel design, while the RE design has close to the same net reactivity at EOL. The smaller negative slope of the linear change in reactivity as a function of time for the three LEU designs (after the first burn cycle for the ICBA design) is a result of plutonium production in the LEU fuel due to neutron capture in ^{238}U, which partially offsets the loss of ^{235}U. The HEU design shows a faster decrease in reactivity due to the reduced level of Pu breeding as a result of its small ^{238}U inventory relative to LEU fuel. The difference between the HPZ design and the RE design is the mass of fuel present. While not needing as much fuel at BOL as the HPZ design due to the lack of hafnium poisoning, the reduced inventory must deplete at a faster rate per initial mass of fuel to maintain the same power level. The boron-bearing ICBA design shows a clear reactivity advantage at end of life due to the complete burnout of boron poisons. Clearly, however, both the HPZ and RE concepts may be viable alternatives to a boron-poisoned fuel design in terms of matching the lifetime of the current HEU fuel. Neither of these designs would be expected to result in blistering concerns, as natural hafnium isotopes decay only by beta emission, so helium will not be created with the material.
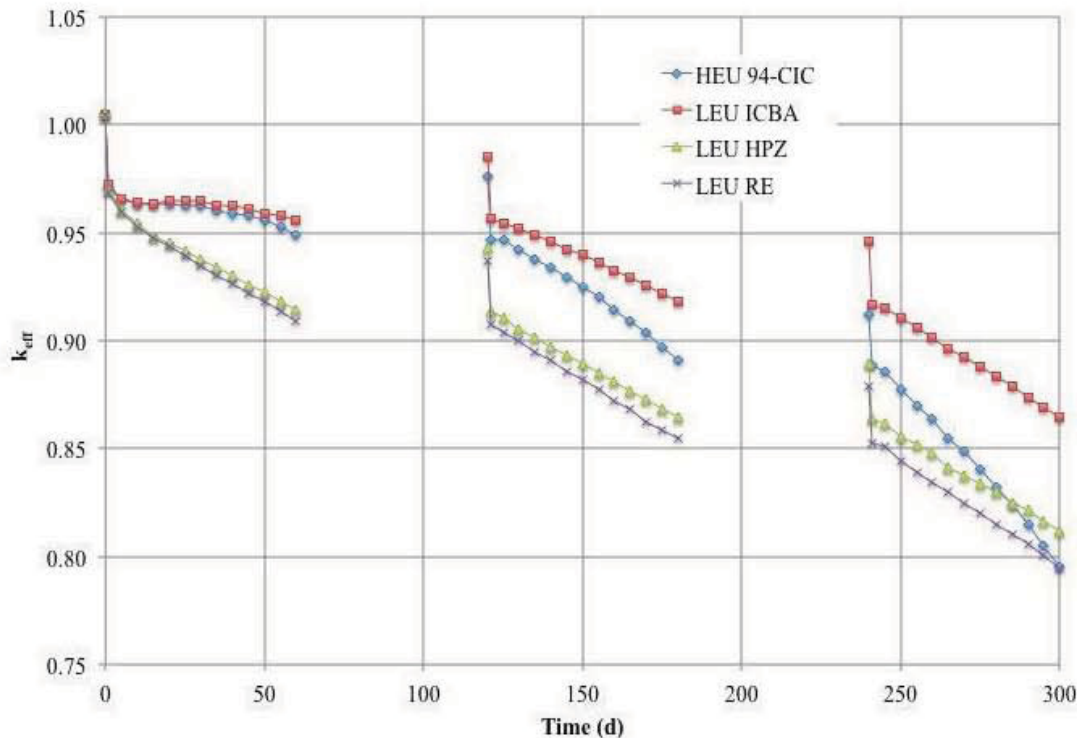
Fig. 3. Results of depletion calculations for four fuel element designs.

Plate Power Distributions

Safety limits for the ATR are determined by the ability of coolant to remove power from fuel elements in the event of an accident scenario. In turn, this is dependent on the heat flux at any given point on the fuel plate surface. Typically, thermal/hydraulic calculations are performed based coolant flow through fuel element flow channels and heat transfer coefficients for each channel. Such calculations are beyond the scope of this work; however, it is possible to examine the heat source for each fuel element design to determine the heat flux distribution for each fuel plate in an average assembly relative to that of the current HEU design. Serpent may be used to calculate fission densities and the total fission count in each plate location in an assembly. Total fissions may be assumed to represent power in each fuel plate. Figure 4 shows the total fission rate (power) calculated for each fuel plate location, normalized to an average of 1.0. It is clear that all four fuel designs produce similar power profiles, with maximum powers occurring in plate 15 for the HEU and LEU ICBA designs, and in plate 13 for the LEU HPZ and RE designs. The shift is a result of reduced thickness plates proposed by Chang for innermost and outermost plates to reduce power peaking. Note that the radial power profile is sensitive to OSCC rotation. Although depletion calculations were performed with states described in Table 3, the LEU ICBA calculation was performed again with a 51.8° OSCC rotation to get and "apples-to-apples" comparison with other radial power profiles.

Total powers show increasing values with plate number, due to the fact that plate volumes generally increase with increasing plate number, since the radius curvature of the fuel plate increases with plate number. Note that for the three LEU designs, reduced thicknesses result in an offsetting reduction in volume in the innermost and outmost plates.

85
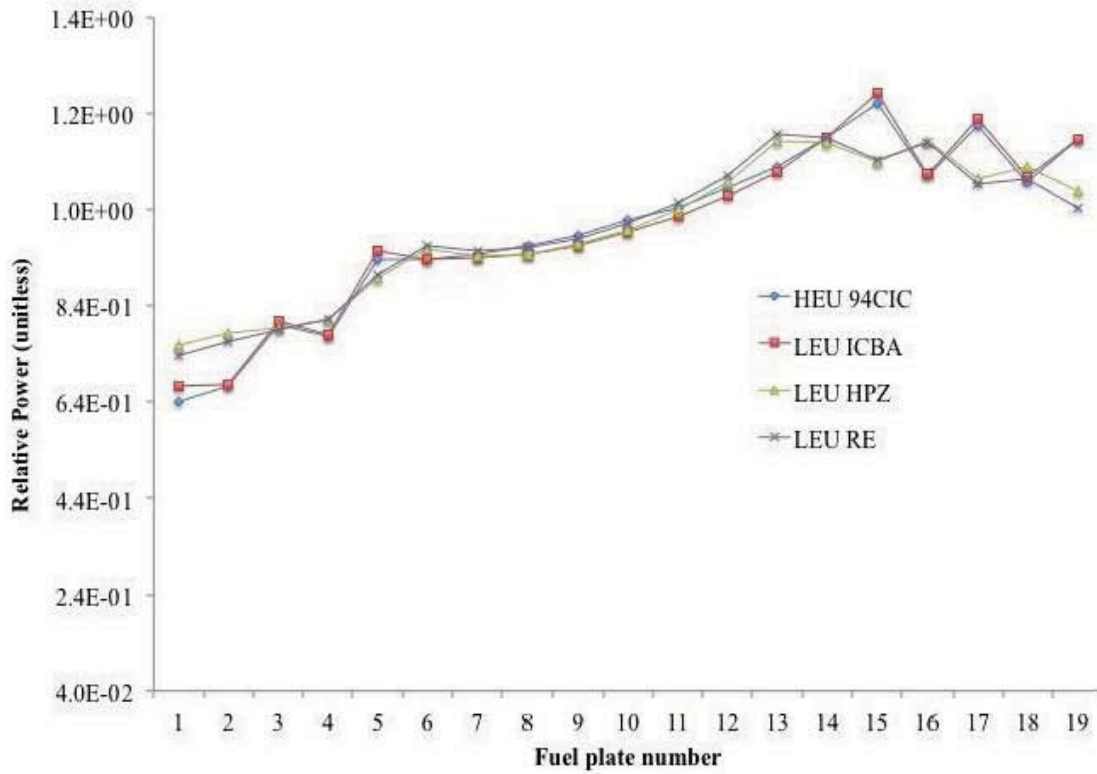
Fig. 4. Average fuel fission power for 51.8° OSCC rotation.

Heat fluxes on fuel surfaces are also dependent on the volume of each fuel region. Since the total power P in a fuel region is the product of the volume of the fuel meat V_f and the power density p in that fuel,

$$P - p \cdot V_f$$

and the heat flux Q'' is the total power divided by the total surface area S_f,

$$Q'' - P/S_f - p \cdot V_f/S_f$$

then because for thin fuel foils of thickness t,

$$V_f \cong S_f \cdot \square$$

and the total surface heat flux is closely approximated by

$$Q'' - p \cdot t, \text{ or } p \cdot t/2 \text{ on each side.}$$

Figure 5 shows the calculated heat flux for the four fuel designs (again, all with a 51.8° OSCC rotation). Heat flux profiles are more flattened across plates, with heat flux peaks in plate 5 for HEU and ICBA designs, and plate 1 in the HPZ and RE designs. The peaking in plate 1 indicates that perhaps a thinner fuel meat would be needed in plate 1. Assuming the heat flux changes with the ratio of change in fuel thickness (which represents change in fission power), changing the thickness of plate 1 from 9 mils to 8 mils would reduce the normalized plate power from ~1.30 to ~1.15 for the HPZ and RE designs. Ideally,

86

it would be desirable to match the HEU heat flux profile, since this is the profile upon which current safety limit calculations are based. However, assuming that only method to control heat flux profiles is by the thickness of the fuel meat within each plate, and assuming a manufacturing tolerance of +/- 1 mil, it is impractical to try to exactly match the current HEU power profiles.

Core Neutron Fluxes

Because the purpose of the ATR to provide neutrons to perform irradiation of experiments, it is important to ensure that changes in fuel designs do not have a significant effect on neutron fluxes and spectra in irradiation locations. For the Serpent calculations reported here, fluxes were calculated for specific regions in the core to determine flux changes as a result of fuel design. Table 5 provides a list of locations in which fluxes were tallied. These locations were selected as they represent the 5 lobes of the ATR, target positions between the core and the OSCCs, and fluxes in the OCSS
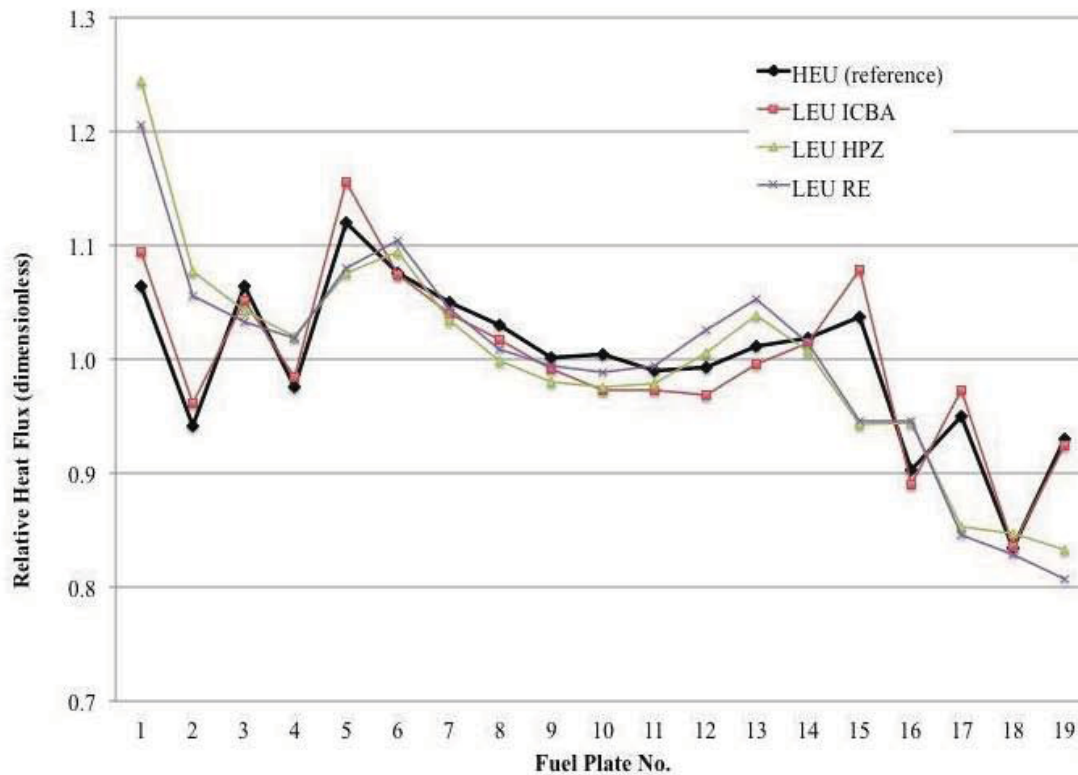
Fig. 5. Average fuel heat flux distribution for 51.8° OSCC rotation.

Table 5. Location of Flux Tallies in ATR Core Calculations

Target Location	Media Within Target Area
NE Flux Trap	Water around targets in central zone
NW Flux Trap	Central aluminum
SE Flux Trap	Central water
SW Flux Trap	Central water
Center Flux Trap	Water around targets in central zone
OSCC Position N1	Interior beryllium

87

OSCC Position N2	Interior beryllium
Small B-Hole B1	Beryllium
Large B-Hole B9	Beryllium

positions, and represent a variety of target configurations. For each location, fluxes were tallied in both a 238-group and 2-group energy structure. The 238-group tallies were based on the SCALE 238-group energy structure for easy comparison to earlier results generated by SCALE (not reported here). The 2-group structure is a tally of neutrons having energies above and below 1.25 eV, representing fast and thermal fluxes.

Figures 6 – 10 show the neutron flux spectra computed in each target position in the five target positions. For reference, Fig. 11 is a drawing of the ATR 94-CIC configuration that shows the nature/layout of each flux trap. Spectral plots were not generated for B-Hole or OSCC positions, although the data is available. Fluxes represent the spatially integrated flux in

Figure 6a shows that in general fluxes in the NE flux trap are not strongly affected by the fuel design, however, the LEU HZP design does show a slightly reduced thermal peak in this location relative to the other fuel designs (the thermal flux detail is shown in Fig 6b). The flux represents the average of all neutrons simulated in the water region surrounding targets in the NE flux trap.

Figure 7a shows the fluxes tallied in the central aluminum filler; Fig. 7b is zoomed in to show the thermal energy peak. As discussed in Ref. 4, this region represents perhaps the hardest spectrum of all targets due to the lack of moderating material. A significant difference is seen between HEU and all LEU designs, due to the lack of moderation in this region. Also visible in Fig. 7a is the structure in the resonance energy range due to fuel resonances, another indicator of lack of moderation.

Figures 8 and 9 (a and b) illustrate the fluxes in water regions in the centers the SE and SW flux traps respectively. Because these flux traps contain identical configurations and are symmetric with respect to the fuel placement, they show almost identical flux spectra. Both show very similar fluxes for all LEU fuel designs, with a slight decrease in the thermal flux relative to HEU fuel. Figures 10 a and b shows fluxes averaged over the water region within the center of the center flux trap. Similar trends are seen here relative to other water regions in NE, SE and SW flux traps. All cases show a small reduction of thermal fluxes relative to the HEU design, with ICBA having the highest thermal flux and HPZ the lowest.

Although these figures show detail in flux spectra and illustrated differences between target region fluxes for the four fuel designs, the differences are hard to quantify in terms of absolute effect. Thus, review of the two-group fluxes in each region would be of value. These results will show the integrated flux in fast and thermal regions, where the fast/thermal boundary was selected to be 1.25eV.
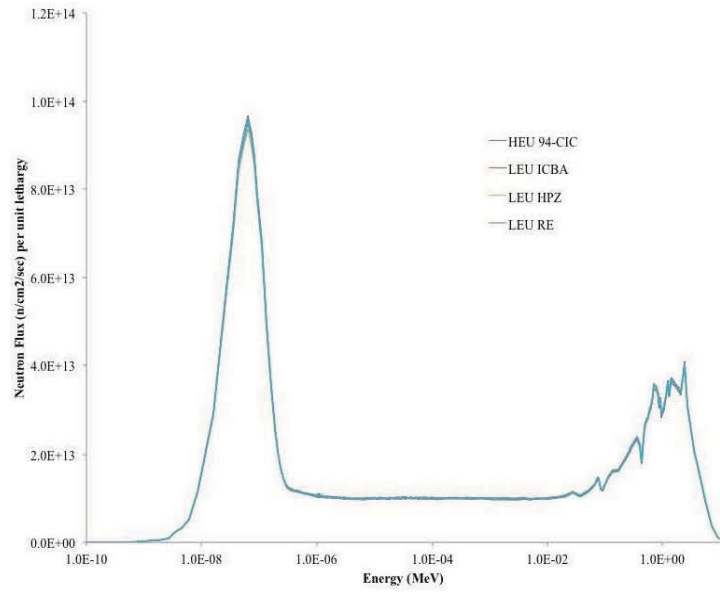
(a)
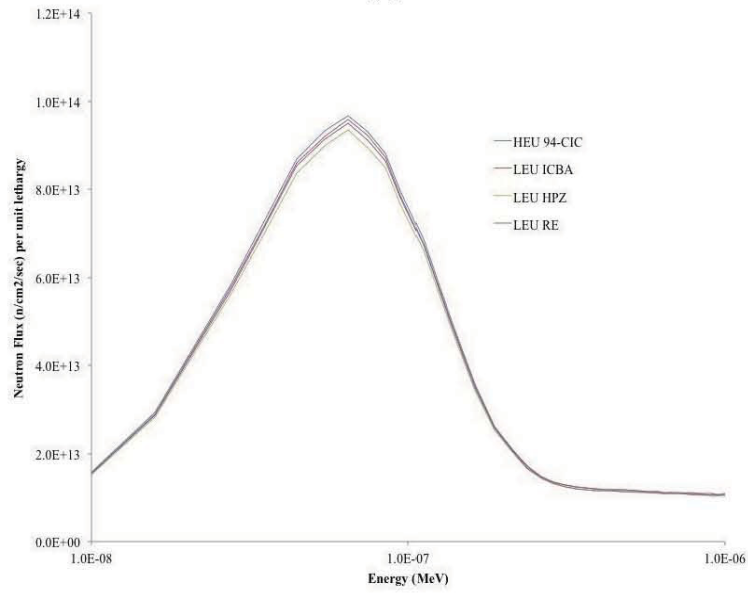
(b)

Fig. 6. Flux spectrum (per unit lethargy) in NE flux trap: (a) full energy range and (b) thermal peak.
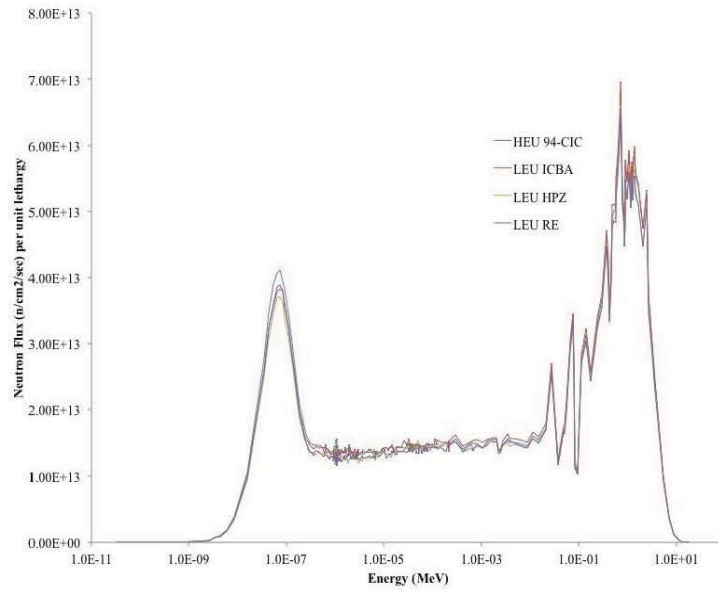
(a)
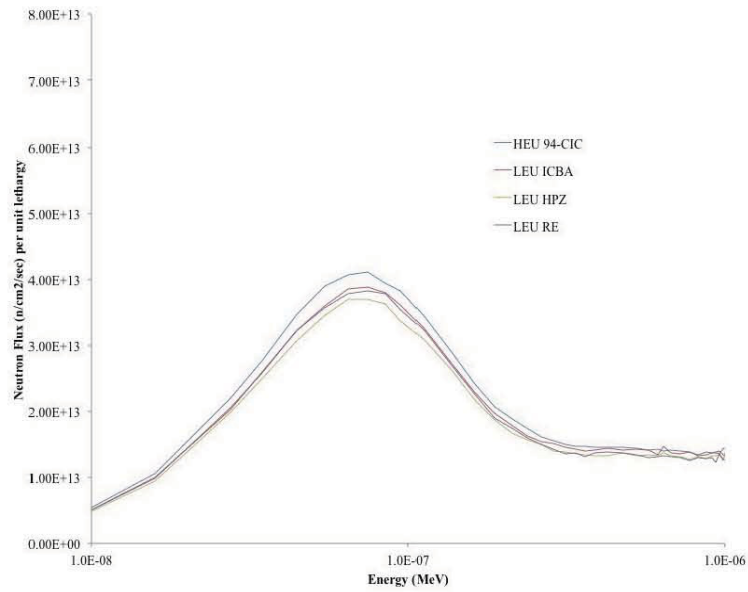
(b)

Fig. 7. Flux spectrum (per unit lethargy) in NW flux trap: (a) full energy range and (b) thermal peak.
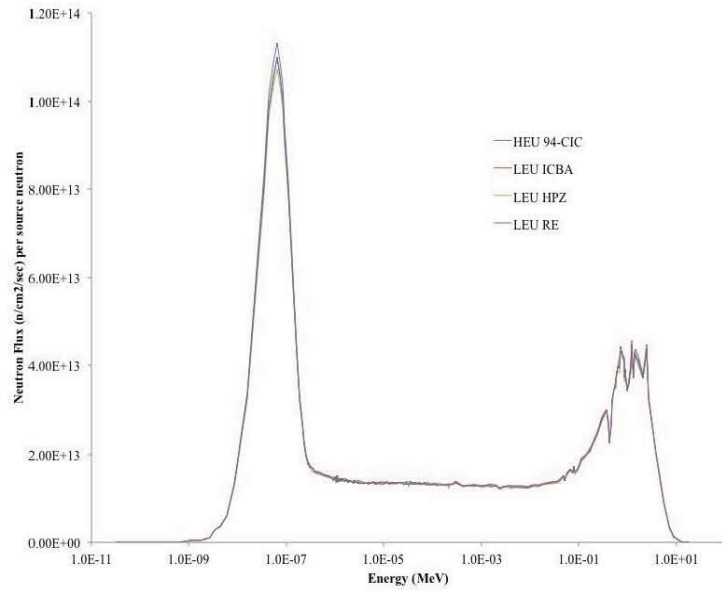
(a)
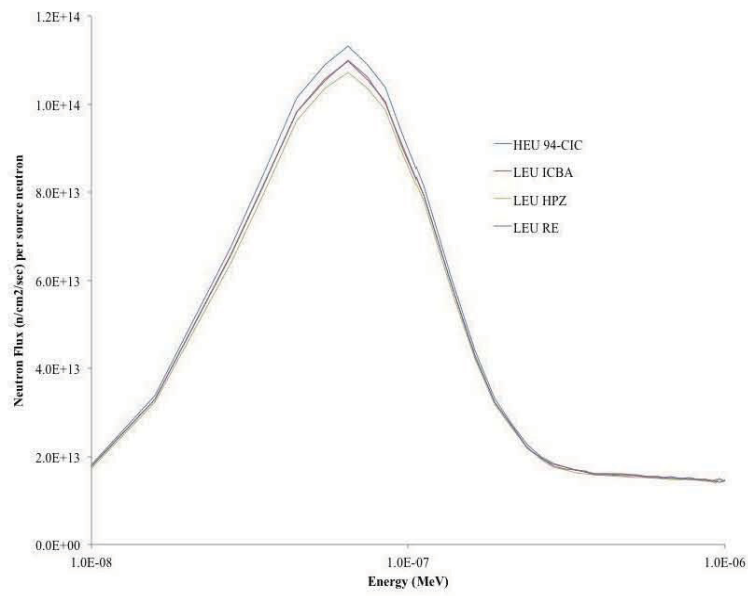
(b)

Fig. 8. Flux spectrum (per unit lethargy) in SE flux trap: (a) full energy range and (b) thermal peak.
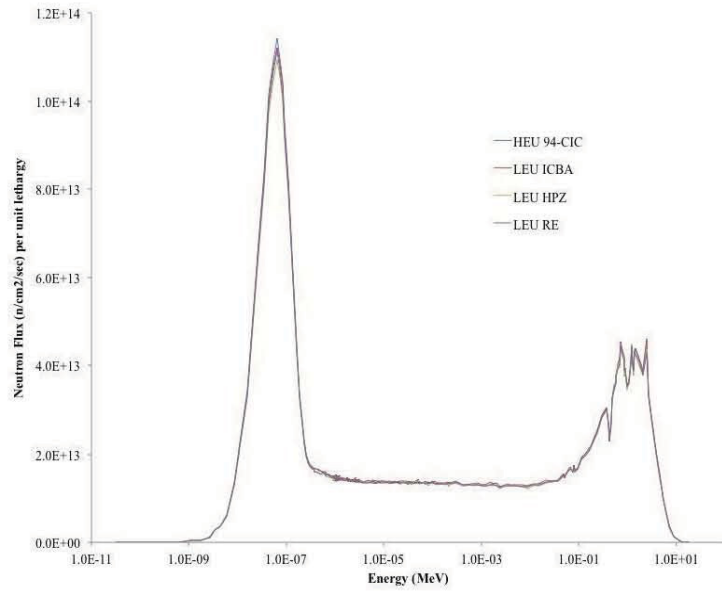
(a)
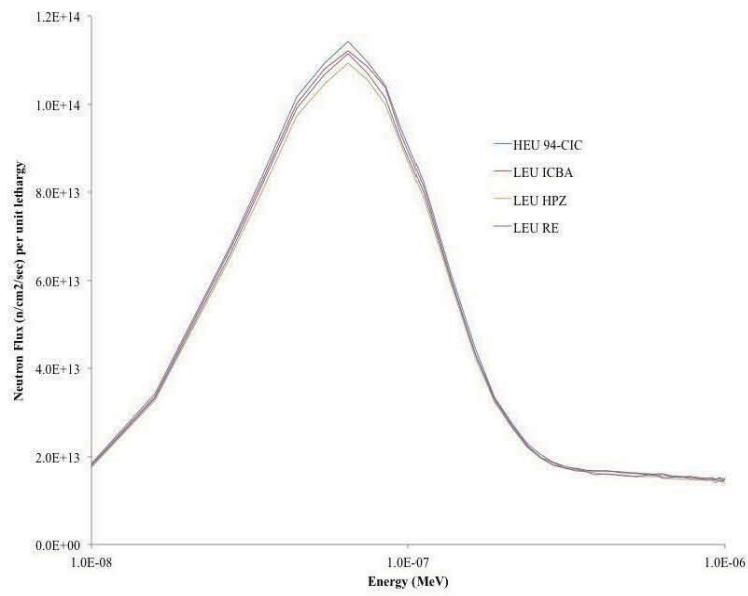
(b)

Fig. 9. Flux spectrum (per unit lethargy) in SW flux trap: (a) full energy range and (b) thermal peak.
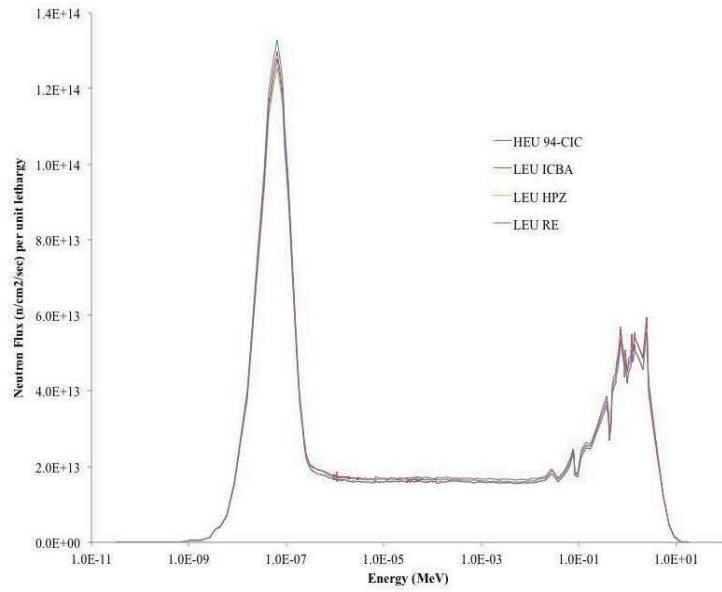
(a)
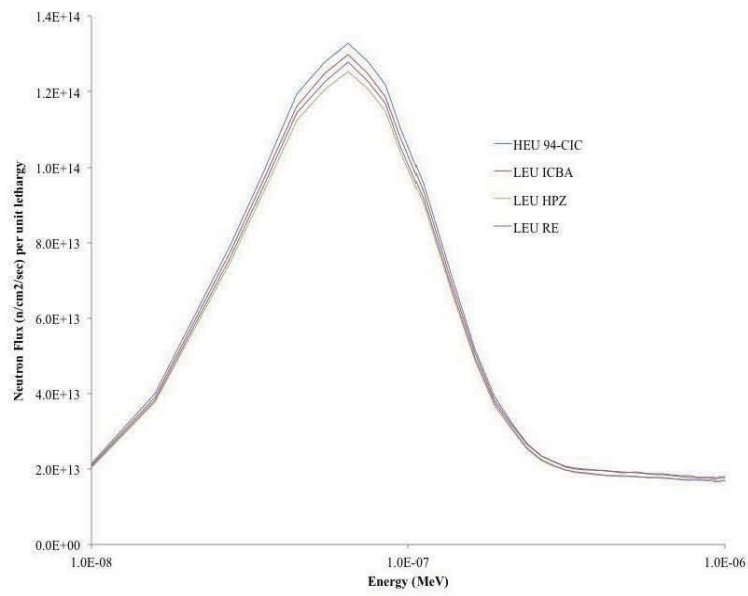
(b)

Fig. 10. Flux spectrum (per unit lethargy) in center flux trap: (a) full energy range and (b) thermal peak.
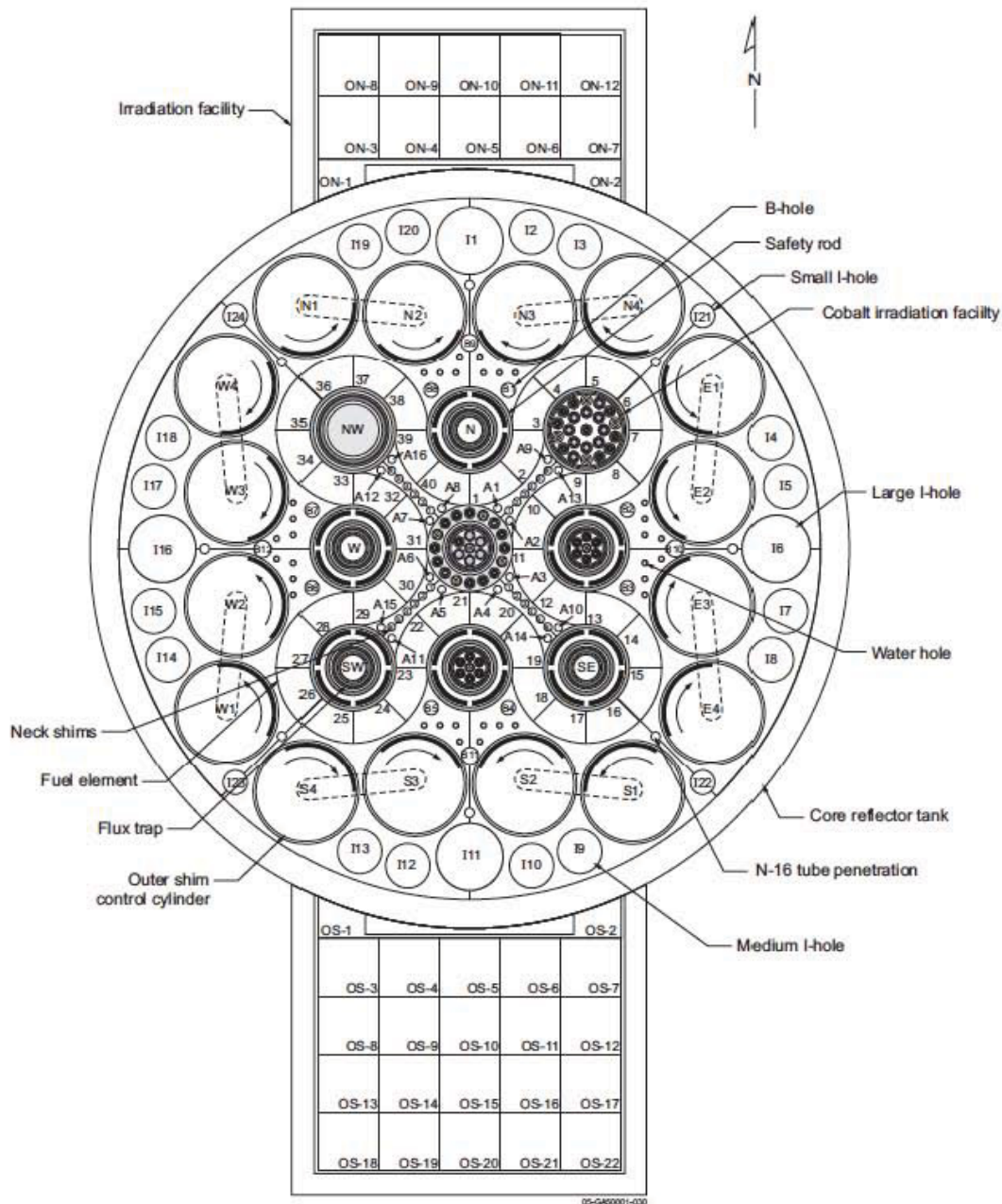
Fig. 11. ATR core configuration showing locations of irradiation/control positions used in flux calculations (Ref. 13)

Tables 6 and 7 provide the calculated fluxes for the nine irradiation positions listed earlier. In each table, the second column provides the calculated flux for the current Mark VII fuel in the 94-CIC configuration. Fluxes computed based on the three LEU fuel designs are given in the following columns, followed by the percentage change relative to the HEU fuel. The fast (E > 1.25 eV) results in Table 6 show that all three LEU designs have for the most part a reduced fast flux in the range of 0-4% for the five in-pile locations, and a similar reduction on the order of 0-6% for outer target and OSCC positions for the ICBA and HPZ designs, with larger (0-16%) differences associated with the RE design.

Table 7 shows changes in thermal fluxes. In general, thermal fluxes are reduced less than 3% for the in-pile locations (the exception being the solid-filled NW in-pile tube), with differences on about the same order for outer positions.

Table 6. Fast Fluxes and Difference Relative to HEU Fuel for Irradiation Positions

	HEU 94-CIC	LEU ICBA		LEU HPZ		LEU RE	
NE	2.16E+14	2.21E+14	2.6%	2.15E+14	-0.1%	2.16E+14	1.7%
NW	3.33E+14	3.39E+14	1.9%	3.23E+14	-3.1%	3.22E+14	-2.3%
SE	2.73E+14	2.75E+14	0.5%	2.69E+14	-1.6%	2.71E+14	-5.7%
SW	2.77E+14	2.81E+14	1.2%	2.74E+14	-1.2%	2.75E+14	-5.6%
C	3.43E+14	3.50E+14	2.0%	3.31E+14	-3.6%	3.29E+14	4.4%
N1 OSCC	7.67E+13	7.67E+13	0.0%	7.18E+13	-6.5%	7.18E+13	-15.9%
N2 OSCC	1.02E+14	1.02E+14	0.0%	9.56E+13	-5.8%	9.58E+13	-9.6%
B-1	1.52E+13	1.54E+13	1.8%	1.48E+13	-2.3%	1.48E+13	1.8%
B-9	6.16E+12	6.28E+12	2.0%	5.97E+12	-3.1%	5.93E+12	-0.1%

To put the results of Tables 6 and 7 in a different perspective, Figs. 12 and 13 are provided to give a graphical representation of fluxes in the five interior flux trap positions. These results show that in general the HPZ and RE fuel designs have very similar behavior in terms of fluxes seen in the irradiation positions. These results suggest that the hafnium poison in the LEU HPZ design has little effect on fluxes outside the fuel region. This in turn would suggest that differences in fluxes are a result of the LEU fuel behavior itself – primarily due to neutron capture in ^{238}U resonances.

Table 7. Thermal Fluxes and Difference Relative to HEU Fuel for Irradiation Positions

	HEU 94-CIC	LEU ICBA		LEU HPZ		LEU RE	
NE	2.04E+14	2.02E+14	-1.0%	1.97E+14	-3.6%	2.00E+14	-2.0%
NW	1.06E+14	1.01E+14	-5.1%	9.59E+13	-9.5%	9.87E+13	-7.0%
SE	2.44E+14	2.38E+14	-2.6%	2.33E+14	-4.5%	2.37E+14	-2.7%
SW	2.46E+14	2.43E+14	-1.2%	2.36E+14	-4.1%	2.40E+14	-2.6%
C	2.88E+14	2.82E+14	-2.0%	2.72E+14	-5.6%	2.76E+14	-4.2%
N1 OSCC	9.38E+13	9.23E+13	-1.6%	8.74E+13	-6.7%	8.85E+13	-5.7%
N2 OSCC	1.08E+14	1.05E+14	-2.7%	1.01E+14	-6.7%	1.02E+14	-5.9%
B-1	1.27E+13	1.24E+13	-2.7%	1.22E+13	-3.8%	1.26E+13	-0.4%
B-9	7.28E+12	7.19E+12	-1.2%	7.00E+12	-3.9%	6.96E+12	-4.4%
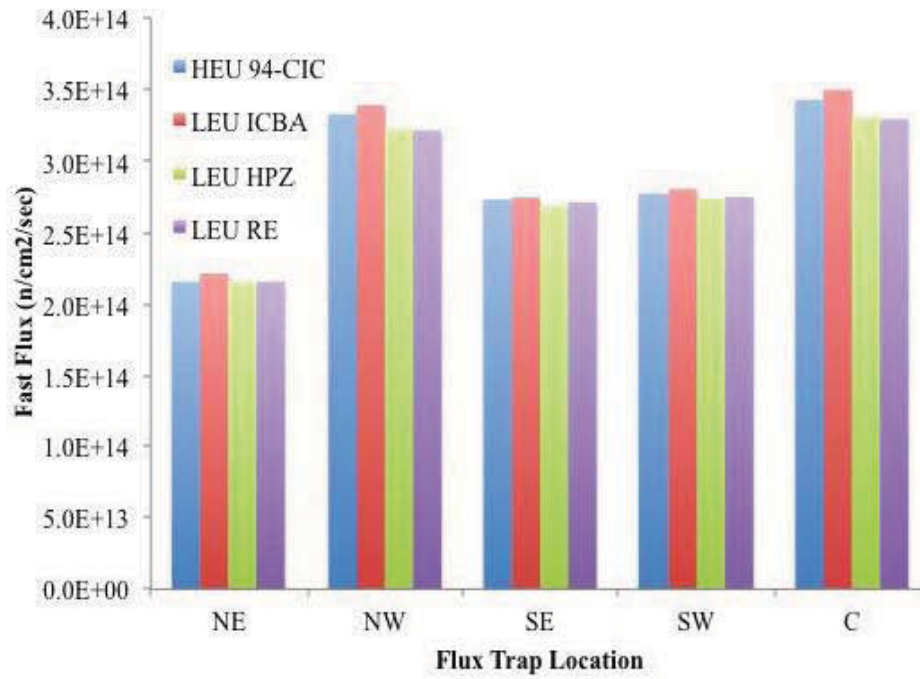
Fig. 12. Fast Fluxes for Lobe Flux Trap Locations.
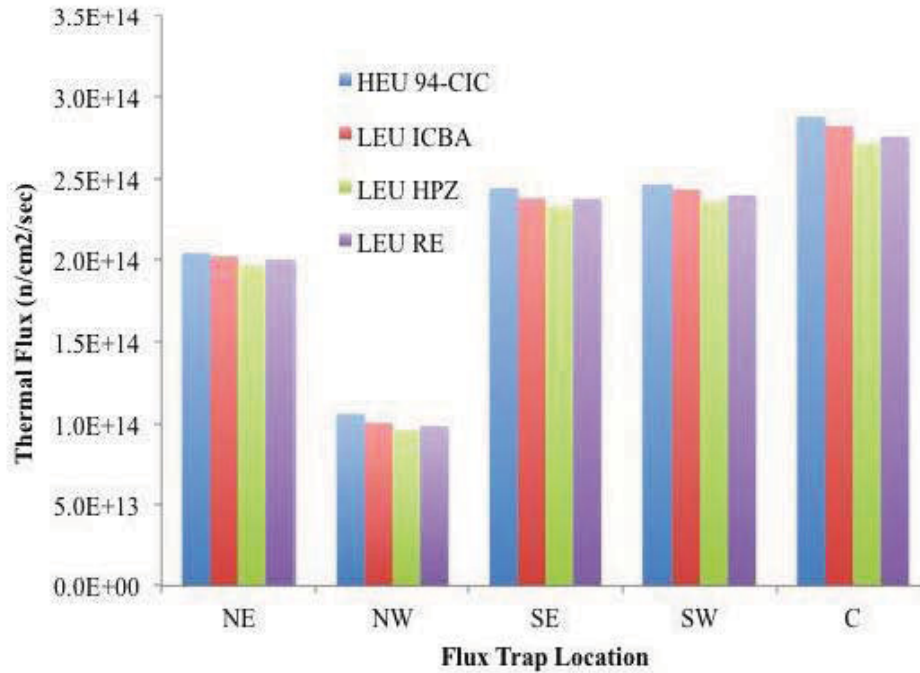
Fig. 13. Thermal Fluxes for Lobe Flux Trap Locations.

OSCC Worth

The next aspect of core performance studied for the considered fuel designs it the worth of the OSCC control elements. Earlier work described in Ref. 4 showed that OSCC drums had less reactivity worth per degree of rotation for the ICBA fuel relative to the HEU fuel, presumably because they see a harder neutron spectra. These calculations were repeated using Serpent, for drum rotations of 0° to 160° in 20° increments. Figure 14 shows drum worths (Δk_{eff} relative to 0°) for all four fuel designs. As expected, the ICBA design shows reduced OSCC worth relative to HEU fuel. However, both the HPZ and RE designs show that OSCC worth is increased relative to HEU fuel. Because the two results are virtually identical, this behavior is not a result of the hafnium present in the HPZ design, and must therefore be due to the LEU itself.
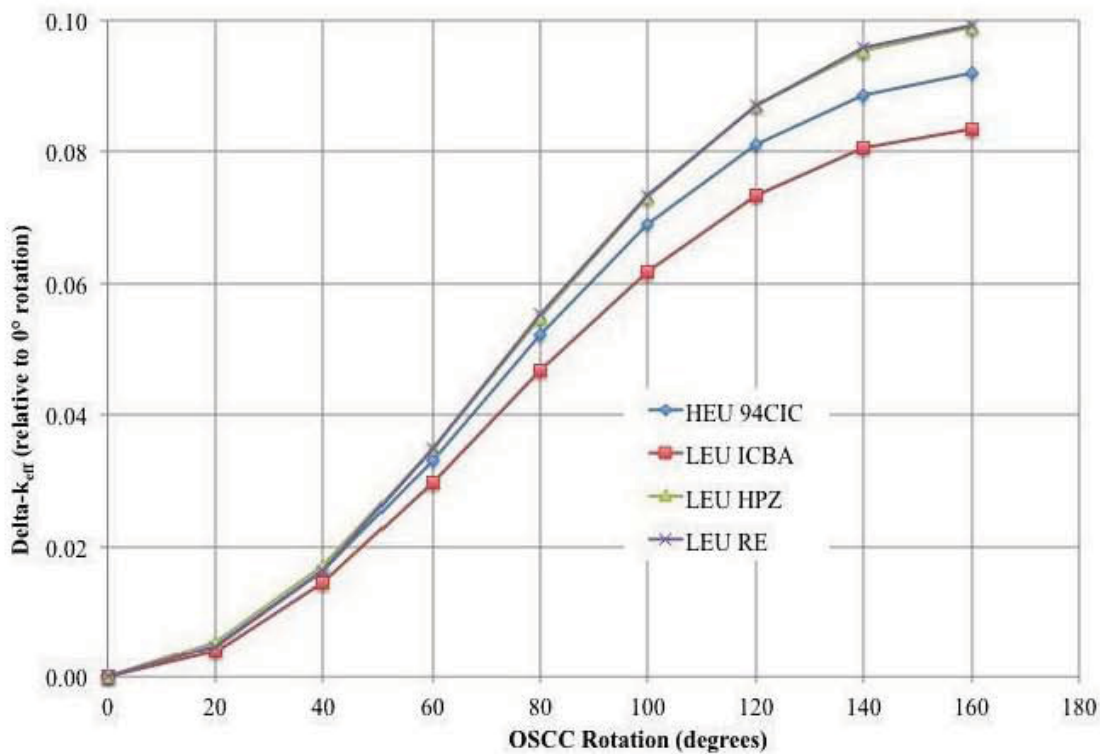
Fig. 14. Δk_{eff} worth of OCSSs as a function of rotation angle.

Delayed Neutron Fraction

The final issue studied for the four fuel designs was the behavior of the delayed neutron fraction as a function of burnup. This is an important consideration for safety analyses in the case of reactivity-driven off-normal events in the ATR. This capability is not available in SCALE, and was not studied in Ref. 4. Intuitively, it is expected that the delayed neutron fraction β_{eff} will decrease with burnup as more plutonium fission becomes a larger component of total fissions. However, the magnitude of the change has not yet been studied. Figure 15 shows a plot of β_{eff} for the four fuel types. There is a considerable amount of stochastic error associated with these results, so error bars are included. Also, to better visualize trends, a linear fit was added to each set of data to show trends. As expected, very little change

97

is seen in the β_{eff} value for HEU fuel over the core lifetime, and a significant decrease is seen for LEU fuels. The delayed neutron fraction is on the order just above 0.0070 at BOL for all fuels, with a very slight change over the HEU lifetime to closer to 0.0070. LEU fuel designs appear to have a statistically identical trend with burnup, with an EOL value for β_{eff} around 0.0065
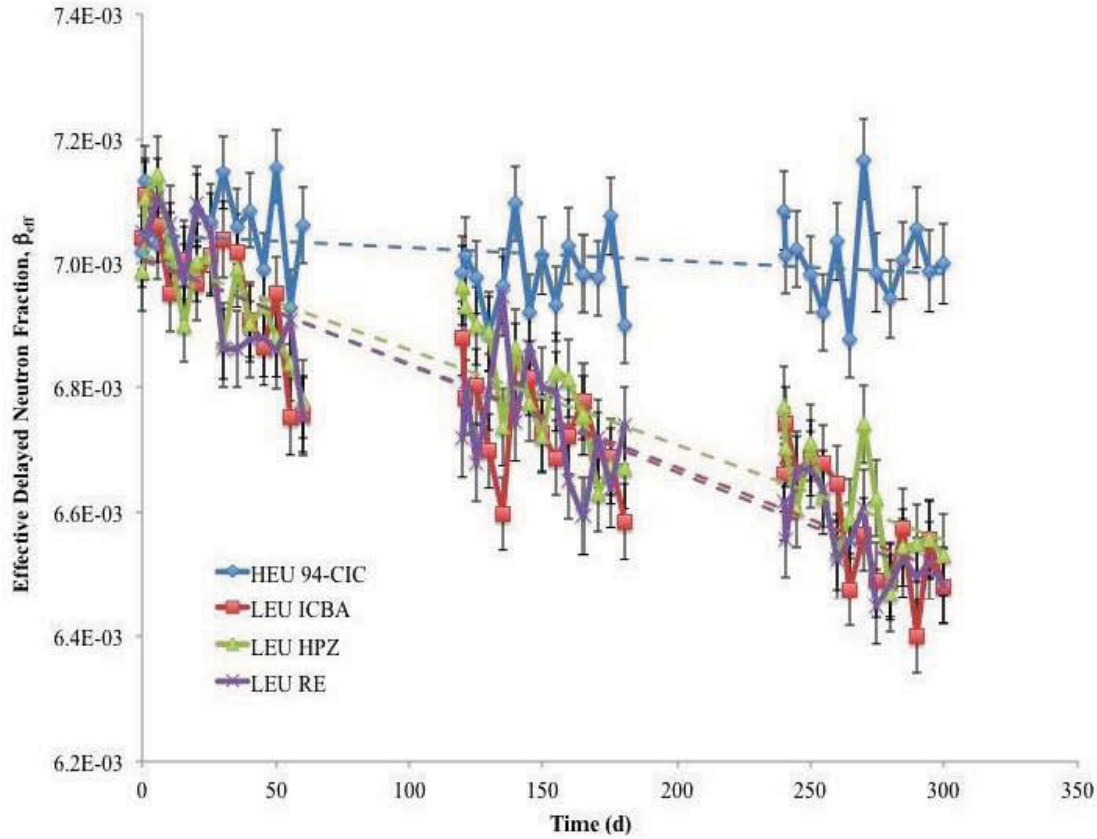
Fig. 15. Delayed neutron fraction β_{eff} as a function of time for HEU and LEU fuels.

Phase II: Viability of an Alternative Unpoisoned Fuel Element Design

Although the hafnium-poisoned zirconium design shows the ability to match the reactivity of the current HEU fuel at end of life, it is not clear if the fresh fuel provides enough excess reactivity to drive a single cycle loaded with once-burned and twice-burned fuel. A single cycle operating history of 56 days at 120 MW total core power was assumed based on a functional requirements specification for ATR. Calculations were performed to estimate once-burned fuel plate isotopic concentrations for an average assembly assuming 56 days operation at 120 MW followed by a 56-day down time; twice-burned isotopic concentrations were generated assuming two such cycles. Both calculations were performed beginning with a fully fresh core, OSCCs rotated to 80° and the 12 outermost neck shims removed for the entirety of the burn cycle(s). Each of the calculations resulted in isotopic inventories for each of the 19 fuel plate locations and corresponding hafnium-bearing zirconium barrier regions. Note that each plate's nuclides were depleted individually using the average flux in that plate location; a single zirconium/hafnium mixture was assumed for barriers on each side of each fuel plate, so 19 zirconium mixtures were tracked.

Using the result of these two calculations with fresh fuel inventories, three sets of nuclide concentrations were available to approximate a prototypic fuel cycle. Based on discussion of loading philosophies and fuel loading examples for ATR cycles 145A and 151A [16, 17], a core loading was assumed using 18 fresh assemblies, 14 once-burned assemblies, and 8 twice-burned assemblies, as illustrated in Fig. 15. A depletion calculation was performed using this loading, depleting all 57 fuel materials and the 57 hafnium poisoned zirconium barriers. For this calculation, all neck shims were modeled as fully withdrawn and outer shims rotated to 180 degrees. No control changes were made during the calculation; if the fuel is viable than the core should remain above critical (~1.005) for a full 56 day cycle. Figure 16 shows the results of these calculations. Clearly, these results indicate that the fresh fuel is over-poisoned, and does not have sufficient excess reactivity to maintain a critical core over a full burn cycle.
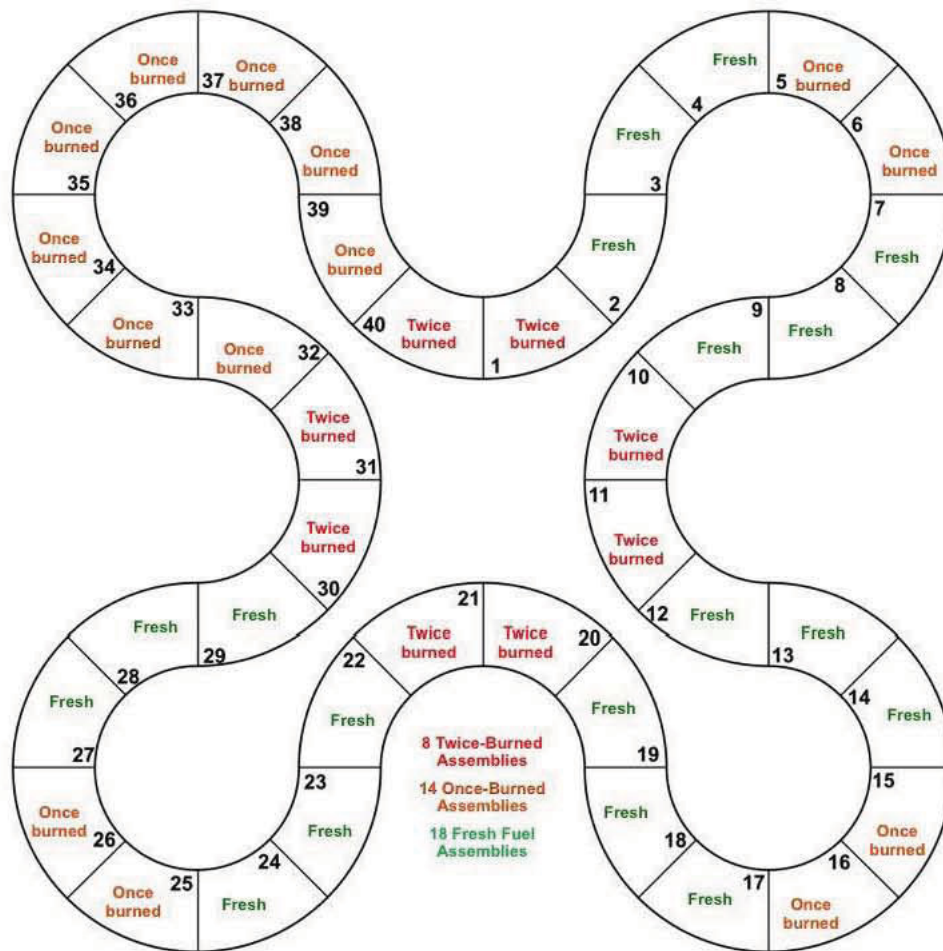
Fig. 15. Loading pattern assumed for prototypic cycle calculations.
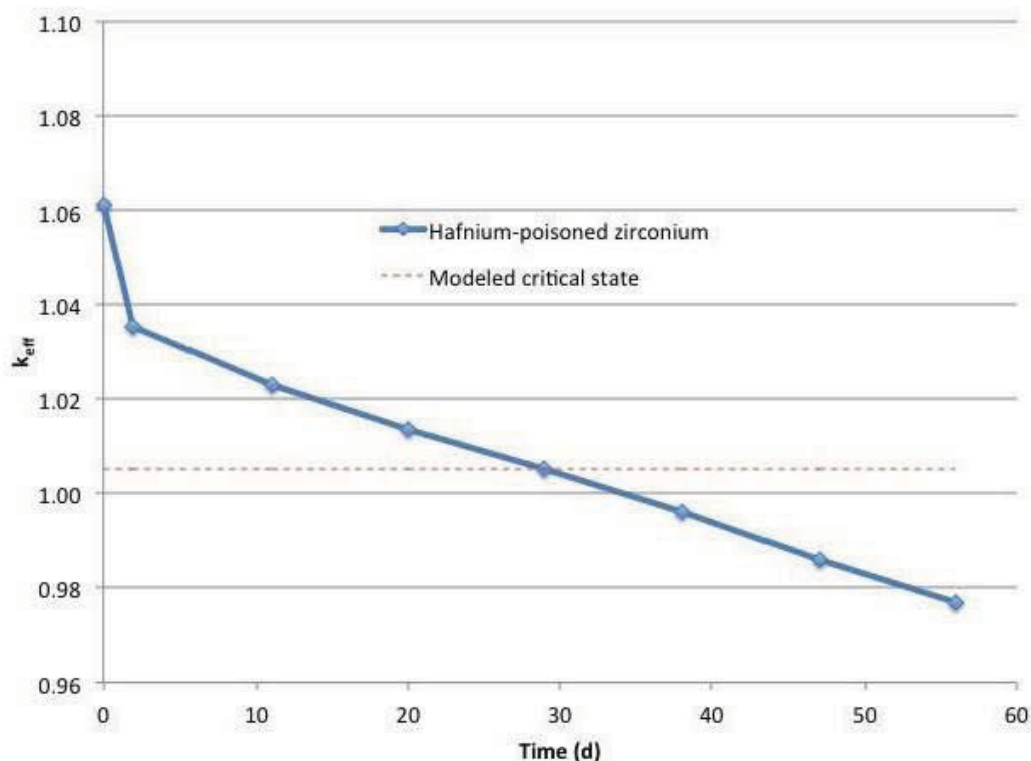
Fig. 16. Performance of HPZ fuel design for a prototypic cycle calculation.

Because the reduced enrichment (RE) design shows less reactivity than the HPZ over the lifetime of the fuel, this set of calculations was not repeated for the RE design. At this point, however, a new design was considered   a fresh 19.75 wt% enriched LEU design with no poison introduced. Although a fresh core fully loaded with such fuel would most likely have significant excess reactivity beyond the typical operational limits, the ATR is very rarely operated in this state. The availability of burned fuel and the need to fully utilize that fuel means that excess reactivity control required for an unpoisoned fresh fuel element could conceivably be handled simply through appropriate core loading. Hence, the prototypic core calculations described above were repeated with a zirconium barrier comprised of 100% natural zirconium. Again, isotopic concentrations for once- and twice-burned fuels were estimated using the approach described above, although depletion of the zirconium materials was not performed. The core loading of Fig. 15 was again utilized to approximate a "typical" ATR cycle, and depletion calculations were performed with all shim control removed/minimized to determine the maximum cycle length of an unpoisoned LEU fuel element. Note that the fuel plate thicknesses used for the HPZ and RE designs (last column of Table 2) were used in these analyses, but that this is a new fuel design in that full enrichment (19.75 wt% ^{235}U) was modeled and no neutron poisons were included in the fuel assembly.
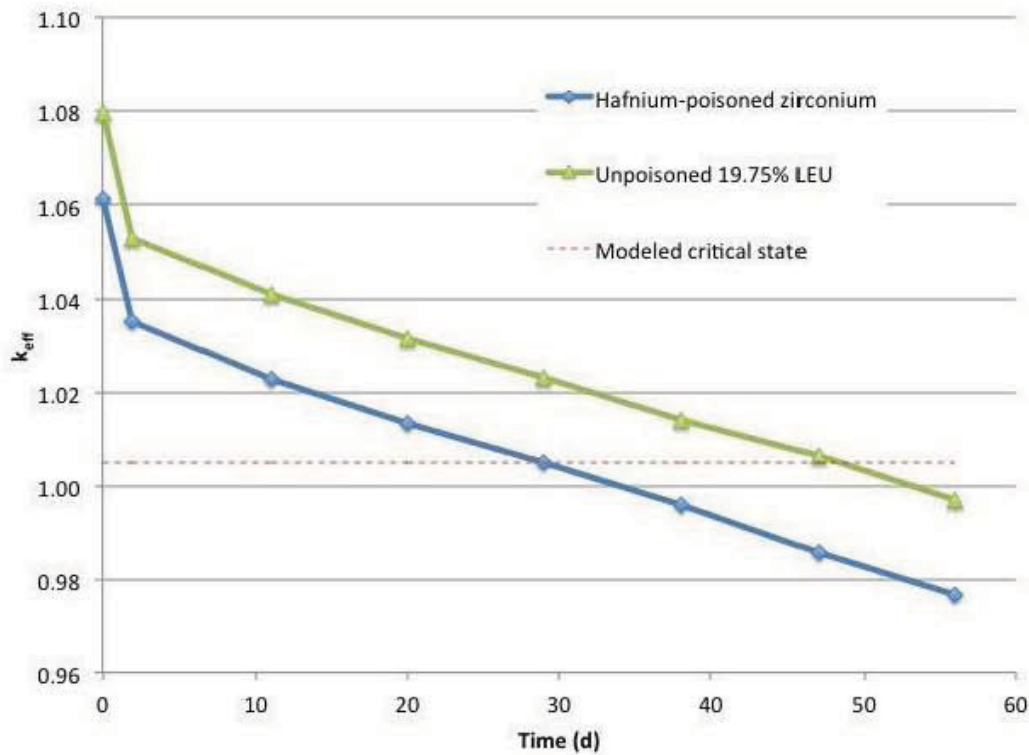
Fig. 17. Performance of unpoisoned and HPZ fuel designs for a prototypic cycle calculation.

Results of these calculations are shown in Fig. 17. The plot shows both the previous (HPZ) and unpoisoned results, and shows the maximum lifetime of a core loaded with this fuel design would be on the order of 50 days. This suggests that even in the absence of poison that the fuel does not possess enough initial reactivity to allow a 56-day burn at a 120 MW core power level in a representative core configuration. Hence, the assumed fuel design of Table 2 needs to be adjusted to improve this performance.

The simplest way to do increase reactivity is to add more fuel to each element. However, plate power distribution issues discussed earlier make this a non-trivial exercise. A summary of the process used to identify a new candidate design that shows intermediate

Table 8. Original Chang LEU Design and Candidate Dimensions for Increased Fuel Reactivity with ELF Design

Fuel Plate No.	LEU HPZ and LEU RE (From Table 2)	Candidate LEU Fuel Design
1	0.02413 (9)	0.02032 (8)
2	0.02286 (9)	0.02286 (9)
3	0.02540 (10)	0.02540 (10)
4	0.02794 (11)	0.03048 (12)
5	0.03302 (13)	0.03302 (13)
6	0.03683 (14.5)	0.03556 (14)
7	0.03683 (14.5)	0.03810 (15)
8	0.03683 (14.5)	0.03810 (15)
9	0.03683 (14.5)	0.03810 (15)
10	0.03683 (14.5)	0.03810 (15)
11	0.03683 (14.5)	0.03810 (15)
12	0.03683 (14.5)	0.03810 (15)
13	0.03683 (14.5)	0.03810 (15)
14	0.03302 (13)	0.03556 (14)
15	0.02794 (11)	0.03048 (12)
16	0.0254 (10)	0.02794 (11)
17	0.02032 (8)	0.02286 (9)
18	0.01778 (7)	0.02032 (8)
19	0.01524 (6)	0.01778 (7)

Note: Dimensions are in cm, followed by mils in parentheses.
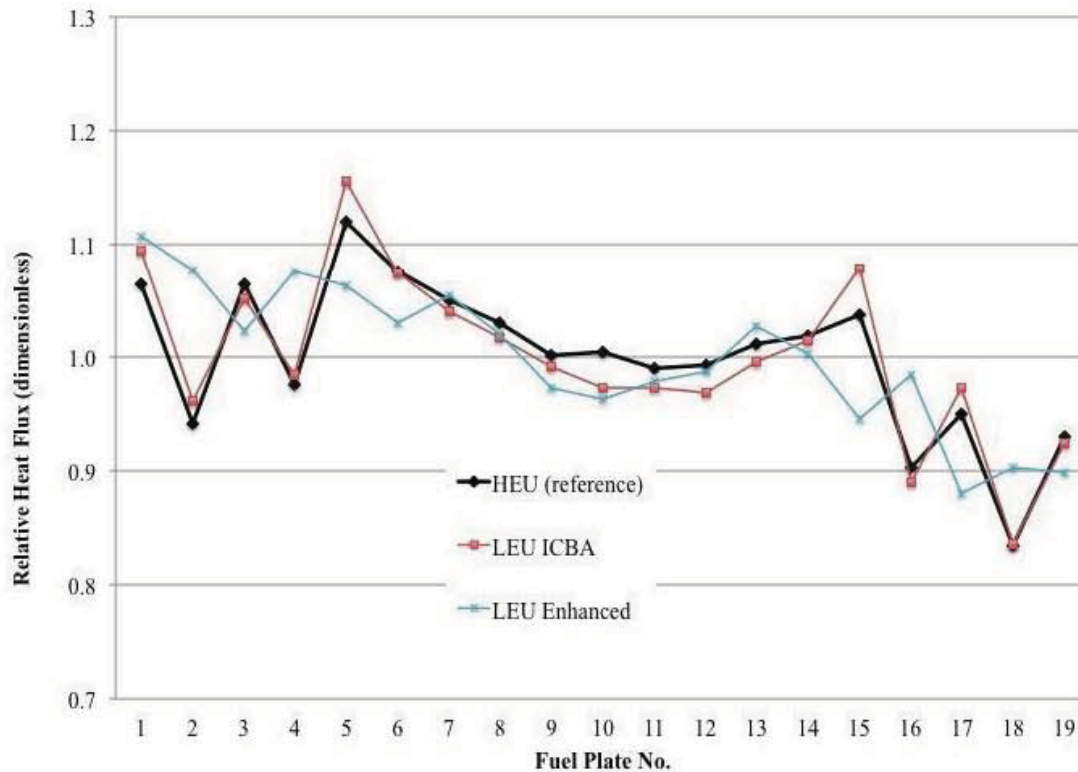
Fig. 18. Heat flux profiles for reference HEU, LEU ICBA and enhanced fuel meat thickness designs.

results would have limited value and is not described here. However, an iterative process in which fuel meat thicknesses were initially adjusted up then selectively reduced to minimize power peaking resulted in a candidate design with 1491 kg of ^{235}U (compared to 1431 kg in previous design, or a 4.2% increase). Fuel thicknesses for this candidate design are given in Table 8. This design is referred to hereafter as simply an Enhanced LEU Fuel (ELF) design. The fuel plate heat flux profile for the ELF assembly configuration is illustrated in Fig. 18; profiles for the reference HEU case and the optimized LEU ICBA case are also shown for comparison. The new enhanced fuel meat thickness of the ELF design shows a significantly flattened radial heat flux profile across the assembly. Note that unlike the HEU and LEU ICBA designs, this heat flux distribution is a function solely of fuel meat thicknesses, as burnable poisons are not included in the ELF assembly design.

As for the earlier prototypic depletion studies, this fuel design was used in a Serpent depletion model under the same burn cycle assumptions. Figure 19 illustrates the results of the prototypic fuel cycle with a core loaded with fresh, once-burned, and twice-burned enhanced fuel assemblies. This figure shows the results of these depletion calculations relative to earlier results, but also demonstrates that the enhanced fuel design appears to meet requirements for three cycles of operation, assuming 56 days per cycle at 120 MW core power. The key point of this calculation is an illustration that with modest increases in fuel masses with an appropriate distribution of fuel meat thicknesses, minimum operating history requirements can be met.
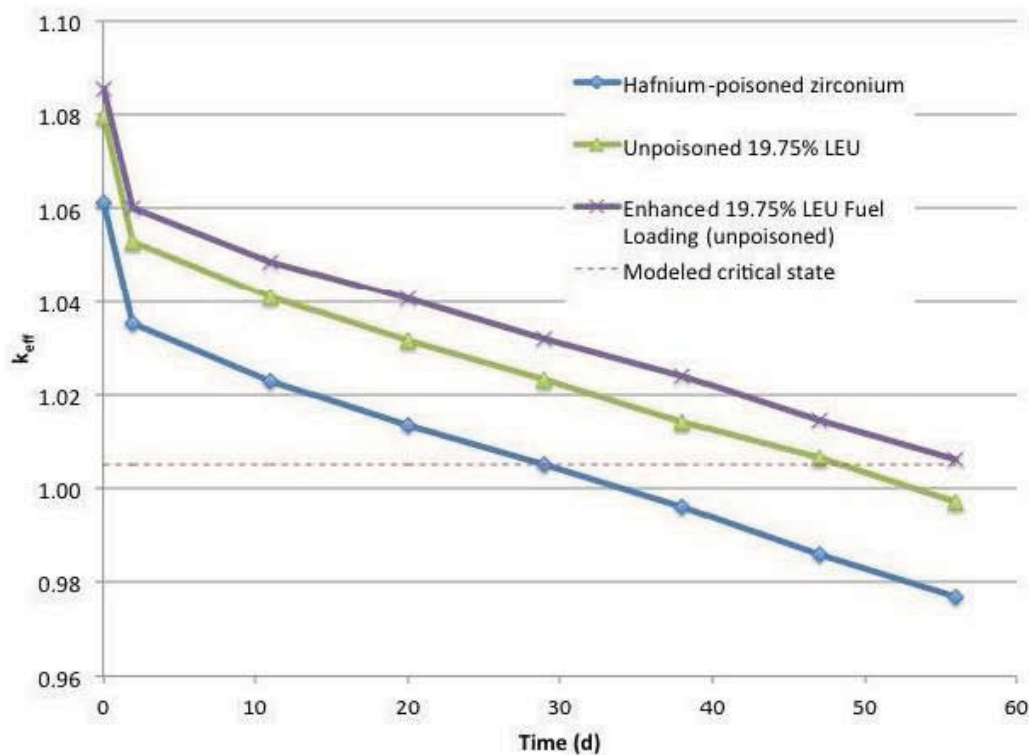
Fig. 19. Performance of enhanced fuel thickness design relative to unpoisoned and HPZ fuel designs for a prototypic cycle calculation.

The ELF design represents a significant change from other fuel design concepts in that it does not use any kind of added poison for reactivity control. While power peaking is controlled by appropriate selection of fuel meat thicknesses, no poison is used to offset the initial excess reactivity of the fuel. However, in normal operation with a significant portion of the core loaded with burned fuel, the reduced reactivity of this burned fuel can be used to offset the excess reactivity of the ELF fuel. For the prototypic loading, the beginning of cycle state was taken critical with 16 neck shims withdrawn and OSCCs set to 54 degrees. Figures 20 and 21 show the number of neck shims removed and OCSS rotations used to perform a depletion simulation with the core maintained close to the critical state (in the range 1.004 to 1.006). Thus, from a reactivity perspective, the ELF design does not appear to provide any operational obstacles in a partially burned core.
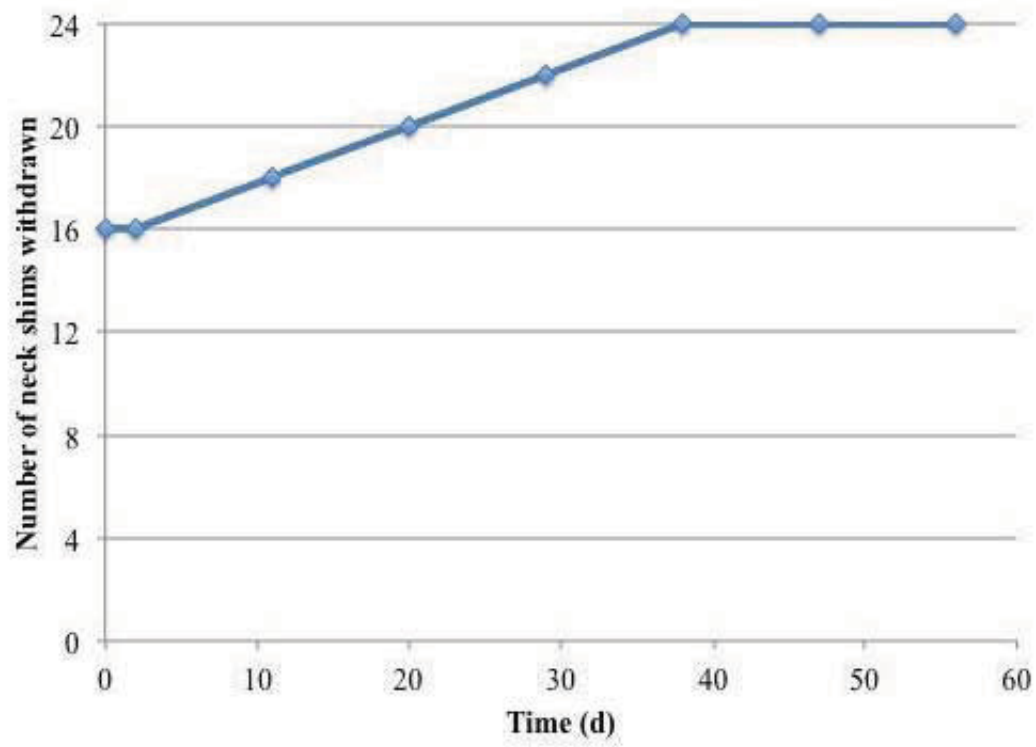
Fig. 20. Number of neck shims removed to maintain ATR criticality during a prototypic depletion cycle.
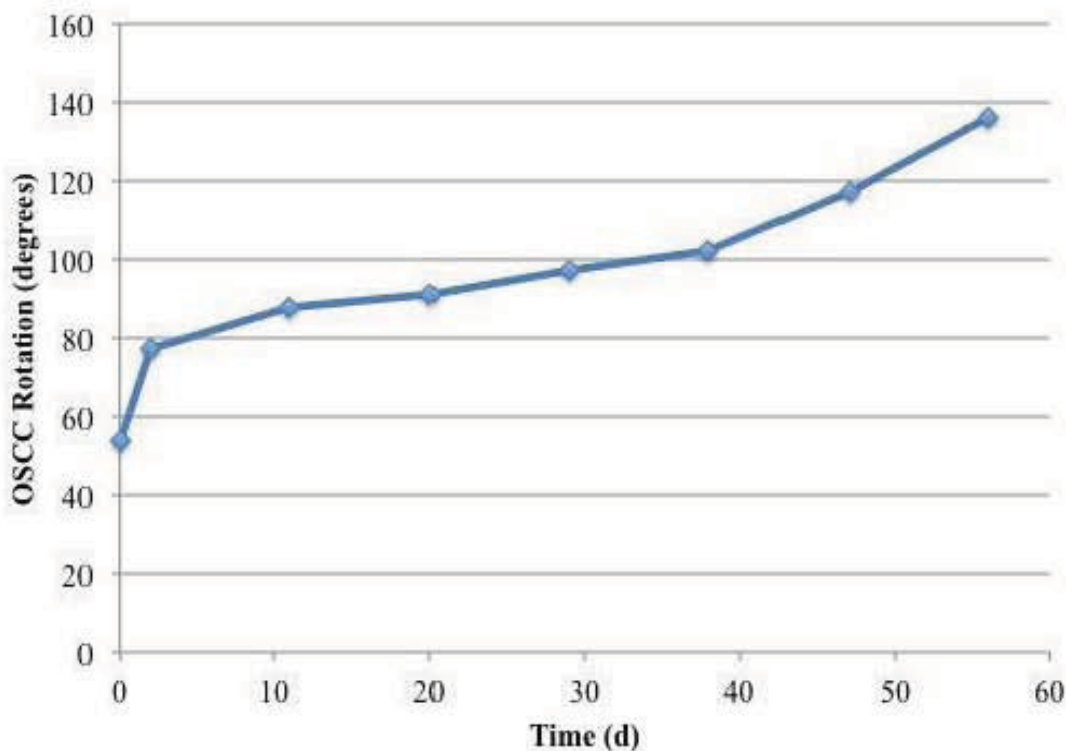
Fig. 21. OSCC rotation needed to maintain ATR criticality during a prototypic depletion cycle.

Additional calculations were performed simulating a core fully loaded with fresh ELF fuel to assess the reactivity control available for such a core. With all neck shims inserted, OSCCs must be rotated to 25° to obtain the critical state. Based on Fig. 14, this represents approximately $1 of excess reactivity, and does not constitute sufficient excess reactivity margin for startup. This fact suggests that a core fully loaded with ELF fuel would not normally be acceptable without additional poisoning; however, other poisoning options external to the fuel (e.g., removable hafnium or fixed/removable borated rods in A positions in the neck region) may be possible.

To conclude this phase of this analysis, depletion and flux calculations performed earlier (as show in Figs. 3, 6-10, and 12-14) were repeated for ELF fuel. Figure 22 shows the eigenvalue as a function of time for Mark VII HEU fuel, the ICBA design (considered to be a reactivity-optimized poisoned design, and the unpoisoned ELF design. The burnup history of Table 4 was again used for this calculation. At first it appears that the ICBA fuel is more reactive than the ELF fuel design; however, one must bear in mind that the results for the ICBA design was calculated with OSCCs rotated to 96.5°, while the ELF design was burned with OSCCs set to 25° to control the excess reactivity, so that all calculations started at the same critical state. At a 96.5° rotation, the ELF design loaded with fresh fuel has an eigenvalue of approximately 1.07, a margin of about 0.065 Δk. With this margin, the ELF would be more reactive than ICBA for the entire life of the fuel. The purpose of this figure is to show the trend of the different fuel types with burnup. Because the ELF design does not contain a burnable absorber, it does not show there reactivity gain at BOL seen in the other two designs. Like ICBA, the ELF design shows a flatter burnup profile than the HEU fuel, due to fissile plutonium production. Looking at the last cycle, is can be seen

107

that the eigenvalue calculated for the ELF design has a slightly shallower profile relative to the ICBA design, due to the increased fissile mass used in the former.
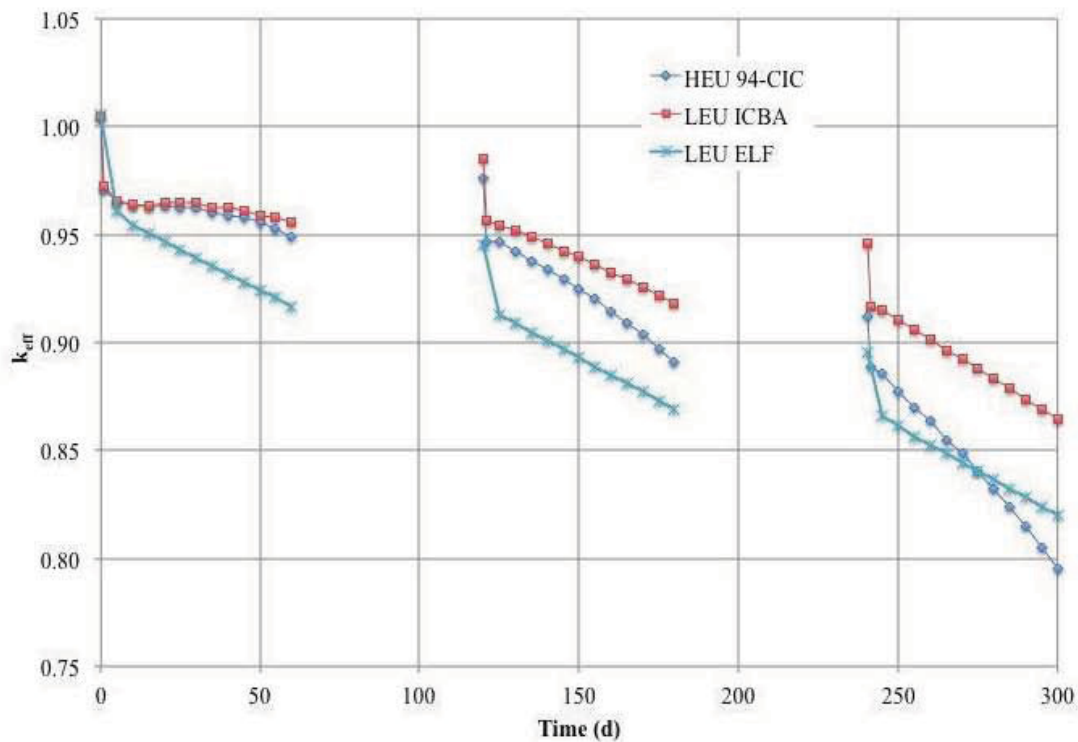
Fig. 22. Results of depletion calculations for HEU Mark 7 and Enhanced LEU Fuel (ELF) designs..

Figures 23-27 show the fluxes for HEU Mark 7 fuel compared to the ELF fuel design. For reference, the results of the earlier ICBA design are also include. Again, each plot shows (a) the full energy range flux profile, and (b) the thermal flux peak in the 0.01eV to 1.0 eV range. At first glance, it appears that the ELF fuel design results in a significant reduction in thermal fluxes, greater than that of the other fuel designs. However, on closer inspection, it is clear that for most lobes the entire flux spectrum is reduced. This is most obvious for the SE (Fig. 25a) and SW (Fig. 25b) flux traps. Clearly, the core configuration with the new fuel design has resulted in a change in the lobe-to-lobe power split. Most likely, the amount of OSCC control required to take this fuel critical (25° rotation) results in suppressed thermal fluxes in the four corner lobes, forcing powers toward the center lobe. This is certainly not an expected operational state – this fuel is so reactive without additional poisons that a core fully loaded with fresh fuel would be very unlikely.

Table 9 provides the power split by lobe for cores operation at 110MW. Unfortunately, this power split makes it difficult to perform an apples-to-apples comparison of target region fluxes. At issue with the conversion of the ATR to LEU is the loss of thermal neutrons due to increased capture in ^{238}U during the slowing down process. The spectral plots have been generated to demonstrate the magnitude of the spectral shift seen in target regions; however, when powers are redistributed between lobes, a visual inspection of the spectra is misleading. Hence, it is perhaps better to devise a comparison that is independent of local power. It is believed that the ratio of fast to thermal fluxes provides a more reasonable assessment of the impact of fuel design on localized spectra. Table 10 shows the fast (E >1.25 eV) to thermal (E < 1.25 eV) ratio within each of the target and other locations tallied for HEU and for each of the other fuel designs analyzed in this report. For all LEU designs, a percentage change relative

to the HEU core is provided. All designs show an average of about 5% or less change (increase) relative to HEU (with the exception of the aluminum filler in the NW in-pile tube). Because fast flux scales to power in each lobe, an increasing ratio represents a decrease in thermal flux for a given power. These results are also illustrated in Fig. 28, which provides a sense of the magnitude of the variations for the various fuel designs. Clearly, for all of the reactivity control options considered here, the mechanism for reactivity control has little affect on the target fluxes; all LEU fuels show about the same fast/thermal ratio for the five flux traps analyzed. Interestingly, a slightly smaller change is seen for the reduced enrichment (RE) design relative to the other LEU designs. The reason for this behavior is not clear; intuitively, with decreased enrichment (and increased ^{238}U content) one would expect the opposite behavior. However, this effect has not been studied further here.
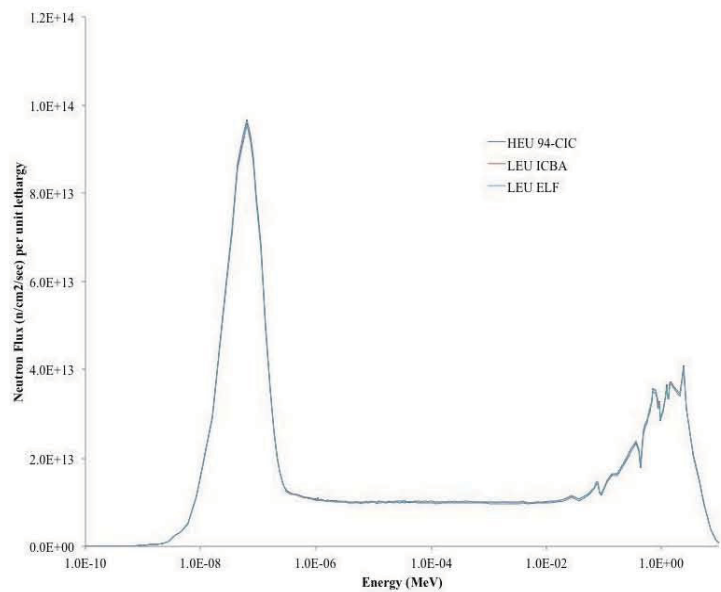
(a)
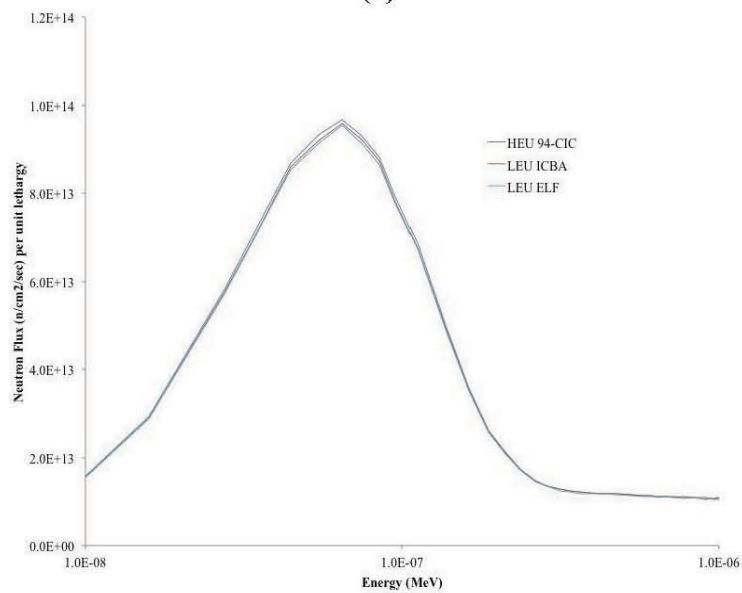
(b)

Fig. 23. Flux spectrum (per unit lethargy) in NE flux trap: (a) full energy range and (b) thermal peak comparing HEU, LEU ICBA, and LEU ELF designs.
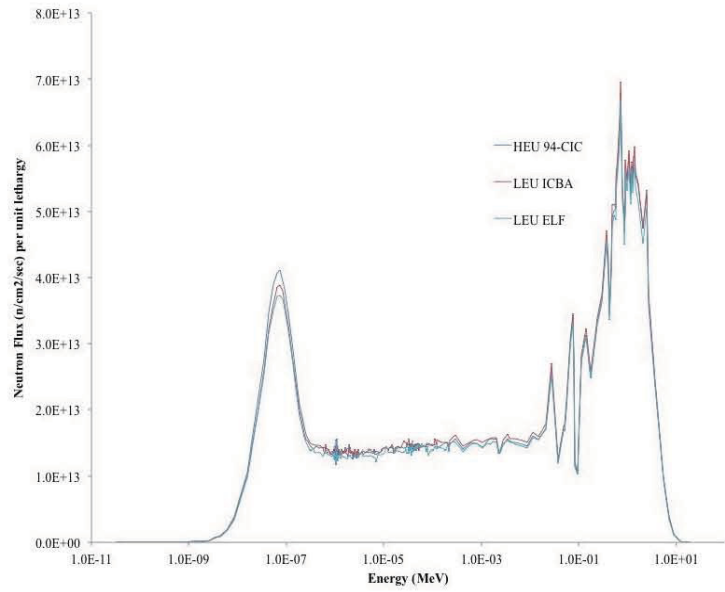
(a)
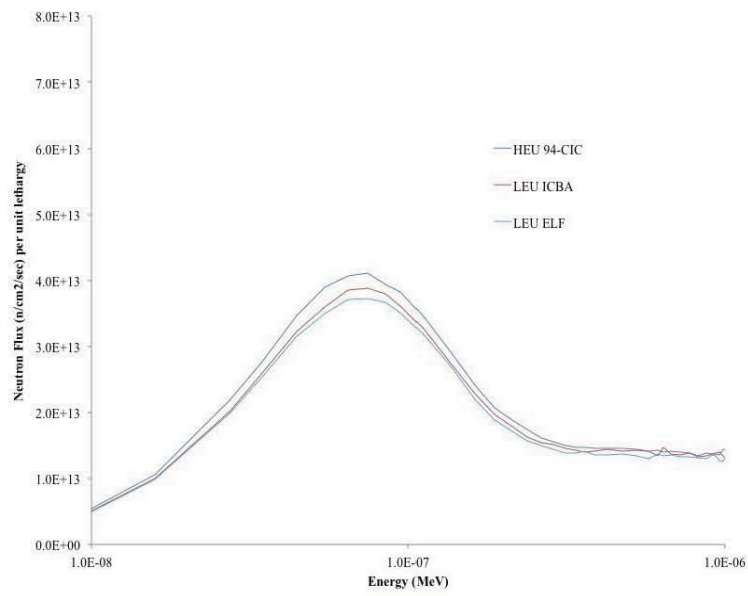
(b)

Fig. 24. Flux spectrum (per unit lethargy) in NW flux trap: (a) full energy range and (b) thermal peak comparing HEU, LEU ICBA, and LEU ELF designs.
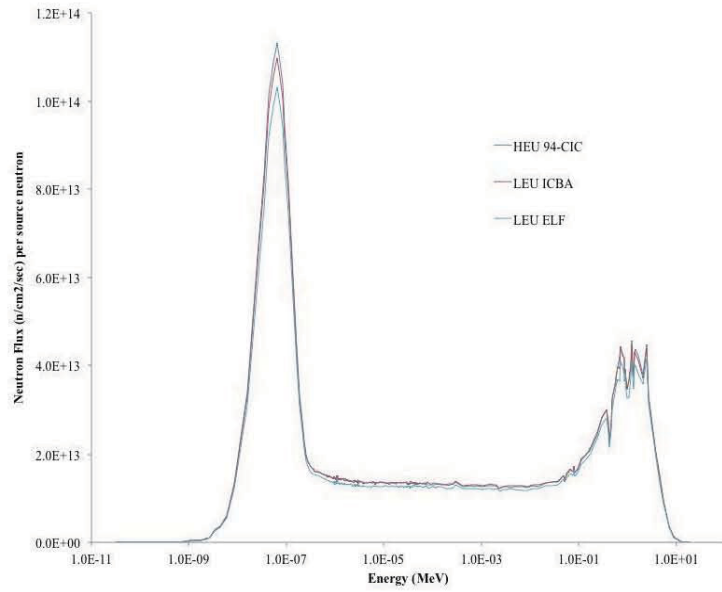
(a)
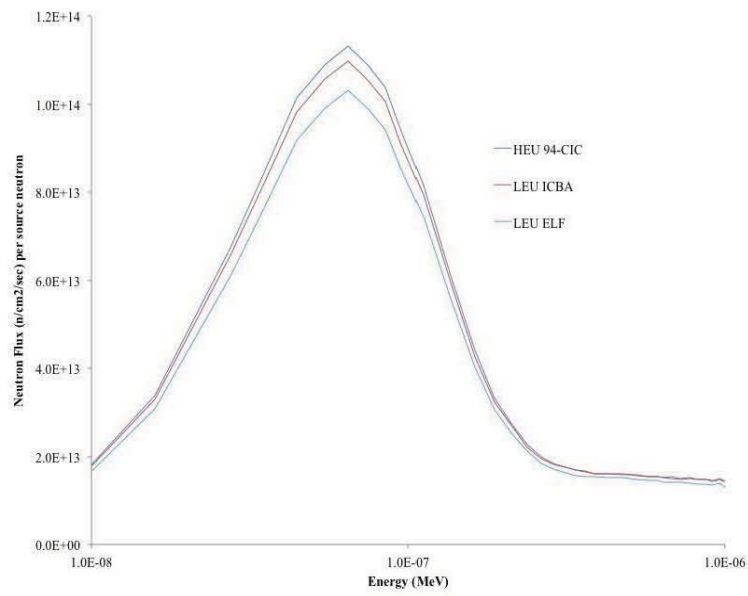
(b)

Fig. 25. Flux spectrum (per unit lethargy) in SE flux trap: (a) full energy range and (b) thermal peak comparing HEU, LEU ICBA, and LEU ELF designs.
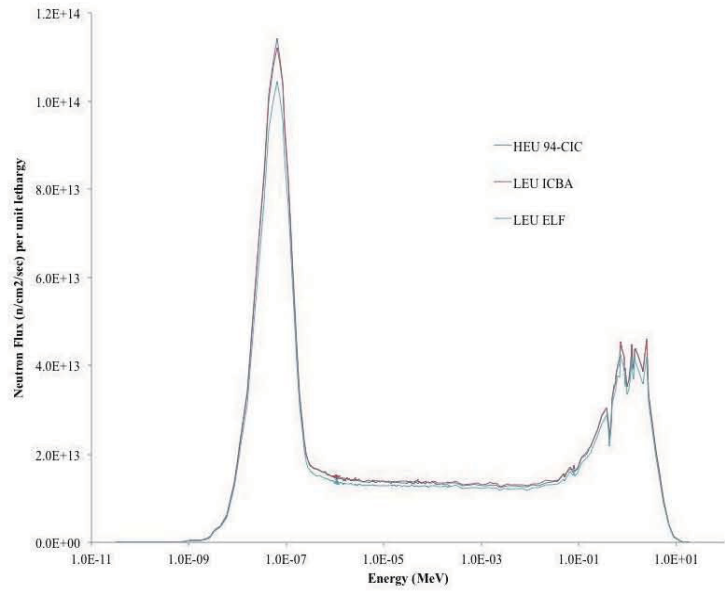
(a)
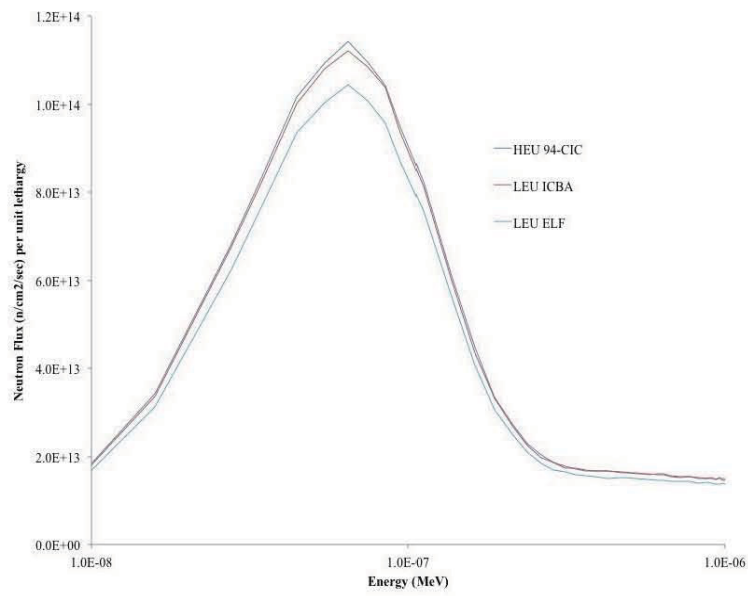
(b)

Fig. 26. Flux spectrum (per unit lethargy) in SW flux trap: (a) full energy range and (b) thermal peak comparing HEU, LEU ICBA, and LEU ELF designs.
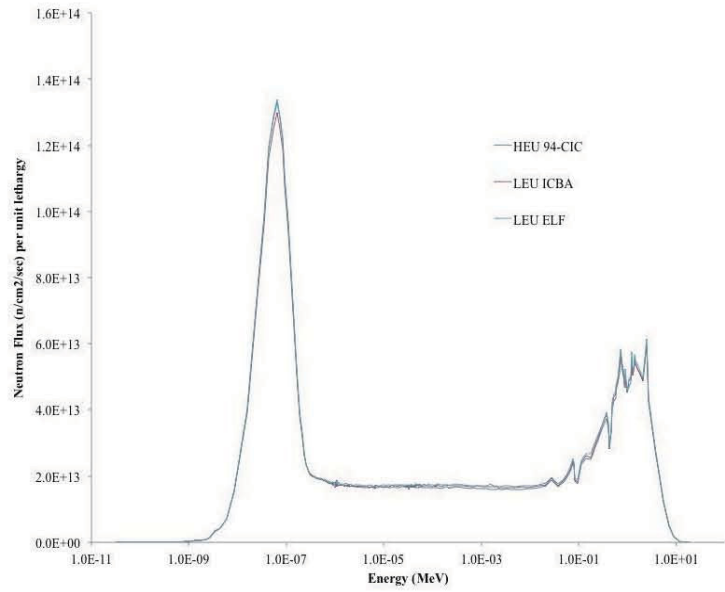
(a)
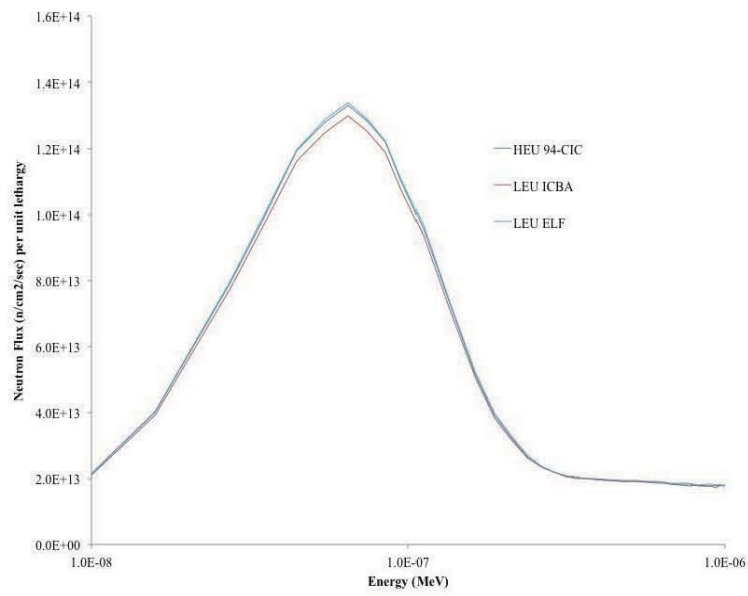
(b)

Fig. 27. Flux spectrum (per unit lethargy) in center flux trap: (a) full energy range and (b) thermal peak comparing HEU, LEU ICBA, and LEU ELF designs.

**Table 9. Comparison of Lobe Power Splits
for HEU and LEU (ELF) Fuel Designs**

| | Lobe Power (MW) | | |
Lobe	HEU	LEU ELF	% Change
NE	18.3	18.8	2.8%
SE	22.7	21.5	-5.0%
SW	22.9	21.7	-5.1%
NW	20.4	20.1	-1.6%
C	25.7	27.8	8.2%

Table 10. Fast to Thermal Flux Ratios and Comparison to HEU Ratios

Location	HEU 94-CIC	LEU ICBA	ICBA Change	LEU HPZ	HPZ Change	LEU RE	RE Change	LEU ELF	ELF Change
NE IPT	1.06	1.09	3.7%	1.09	3.6%	1.08	2.1%	1.09	3.3%
NW IPT	3.14	3.37	7.4%	3.36	7.1%	3.26	3.8%	3.33	6.2%
SE IPT	1.12	1.16	3.2%	1.15	3.1%	1.14	2.1%	1.16	3.3%
SW IPT	1.13	1.15	2.5%	1.16	3.0%	1.15	1.9%	1.16	2.8%
C IPT	1.19	1.24	4.1%	1.22	2.1%	1.20	0.3%	1.23	3.6%
N1 OSCC	0.818	0.832	1.6%	0.821	0.3%	0.812	-0.8%	0.962	17.5%
N2 OSCC	0.940	0.966	2.7%	0.949	0.9%	0.943	0.3%	0.998	6.3%
B-1	1.19	1.25	4.6%	1.21	1.6%	1.17	-1.9%	1.24	3.4%
B-9	0.846	0.874	3.3%	0.853	0.8%	0.852	0.7%	0.851	0.7%
Ave IPTs	1.53	1.60	5.1%	1.60	4.6%	1.56	2.5%	1.59	4.5%
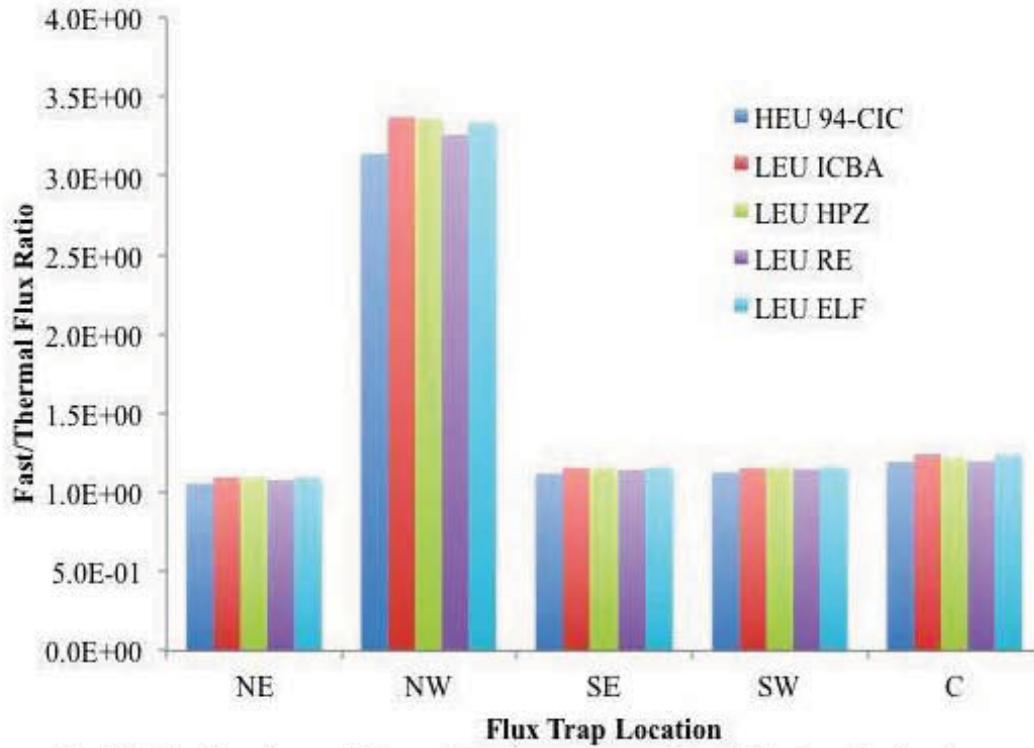
Fig. 28. Fast-to-thermal flux ratios for center region of five in-pile flux traps.

Finally, for completeness, β_{eff} as a function of burnup is plotted in Fig. 29. The results show the same trend as was seen in Fig. 15; HEU and LEU fuels both start with a β_{eff} value around 0.0070 at BOL and around 0.0066 at EOL. Note that the ELF calculations were performed using a greater number of histories than were used in the earlier HEU calculations, so that uncertainties are reduced in the ELF calculations.
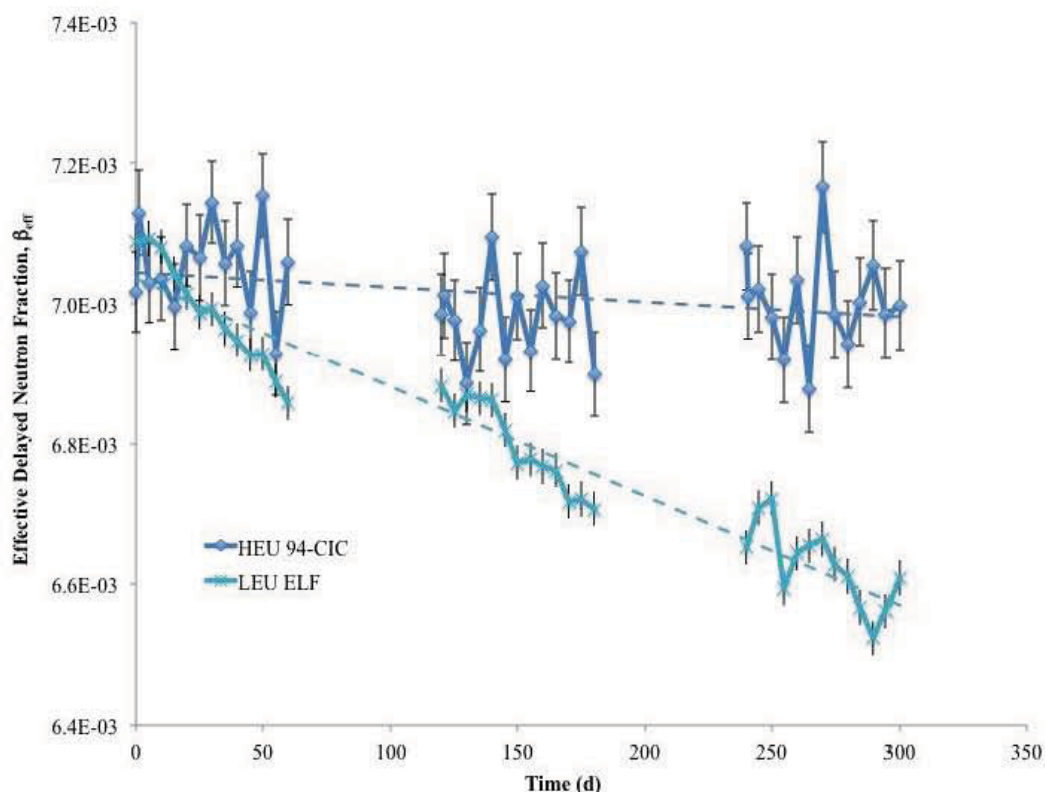
Fig. 29. Delayed neutron fraction β_{eff} as a function of time for HEU Mark 7 and LEU ELF fuel designs.

Summary

Serpent has not been formally validated for ATR calculations and results reported here must be considered in that context. This being said, results reported here are consistent with calculations reported previously for the HEU and LEU ICBA designs. In addition, Serpent has recently performed power prediction calculations based on ATRC experiment 12-5, showing excellent agreement with measured data[18], providing a great deal of confidence in the ability of Serpent to predict ATR behavior for different LEU fuel assembly designs. However, depletion capabilities of Serpent have not been validated in this manner at this time.

This work initially considered a fuel assembly design in which burnable poison boron was replaced by essentially fixed poison hafnium for reactivity control. Hafnium is chemically very similar to zirconium and should be able to be added to the zirconium that is used as a fuel-clad barrier in proposed LEU fuel designs, with no adverse materials effects (although this remains to be determined). A hafnium concentration of approximately 2 wt % in zirconium was found to provide the desired level of excess reactivity.

Initial scoping calculations performed for the hafnium-poisoned barrier used the fuel dimensions specified for the ICBA fuel design. However, this model resulted in an unacceptably increased power and heat flux in outer fuel plates that would eventually cause problems for safety limits. Thus, a more recently proposed set of fuel plate dimensions was adopted. These dimensions are know to be too tightly specified relative to manufacturing tolerances, but were adopted as the best available for this study.

117

Subsequently, the need for hafnium control was questioned, as an equivalent reduction of excess reactivity via a decreased initial fuel enrichment would also serve the same function at beginning of life. Hence, second fuel element design was considered, where pure zirconium was used in the modeled barrier material with just less than 18% ^{235}U enrichment to match the desired initial core reactivity. The two models, named hafnium-poisoned zirconium (HPZ) and reduced enrichment (RE), were analyzed. The current Mark VII HEU fuel assembly design was also modeled, along with the previously studied LEU integral clad burnable absorber (ICBA) design. The latter provided a check on the performance of Serpent by allowing comparison to earlier results, and also highlighted the difference in fuel performance when using a fixed poison in place of a burnable poison.

Results show that both the HPZ and RE fuel element designs are able to match the fuel burnup lifetime of current HEU fuel; because it contains more fissile fuel, the HPZ design has more reactivity at discharge than the RE design. Both designs show slight decreases in both fast and thermal fluxes, although changes vary by core location. Because the fast fluxes reported in this work are a summation of all neutrons with energies above 1.25 eV, it is unclear where in this energy range neutrons are being lost, although it is likely that most "fast" neutrons are lost at energies below 100 keV due to resonance capture.

Unfortunately, because hafnium acts as a fixed absorber with little burnout over the fuel lifetime, it does not allow the reactivity recovery that a burnable poison such as boron provided. In a realistic core, loaded with both fresh fuel and fuel with multiple cycles of burnup, the excess reactivity is insufficient to meet requirements for a full cycle. Removing the hafnium poison and using pure zirconium for the barrier material and calculating the same cycle burnup indicates that this design contains insufficient fuel mass to complete three full prototypic cycles.

Increasing the mass in fuel plates is not as simple as adding a fractional mass of fuel to each plate. It was assumed that the manufacturing process would create fuel meats rolled to the closest 1 mil thickness. Adding 1 mil of fuel to each plate would result in excessing peaking in outer plates. Thus, the thickness of each plate was varied to find a set of thicknesses that would add needed mass without increasing power peaking. A workable design was found and used for further analysis; this is not an optimized design in any way other than trying to minimize peaking. It is simply a design found to be a possible candidate that could be used to complete the analyses documented here. For reference, this candidate design was termed Enhanced LEU Fuel, or ELF.

Because the ELF design is unpoisoned, it relies on reduced reactivity mechanisms elsewhere in the core. Additional poisons inserted in A-holes may be an option, but under normal operation, the ATR is loaded with a mixture of fresh and burned fuels. A scoping calculation representing a "typical" or "prototypic" core loading with fresh, once, and twice burned fuels was found to provide sufficient negative reactivity to be able to provide required startup excess reactivity, and was used to demonstrate that such a core could be operated for three 60 day cycles at 110 MW/cycle with excess reactivity until the end of the third cycle.

A study of spectral shift for the ELF design and a comparison to other designs indicates that a 2-3 percent increase in the fast/thermal ratio is seen for most flux traps, with a larger (5-7%) increase for the bounding case of the solid aluminum filler in the NW flux trap in this model. This increase is primarily indicating a decrease in the thermal flux in each location. This change is seen for all LEU fuel types, irrespective of the type of reactivity control used. These results demonstrate that conversion to LEU fuel will result in slight decreases in thermal fluxes in flux traps, but decreases on the order of only 2-3% will be seen, which is a manageable level.

References

8. G.S. Chang, R.G. Ambrosek, M.A. Lillo, "Advanced Test Reactor LEU Fuel Conversion Feasibility Study (2006 Annual Report),' INL/EXT-06-11887, Idaho National Laboratory. Dec. 2006.

9. G. S. Chang, "ATR LEU Fuel and Burnable Absorber Neutronics Performance Optimization by Fuel Meat Thickness Variation," INL/CON-07-12949, RERTR-2007 - International Meeting on Reduced Enrichment for Research and Test Reactors, Prague, Czech Republic, Sept. 2007.

10. G. S. Chang, "ATR LEU Monolithic Foil-Type Fuel with Integral Cladding Burnable Absorber Design – Neutronics Performance Evaluation," RERTR 2011 – 33rd International Meeting on Reduced Enrichment for Research and Test Reactors, Santiago, Chile, Oct. 2011.

11. M. D. DeHart, W. F. Skerjanc and B. K. Castle, "Evaluation of RERTR LEU Conversion Core Physics Analysis Methods," ECAR-1819, Idaho National Laboratory, Feb. 20, 2012.

12. M. D. DeHart, W. F. Skerjanc and S. R. Morrell, "Analysis of the Reactor Physics of Low-Enrichment Fuel for the INL Advanced Test Reactor in support of RERTR," Proc. ANS Annual Meeting, American Nuclear Society, Chicago, IL, June 2012.

13. R. Stamm'ler et al., "User's Manual for HELIOS," Studsvik/Scandpower (1994).

14. D. S. Lucas, "Core Modeling of the Advanced Test Reactor with the Attila Code," M&C 2005: International Topical Meeting on Mathematics and Computation, Supercomputing, Reactor Physics, and Nuclear and Biological Applications, Avignon, France, 2005.

15. J. Leppänen, "A New Assembly-level Monte Carlo neutron transport code for reactor physics calculations." Proc. M&C 2005. Avignon, France, Sept. 12-15 2005.

16. M. D. DeHart and S. M. Bowman, "High-Fidelity Lattice Physics and Depletion Analysis Capabilities of the SCALE 6.0 Code System Using TRITON," *Nuclear Technology*, **174**, 2, 196-213, May 2011.

17. F. B. Brown, et al., "MCNP Version 5," Trans. Am. Nucl. Soc., **87**, 273 (November 2002).

18. G. S. Chang M. A. Lillo R. G. Ambrosek, "Neutronics and Thermal Hydraulics Study for Using a Low-Enriched Uranium Core in the Advanced Test Reactor 2008 Final Report," INL/EXT-08-13980, Idaho National Laboratory, June 2008.

19. G. A. Moore et al., "Full Size U-10Mo Monolithic Fuel Foil and Fuel Plate Fabrication – Technology Development," INL/CON-09-17519, 14th International Topical Meeting on Research Reactor Fuel Management (RRFM), Marrakech, Morocco, March 2010.

20. S.S. Kim, B.G. Schnitzler, "Advanced Test Reactor: Serpentine Arrangement of Highly Enriched Water-Moderated Uranium-Aluminide Fuel Plates Reflected by Beryllium", NEA/NSC/DOC/(95)03/II, Volume II, HEU-MET-THERM-022.

21. G. Chang, personal communication, May 29, 2012.

22. A. P. Cochran Letter to A. J. Bieniawski, "Naval Reactors Functional Requirements for the

Advanced Test Reactor," NR:RM:APCochran S#08-04461, Dec 11, 2008.

23. E. Swain, personal communication, July 25, 2012.

24. B. Chase, personal communication, July 25, 2012.

25. D. W. Nigg et al., "Advanced Test Reactor Core Modeling Update Project - Annual Report for Fiscal Year 2012," Draft

Appendix C – MCNP Neutronic Analyses for ICBA and ISBA Fuel Element Designs on LEU Conversion at Beginning of Life

C.R. Glass
G.S. Chang

Nuclear Science and Technology Directorate

Title: MCNP Neutronic Analyses for ICBA and ISBA Fuel Element Designs on LEU Conversion at Beginning of Life

ECAR No.:   2043   ECAR Rev. No.: Rev. 0   Project File No.: 31230   Date: Sept 2012

5.   Review (R) and Approval (A) and Acceptance (Ac)[1]:

		Typed Name/Organization	Signature or eCR No. [2]
Performer/Author		C. R. Glass / C660	9/12/12
		G. S. Chang / C110	Greg S Chang 09/12/2012
Technical Checker	R	M. D. DeHart / C110	
Independent Peer Reviewer[3]	R	D. W. Nigg / C100	P.P DAVID NIGG
Performer's Manager	A	G. J. Youinou / C110	
Requester	Ac	S. R. Morrell / D210	9/13/2013
Controlled Unclassified Information	R	C. R. Glass / C660	9/12/12
Nuclear Safety[3]	Ac	N/A	

1   Review and Approval are required. See LWP-10200 for definitions and responsibilities.

2   Electronic Change Request (ECR) numbers in lieu of signatures on this page indicate electronic final review, approval and acceptance by the listed individuals.

3   If Required, per LWP-10200.

1. SCOPE AND BRIEF DESCRIPTION

The purpose of this ECAR is to document the physics analysis of three proposed Reduced Enrichment Research and Test Reactor (RERTR) Full Element designs impact on the full core conversion of the Advanced Test Reactor (ATR). Included in this analysis are results for assembly power profiles and relative radial, axial, and azimuthal power profiles. These calculations were performed using the MCNP computer code. The neutronics model, analysis details, and results are presented in the attached report.

2. MODEL DEVELOPMENT AND VERIFICATION

The analysis considered a 19-plate full core model of the ATR. The base model to compare the effects of the new assembly designs on ATR is of the core internals after the Core Internal Changeout (CIC) of 1994. This core model was first developed in Reference [1]. Figure 1 is a top view sketch of the model, and Figure 2 is a side view sketch of the model. Figure 3 is a top view sketch of the model used to describe the ATR fuel element in the model.

Verification of this MCNP model was performed by comparing measurement data from both ATR and ATRC. Both K_{eff} and assembly power distributions were compared. Table 9 and Table 10 in Appendix A show the element powers and their percent differences for ATR measurement, ATRC measurement, and the HEU MCNP model. It should be noted that ATR and ATRC are nearly identical reactor cores which utilize the same fuel in the same configuration with most of the other components of the cores being the same as well. As such it would be expected that the measurement comparisons between the 2 cores should be fairly close, with any differences in assembly power measurements being due to either measurement uncertainty or fluxuations in the manufacturing or impurities of the fuel, control drums and shims, and the reflector. When the ATR and ATRC measurements are compared, we see a maximum assembly difference of 12.85% and a standard deviation of the % differences between the assembly powers of 4.83%. When the same comparison is made between the MCNP HEU model (Case-A) and ATR, the maximum assembly difference drops to -8.74% with a standard deviation of 4.09%. The K_{eff} of the MCNP model for the same control drum and rod configurations as those from the first critical following the CIC of 1994 was also calculated as 0.99994 +/- 0.00004. The conclusion of these two comparisons shows that the HEU MCNP model is at least as good as using ATRC measurements to predict ATR behavior. Any differences between the MCNP model and ATR measurements are likely due to measurement uncertainty along with minor assumptions in the modeling and unknowns in material impurities and fabrication.

This now verified model was used throughout the analysis, with the description of only the fuel elements changed for the different cases. In the base case (Case-A), all 40 elements were modeled as fresh, standard 7F, HEU type fuel elements. For subsequent cases, a LEU element with Integral Cladding Burnable Absorber (ICBA) replaced all 40 fuel elements (Case-B), an LEU element with Integral Side-plate Burnable Absorber (ISBA) comprised of ^{10}B replaced all 40 fuel elements (Case-C), or an LEU element with ISBA comprised of Cadmium replaced all 40 elements (Case-D). Table 1 shows the specifications

for a typical type 7F fuel element. Table 2 shows the specifications of LEU-ICBA, Table 3 the specifications for the ^{10}B LEU-ISBA, and Table 4 the specifications of the Cd LEU-ISBA.
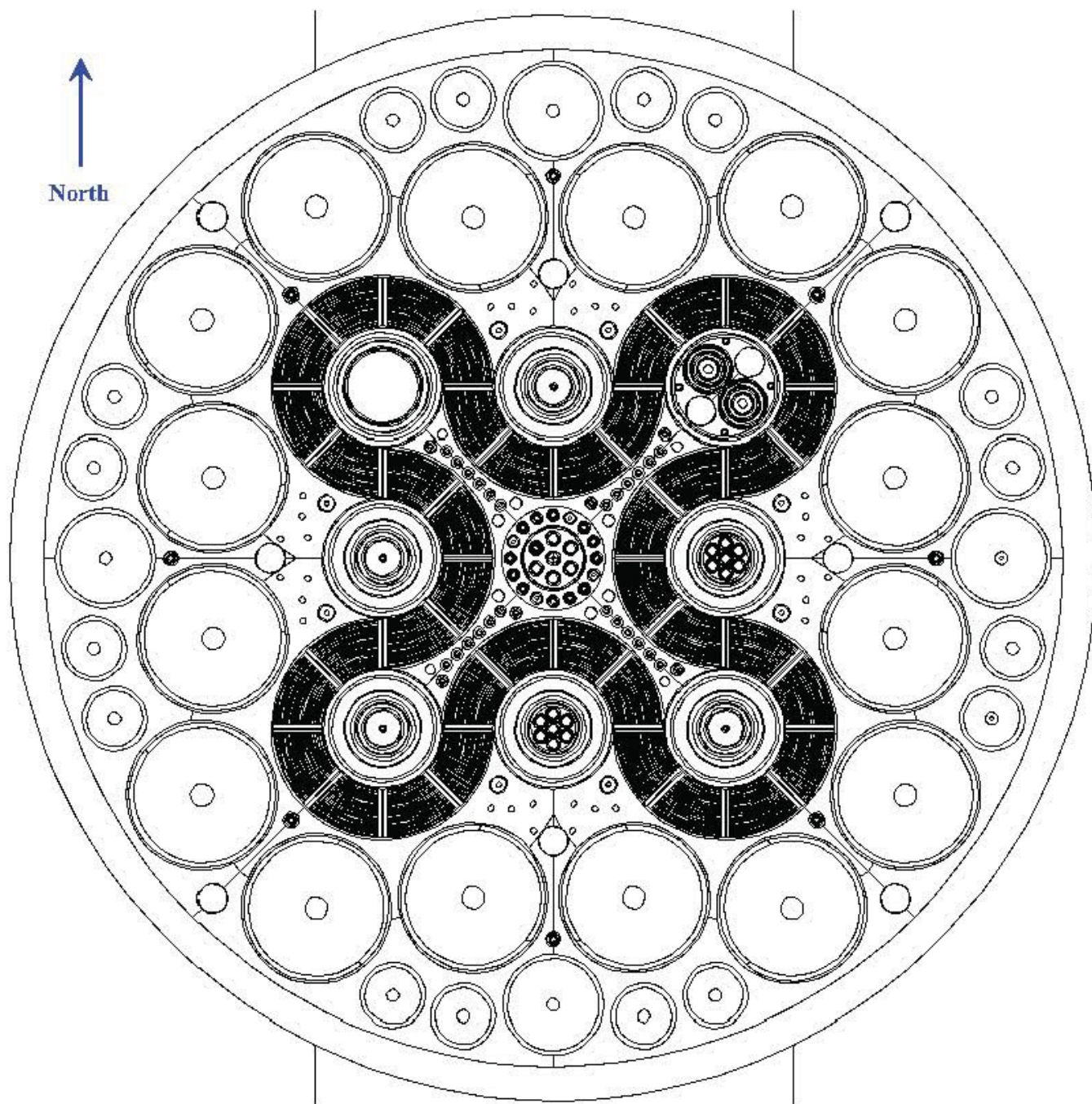
Figure 1. Radial cross section view of MCNP model used to describe CIC-1994.
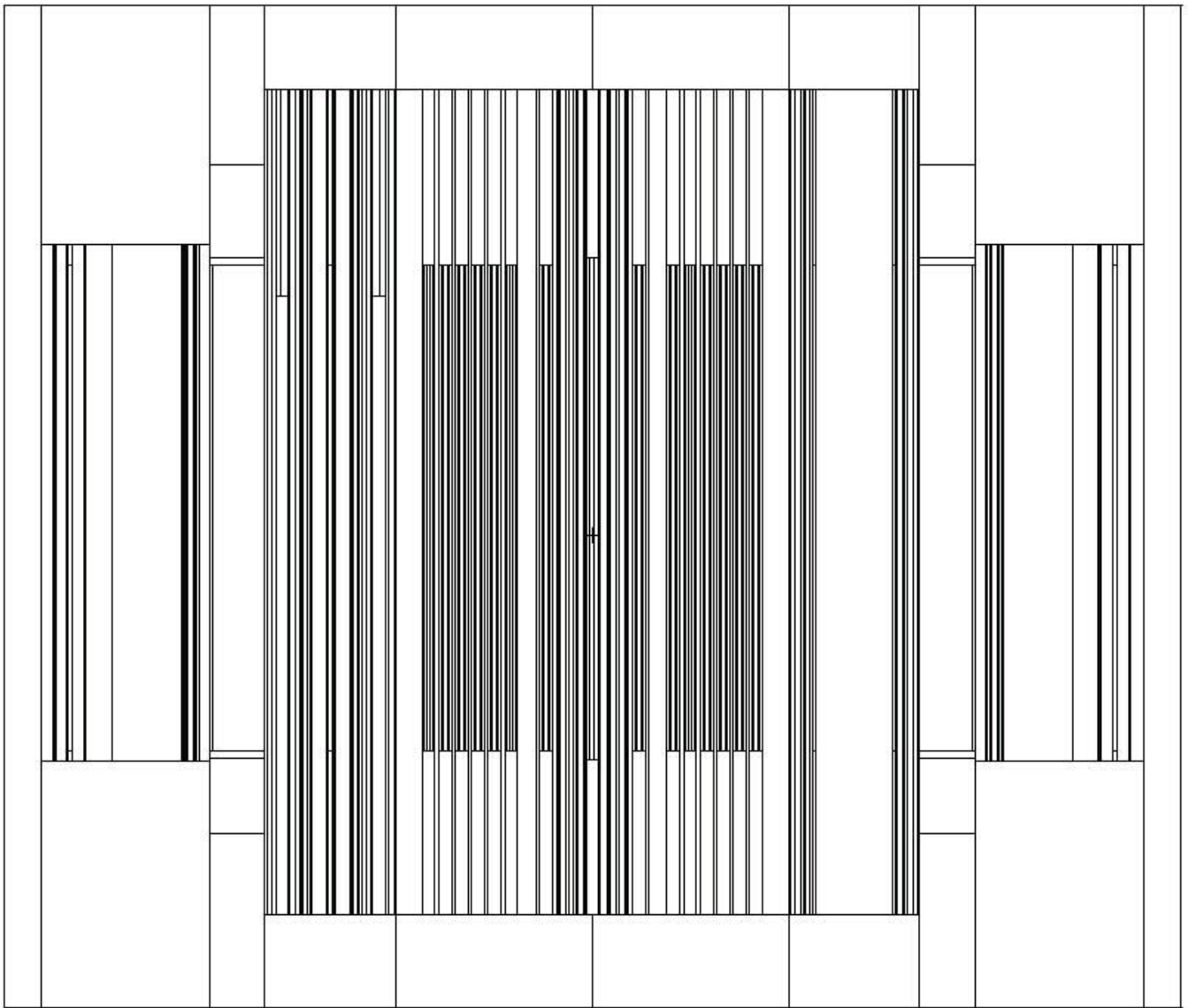
Figure 2. Axial cross section view of MCNP model used to describe CIC-1994.
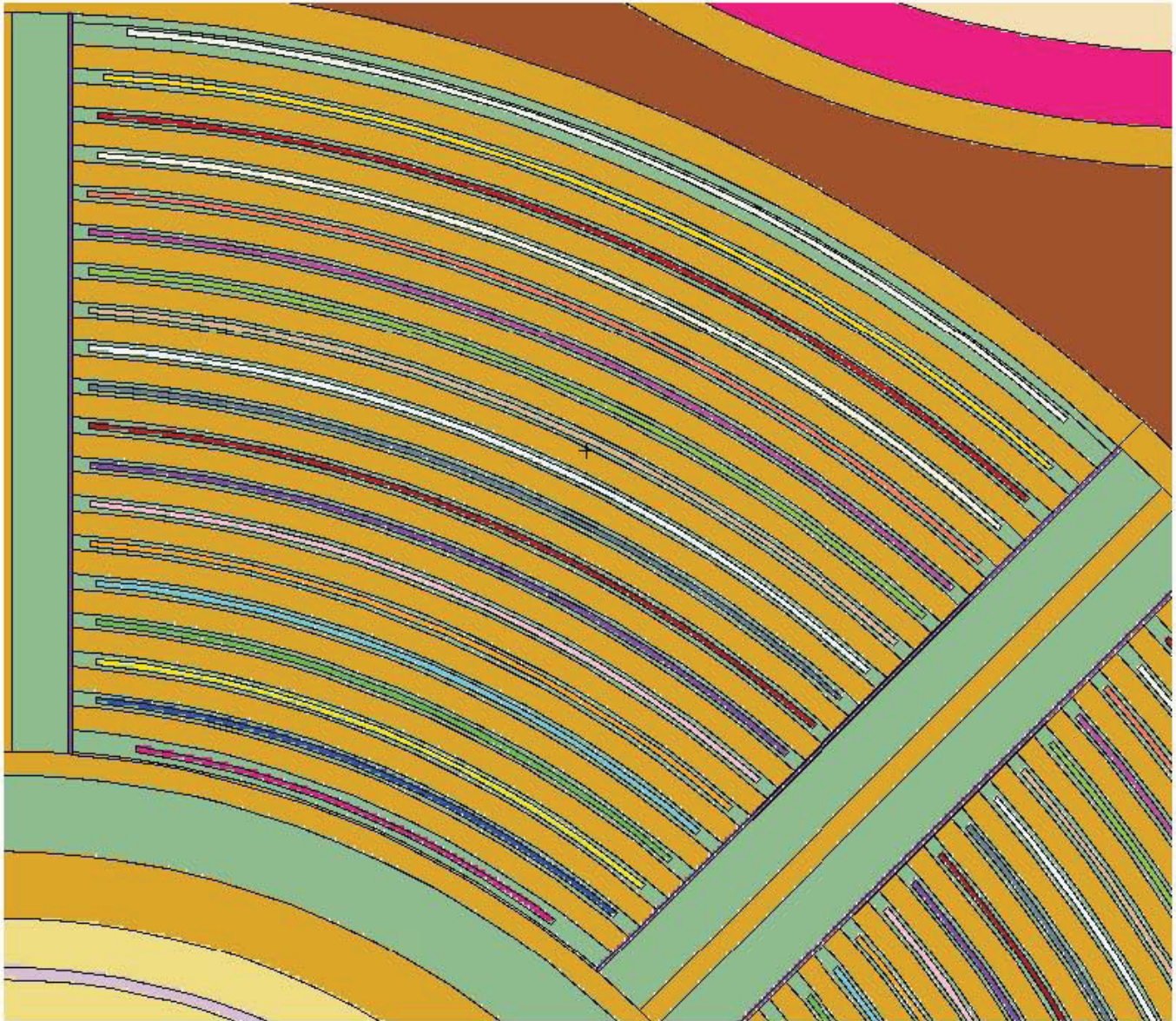
Figure 3. Top view of the MCNP model of an ATR fuel element used to describe CIC-1994.

Table 1. Specifications for a type 7F ATR Fuel Element.

Plate	Fuel Meat Thickness (mil)	U-235 Mass (g)	B-10 Mass (g)
Plate-1	20.00	24.30	0.063
Plate-2	20.00	29.10	0.078
Plate-3	20.00	38.70	0.044
Plate-4	20.00	40.40	0.045
Plate-5	20.00	52.10	--
Plate-6	20.00	54.60	--
Plate-7	20.00	57.00	--
Plate-8	20.00	59.40	--
Plate-9	20.00	61.80	--
Plate-10	20.00	64.20	--
Plate-11	20.00	66.60	--
Plate-12	20.00	69.00	--
Plate-13	20.00	71.40	--
Plate-14	20.00	73.80	--
Plate-15	20.00	76.30	--
Plate-16	20.00	64.00	0.071
Plate-17	20.00	65.90	0.073
Plate-18	20.00	53.80	0.143
Plate-19	20.00	52.60	0.143
Total		1075.00	0.660

Table 2. Specifications for Case-B, LEU-ICBA.

Plate	Fuel Meat Thickness (mil)	U-235 Mass (g)	B-10 Mass (g)
Plate-1	8	32.876	0.058
Plate-2	10	35.016	0.149
Plate-3	10	46.150	0
Plate-4	11	48.512	0
Plate-5	13	66.162	0
Plate-6	13	69.247	0
Plate-7	13	72.339	0
Plate-8	13	75.450	0
Plate-9	13	78.536	0
Plate-10	13	81.623	0
Plate-11	13	84.707	0
Plate-12	13	87.805	0
Plate-13	13	90.869	0
Plate-14	13	93.981	0
Plate-15	13	97.049	0
Plate-16	10	77.049	0
Plate-17	10	79.417	0
Plate-18	9	65.439	0.111
Plate-19	8	67.704	0.317
Total	--	1349.931	0.636

Table 3. Specifications for Case-C, LEU-ISBA (^{10}B).

Plate	Fuel Meat Thickness (mil)	U-235 Mass (g)
Plate-1	9.0	37.01
Plate-2	9.0	35.04
Plate-3	10.0	46.17
Plate-4	11.0	53.38
Plate-5	13.0	66.19
Plate-6	14.5	77.27
Plate-7	14.5	80.71
Plate-8	14.5	84.17
Plate-9	14.5	87.62
Plate-10	14.5	91.07
Plate-11	14.5	94.51
Plate-12	14.5	97.97
Plate-13	14.5	101.40
Plate-14	13.0	104.86
Plate-15	11.0	82.15
Plate-16	10.0	77.07
Plate-17	8.0	63.55
Plate-18	7.0	57.27
Plate-19	6.0	50.79
Total	--	1388.21

*0.68g ^{10}B per FE

Table 4. Specifications for Case-D, LEU-ISBA (Cd).Table 5

Plate	Fuel Meat Thickness (mil)	U-235 Mass (g)
Plate-1	9.0	37.01
Plate-2	9.0	35.04
Plate-3	10.0	46.17
Plate-4	11.0	53.38
Plate-5	13.0	66.19
Plate-6	14.5	77.27
Plate-7	14.5	80.71
Plate-8	14.5	84.17
Plate-9	14.5	87.62
Plate-10	14.5	91.07
Plate-11	14.5	94.51
Plate-12	14.5	97.97
Plate-13	14.5	101.40
Plate-14	13.0	104.86
Plate-15	11.0	82.15
Plate-16	10.0	77.07
Plate-17	8.0	63.55
Plate-18	7.0	57.27
Plate-19	6.0	50.79
Total	--	1388.21

*33.49g Cd per FE

3. BACKGROUND DATA

For CIC-1994 (NT-3 of Cycle 103A-2), the ATR was loaded with 40 new (fresh) type 7F fuel elements. The Large Inpile Tube (LIPT) in the northwest flux trap was empty. The Standard Inpile Tube (SIPT) in the north, west, southwest, and southeast flux traps had stainless steel flow tubes installed. The northeast flux trap was loaded with the 23-position Large Irradiation Housing Assembly (LIHA), with aluminum fillers in positions NE-2, NE-9 and NE-15 through NE-21, with Low Specific Activity (LSA) Cobalt capsule trains loaded in positions NE-3, NE-5 through NE-7, NE-10, NE-12 through NE-14, and NE-22, and the remaining positions (NE-1, NE-4, NE-8, NE-11, and NE-23) containing flux monitor wire holders. Six of the Small Irradiation Housing Assembly (SIHA) positions in the east flux trap were loaded with LSA Cobalt, with position E-7 containing a flux monitor wire holder. Six of the SIHA positions in the south flux trap were loaded with LSA Cobalt, with position S-7 containing a flux monitor wire holder. Position C-6 of the SIHA in the center flux trap was loaded with LSA Cobalt, position C-7 contained a flux monitor wire holder, and the remaining positions were loaded with aluminum fillers. Positions H-1, H-4, H-5, H-7 through H-9, H-12, H-13, H-15, and H-16 were loaded with LSA Cobalt. A re-entrant tube for the ^{16}N power monitoring system was installed in positions H-3 and H-11. The remaining H-hole positions (which surround the center flux trap) contained flux monitor wire holders. A Solid Flow Restrictor (SFR) was loaded into each of the inboard A positions (A-1 through A-8). An SFR was loaded into positions A-9 through A-12, and a short aluminum flow restricting rod was loaded into each of the remaining outboard A positions (A-13 through A-16). The startup source (SUS) was loaded into position B-4, and SFRs were loaded into each of the remaining small B positions. Beryllium fillers were loaded into each of the large B positions and each of the small, medium, and large I holes. All neck shim rods were fully inserted, and the two regulating rods (SW-4 and SE-4) were fully withdrawn. Table 6 shows the core loading for CIC-1994 (NT-3 of Cycle 103A-2).

Table 6. Core Loadings.

Core Position	Cycle 103A-2 (NT-3)	Drawing / Reference
Fuel Annulus		
F-1 through F-40	40 new 7F-type fuel elements	405400
Large Inpile Tube		
Northwest	FMWH with IR-1, 2, 3, 4	403870, 035561
Standard Inpile Tubes		
North	SS Flow Tube	9074D35
West	SS Flow Tube	9074D35
Southwest	SS Flow Tube	9074D35
Southeast	SS Flow Tube	9074D35
Safety Rod Monitor Positions		
North	Empty, Safety Rod	
West	Empty, Safety Rod	
East	SR-1 through SR-4, Safety Rod	417424
Southwest	SR-5 through SR-8, Safety Rod	417424

Table 6. Core Loadings.

Core Position	Cycle 103A-2 (NT-3)	Drawing / Reference
South	SR-9 through SR-12, Safety Rod	417424
Southeast	SR-13 through SR-16, Safety Rod	417424
NE Flux Trap Irradiation Facility with 23-hole LIHA		
NE-1	LMWH-1	443656
NE-2, NE-9, NE-15 through NE-21	Aluminum Filler	
NE-3, NE-5 through NE-7, NE-10, NE-12 through NE-14, NE-22	ATRC LSA Cobalt	LSL-24-94
NE-4	LMWH-2	443656
NE-8	LMWH-3	443656
NE-11	LMWH-4	443656
NE-23	LMWH-5	443656
East Flux Trap Irradiation Facility with 7-hole SIHA		
E-1 through E-6	ATRC LSA Cobalt	LSL-24-94
E-7	SMWH-1	443656
South Flux Trap Irradiation Facility with 7-hole SIHA		
S-1 through S-6	ATRC LSA Cobalt	LSL-24-94
S-7	SMWH-2	443656
Center Flux Trap Irradiation Facility with 7-hole SIHA		
C-1 through C-5	Aluminum Filler	
C-6	ATRC LSA Cobalt	LSL-24-94
C-7	CMWH-1	443656
H Positions		
H-1, H-4, H-5, H-7 through H-9, H-12, H-13, H-15, H-16	ATRC LSA Cobalt	LSL-24-94
H-3, H-11	^{16}N Tube	443656
H-2	FMWH-1	424852
H-6	FMWH-2	424852
H-10	FMWH-3	424852
H-14	FMWH-4	424852
Neck Shim Positions		
SW-4 and SE-4	Regulating Rod (fully withdrawn)	120471
All but SW-4 and SE-4	Neck Shim Rod (fully inserted)	120471
Inboard A Positions		
A-1 through A-8	SFR	120421
Outboard A Positions		
A-9 through A-12	SFR	120421
A-13 through A-16	Short FR	446643-2
Reflector		
All	Beryllium Reflector Blocks	419609

132

Table 6. Core Loadings.

Core Position	Cycle 103A-2 (NT-3)	Drawing / Reference
Outer Shim Control Cylinders		
All	Rotated to 51.8°	401795 - 401798
Small B Positions		
B-1 through B-3, B-5 through B-8	SFR	035140
B-4	Startup Source	Tom-11-94
Large B Positions		
B-9 through B-12	Beryllium Filler	120391
I Positions		
I-1 through I-20	Beryllium Filler	120391
I-21 through 1-24	Beryllium Filler	418780

4. ASSUMPTIONS

Some of the assumptions included in the MCNP models are:

- Uniform fuel enrichment (93 wt% U-235 or 19.75 wt% U-235).

- Uniform fuel mass per element.

- No significant fuel impurities.

- Uniform burnable poison mass per element.

- Natural B-10 content (19.9 at%) in Boron.

- No significant impurities in B_4C.

- No significant impurities in aluminum powder.

- Uniform 7% void in fuel matrix.

- No significant clad impurities.

- Uniform nominal density (2.7 g/cm^3) of Al clad.

- Uniform nominal density (6.5 g/cm^3) of Zr clad.

- Uniform UMo(10) density (16.9 g/cm^3) of RERTR fuel.

- Uniform nominal cobalt density (8.9 g/cm^3) in cobalt irradiation facilities.

- No significant impurities in Hf in safety rods, neck shims, and OSCCs.

- Uniform Hf density.

- No significant impurities in Be reflector.

- Uniform nominal dimensions of fuel elements.

- Uniform water temperature.

- The startup source in position B-4 was not modeled (replaced with water).

The ATR reactivity calculations used a delayed neutron fraction (β) value of 0.0075.[2] Table 1 through Table 4 show how the type 7F ATR fuel element and the RERTR fuel elements were modeled.

5. COMPUTER CODE VALIDATION

MCNP was used to perform this analysis. The codes are listed as verified and validated software in the INL Enterprise Architecture Repository (see Table 7) and are accepted as qualified scientific and engineering analysis software.

MCNP has been validated for use at the INL by running the 42 sample problems transmitted on the Radiation Safety Information Computational Center (RSICC) installation CD and comparing the results against the standard results provided on the CD.[3,4] The validation process was performed on the icestorm computer system for MCNP. The sample problems were run on icestorm and the results were in agreement with the standard results provided on the RSICC CD. Additionally, the input model for the ATR criticality benchmark[5] was executed on icestorm, and results in agreement with the published results were obtained. The computer configurations listed in Table 8 were used to perform the calculations reported in this ECAR.

Table 7. INL Qualified Analysis Software Version and Tracking Number.

Code Name	Version	V&V Tracking Number
MCNP	5 (Release 1.40)	234166

Table 8. Computer Configurations for INL Qualified MCNP Installations.

Computer Model	Processor	Operating System
MCNP		
Dell PowerEdge 1950 (w/166 dual socket nodes)	126 nodes w/dual core Intel Xeon 5150 processors (2.66 GHz), 8 GB RAM 40 nodes w/quad core Intel Xeon X5355 processors (2.66 GHz), 16 GB RAM	openSUSE 10.2, gcc version 4.1.2, kernel version 2.6.18.8-0.3 (all nodes)

6. LEU CONVERSION DISCUSSION/ANALYSIS

6.1. Fuel Element Power Distribution

Fuel element power for each case was calculated using MCNP. The results were normalized to a total core power of 250 MW. The reference case, Case-A, was validated by comparing MCNP calculated results to measured ATR assembly power distribution data. This comparison showed that there is a modeling bias in the assembly power distribution. However, this bias is less than the difference between measured results between ATR and ATRC, two nearly identical reactors. The power distributions for Cases B, C, and D do not vary significantly with respect to Case-A when compared to the model bias between measurement and Case-A. Detailed comparison plots between for all the comparisons can be found in Appendix A. The results show that the assembly power distribution is not expected to vary significantly for full core LEU conversion with any of the three proposed designs at beginning of life.

6.2. Radial Fuel Power Profile

MCNP was used to find the radial fuel power in all forty fuel elements at BOC. This radial power was then converted to heat flux before normalized in order to capture the effect of varying size fuel plates throughout the fuel assembly. The radial results were normalized to the average heat flux within each fuel element. Tabular data for each of the four proposed fuel designs are presented in Appendix A under Table 11 through Table 14. Graphical representations of this normalized power distribution are shown in four fuel elements (elements 18, 19, 22, and 38) in Figure 9 through Figure 12, also in Appendix A. The radial power profile for each of the 3 LEU designs varies noticeably from the HEU reference case. However, the power profiles for all the designs are still relatively flat and remain below the current limit of existing analyses.

6.3. Axial and Azimuthal Fuel Power Distribution

MCNP was used to find the axial and azimuthal power distribution in the same four fuel elements (18, 19, 22, and 38), again at BOC. The results were again normalized, this time to the average power of the fuel plate being tallied. Although power distributions were generated for each of the plates within these assemblies, only the results for plate 15 are presented as all the plates within the assembly show similar profiles and trends. Graphical representations of the azimuthal power distributions are shown in Figure 13 through Figure 16. The graphs of the axial power distributions are shown in Figure 17 through Figure 20. The azimuthal power profiles for all 3 designs are relatively flat and have peaks lower than the current thermal hydraulic analyses. However, the ISBA (B-10) design in its current form performs the best with the lowest peak in all four of the fuel elements considered. As for the axial power profile comparisons, there is little to no discernible differences in the axial power profiles of any of the designs.

7. CONCLUSION

The 19-plate, full core, MCNP model of ATR first presented in Reference 1 has been validated and been shown to be as accurate as measurement data. Both the maximum and standard deviation in the assembly power distribution of the MCNP model vs. the ATR measurement data has been shown to be lower than the differences between ATR measurements and ATRC measurements. Three possible LEU designs (ICBA, ISBA-^{10}B, and ISBA-Cd) have been compared to the HEU benchmark using MCNP. Core power maps, radial power distribution, axial power distributions, and azimuthal power distributions were compared for each design. The results show that there should be little to no impact on the axial power profile of the ATR, and that small differences in the assembly power distribution are less than the modeling bias between measured and calculated results. The radial and azimuthal power profiles do show some variation between all of the designs and the reference HEU case. However, the maximum local to average peaking factors for all of the designs remain below established limits for the HEU fuel. Further work should be done to consider the effects of burnup on these proposed designs throughout the fuel's lifecycle.

8. REFERENCES

[1]. M.N. Neeley, G. S. Chang., "MCWO Neutronics Analysis of RERTR Full Element Demonstration in Position 38 of the ATR," ECAR-1357, February 2011.

[1]. W. C. Cook, A. C. Smith, "ATR CSAP Code Package on the Workstation Version 1," PG-T-96-002, May 1996.

[1]. Tim Goorley, et. al., "Release of MCNP5_RSICC_1.30," Trans. Am. Nucl. Soc., Vol. 91, 693-694 (2004).

[1]. X-5 Monte Carlo Team, "MCNP-A General Monte Carlo N-Particle Transport Code, Version 5," Volume I, LA-UR-03-1987, Los Alamos National Laboratory, April 24, 2003 (Revised 6/30/2004) and Volume II, LA-CP-0245, Los Alamos National Laboratory, April 24,2003 (Revised 6/30/2004) (Vol. II is available with a licensed copy of MCNP)

[1]. S. S. Kim, B. G. Schnitzler, "Advanced Test Reactor: Serpentine Arrangement of Highly Enriched Water-Moderated Uranium-Aluminide Fuel Plates Reflected by Beryllium," HEU-MET-THERM-022, NEA/NSC/DOC/(95)03/II, International Handbook of Evaluated Criticality Safety Benchmark Experiments, Volume II: Highly Enriched Uranium Systems, March 2009.

1.1 Appendix A: Power Distribution Plots

Table 9: Assembly Power Comparisons between Measurement, HEU, and LEU

Assembly	ATR	ATRC	Case-A	Case-B	Case-C	Case-D
1	6.66	6.70	7.04	7.08	7.01	6.97
2	6.18	6.21	6.50	6.57	6.56	6.53
3	5.57	5.63	5.77	5.88	5.93	5.93
4	4.32	4.46	4.41	4.46	4.49	4.53
5	3.39	3.89	3.62	3.68	3.65	3.72
6	3.61	3.86	3.59	3.64	3.62	3.68
7	4.28	4.64	4.46	4.51	4.57	4.60
8	6.07	6.20	6.11	6.23	6.31	6.34
9	6.53	6.51	6.78	6.86	6.85	6.85
10	6.93	6.89	7.26	7.31	7.25	7.22
11	7.67	7.17	7.61	7.63	7.56	7.54
12	8.09	7.46	7.58	7.58	7.55	7.57
13	7.40	7.10	7.16	7.19	7.24	7.30
14	6.45	6.02	5.85	5.79	5.85	5.90
15	5.16	5.22	4.89	4.84	4.83	4.89
16	5.16	5.34	4.92	4.87	4.85	4.91
17	6.45	6.11	5.93	5.87	5.93	5.98
18	7.40	7.38	7.43	7.45	7.56	7.59
19	8.09	7.56	7.76	7.73	7.74	7.74
20	7.99	7.54	7.83	7.83	7.75	7.74
21	8.01	7.82	7.93	7.91	7.84	7.83
22	8.04	7.92	7.77	7.73	7.73	7.74
23	7.73	7.76	7.38	7.37	7.48	7.48
24	6.24	6.38	5.94	5.86	5.94	5.95
25	4.90	5.48	4.92	4.87	4.84	4.88
26	5.06	5.47	4.90	4.83	4.81	4.86
27	5.99	6.36	5.84	5.75	5.83	5.84
28	7.12	7.47	7.11	7.09	7.17	7.17
29	7.68	7.51	7.56	7.51	7.50	7.47
30	7.42	7.47	7.63	7.61	7.54	7.49
31	7.08	7.00	7.35	7.33	7.25	7.19
32	6.83	6.77	7.03	7.01	6.97	6.91
33	6.15	6.43	6.61	6.64	6.68	6.62
34	5.07	5.19	5.30	5.27	5.28	5.24
35	4.11	4.36	4.36	4.34	4.28	4.27
36	4.31	4.25	4.33	4.31	4.26	4.25

37	5.04	5.08	5.20	5.18	5.20	5.17
38	6.30	6.15	6.39	6.43	6.46	6.42
39	6.65	6.49	6.85	6.85	6.81	6.75
40	6.88	6.74	7.08	7.10	7.02	6.94

Table 10: Percent Differences in Assembly Power for Measurement, HEU, and LEU

Assembly	Diff % ATRC vs. ATR	Diff % Case-A vs. ATR	Diff % Case-B vs. Case-A	Diff % Case-C vs. Case-A	Diff % Case-D vs. Case-A
1	0.60	5.37	0.64	-0.37	-1.01
2	0.48	4.92	1.13	0.97	0.51
3	1.07	3.51	1.94	2.73	2.77
4	3.14	2.01	1.08	1.84	2.87
5	12.85	6.24	1.90	1.06	2.93
6	6.48	-0.63	1.57	0.88	2.54
7	7.76	4.12	1.06	2.29	3.16
8	2.10	0.67	1.99	3.21	3.82
9	-0.31	3.68	1.18	1.10	1.05
10	-0.58	4.60	0.61	-0.19	-0.62
11	-6.97	-0.74	0.16	-0.73	-1.00
12	-8.45	-6.74	-0.05	-0.40	-0.16
13	-4.23	-3.34	0.42	1.09	1.88
14	-7.14	-6.92	-1.02	0.05	0.86
15	1.15	-5.43	-1.03	-1.39	0.01
16	3.37	-4.81	-1.07	-1.40	-0.31
17	-5.56	-8.74	-1.10	0.06	0.80
18	-0.27	0.47	0.17	1.73	2.14
19	-7.01	-4.25	-0.35	-0.32	-0.21
20	-5.97	-1.99	-0.03	-1.04	-1.15
21	-2.43	-1.05	-0.26	-1.04	-1.25
22	-1.52	-3.43	-0.55	-0.56	-0.47

23	0.39	-4.72	-0.10	1.27	1.40
24	2.19	-5.05	-1.37	0.08	0.11
25	10.58	0.42	-1.07	-1.61	-0.89
26	7.50	-3.27	-1.40	-1.75	-0.87
27	5.82	-2.49	-1.58	-0.33	-0.13
28	4.69	-0.09	-0.27	0.78	0.83
29	-2.26	-1.55	-0.69	-0.83	-1.20
30	0.67	2.79	-0.27	-1.17	-1.81
31	-1.14	3.63	-0.20	-1.31	-2.19
32	-0.89	2.79	-0.27	-0.83	-1.67
33	4.35	6.94	0.49	1.01	0.13
34	2.31	4.29	-0.61	-0.26	-1.00
35	5.73	5.63	-0.33	-1.81	-2.06
36	-1.41	0.51	-0.49	-1.61	-1.86
37	0.79	3.06	-0.40	-0.01	-0.57
38	-2.44	1.45	0.61	1.11	0.40
39	-2.47	2.87	0.07	-0.54	-1.42
40	-2.08	2.85	0.21	-0.88	-2.02
max	12.85	6.94	1.99	3.21	3.82
min	-8.45	-8.74	-1.58	-1.81	-2.19
std dev	4.83	4.09	0.94	1.28	1.63
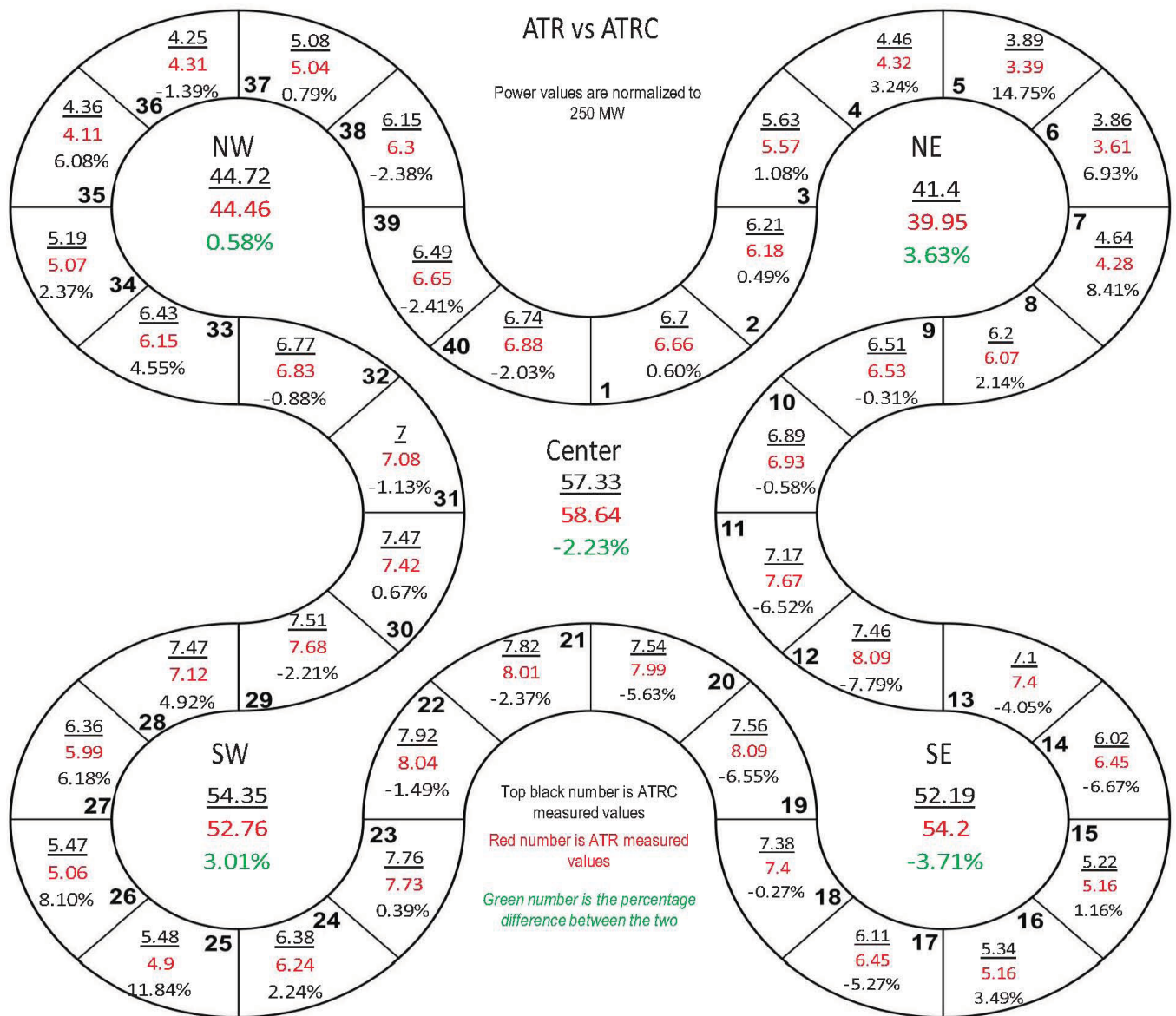
Figure 4: ATR vs ATRC Measured Power Distribution Comparison
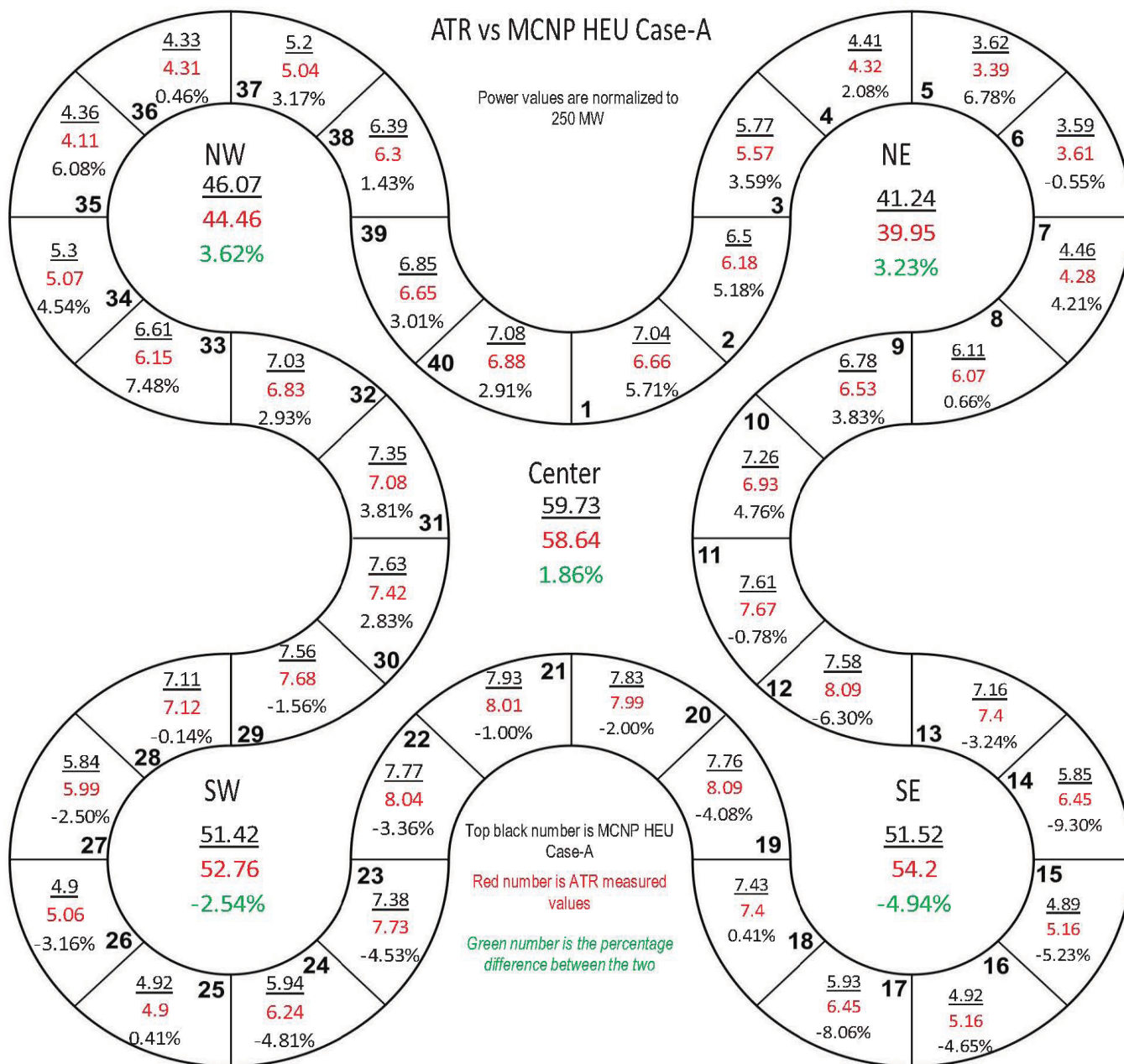
Figure 5: ATR Measurement vs Case-A Power Distribution Comparison
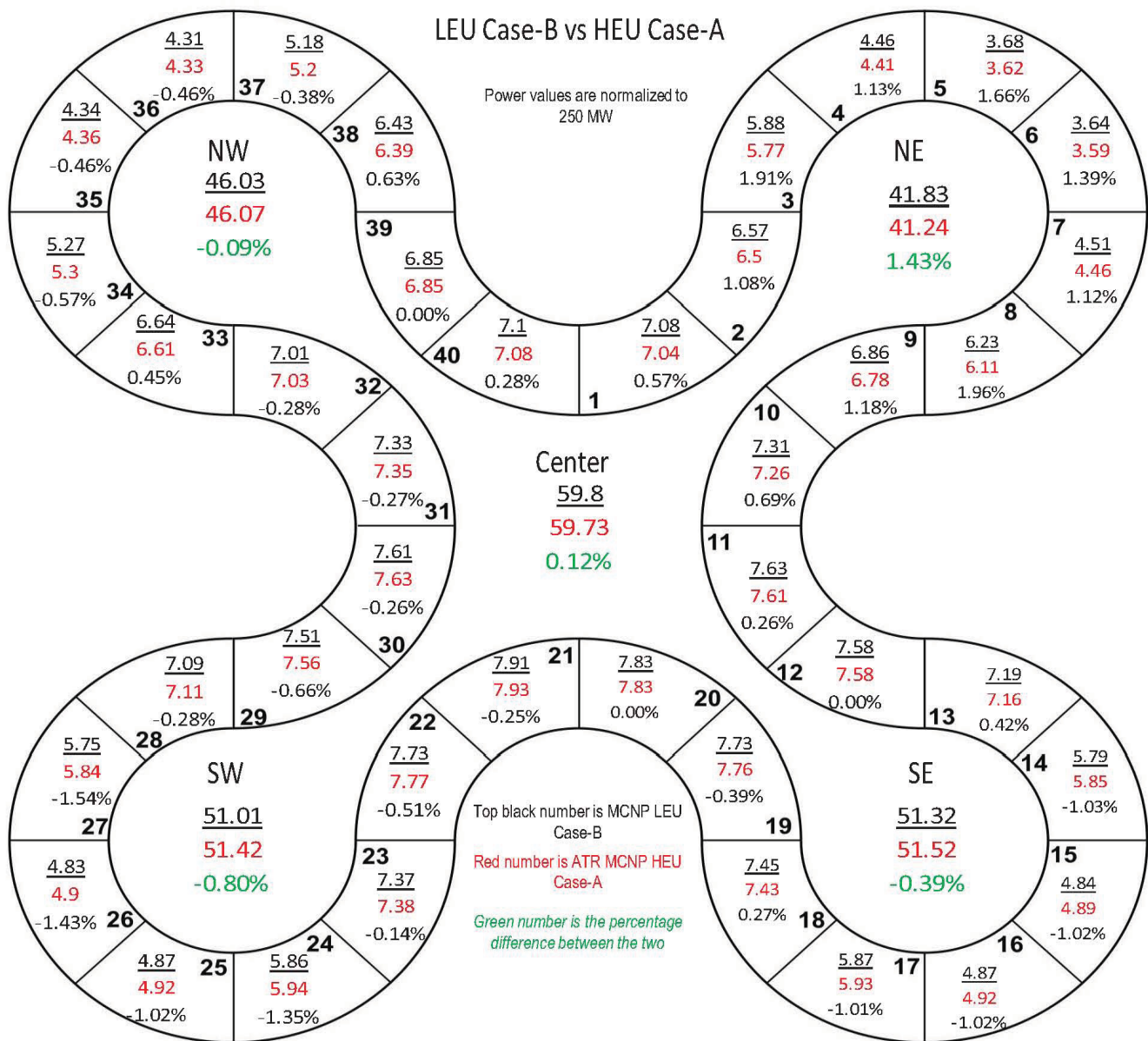
Figure 6: LEU Case-B vs HEU Case-A Power Distribution Comparison

144
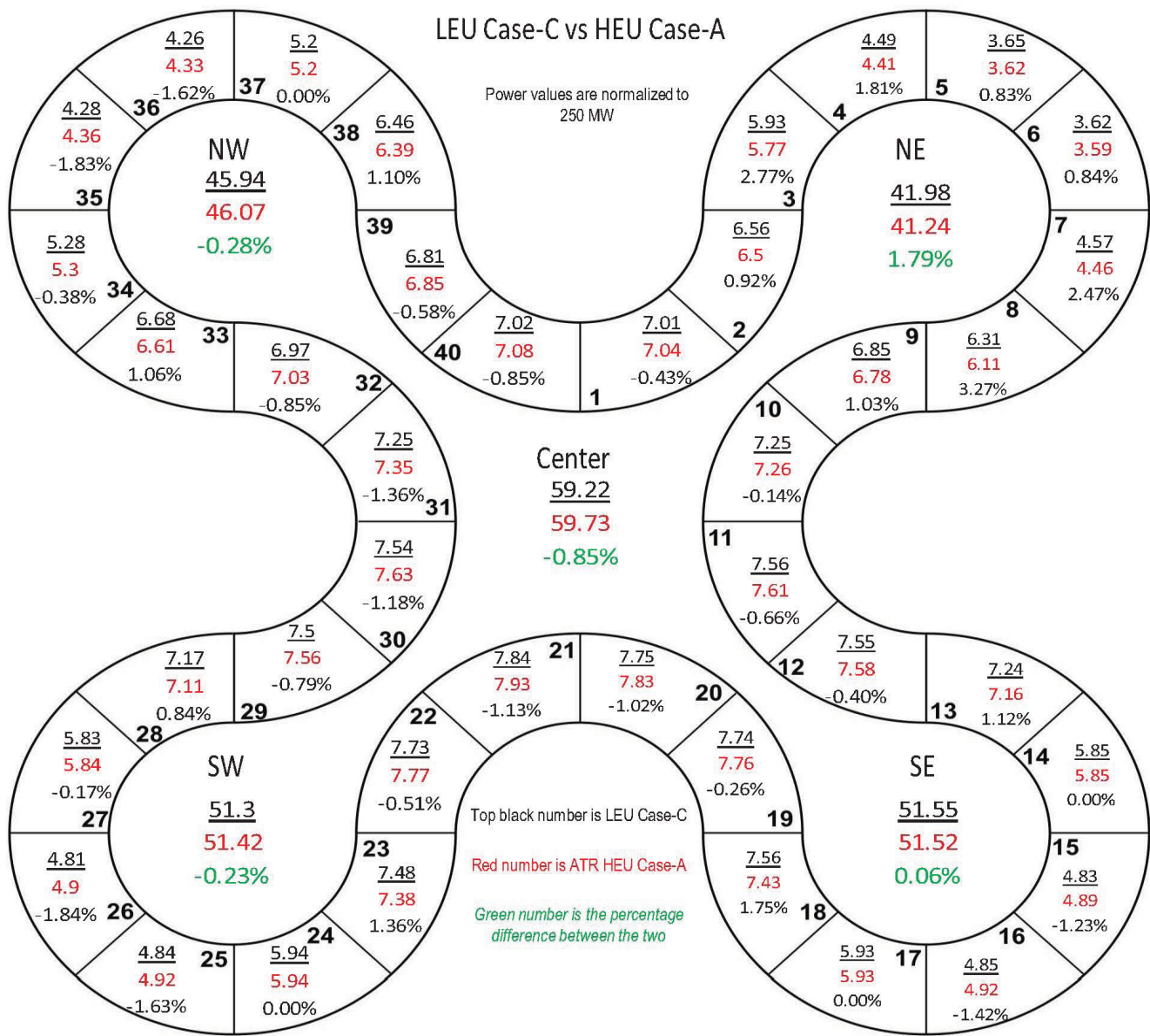
Figure 7: LEU Case-C vs HEU Case-A Assembly Power Distribution Comparison
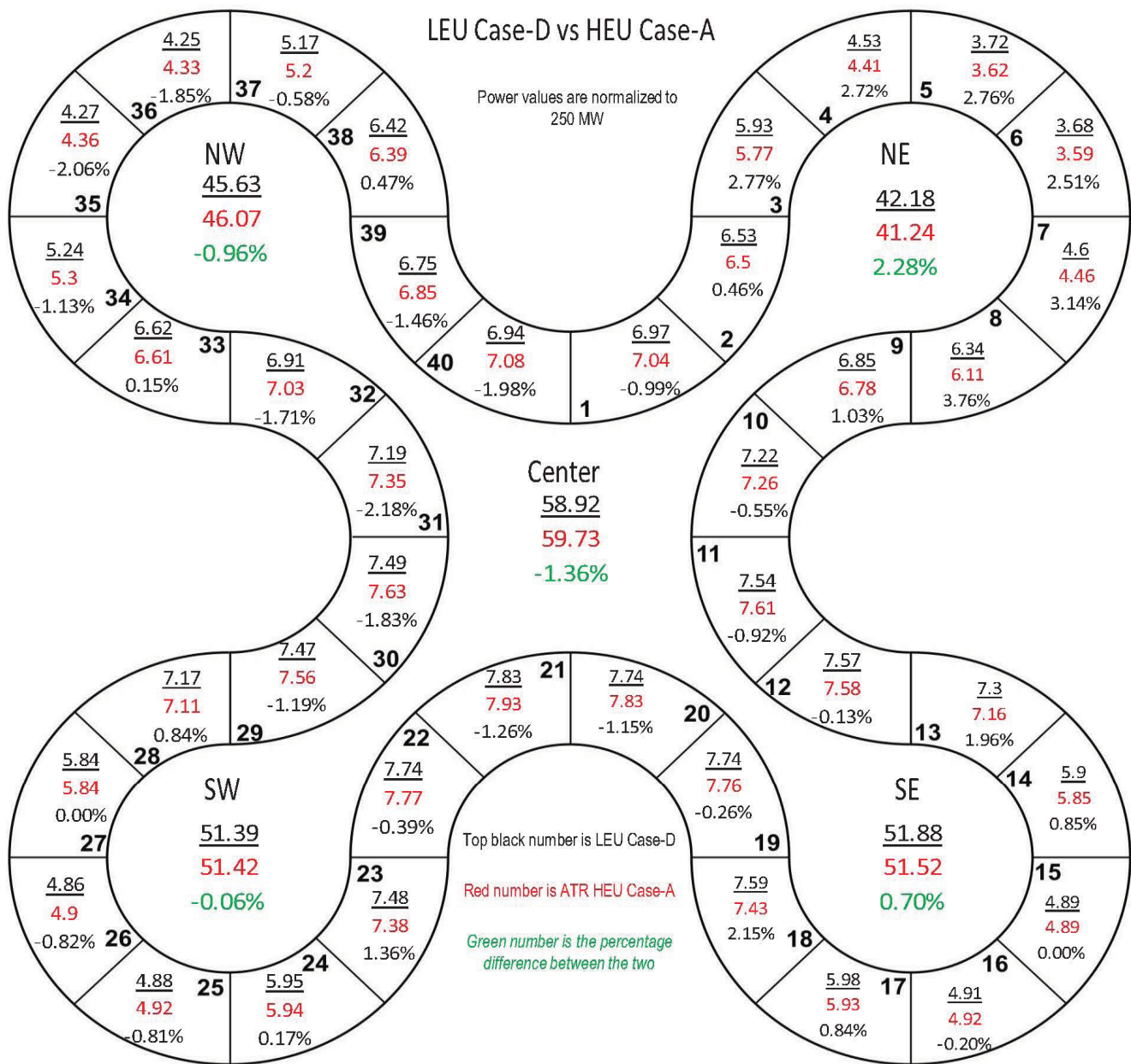
Figure 8: LEU Case-D vs HEU Case-A Power Distribution Comparison

146

Table 11: Detailed HEU Radial Power Profile

Assembly	Plate 1	Plate 2	Plate 3	Plate 4	Plate 5	Plate 6	Plate 7	Plate 8	Plate 9	Plate 10	Plate 11	Plate 12	Plate 13	Plate 14	Plate 15	Plate 16	Plate 17	Plate 18	Plate 19
1	1.077	0.928	1.050	0.975	1.122	1.090	1.063	1.038	1.031	1.018	1.017	1.011	1.021	1.033	1.056	0.887	0.921	0.791	0.871
2	1.130	0.948	1.072	0.984	1.122	1.077	1.046	1.013	1.005	0.991	0.988	0.988	0.992	1.011	1.040	0.887	0.941	0.825	0.941
3	1.120	0.932	1.035	0.939	1.071	1.033	0.987	0.969	0.955	0.951	0.957	0.969	0.983	1.023	1.070	0.933	1.027	0.936	1.111
4	1.245	1.025	1.135	1.007	1.133	1.077	1.033	0.985	0.970	0.952	0.944	0.944	0.956	0.974	1.007	0.866	0.933	0.835	0.978
5	1.503	1.184	1.268	1.112	1.227	1.143	1.068	1.021	0.976	0.955	0.940	0.922	0.911	0.903	0.914	0.758	0.787	0.669	0.737
6	1.426	1.148	1.237	1.096	1.217	1.146	1.079	1.030	0.995	0.963	0.944	0.928	0.925	0.916	0.932	0.776	0.809	0.686	0.747
7	1.207	0.999	1.094	0.991	1.124	1.072	1.020	0.995	0.976	0.963	0.952	0.953	0.968	0.984	1.028	0.882	0.948	0.854	0.991
8	1.132	0.939	1.034	0.934	1.062	1.015	0.976	0.953	0.939	0.934	0.937	0.958	0.982	1.022	1.079	0.948	1.045	0.961	1.151
9	1.197	0.988	1.106	1.005	1.143	1.091	1.049	1.014	0.994	0.977	0.972	0.969	0.971	0.991	1.019	0.863	0.916	0.811	0.924
10	1.147	0.970	1.091	0.998	1.154	1.095	1.073	1.050	1.026	1.014	1.000	0.996	0.996	1.009	1.027	0.858	0.897	0.764	0.838
11	1.135	0.955	1.073	0.992	1.138	1.107	1.063	1.048	1.024	1.014	1.013	1.003	1.009	1.017	1.033	0.868	0.900	0.767	0.841
12	1.154	0.973	1.079	0.982	1.128	1.087	1.049	1.021	1.006	0.995	0.987	0.993	0.999	1.009	1.036	0.877	0.926	0.803	0.897
13	1.046	0.895	1.003	0.932	1.077	1.041	1.011	0.981	0.972	0.969	0.970	0.977	0.998	1.031	1.081	0.942	1.029	0.936	1.110
14	1.130	0.962	1.085	0.977	1.120	1.079	1.042	1.010	0.988	0.977	0.970	0.970	0.982	0.994	1.036	0.886	0.951	0.850	0.990
15	1.242	1.048	1.156	1.055	1.207	1.145	1.095	1.054	1.023	0.996	0.979	0.974	0.964	0.958	0.966	0.805	0.834	0.716	0.780
16	1.236	1.033	1.159	1.056	1.197	1.144	1.099	1.059	1.027	1.002	0.979	0.971	0.968	0.960	0.970	0.803	0.843	0.714	0.781
17	1.131	0.955	1.070	0.980	1.116	1.075	1.038	1.006	0.994	0.978	0.967	0.977	0.982	0.997	1.037	0.886	0.956	0.853	1.000
18	1.021	0.870	0.984	0.910	1.050	1.019	0.993	0.975	0.965	0.961	0.962	0.978	0.996	1.029	1.096	0.962	1.066	0.979	1.185
19	1.189	0.990	1.100	1.007	1.144	1.096	1.054	1.023	1.005	0.991	0.985	0.979	0.986	0.998	1.023	0.860	0.904	0.787	0.879
20	1.161	0.978	1.101	1.008	1.157	1.114	1.080	1.048	1.020	1.015	1.007	0.996	0.996	1.007	1.022	0.852	0.883	0.746	0.809

Table 11: Detailed HEU Radial Power Profile Continued

Assembly	Plate 1	Plate 2	Plate 3	Plate 4	Plate 5	Plate 6	Plate 7	Plate 8	Plate 9	Plate 10	Plate 11	Plate 12	Plate 13	Plate 14	Plate 15	Plate 16	Plate 17	Plate 18	Plate 19
21	1.160	0.975	1.096	0.997	1.147	1.110	1.069	1.034	1.018	1.002	0.997	0.995	0.998	1.009	1.030	0.858	0.895	0.769	0.844
22	1.180	0.989	1.097	0.998	1.141	1.093	1.049	1.018	1.004	0.994	0.985	0.983	0.987	1.004	1.027	0.869	0.915	0.789	0.878
23	1.032	0.881	0.995	0.925	1.061	1.028	1.001	0.983	0.964	0.960	0.973	0.985	1.002	1.035	1.090	0.952	1.040	0.951	1.143
24	1.134	0.957	1.070	0.985	1.120	1.080	1.040	1.006	0.992	0.973	0.969	0.968	0.976	0.997	1.038	0.887	0.955	0.856	0.997
25	1.234	1.039	1.160	1.047	1.190	1.138	1.090	1.059	1.030	1.000	0.984	0.977	0.967	0.969	0.977	0.805	0.839	0.719	0.780
26	1.246	1.041	1.152	1.056	1.201	1.140	1.092	1.047	1.026	0.998	0.987	0.971	0.966	0.962	0.976	0.812	0.836	0.711	0.779
27	1.137	0.954	1.075	0.982	1.125	1.084	1.036	1.016	0.998	0.977	0.969	0.969	0.977	0.997	1.034	0.883	0.951	0.849	0.989
28	1.055	0.897	1.014	0.936	1.080	1.044	1.012	0.989	0.980	0.972	0.976	0.986	0.997	1.030	1.073	0.931	1.018	0.921	1.089
29	1.116	0.945	1.064	0.976	1.130	1.085	1.049	1.033	1.022	1.004	1.002	1.000	1.003	1.015	1.041	0.879	0.926	0.810	0.900
30	1.088	0.936	1.065	0.985	1.134	1.101	1.067	1.048	1.032	1.020	1.017	1.012	1.015	1.026	1.050	0.876	0.908	0.773	0.847
31	1.115	0.949	1.077	1.001	1.155	1.113	1.076	1.053	1.039	1.026	1.015	1.013	1.012	1.019	1.034	0.858	0.887	0.751	0.809
32	1.141	0.968	1.084	0.993	1.148	1.110	1.074	1.042	1.023	1.016	1.010	1.006	0.998	1.003	1.029	0.858	0.893	0.763	0.841
33	0.935	0.826	0.956	0.905	1.059	1.035	1.008	0.996	0.988	0.993	0.992	0.998	1.029	1.055	1.108	0.965	1.052	0.960	1.141
34	1.018	0.894	1.031	0.955	1.102	1.078	1.041	1.023	1.001	0.995	0.988	0.992	1.011	1.028	1.065	0.912	0.977	0.875	1.014
35	1.102	0.954	1.096	1.019	1.186	1.147	1.107	1.072	1.057	1.028	1.011	0.998	0.996	0.995	1.008	0.833	0.860	0.731	0.801
36	1.101	0.962	1.103	1.024	1.181	1.140	1.110	1.071	1.055	1.028	1.016	1.004	0.989	0.989	0.993	0.829	0.860	0.737	0.809
37	1.005	0.886	1.029	0.955	1.112	1.076	1.052	1.025	1.007	0.992	0.992	0.997	1.008	1.025	1.066	0.909	0.974	0.871	1.020
38	0.950	0.832	0.967	0.908	1.062	1.039	1.019	1.006	0.997	0.991	0.996	1.005	1.021	1.053	1.103	0.956	1.042	0.939	1.113
39	1.124	0.951	1.071	0.981	1.139	1.100	1.060	1.039	1.023	1.011	1.008	1.004	1.009	1.018	1.041	0.872	0.911	0.782	0.855
40	1.088	0.938	1.064	0.982	1.131	1.103	1.073	1.047	1.035	1.028	1.025	1.024	1.024	1.033	1.047	0.870	0.904	0.761	0.823

148

Table 12: Detailed ICBA Radial Power Profiles

Assembly	Plate 1	Plate 2	Plate 3	Plate 4	Plate 5	Plate 6	Plate 7	Plate 8	Plate 9	Plate 10	Plate 11	Plate 12	Plate 13	Plate 14	Plate 15	Plate 16	Plate 17	Plate 18	Plate 19
1	0.997	1.007	0.952	0.963	1.057	1.016	0.985	0.972	0.961	0.960	0.968	0.979	1.005	1.049	1.113	0.949	1.033	1.013	1.020
2	1.076	1.079	0.981	0.990	1.071	1.016	0.982	0.966	0.951	0.948	0.951	0.961	0.980	1.020	1.081	0.920	1.003	0.998	1.028
3	1.108	1.079	0.979	0.971	1.048	0.983	0.942	0.921	0.904	0.903	0.910	0.935	0.965	1.012	1.091	0.948	1.065	1.087	1.152
4	1.225	1.181	1.048	1.031	1.096	1.015	0.970	0.938	0.916	0.907	0.904	0.917	0.927	0.963	1.041	0.898	0.982	0.996	1.046
5	1.394	1.305	1.133	1.079	1.128	1.030	0.971	0.932	0.899	0.884	0.882	0.884	0.894	0.927	0.981	0.838	0.926	0.935	0.977
6	1.329	1.257	1.113	1.066	1.110	1.031	0.969	0.938	0.911	0.894	0.891	0.893	0.910	0.942	0.999	0.855	0.946	0.952	0.994
7	1.172	1.141	1.033	1.020	1.092	1.022	0.967	0.939	0.919	0.906	0.910	0.923	0.942	0.986	1.049	0.899	1.000	1.013	1.067
8	1.120	1.093	0.974	0.962	1.040	0.975	0.934	0.914	0.895	0.894	0.901	0.927	0.952	1.008	1.097	0.956	1.072	1.105	1.179
9	1.146	1.123	1.021	1.010	1.088	1.022	0.976	0.951	0.937	0.932	0.932	0.944	0.961	1.001	1.060	0.907	0.991	0.988	1.011
10	1.067	1.064	0.983	0.985	1.073	1.015	0.988	0.973	0.962	0.953	0.957	0.974	0.997	1.034	1.088	0.924	1.001	0.981	0.982
11	1.048	1.052	0.971	0.974	1.074	1.016	0.991	0.974	0.963	0.956	0.971	0.977	1.003	1.035	1.099	0.933	1.003	0.981	0.980
12	1.105	1.098	1.007	1.010	1.092	1.029	0.997	0.969	0.956	0.947	0.954	0.965	0.982	1.017	1.072	0.906	0.979	0.957	0.959
13	1.020	1.037	0.960	0.961	1.044	0.994	0.964	0.948	0.930	0.925	0.930	0.945	0.974	1.019	1.099	0.949	1.063	1.088	1.150
14	1.091	1.098	1.000	1.008	1.090	1.020	0.989	0.964	0.947	0.939	0.931	0.943	0.958	0.992	1.061	0.909	0.998	1.011	1.051
15	1.122	1.127	1.025	1.027	1.101	1.044	0.994	0.963	0.938	0.928	0.926	0.935	0.945	0.985	1.040	0.898	0.981	0.990	1.032
16	1.116	1.127	1.030	1.029	1.116	1.039	0.998	0.968	0.941	0.935	0.929	0.933	0.941	0.978	1.045	0.890	0.979	0.982	1.023
17	1.081	1.091	1.009	1.006	1.091	1.021	0.992	0.956	0.938	0.937	0.930	0.937	0.957	0.997	1.064	0.908	1.003	1.019	1.062
18	1.004	1.014	0.936	0.950	1.032	0.978	0.948	0.927	0.918	0.911	0.921	0.940	0.970	1.027	1.115	0.971	1.087	1.134	1.216
19	1.137	1.125	1.028	1.024	1.096	1.033	0.990	0.967	0.955	0.943	0.948	0.957	0.971	1.009	1.068	0.896	0.967	0.945	0.941
20	1.073	1.081	0.994	0.999	1.091	1.030	0.996	0.979	0.963	0.958	0.970	0.974	0.991	1.027	1.079	0.914	0.982	0.954	0.945

Table 12: Detailed ICBA Radial Power Profiles Continued

Assembly	Plate 1	Plate 2	Plate 3	Plate 4	Plate 5	Plate 6	Plate 7	Plate 8	Plate 9	Plate 10	Plate 11	Plate 12	Plate 13	Plate 14	Plate 15	Plate 16	Plate 17	Plate 18	Plate 19
21	1.063	1.064	0.985	0.989	1.079	1.024	0.992	0.973	0.959	0.956	0.959	0.974	0.995	1.027	1.081	0.922	0.994	0.980	0.983
22	1.134	1.122	1.015	1.015	1.096	1.035	0.992	0.975	0.956	0.949	0.950	0.957	0.980	1.013	1.061	0.894	0.968	0.945	0.943
23	1.005	1.018	0.947	0.951	1.037	0.983	0.951	0.934	0.921	0.925	0.931	0.951	0.983	1.029	1.113	0.967	1.080	1.103	1.172
24	1.092	1.096	1.011	1.006	1.086	1.021	0.987	0.950	0.932	0.926	0.931	0.940	0.964	0.999	1.062	0.914	1.006	1.016	1.060
25	1.130	1.129	1.032	1.026	1.112	1.039	0.996	0.964	0.945	0.926	0.927	0.929	0.944	0.975	1.046	0.892	0.976	0.987	1.026
26	1.130	1.129	1.027	1.028	1.109	1.045	1.002	0.968	0.935	0.927	0.924	0.934	0.944	0.975	1.038	0.885	0.984	0.985	1.029
27	1.094	1.098	1.010	1.015	1.097	1.025	0.989	0.951	0.941	0.929	0.929	0.936	0.960	0.996	1.061	0.906	0.998	1.012	1.054
28	1.028	1.037	0.954	0.960	1.055	0.993	0.974	0.949	0.935	0.933	0.939	0.953	0.975	1.022	1.098	0.948	1.049	1.069	1.128
29	1.065	1.071	0.995	0.998	1.085	1.029	0.993	0.976	0.962	0.959	0.960	0.976	0.995	1.022	1.082	0.913	0.984	0.970	0.967
30	1.009	1.029	0.960	0.982	1.078	1.020	0.992	0.976	0.970	0.967	0.971	0.978	1.008	1.045	1.108	0.935	1.006	0.984	0.983
31	1.024	1.043	0.976	0.990	1.083	1.029	0.997	0.978	0.968	0.965	0.978	0.989	1.007	1.038	1.097	0.921	0.994	0.966	0.959
32	1.084	1.096	1.008	1.013	1.106	1.047	1.008	0.990	0.968	0.966	0.965	0.974	0.988	1.013	1.072	0.897	0.958	0.931	0.914
33	0.904	0.953	0.909	0.945	1.041	0.994	0.968	0.954	0.946	0.946	0.957	0.965	0.998	1.048	1.130	0.980	1.088	1.104	1.170
34	0.960	1.006	0.958	0.984	1.080	1.026	0.996	0.971	0.958	0.951	0.954	0.968	0.981	1.027	1.090	0.934	1.030	1.038	1.087
35	1.007	1.049	0.990	1.006	1.098	1.041	1.004	0.981	0.957	0.949	0.948	0.949	0.972	1.006	1.067	0.911	1.002	1.013	1.050
36	1.008	1.044	0.982	1.008	1.096	1.037	1.004	0.979	0.959	0.953	0.946	0.954	0.971	1.009	1.067	0.916	1.004	1.005	1.057
37	0.977	1.021	0.968	0.990	1.078	1.025	0.997	0.968	0.953	0.952	0.951	0.960	0.988	1.021	1.087	0.930	1.027	1.033	1.073
38	0.925	0.973	0.928	0.952	1.043	1.003	0.974	0.956	0.946	0.951	0.953	0.970	0.993	1.038	1.114	0.970	1.072	1.091	1.146
39	1.067	1.075	0.999	1.002	1.089	1.035	1.002	0.979	0.969	0.964	0.968	0.979	0.999	1.029	1.085	0.908	0.974	0.947	0.933
40	1.014	1.031	0.967	0.975	1.073	1.022	0.994	0.979	0.966	0.970	0.980	0.990	1.007	1.048	1.106	0.930	1.004	0.973	0.970

Table 13: Detailed ISBA (B-10) Radial Power Distribution

Assembly	Plate 1	Plate 2	Plate 3	Plate 4	Plate 5	Plate 6	Plate 7	Plate 8	Plate 9	Plate 10	Plate 11	Plate 12	Plate 13	Plate 14	Plate 15	Plate 16	Plate 17	Plate 18	Plate 19
1	1.245	1.070	1.040	1.023	1.086	1.116	1.066	1.035	1.019	1.008	1.015	1.034	1.068	1.020	0.931	0.920	0.810	0.773	0.722
2	1.302	1.103	1.064	1.029	1.084	1.104	1.042	1.003	0.983	0.976	0.979	0.995	1.032	0.993	0.922	0.925	0.835	0.826	0.805
3	1.282	1.066	1.009	0.972	1.017	1.030	0.971	0.943	0.929	0.928	0.945	0.977	1.032	1.017	0.971	1.007	0.943	0.969	0.992
4	1.459	1.192	1.113	1.052	1.083	1.083	1.011	0.966	0.937	0.928	0.931	0.947	0.988	0.958	0.902	0.914	0.842	0.847	0.846
5	1.773	1.404	1.273	1.176	1.179	1.150	1.050	0.987	0.948	0.921	0.909	0.907	0.920	0.870	0.790	0.774	0.686	0.658	0.627
6	1.687	1.353	1.244	1.158	1.173	1.152	1.058	0.999	0.962	0.933	0.923	0.924	0.940	0.887	0.806	0.794	0.697	0.670	0.641
7	1.406	1.157	1.085	1.037	1.071	1.078	1.011	0.968	0.945	0.935	0.933	0.959	1.002	0.975	0.915	0.932	0.857	0.865	0.868
8	1.299	1.070	1.008	0.963	1.000	1.016	0.959	0.928	0.911	0.911	0.930	0.968	1.027	1.019	0.977	1.019	0.965	0.998	1.030
9	1.387	1.156	1.094	1.050	1.093	1.105	1.039	0.998	0.971	0.960	0.961	0.975	1.012	0.972	0.904	0.909	0.819	0.808	0.790
10	1.332	1.124	1.084	1.050	1.106	1.128	1.068	1.030	1.010	0.998	1.003	1.017	1.046	0.994	0.906	0.892	0.783	0.742	0.687
11	1.309	1.110	1.068	1.042	1.099	1.122	1.068	1.032	1.012	1.007	1.008	1.022	1.053	1.002	0.916	0.899	0.788	0.748	0.696
12	1.343	1.125	1.072	1.039	1.089	1.106	1.042	1.009	0.989	0.981	0.988	1.005	1.039	0.999	0.920	0.913	0.811	0.784	0.744
13	1.191	1.017	0.986	0.965	1.020	1.041	0.995	0.962	0.948	0.950	0.959	0.990	1.045	1.029	0.980	1.013	0.947	0.972	0.992
14	1.294	1.097	1.056	1.026	1.075	1.093	1.034	0.991	0.968	0.959	0.964	0.982	1.019	0.989	0.924	0.938	0.862	0.865	0.864
15	1.436	1.207	1.157	1.115	1.158	1.167	1.092	1.033	1.000	0.983	0.970	0.975	0.989	0.930	0.848	0.830	0.732	0.705	0.673
16	1.434	1.210	1.155	1.111	1.158	1.165	1.086	1.036	1.001	0.979	0.972	0.970	0.991	0.935	0.847	0.834	0.737	0.707	0.674
17	1.292	1.093	1.055	1.020	1.072	1.090	1.029	0.988	0.967	0.956	0.961	0.981	1.022	0.991	0.928	0.944	0.865	0.873	0.872
18	1.159	0.990	0.960	0.940	0.997	1.020	0.972	0.945	0.935	0.938	0.955	0.987	1.047	1.037	0.998	1.043	0.987	1.025	1.063
19	1.381	1.153	1.094	1.050	1.097	1.113	1.049	1.010	0.988	0.980	0.983	0.995	1.029	0.984	0.903	0.895	0.798	0.769	0.728
20	1.341	1.138	1.092	1.058	1.113	1.137	1.074	1.038	1.018	1.006	1.005	1.017	1.042	0.987	0.901	0.880	0.766	0.722	0.665

Table 13: Detailed ISBA (B-10) Radial Power Distribution Continued

Assembly	Plate 1	Plate 2	Plate 3	Plate 4	Plate 5	Plate 6	Plate 7	Plate 8	Plate 9	Plate 10	Plate 11	Plate 12	Plate 13	Plate 14	Plate 15	Plate 16	Plate 17	Plate 18	Plate 19
21	1.333	1.127	1.084	1.050	1.104	1.129	1.066	1.028	1.011	1.000	0.999	1.012	1.043	0.992	0.906	0.892	0.785	0.745	0.694
22	1.375	1.148	1.092	1.050	1.097	1.114	1.049	1.010	0.988	0.980	0.983	0.997	1.030	0.986	0.908	0.898	0.798	0.769	0.728
23	1.170	1.001	0.970	0.950	1.006	1.028	0.984	0.958	0.946	0.947	0.963	0.993	1.051	1.036	0.989	1.029	0.964	0.993	1.019
24	1.290	1.093	1.055	1.023	1.074	1.090	1.029	0.986	0.965	0.958	0.961	0.983	1.025	0.991	0.929	0.945	0.864	0.869	0.870
25	1.437	1.210	1.153	1.111	1.156	1.163	1.090	1.039	1.004	0.983	0.968	0.970	0.989	0.933	0.850	0.834	0.734	0.705	0.673
26	1.436	1.214	1.159	1.117	1.157	1.166	1.092	1.039	1.004	0.982	0.968	0.967	0.984	0.931	0.846	0.829	0.732	0.705	0.672
27	1.297	1.100	1.056	1.026	1.075	1.093	1.030	0.991	0.970	0.957	0.958	0.978	1.021	0.987	0.926	0.943	0.863	0.865	0.864
28	1.197	1.021	0.992	0.968	1.023	1.051	0.997	0.969	0.952	0.954	0.965	0.994	1.048	1.027	0.974	1.005	0.935	0.956	0.971
29	1.289	1.093	1.055	1.027	1.085	1.109	1.051	1.016	0.999	0.993	1.000	1.016	1.050	1.006	0.927	0.920	0.819	0.792	0.752
30	1.259	1.083	1.050	1.031	1.095	1.124	1.070	1.040	1.022	1.015	1.021	1.032	1.065	1.014	0.924	0.906	0.794	0.755	0.698
31	1.286	1.101	1.070	1.051	1.111	1.138	1.081	1.047	1.027	1.017	1.018	1.028	1.057	1.001	0.912	0.888	0.774	0.728	0.666
32	1.335	1.129	1.083	1.055	1.110	1.128	1.067	1.030	1.010	0.998	0.997	1.010	1.044	0.992	0.908	0.893	0.783	0.742	0.687
33	1.056	0.937	0.938	0.937	1.006	1.042	1.002	0.977	0.968	0.972	0.984	1.018	1.076	1.057	1.008	1.045	0.971	0.993	1.013
34	1.152	1.017	1.001	0.993	1.061	1.091	1.038	1.007	0.991	0.984	0.990	1.009	1.053	1.019	0.952	0.969	0.889	0.891	0.892
35	1.281	1.126	1.103	1.088	1.150	1.171	1.108	1.061	1.027	1.008	0.996	0.999	1.018	0.960	0.874	0.858	0.753	0.727	0.691
36	1.284	1.121	1.106	1.081	1.151	1.173	1.104	1.059	1.031	1.007	0.997	0.999	1.021	0.961	0.876	0.859	0.755	0.726	0.691
37	1.159	1.019	1.010	0.999	1.066	1.096	1.043	1.010	0.988	0.983	0.987	1.008	1.046	1.012	0.951	0.963	0.884	0.889	0.887
38	1.074	0.949	0.944	0.942	1.015	1.051	1.008	0.985	0.972	0.975	0.987	1.020	1.074	1.052	0.999	1.029	0.956	0.978	0.991
39	1.299	1.108	1.067	1.039	1.095	1.123	1.064	1.029	1.011	1.003	1.007	1.023	1.054	1.006	0.920	0.903	0.791	0.756	0.701
40	1.258	1.082	1.052	1.032	1.098	1.132	1.080	1.045	1.029	1.024	1.026	1.038	1.069	1.013	0.922	0.901	0.786	0.739	0.676

Table 14: Detailed ISBA (Cd) Radial Power Profile

Assembly	Plate 1	Plate 2	Plate 3	Plate 4	Plate 5	Plate 6	Plate 7	Plate 8	Plate 9	Plate 10	Plate 11	Plate 12	Plate 13	Plate 14	Plate 15	Plate 16	Plate 17	Plate 18	Plate 19
1	1.115	1.083	0.940	0.954	0.989	1.019	0.988	0.949	0.952	0.973	0.981	1.028	1.100	0.970	1.020	1.031	0.951	0.979	0.977
2	1.247	1.150	1.004	0.968	1.028	1.044	0.976	0.958	0.934	0.936	0.961	0.981	1.026	0.915	0.985	1.002	0.933	0.967	0.985
3	1.243	1.166	0.971	0.939	0.978	0.981	0.946	0.906	0.895	0.897	0.919	0.955	1.021	0.889	0.997	1.056	1.028	1.064	1.150
4	1.363	1.264	1.039	0.969	1.015	0.987	0.905	0.902	0.894	0.888	0.910	0.929	0.994	0.894	0.987	1.021	0.948	1.018	1.076
5	1.524	1.311	1.107	1.003	1.012	1.021	0.938	0.933	0.883	0.883	0.883	0.876	0.955	0.842	0.914	0.985	0.923	0.982	1.027
6	1.421	1.298	1.066	0.997	1.062	1.030	0.939	0.900	0.889	0.877	0.871	0.888	0.961	0.875	0.948	0.990	0.958	0.980	1.048
7	1.297	1.162	0.966	0.951	0.977	1.014	0.947	0.945	0.902	0.902	0.915	0.931	0.995	0.913	0.978	1.031	0.979	1.054	1.142
8	1.289	1.163	0.997	0.954	0.966	0.967	0.918	0.894	0.881	0.883	0.915	0.932	1.003	0.913	0.990	1.048	1.027	1.100	1.162
9	1.321	1.226	1.025	0.995	1.027	1.054	0.967	0.945	0.932	0.915	0.938	0.958	1.019	0.904	0.944	0.987	0.923	0.949	0.973
10	1.234	1.155	1.008	0.982	1.032	1.038	0.977	0.953	0.953	0.945	0.962	0.985	1.055	0.920	0.990	1.003	0.928	0.926	0.953
11	1.215	1.135	0.984	0.956	1.026	1.035	1.004	0.979	0.968	0.961	0.977	1.004	1.068	0.917	0.985	0.998	0.923	0.935	0.933
12	1.305	1.206	1.056	0.993	1.049	1.032	0.997	0.958	0.940	0.928	0.940	0.988	1.019	0.908	0.952	0.997	0.914	0.906	0.914
13	1.154	1.084	0.956	0.923	1.009	1.002	0.938	0.934	0.941	0.921	0.913	0.969	1.017	0.943	1.022	1.075	1.020	1.055	1.124
14	1.229	1.167	0.990	0.967	1.009	1.019	0.974	0.927	0.927	0.918	0.897	0.948	1.004	0.908	0.985	1.028	0.991	1.034	1.077
15	1.245	1.178	1.002	0.969	1.017	1.023	0.956	0.926	0.896	0.911	0.927	0.970	1.015	0.901	0.969	1.027	0.962	1.018	1.086
16	1.240	1.170	0.972	0.962	1.006	1.021	0.992	0.943	0.922	0.904	0.924	0.972	1.006	0.897	0.960	1.012	0.973	1.032	1.094
17	1.222	1.160	0.981	0.929	0.994	0.992	0.933	0.910	0.903	0.923	0.926	0.953	1.013	0.911	1.001	1.060	1.000	1.067	1.121
18	1.163	1.093	0.935	0.905	0.963	0.978	0.915	0.885	0.893	0.891	0.911	0.948	1.028	0.963	1.031	1.096	1.069	1.131	1.205
19	1.305	1.224	1.049	1.022	1.054	1.066	1.010	0.956	0.936	0.941	0.945	0.986	1.020	0.910	0.942	0.971	0.894	0.886	0.884
20	1.276	1.196	1.012	0.995	1.016	1.046	0.988	0.964	0.950	0.949	0.969	1.004	1.061	0.923	0.974	0.984	0.899	0.902	0.892

153

Table 14: Detailed ISBA (Cd) Radial Power Profile Continued

| Assembly	Plate 1	Plate 2	Plate 3	Plate 4	Plate 5	Plate 6	Plate 7	Plate 8	Plate 9	Plate 10	Plate 11	Plate 12	Plate 13	Plate 14	Plate 15	Plate 16	Plate 17	Plate 18	Plate 19
21	1.243	1.149	1.001	0.977	1.023	1.034	0.997	0.955	0.942	0.936	0.960	1.003	1.057	0.927	0.989	1.018	0.927	0.929	0.935
22	1.325	1.228	1.039	1.018	1.047	1.075	0.989	0.958	0.926	0.934	0.942	0.969	1.032	0.908	0.958	0.972	0.896	0.894	0.891
23	1.142	1.102	0.954	0.920	0.958	0.985	0.947	0.906	0.881	0.916	0.925	0.981	1.034	0.933	1.022	1.084	1.038	1.108	1.165
24	1.207	1.131	0.981	0.936	0.991	1.005	0.960	0.926	0.929	0.930	0.942	0.981	1.026	0.924	0.975	1.024	0.991	1.047	1.095
25	1.208	1.173	1.006	0.986	1.004	1.021	0.982	0.935	0.907	0.915	0.919	0.946	1.002	0.890	0.984	1.017	0.982	1.036	1.087
26	1.243	1.142	1.000	0.957	1.011	1.041	0.967	0.945	0.887	0.912	0.932	0.962	1.018	0.916	0.973	1.028	0.988	1.009	1.070
27	1.192	1.119	0.973	0.955	1.015	1.005	0.949	0.924	0.914	0.921	0.950	0.988	1.038	0.918	0.991	1.025	0.991	1.034	1.098
28	1.203	1.121	0.970	0.933	0.991	0.993	0.936	0.913	0.919	0.915	0.940	0.976	1.023	0.921	0.996	1.072	0.999	1.057	1.122
29	1.265	1.173	1.011	0.967	1.031	1.047	0.994	0.977	0.949	0.971	0.972	0.984	1.040	0.919	0.974	1.002	0.894	0.918	0.913
30	1.162	1.115	0.974	0.962	0.999	1.050	0.995	0.939	0.963	0.974	0.975	1.004	1.075	0.947	1.005	1.012	0.946	0.958	0.946
31	1.187	1.156	0.986	0.951	1.017	1.055	0.993	0.989	0.964	0.950	0.979	1.006	1.078	0.944	0.990	1.009	0.920	0.918	0.909
32	1.277	1.207	1.052	0.999	1.045	1.066	1.006	0.985	0.960	0.948	0.967	0.978	1.036	0.910	0.947	0.978	0.887	0.886	0.866
33	1.042	1.021	0.909	0.902	0.953	1.001	0.958	0.927	0.921	0.941	0.954	1.000	1.082	0.954	1.029	1.088	1.052	1.110	1.157
34	1.060	1.032	0.928	0.896	1.003	1.057	0.978	0.954	0.946	0.937	0.945	0.990	1.049	0.937	0.998	1.067	1.026	1.081	1.116
35	1.083	1.087	0.967	0.922	1.000	1.036	0.972	0.951	0.945	0.919	0.946	0.989	1.031	0.932	0.997	1.045	0.994	1.053	1.132
36	1.104	1.115	0.975	0.960	1.009	1.015	0.961	0.938	0.947	0.960	0.929	0.954	1.023	0.918	1.012	1.047	0.999	1.032	1.101
37	1.066	1.065	0.927	0.907	1.009	1.011	0.968	0.945	0.930	0.950	0.965	0.998	1.054	0.946	1.010	1.059	0.999	1.065	1.125
38	1.030	1.043	0.922	0.917	0.988	1.038	0.962	0.945	0.926	0.948	0.952	1.004	1.054	0.928	1.016	1.066	1.038	1.080	1.145
39	1.242	1.143	1.003	0.986	1.054	1.067	0.996	0.981	0.939	0.974	0.986	1.000	1.057	0.922	0.978	0.982	0.897	0.908	0.883
40	1.131	1.095	0.993	0.967	1.042	1.044	0.999	0.979	0.985	0.987	0.992	1.032	1.051	0.929	0.992	1.004	0.920	0.921	0.935
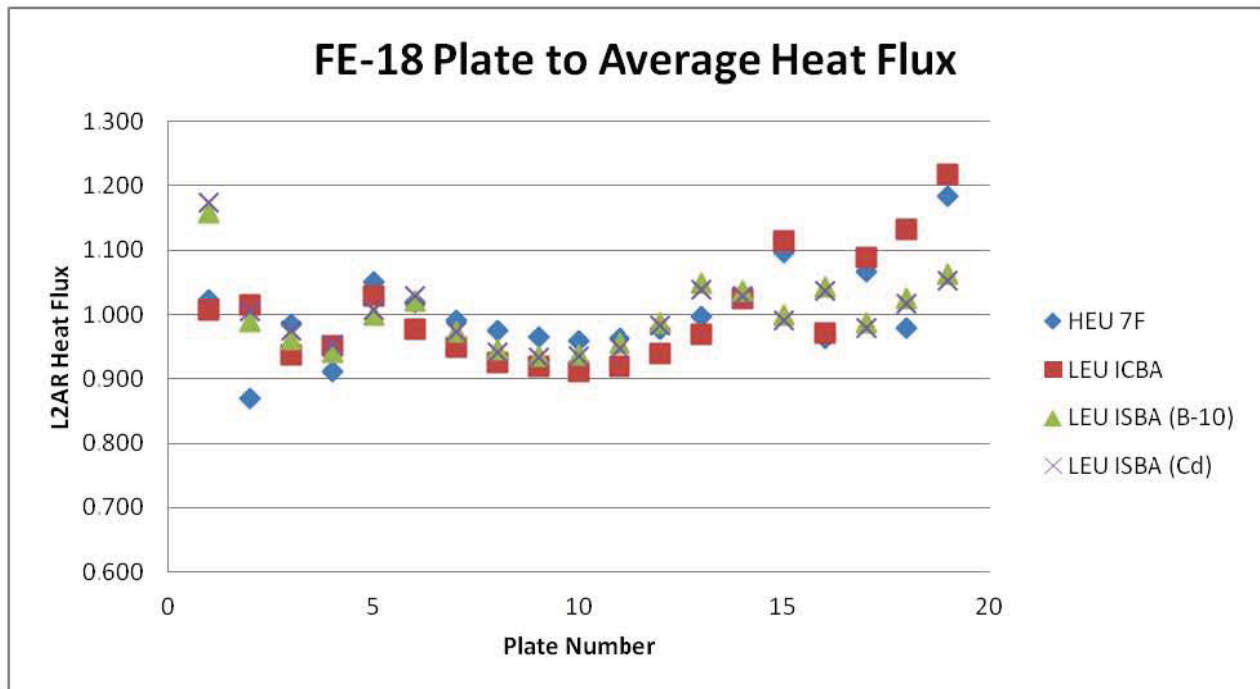
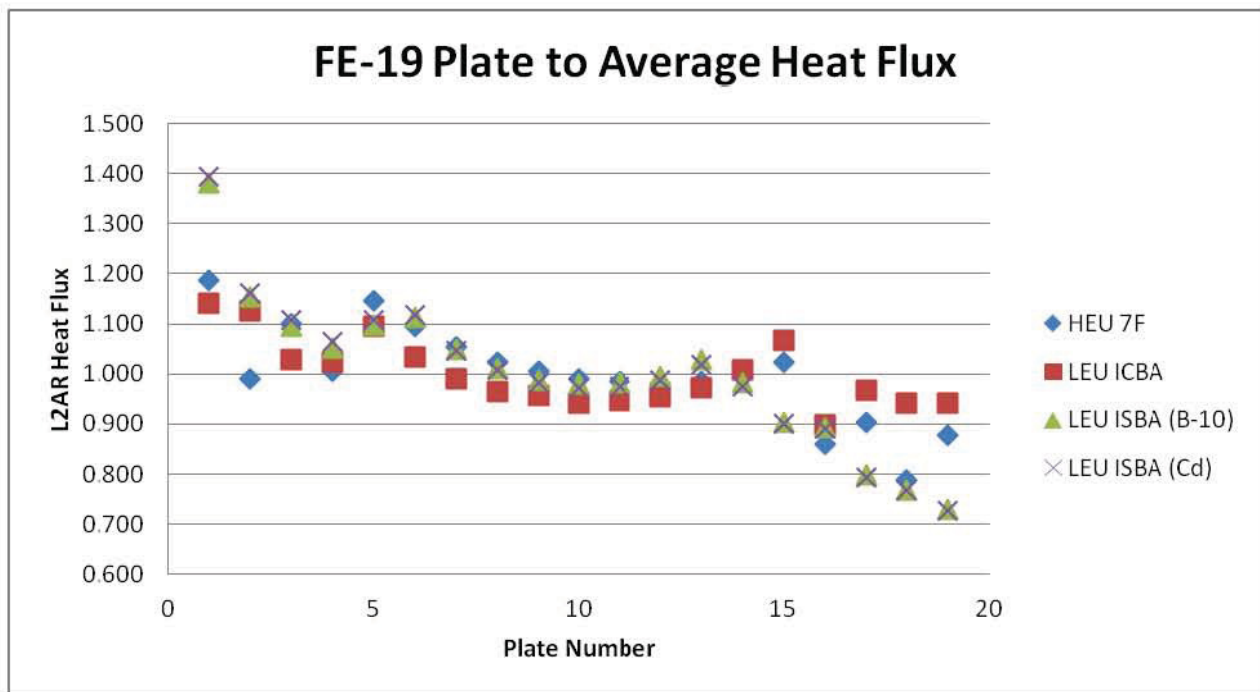Figure 9: Fuel Element 18 Normalized Heat Flux

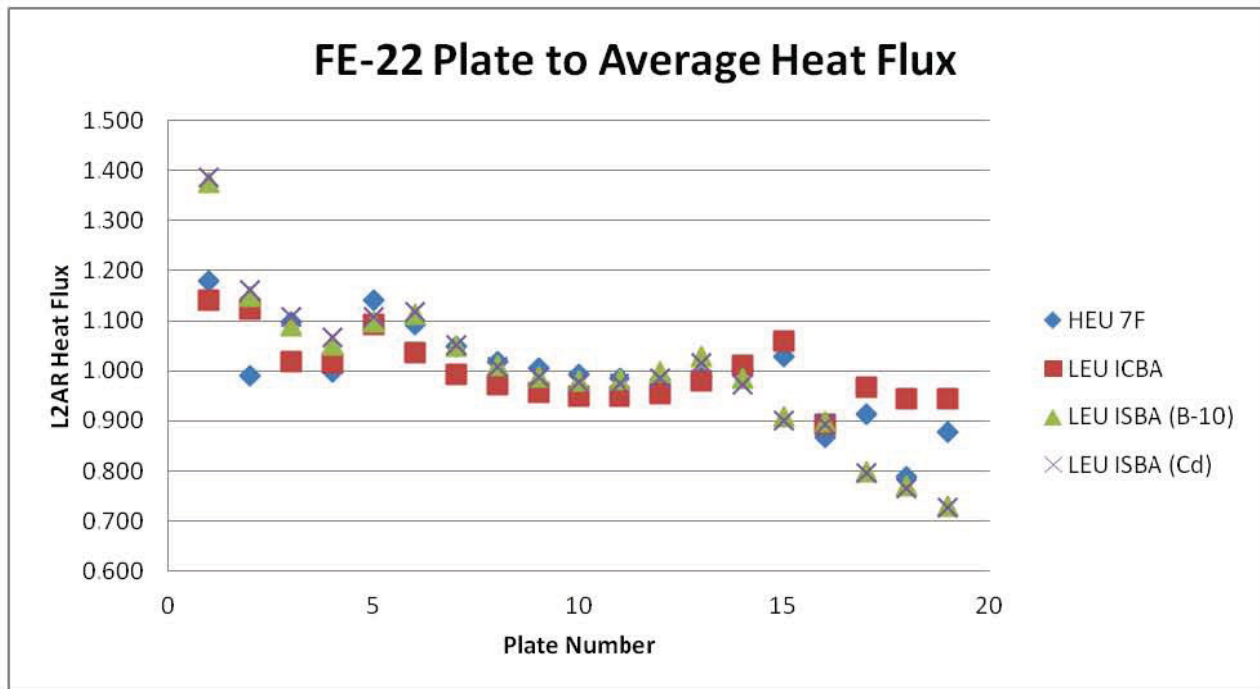Figure 10: Fuel Element 19 Normalized Heat Flux

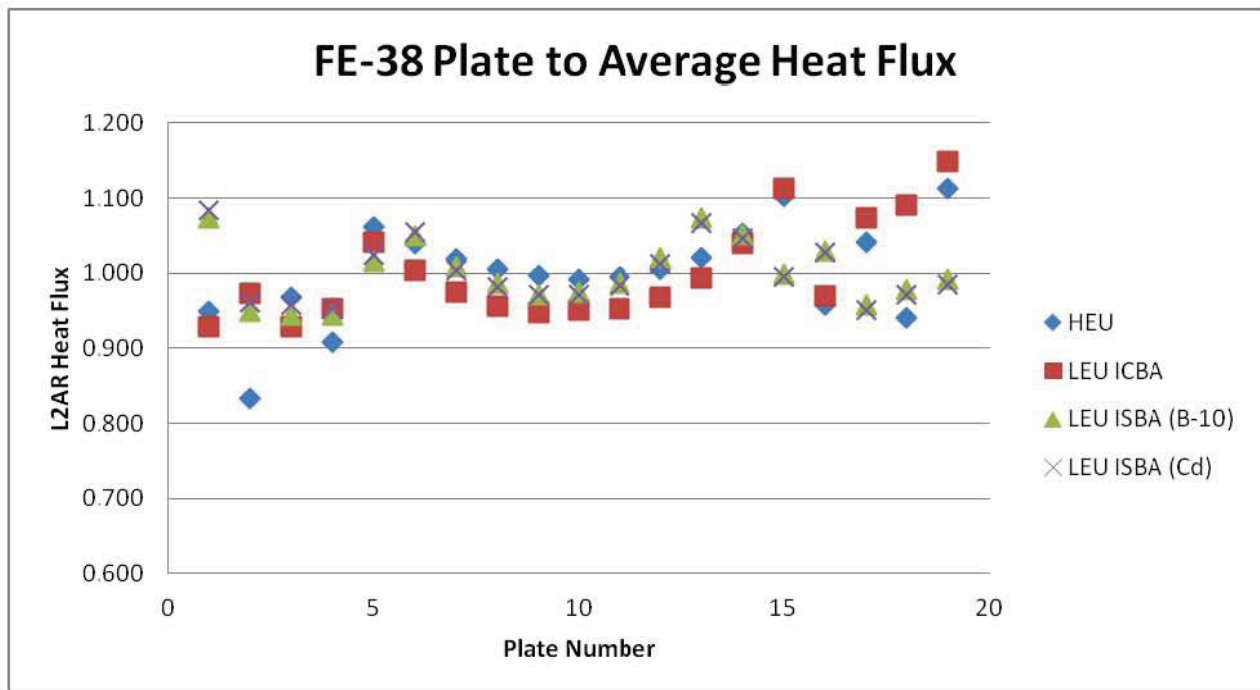Figure 11: Fuel Element 22 Normalized Heat Flux

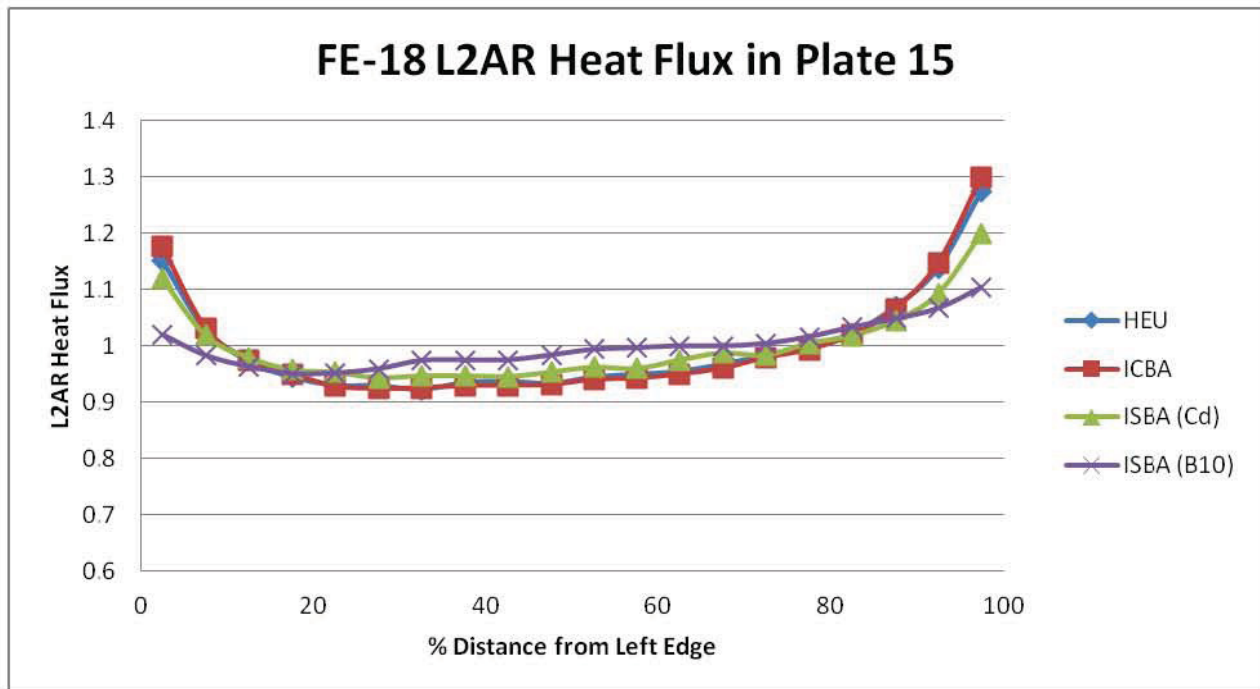Figure 12: Fuel Element 38 Normalize Heat Flux

Figure 13: Fuel Element 18, Plate 15 Azimuthal Power Profile
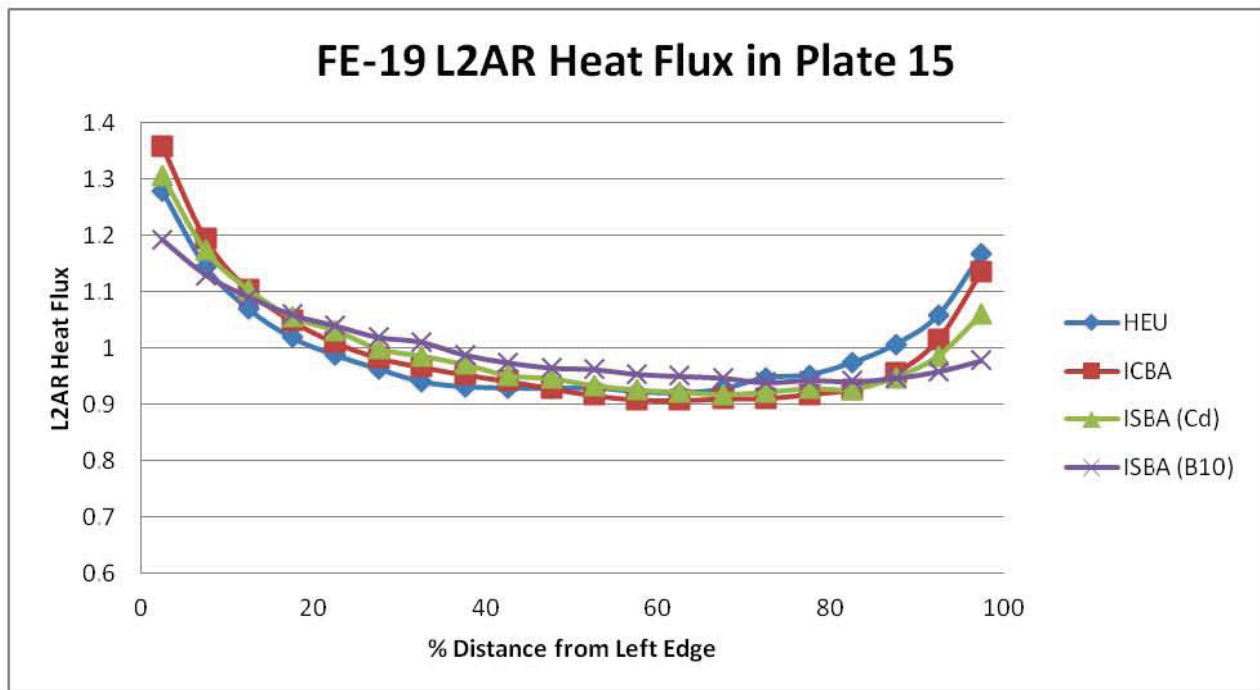

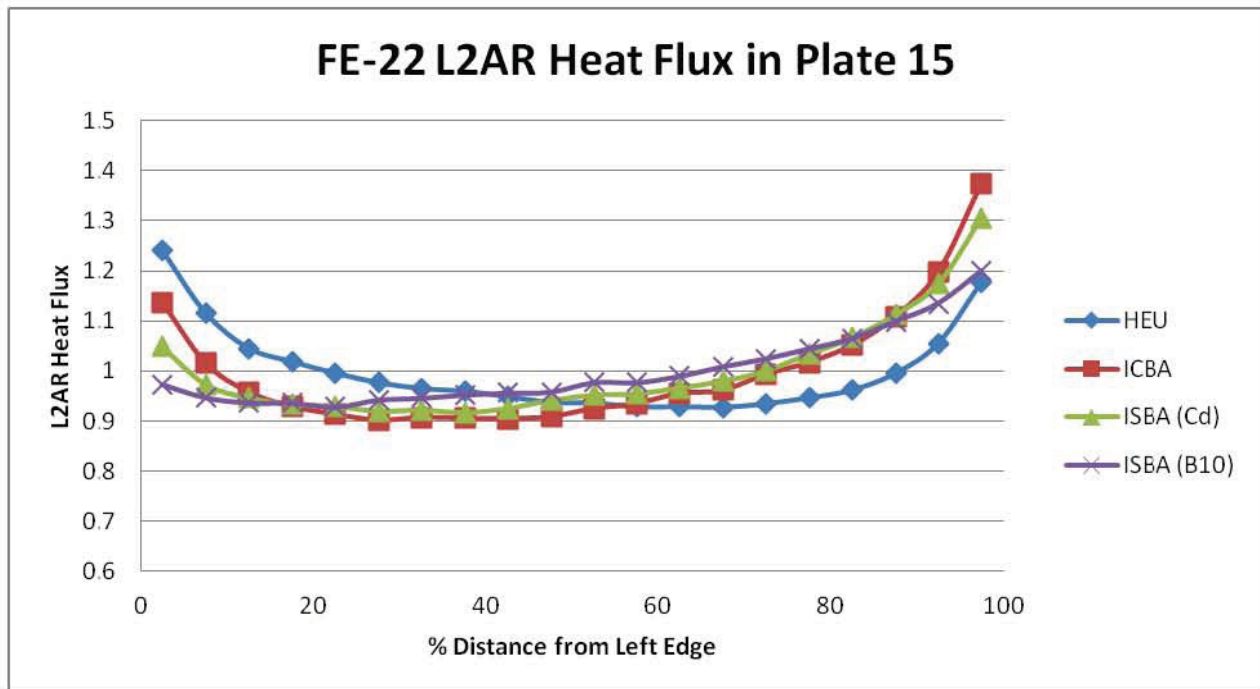Figure 14: Fuel Element 19, Plate 15 Azimuthal Power Profile

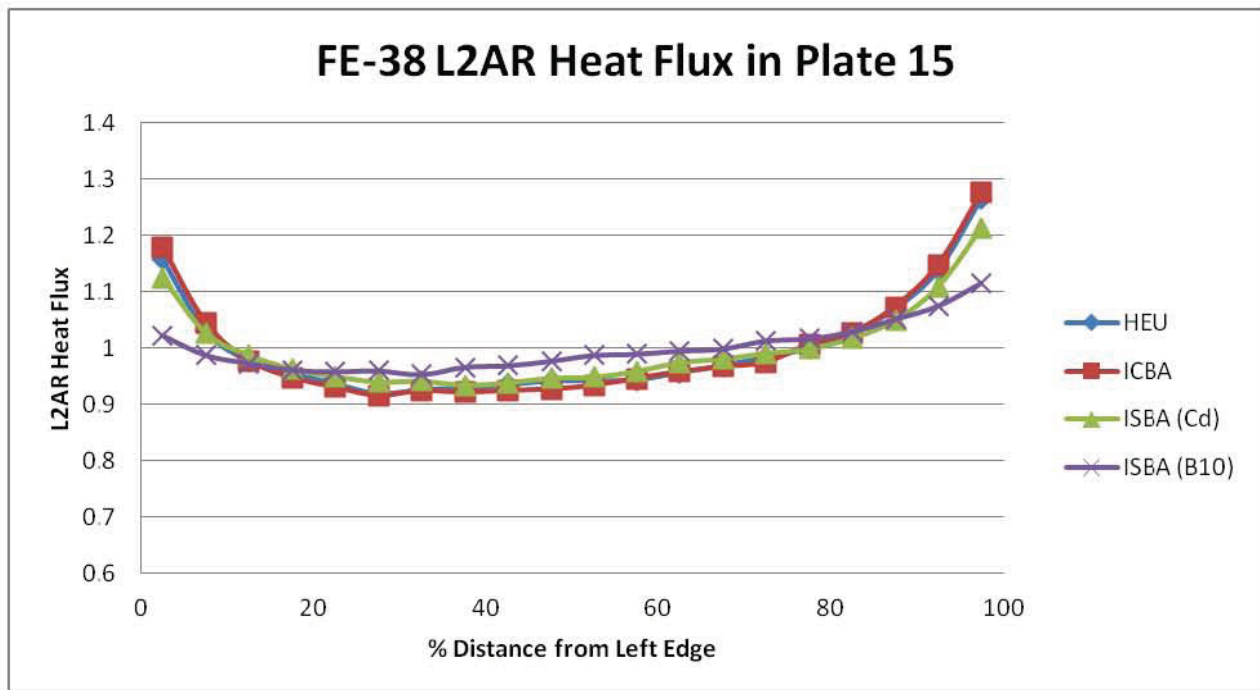Figure 15: Fuel Element 22, Plate 15 Azimuthal Power Profile

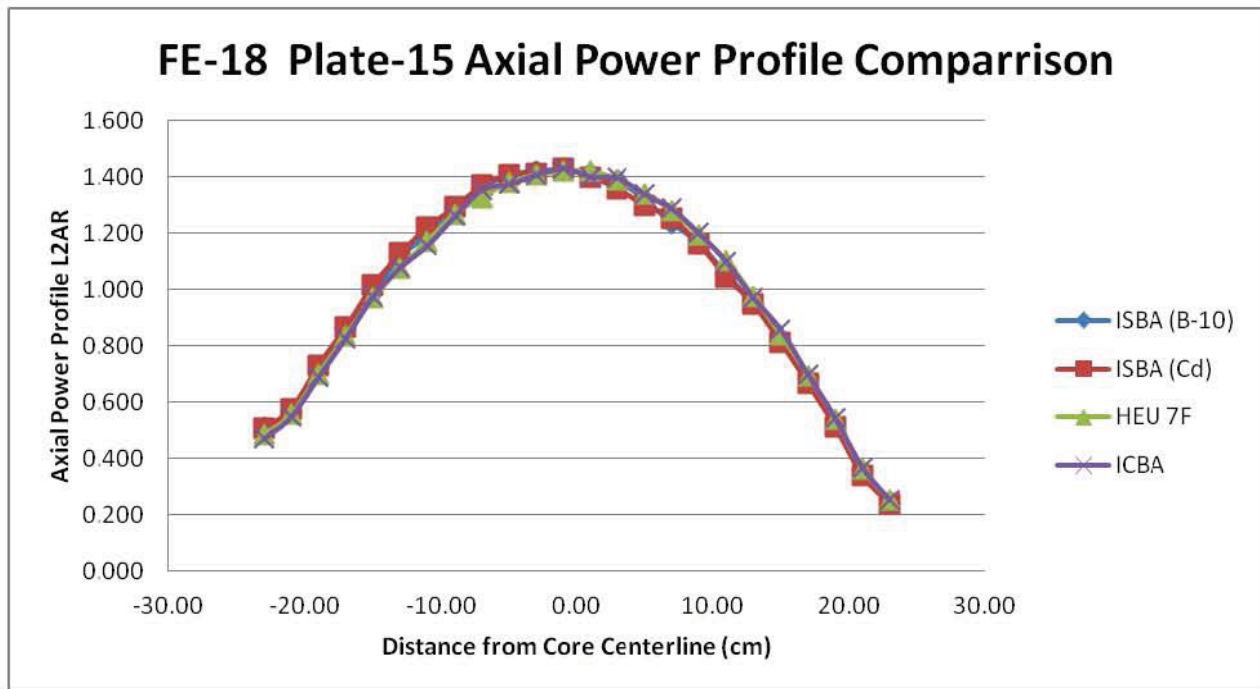Figure 16: Fuel Element 38, Plate 15 Azimuthal Power Profile

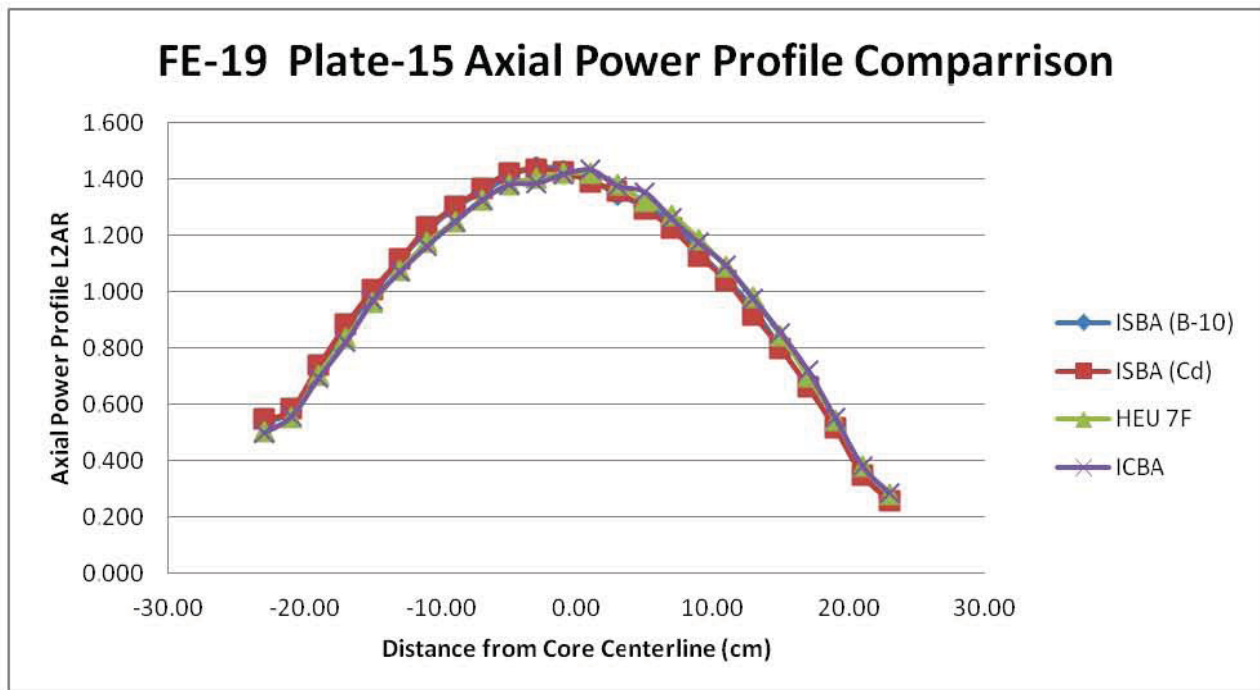Figure 17: Fuel Element 18, Plate 15 Axial Power Profile

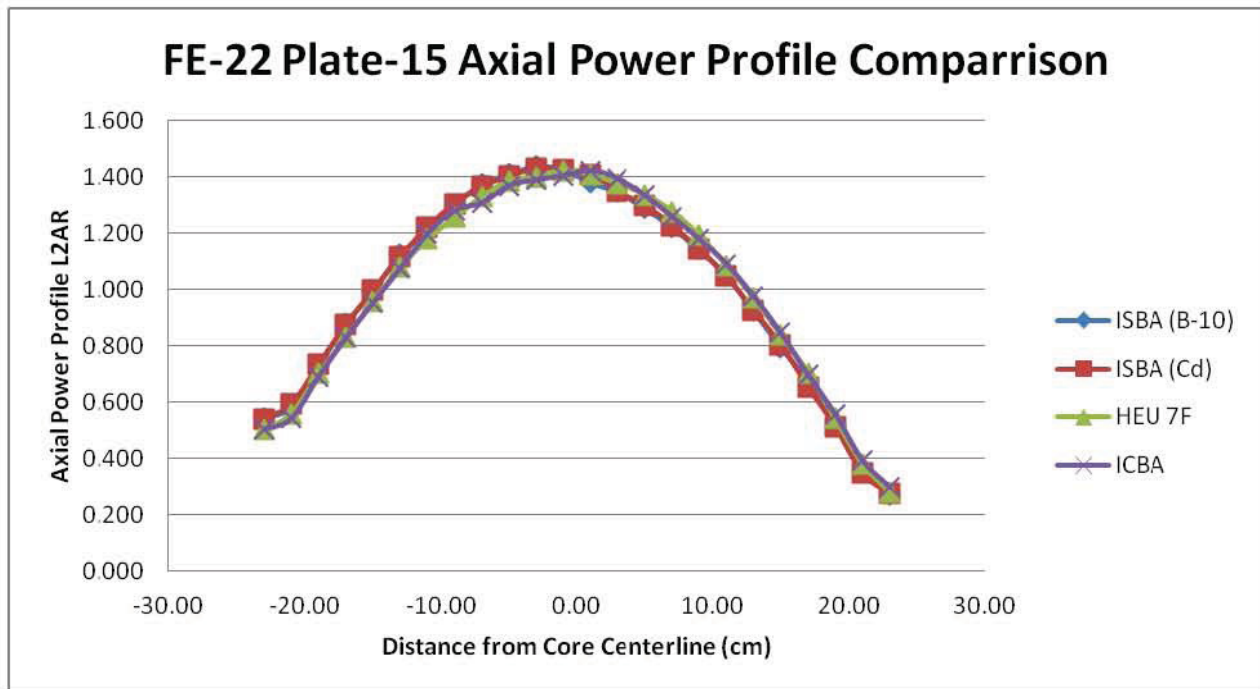Figure 18: Fuel Element 19, Plate 15 Axial Power Profile

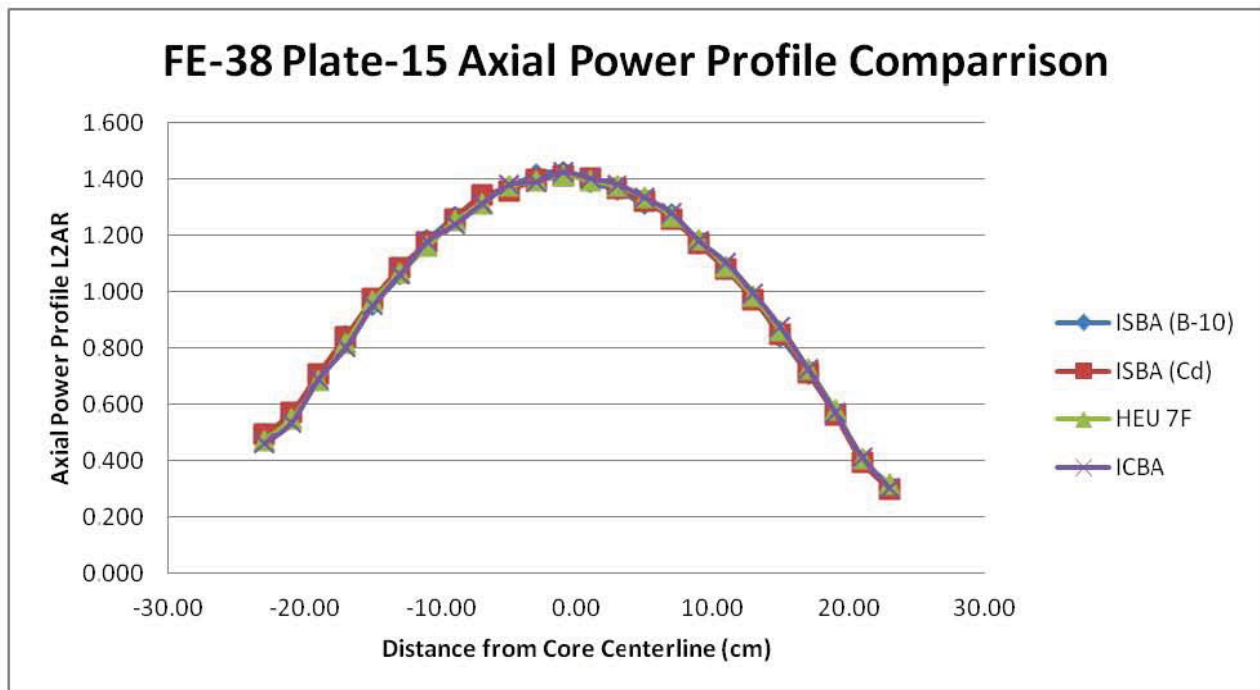Figure 19: Fuel Element 22, Plate 15 Axial Power Profile

Figure 20: Fuel Element 38, Plate 15 Axial Power Profile

1. M.N. Neeley, G. S. Chang., "MCWO Neutronics Analysis of RERTR Full Element Demonstration in Position 38 of the ATR," ECAR-1357, February 2011.

2. W. C. Cook, A. C. Smith, "ATR CSAP Code Package on the Workstation Version 1," PG-T-96-002, May 1996.

3. Tim Goorley, et. al., "Release of MCNP5_RSICC_1.30," Trans. Am. Nucl. Soc., Vol. 91, 693-694 (2004).

4. X-5 Monte Carlo Team, "MCNP-A General Monte Carlo N-Particle Transport Code, Version 5," Volume I, LA-UR-03-1987, Los Alamos National Laboratory, April 24, 2003 (Revised 6/30/2004) and Volume II, LA-CP-0245, Los Alamos National Laboratory, April 24,2003 (Revised 6/30/2004) (Vol. II is available with a licensed copy of MCNP)

5. S. S. Kim, B. G. Schnitzler, "Advanced Test Reactor: Serpentine Arrangement of Highly Enriched Water-Moderated Uranium-Aluminide Fuel Plates Reflected by Beryllium," HEU-MET-THERM-022, NEA/NSC/DOC/(95)03/II, International Handbook of Evaluated Criticality Safety Benchmark Experiments, Volume II: Highly Enriched Uranium Systems, March 2009.